



**Scaleable Oral Dose Formulations**

**By**

**Elanor Michelle Brammer**

A thesis in fulfilment of the requirements for the degree of Doctor of  
Philosophy

Strathclyde Institute of Pharmacy and Biomedical Sciences,

The University of Strathclyde,

Glasgow, United Kingdom

2023

# Scaleable Oral Dose Formulations

Elanor Brammer

## **Declaration of Authenticity and Author's Rights**

This thesis is the result of the author's original research. It has been composed by the author and has not been previously submitted for examination which has led to the award of a degree. The copyright of this thesis belongs to the author under the terms of the United Kingdom Copyright Acts as qualified by University of Strathclyde Regulation 3.50. Due acknowledgement must always be made of the use of any material contained in, or derived from, this thesis.

Signed:

Date:

The data underpinning this publication will be available from the University of Strathclyde KnowledgeBase at <https://doi.org/10.15129/c8874cdb-adda-4dea-946d-2822059ad8ca>. Further details relating to the data can be accessed from the portal.

# Acknowledgements

Thanks to Professor Gavin Halbert, you have been a fantastic supervisor to work with and your guidance and enthusiasm throughout my PhD has been invaluable. Thanks also to my second supervisor, John Robertson, who was a late addition to my mentoring, but who has helped considerably with a number of lab related problems throughout my PhD journey!

Huge thanks are also due to all the other members of CMAC, especially the National Facility team, who provided excellent training on various pieces of equipment throughout my time in the university and were always on hand with expert advice whenever I encountered unexpected results!

I would like to express my gratitude to the Engineering and Physical Sciences Research Council (EPSRC) for the generous funding which allowed this research to be undertaken, and to the numerous CMAC industry partners who have guided the direction of this research throughout my time on the project.

To my wonderful family and fantastic group of friends (with special thanks to Sarahjane for keeping me sane in the lab and to Alice for the copious amount of wine and Zoom calls towards the end), I couldn't have done this without you! Despite the struggles of raising children while studying for both an undergraduate and postgraduate degree, I don't regret anything and believe my children have spurred me on to be the best possible version of myself!

## Abbreviations

3D	Three Dimensional
3DP	Three Dimensional Printing
3TC	Lamivudine
Å	Angstrom
ABS	Acrylonitrile butadiene styrene
ACN	Acetonitrile
AFM	Atomic Force Microscopy
API	Active Pharmaceutical Ingredient
AZT	Zidovudine
BCS	Biopharmaceutics Classification System
BNF	British National Formulary
CAD	Computer-Aided Design
CAR	Carvedilol
cm	Centimetres
CMAC	Continuous Manufacturing and Crystallisation
Da	Dalton
DAD	Diode-Array Detection
DC	Direct Compression

DED	Directed energy deposition
DMLS	Direct Metal Laser Sintering
DMSO	Dimethyl Sulfoxide
DoE	Design of Experiments
DSC	Differential Scanning Calorimetry
DTC	Doctoral Training Centre
EC	Ethyl cellulose
EHD DOD	Electrohydrodynamic Drop-on-Demand
EPSRC	Engineering and Physical Sciences Research Council
FDA	Food and Drug Administration
FDM	Fused Deposition Modelling
FFF	Fused Filament Fabrication
g	Grams
GCIB	Gas Cluster Ion Beam
H <sub>2</sub> O	Water
HCl	Hydrochloric Acid
HIV	Human Immunodeficiency Virus
HME	Hot Melt Extrusion
HPC	Hydroxypropylcellulose
HPLC	High Performance Liquid Chromatography

HPMC	Hydroxypropyl methylcellulose
kbar	kilo bar
kg	kilo grams
kV	kilo volts
L	litres
LMIG	Liquid Metal Ion Gun
m	Metres
mA	milli amps
MAN	Mannitol
µg	micro grams
mg	milli grams
MIBK	Methyl Isobutyl Ketone
min	minutes
MIT	Massachusetts Institute of Technology
µL	micro litres
mL	milli litres
µm	micro metres
mm	milli metres
mM	Millimolar
mN	milli Newton

mPa	milli Pascal
MPa	megapascal
mW	milliwatt
MWt	Molecular Weight
N	Newton
NaCl	Sodium Chloride
Nano-CT	Nano-Computed Tomography
nm	Nanometres
NPL	National Physical Laboratory
NRTIs	Nucleoside Transcriptase Reverse Inhibitors
PDA	Personal Digital Assistant
PDE	Permitted Daily Exposure
PE	Piezoelectric
PEG	Polyethylene Glycol
PET	Polyethylene Terephthalate
PG	Propyleneglycol
PLA	Poly(l-Lactic Acid)
PTFE	Polytetrafluoroethylene
PVA	Polyvinyl Alcohol
PVP	Polyvinylpyrrolidone

R&D	Research and Development
rpm	Revolutions per minute
s	Seconds
SEM	Scanning Electron Microscope
SFO	Sheet Fed Offset
SGF	Simulated Gastric Fluid
SLS	Selective Laser Sintering
STL	Stereolithography
T <sub>g</sub>	Glass Transition Temperature
TGA	Thermal Gravimetric Analysis
TIJ	Thermal Inkjet Printing
ToF-SIMS	Time of Flight Secondary Ion Mass Spectrometry
UK	United Kingdom
USA	United States of America
USP	United States Pharmacopeia
UV	Ultra-violet
v/v	Volume to volume
vs	Versus
w/w	Weight to weight
XRPD	X-Ray Powder Diffraction



## **Abstract**

This thesis explores the manufacture of personalised medicine for solid oral dosage forms, with the main area of research focused on the use of Fused Filament Fabrication (FFF), a 3-dimensional printing (3DP) technique which utilises a polymer filament as feedstock. Two different techniques for the incorporation of a drug within this filament feedstock, solution loading and extrusion loading, are examined in order to investigate the applicability of this technique in the production of varying doses of carvedilol. The solution loading method is highlighted as having the potential to be beneficial when concerned with the manufacture of low dose drugs, whereas the extrusion loading method allows for higher dose drugs to be produced with greater overall dose variation.

In terms of how these new dosage forms behave, the FFF 3DP technique lends itself to the production of tablets with sustained release characteristics, alteration of which is difficult to achieve even with the use of pharmaceutical disintegrants. Despite various attempts to alter this release, through the use of different additives or structural changes to the dosage forms, sustained release remains the mechanism by which any active pharmaceutical ingredient (API) will be released within the body.

Carvedilol is currently marketed as both an immediate release and as a controlled release product. While investigation has concluded that immediate release is not achievable with this manufacturing method, this thesis demonstrates the production of sustained release dosage forms of carvedilol in a range of 7-101 mg, which exceeds the range of 10-80 mg currently available for the controlled release product.

While this area of research is still in its infancy, this thesis provides an in-depth investigation into FFF as a manufacturing technique and acts as a starting point for the consideration of adopting this technique as a viable method of production in the pharmaceutical industry.

# Table of Contents

1	Introduction .....	1
1.1	Background – Dosage Forms .....	1
1.2	Oral Dosage Forms.....	1
1.3	Current Manufacturing of Oral Doses.....	2
1.4	Personalised Medicine.....	3
1.4.1	Methods of Applying Personalised Medicine .....	4
1.5	Scaling Doses Based on Current Manufacturing Techniques .....	6
1.6	Initial Attempts at Altering Manufacture .....	7
1.6.1	Tablets Manufactured with a Drug Free Splittable Layer.....	7
1.6.2	Tablet-Like Slices Produced with a Novel Cutting Tool.....	9
1.6.3	Inkjet Printing of Oral Dosage Forms.....	10
1.6.4	Flexographic Printing.....	17
1.7	Additive Manufacturing and 3-Dimensional Printing (3DP).....	18
1.7.1	Metals.....	20
1.7.2	Food .....	21
1.7.3	Medical Applications .....	22
1.8	3D Printing of Solid Oral Dosage forms .....	23
1.8.1	Inkjet Binder 3D Printing of Dosage Forms .....	23
1.8.2	Stereolithography (STL) Fabrication of Dosage Forms.....	25

1.8.3	Room Temperature Paste Extrusion 3D Printing of Dosage Forms ....	26
1.8.4	Fused Filament Fabrication of Dosage Forms .....	27
1.9	The Current Study .....	31
1.9.1	Method Selection .....	32
1.9.2	Polymer Selection .....	33
1.9.3	API Selection .....	34
1.10	Aims and Objectives .....	39
2	Materials and Methods .....	40
2.1	Introduction .....	40
2.2	Materials .....	40
2.3	Manufacture of 3D Printed Tablets .....	41
2.4	Extrusion of Polymer Filaments .....	42
2.5	Techniques Specific to Chapter 3 and Solution Loading of PVA Filaments	43
2.5.1	Preparation of Drug Loaded Filaments .....	43
2.5.2	Solvent Screening.....	43
2.5.3	Varying the Loading with Solvent Evaporation Rate .....	44
2.5.4	Varying Concentration of Loading Solution.....	44
2.5.5	Varying Loading of Filaments With Time.....	44
2.5.6	Varying Loading of Filaments with Varying Pressure .....	45

2.6	Techniques Specific to Chapter 4 and Extrusion Loading of PVA or Affinisol™	46
2.6.1	Milling of PVA Filament	46
2.6.2	Extrusion of PVA	46
2.6.3	DoE Approach to Extrusion of Affinisol™ with Disintegrants using MODDE Statistical Analysis	47
2.6.4	Extrusion of Affinisol™ with Carvedilol and Varying Mannitol or PEG 4600	49
2.6.5	Extrusion of Affinisol™ with Carvedilol and Superdisintegrants	51
2.6.6	Disintegration of Affinisol™/Carvedilol/Disintegrant Filaments	51
2.7	Techniques Specific to Chapter 5 and the Population of a Ternary Phase Diagram	52
2.7.1	Population of a Ternary Phase Diagram	52
2.7.2	Extrusion of Formulations with 1% Carvedilol	53
2.7.3	Extrusion of Formulations with 5% Carvedilol	54
2.7.4	Extrusion of Formulations with 10.5% Carvedilol	54
2.7.5	Extrusion of Formulations with 20% Carvedilol	54
2.7.6	Extrusion of Formulations with 30% Carvedilol	55
2.7.7	Extrusion of Formulations with 40-50% Carvedilol	56
2.7.8	Extrusion of Formulations with 45% Affinisol™	57
2.7.9	Direct Compression of Affinisol™/Carvedilol/Mannitol Formulations	57

2.8	Analytical Techniques .....	59
2.8.1	Determination of Carvedilol Concentration.....	59
2.8.2	Dissolution Analysis .....	61
2.8.3	Analysis of Drug Distribution.....	61
2.8.4	Determination of Crystallinity .....	64
2.8.5	Surface Morphology.....	65
2.8.6	3-Point Bend Testing .....	66
2.8.7	ANOVA Statistical Analysis .....	67
3	Producing Drug Loaded 3D Printed Tablets via Solution Loading of PVA.....	68
3.1	Introduction .....	68
3.2	Aim.....	68
3.3	Results and Discussion.....	69
3.3.1	Loading of PVA Filaments with Carvedilol .....	69
3.3.2	Production of 3D Printed Tablets.....	81
3.4	Conclusions and Next Steps .....	107
4	Drug Loading of Polymer Filaments via Hot-Melt Extrusion .....	110
4.1	Introduction .....	110
4.2	Aim.....	110
4.3	Results and Discussion.....	111
4.3.1	Extrusion and Milling of PVA.....	111
4.3.2	DoE Approach to Extrusion of Affinisol™ with Disintegrants.....	116

4.3.3	3D Printing of Affinisol™ Formulations .....	130
4.4	Conclusions and Next Steps .....	178
5	Population of a Ternary Phase Diagram to better understand Formulations for 3D Printing.....	180
5.1	Introduction .....	180
5.2	Aim.....	180
5.3	Results and Discussion .....	181
5.3.1	Production of a Ternary Phase Diagram .....	181
5.3.2	Highest and Lowest Achievable Dose.....	205
5.3.3	Comparison to Direct Compression as a Manufacturing Method.....	208
5.4	Conclusion and Next Steps.....	214
6	Conclusions and Future Work.....	219
6.1	Overall Conclusions .....	219
6.2	Further Work .....	222
7	Appendices.....	223
7.1	HME Experimental Screw Configuration .....	223
7.2	Feed Rate of Material Entering Extruder .....	224
7.3	Raman Mapping Images for Carvedilol Loaded Filaments and Tablets...	225
7.3.1	Carvedilol Loaded PVA Filaments .....	225
7.3.2	Carvedilol Loaded PVA Printed Tablets.....	227
7.4	Stress versus Strain Graphs for Different CAR Drug Loadings.....	228

7.5 Flexural Modulus and Maximum Stress Values for Ternary Phase Diagram Formulations .....	232
7.6 Supplementary DSC Data.....	234
References .....	242

# **1 Introduction**

## **1.1 Background – Dosage Forms**

The term ‘dosage form’ refers to the system by which an active pharmaceutical ingredient (API) is delivered into the body, thereby reaching the desired site of action. Dosage forms do not solely consist of a drug, rather they encompass a variety of different components which are added to the formulation during the manufacturing process. These extra components, when combined with the API, serve to protect the active ingredient from any undesirable chemical changes<sup>1</sup> or overcome any undesirable drug properties (e.g. poor solubility<sup>2</sup>) and result in a formulation that is stable and is delivered, at an accurate dose, to the correct site of action within the body. Dosage forms can be administered in a variety of different ways – topical, inhalation, injection and oral to name a few, with the latter of these systems being the most favourable. Early screening of the absorption, distribution, metabolism and excretion aspects of an API, along with investigation into its toxicity are of paramount importance to the drug discovery industry<sup>3</sup> and are factors which must be considered with the development of any new drug and its formulation. As the oral route of administration proves to be the most popular, it is therefore the route where this research will be focussed.

## **1.2 Oral Dosage Forms**

Oral dosage forms remain the preferred method of administration for the vast majority of drugs due to improved patient compliance, accuracy of dosing and the lack of pain associated with administering when compared to injections.<sup>4,5,6</sup> Oral dosage forms are also cheaper to manufacture, as they don’t require sterile preparation, and they don’t require extra personnel to administer, which allows patients to take their medication out with a hospital environment.

Oral dosage forms fall into the categories of solids, semi-solids or liquids, with the most common formulation methods across these categories being tablets, capsules, suspensions, solutions and emulsions.<sup>7</sup> All of these formulations encompass a number of different excipients which are designed to aid the pharmaceutical behaviour during



manufacture of the product, or once it has entered the body. If we consider a simple tablet, the main components are typically: API, disintegrant<sup>8</sup> (for ensuring the break-up of the tablet), binder<sup>9</sup> (for holding powders together), diluent<sup>10</sup> (for bulking the final product to allow adequate patient handling), lubricant<sup>11</sup> (to reduce friction between surfaces of manufacturing equipment) and glidant<sup>11</sup> (lubricants which enhance the powder flow properties of the pharmaceutical blend prior to manufacture). All of these different components ultimately govern how a tablet behaves, and tweaking the composition slightly can potentially alter the overall manufacturing or behaviour within the body.

Oral dosage forms also benefit from the ability to tailor the release mechanism of the API once it has entered the body. These release mechanisms vary between either immediate release, which is defined as releasing 80% of the API within a specified time (typically 45 minutes),<sup>12</sup> sustained release, which releases API consistently over a period of time,<sup>13</sup> or delayed release, which has an initial delay before releasing the API.<sup>14</sup> There is also another release mechanism classed as ‘pulsatile’, which is defined as the ‘rapid and transient release of a certain amount of drug molecules within a short time-period immediately after a predetermined off-release period.’<sup>15</sup>

### **1.3 Current Manufacturing of Oral Doses**

Oral doses can be manufactured in many different forms, however as mentioned above, these generally fall into two main categories – liquid oral doses and solid oral doses. Liquid doses are generally manufactured as emulsions, gels, mixtures, solutions and suspensions, and are easily scaled to individual patients by administering with the use of measuring cups and spoons, or even with convenient dosing syringes in the case of paediatric Calpol®.<sup>16</sup>

Solid oral doses are typically manufactured in the form of capsules, tablets or pellets, with tablets produced via wet granulations and direct compression of API and excipients being the most common method of production and distribution.<sup>17</sup> Despite this popularity, there are still a number of shortcomings associated with the technique, namely: the limited tablet geometries available for production, with most tablets produced as circular solid cylinders with flat or convex faces,<sup>18</sup> the sensitivity of some

APIs to humidity encountered during wet granulation and direct compression,<sup>19</sup> the forceful nature of the tableting technique causing polymorphic changes to the API,<sup>20</sup> and the inherent large supply chain of the manufacturing technique as production is carried out in large batches at licensed facilities, which are often far away from the required point of care of the patient.<sup>21</sup>

These limitations, coupled with the general shift in the pharmaceutical industry towards a more personalised manufacturing approach,<sup>22</sup> mean that alternatives to this traditional manufacturing model must be investigated, leading to the overall focus for this research.

## 1.4 Personalised Medicine

Personalised medicine is a ‘catch all’ term that refers to a number of different ideas and approaches within the overall healthcare sector, not limited purely to manufacturing, but what does it actually mean?

*‘The core definition of personalised medicine is using an individual’s specific biological characteristics to tailor therapies to that person, including drugs, drug dosage and other remedies’ M. Swan, 2009.<sup>23</sup>*

So why is this important to us? A patient population can vary widely with regards to how each individual reacts to different drugs. Figure 1 provides a visual representation of this and highlights the different responses which may occur.

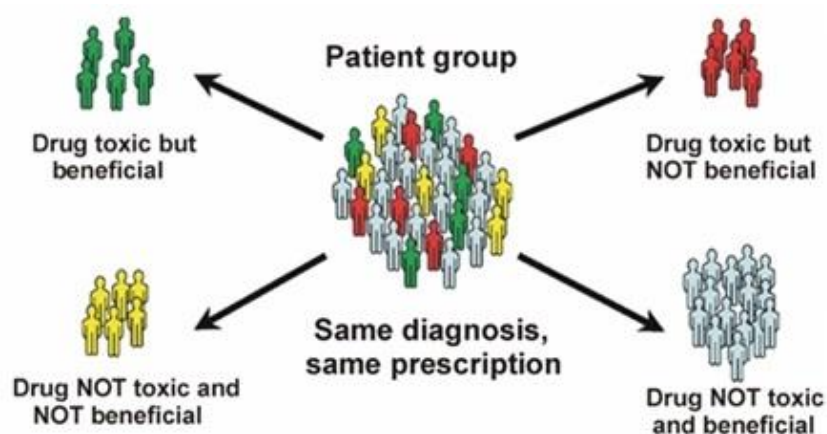


**Figure 1** - Different outcomes of treatment within the same patient population.<sup>24</sup>

There are many factors which have the potential to influence individual patient response to a drug, such as: age, gender, multiple drugs, disease state, past history of any adverse reactions/allergy, genetic factors, large doses etc.<sup>25</sup> Personalised medicine has the ability to offer the right drug for the right disease at the right time and with the right dosage, but this is not a new concept, especially when you consider that historically it was common for pharmacists to prepare individual, patient specific medications on site for their patients.<sup>26</sup>

The current traditional business model, within the pharmaceutical industry, is based around the discovery and development of ‘Blockbuster Drugs,’<sup>27</sup> however the recent expiration of patents on a number of these drugs, combined with decreased R&D productivity means that a change in strategy is required. With the emergence of drugs such as trastuzumab and gefitinib, which target very specific patient groups,<sup>28</sup> perhaps industrial focus could also include a more personalised approach towards development and manufacture, going forward.

Aside from manufacturing approaches, which is the main focus of this research, personalised medicine is already being investigated/applied in other areas, a few of which are discussed below.

#### **1.4.1 Methods of Applying Personalised Medicine**

##### **1.4.1.1 Pharmacokinetic Approaches**

Levofloxacin is an example of a broad spectrum antibiotic which is prescribed to a highly varied patient population.<sup>29</sup> The number of factors to be considered include: obese vs normal-weight, cystic fibrosis vs non cystic fibrosis, male vs female, children vs adults, elderly patients vs younger patients, intensive care patients and patients with a creatinine clearance level less than 50 mL per minute. If we take a couple of these factors as examples, it is possible to see how clinicians can adjust their prescriptions to provide personalised care.

It was found that obese patients with normal kidney function may actually clear levofloxacin more efficiently than patients who fall into a normal weight range. It is important for healthcare workers to take this into account and adjust the prescription

to avoid under dosing, or to use an alternative therapy, such as the antibiotic moxifloxacin instead, as the pharmacokinetics are not significantly affected by obesity.<sup>30</sup>

When investigating the paediatric use of levofloxacin, Chien *et al.* discovered that children under the age of 5 cleared the drug nearly twice as fast as adults.<sup>31</sup> As a result, they recommended that children above the age of 5 receive a dose of 10 mg/kg daily and children between the ages of 6 months and 5 years receive 10 mg/kg twice daily (every 12 hours).

#### **1.4.1.2 Pharmacogenetic Approaches**

Tailoring medicine to treat patients with specific gene mutations through the application of pharmacogenetics is another method of providing individualised healthcare. Vertex, a small pharmaceutical company based in Massachusetts, released their drug Kalydeco (ivacaftor) for the treatment of a specific population of cystic fibrosis patients.<sup>32</sup> The drug is only used in patients above the age of 6 and who have a particular mutation in a specific gene related to cystic fibrosis. This mutation only occurs in 4% of the population of cystic fibrosis sufferers, but there is the potential for Kalydeco to be used for patients with other mutations, widening the pool to 10% of the cystic fibrosis population.<sup>33</sup> Even though this treatment only targets such a small percentage of patients, those patients benefit from a better quality of life and highlights the importance of personalised medicine.

#### **1.4.1.3 Digital Approaches**

Another point to consider when looking into personalised medicine is the ease with which an accurate dose can be determined. Warfarin is another example of a commonly prescribed drug that is required in many different doses. It has a small therapeutic index and the correct dose varies greatly from person to person with factors such as age, diet, gender, other medications, comorbidities (such as diabetes, cancer, renal or liver disease) and even genetic variation playing a part in the quantity prescribed for individual patients.<sup>34</sup> In order to help prescribe doses of warfarin quickly and effectively, Zhao *et al.* have developed a portable tool known as

SmartWarf, which uses an algorithm to calculate a dosing regimen for the patient.<sup>35</sup> SmartWarf can be installed in a personal digital assistant (PDA) allowing a doctor to have access to the information anywhere, which is beneficial in terms of time and ease of dosing, however issues would still remain if the required dose was not one that is currently manufactured. Studies have shown that patient compliance decreases if tablets are required to be split for the correct dose to be achieved,<sup>36</sup> so care would need to be taken to ensure no under or overdosing occurs.

Another method of personalising care is through the use of an Internet Web-application. A recent pilot study was carried out on a group of lung cancer patients with a view to earlier detection of disease relapse.<sup>37</sup> These patients were required to fill in an online form with details of 11 self-assessed symptoms, which was then sent to an oncologist for review. If any of the symptoms matched some predefined criteria, this resulted in an alert email being sent to an oncologist who then phoned the patient to confirm the symptoms and arrange immediate follow-up. It was possible to detect relapses an average of 5 weeks earlier than with planned visits alone and patients also reported feeling less stressed in the lead up to a planned visit by using this system. Although further research is required, with high patient compliance it is likely that this method could lead to more effective treatment. Attention is directed where there is a need, allowing for better distribution of resources.

While all of these examples demonstrate areas where personalised medicine is being investigated, the fact remains that in order to be able to supply a patient with a dose tailored specifically for their own needs, it is essential that there is a viable method of manufacturing the required doses that are called for using these techniques. With the popularity of oral dosing, scaling of oral dose formulations is discussed in more detail below.

## **1.5 Scaling Doses Based on Current Manufacturing Techniques**

While oral dosing is the preferred method of administering an API to the vast majority of the population, across various ages, sizes, etc., care must still be taken to ensure no under or overdosing. This highlights the need for any dosing regime to be easily scaled to mirror individual patient needs.

Scaling of liquid doses is, in theory, relatively easy and is achieved, as mentioned above, by the use of measuring spoons, or syringes.<sup>16</sup> Liquid doses are also ideal for the treatment of young children or the elderly, who may have lost the ability to swallow large solid material.<sup>38</sup> Despite this ease of scaling, there is also the potential for measurement errors to arise,<sup>38,39</sup> especially as the dosing is usually being carried out by individuals with little or no medical training. Despite this, there are also many substances which are unsuitable for manufacture as liquid oral dosage forms.<sup>40</sup>

With regards to scaling solid doses, the current method employed is the production of varying strengths of tablets and capsules, in the hope that a combination of different tablets will produce the required dose for individual patients. Sometimes splitting of tablets is employed as a further method of varying the dose, but this only provides a small number of additional doses and also leads to unacceptable weight differences, and therefore doses, in the fragments.<sup>41</sup> There is some increased flexibility when using pellets, which can be divided into varying quantities using similar methods to liquid dosing, but this can also introduce the errors which are associated with liquid dosing.

Ideally, finding a method of producing solid oral doses in various strengths, with no additional cost or associated error, and with a relatively simple means of manufacture, could help ensure that patients are more easily prescribed the correct dose for their individual needs.

## **1.6 Initial Attempts at Altering Manufacture**

### **1.6.1 Tablets Manufactured with a Drug Free Splittable Layer**

One way of providing personalised doses has been proposed by Green *et al.* and Solomon and Kaplan (Figure 2).<sup>42,43,44</sup> While this method does not increase the number of possible doses over conventional scored tablets (which can normally be halved or quartered), it is possible to overcome the dose variation associated with splitting tablets.

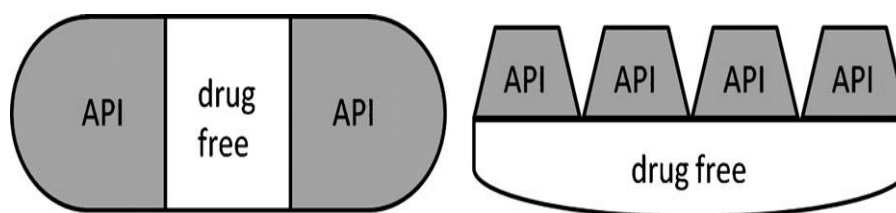


**Figure 2** - Tablets manufactured with 'drug free' layers.<sup>42,43,44</sup>

This method involves manufacturing tablets that have a 'drug free' layer present, through which tablet splitting will occur. This means that accurate splitting of a tablet can be achieved not just by a pharmacist, but by patients themselves. The tablets can be taken whole, or subdivided to provide a select number of varying doses. Although this method provides a relatively easy way to ensure patients are receiving the correct dose, there are still only a small number of different doses which can be administered, with a maximum of four separate segments from the proposed designs.

Another method for providing greater dose variation has been proposed by Remon and co-workers (Figure 3).<sup>45</sup> Although tablet splitting does not occur through a 'drug free' layer, allowing for possible variation in the administered dose, the number of doses has been increased. This allows for greater flexibility of dose, one of the main goals associated with the manufacture of personalised medicine.

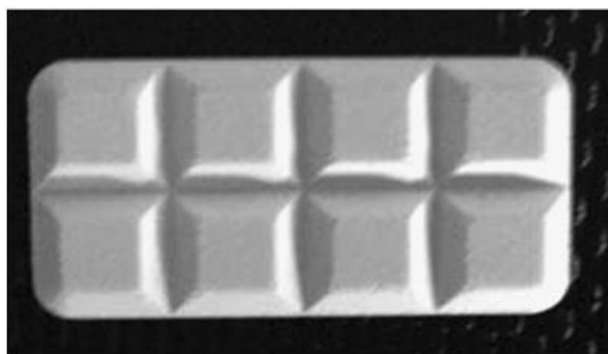


**Figure 3** - Tablet (22.4mm long/11.2mm wide) produced to enable splitting into eight segments.<sup>45</sup>

Remon and co-workers used zidovudine (AZT) and lamivudine (3TC), both Nucleoside Transcriptase Reverse Inhibitors (NRTIs) for the treatment of HIV, as model compounds in their research. There is a great demand for flexibility in dosing

of these types of drug, as a large population of patients are children. By producing a tablet that can be split into a larger number of sections, it is possible to more accurately dose paediatric patients according to their weight, thus avoiding occurrences of toxicity or resistance. Each tablet contained 300 mg AZT and 160 mg 3TC and each segment corresponds to a dose equivalent to 5 kg body weight. This means that the dose is suitable for use in very young children (approx. 1 month) up to adults, where the recommended dose is one tablet (300 mg AZT, 150 mg 3TC) twice daily.<sup>46</sup>

### 1.6.2 Tablet-Like Slices Produced with a Novel Cutting Tool

Wening *et al.*<sup>40</sup> have demonstrated the use of a twin-screw extruder, equipped with a cutting tool, in the production of varying sustained release doses of their model drug, carvedilol. Different diameters of extrudate with varying drug loading could be produced, which were then cut into 'tablet-like' slices of varying diameter. Figure 4 shows the cutting tool used to slice the extrudate and Figure 5 shows the cylindrical extrudate and tablet-like slices.

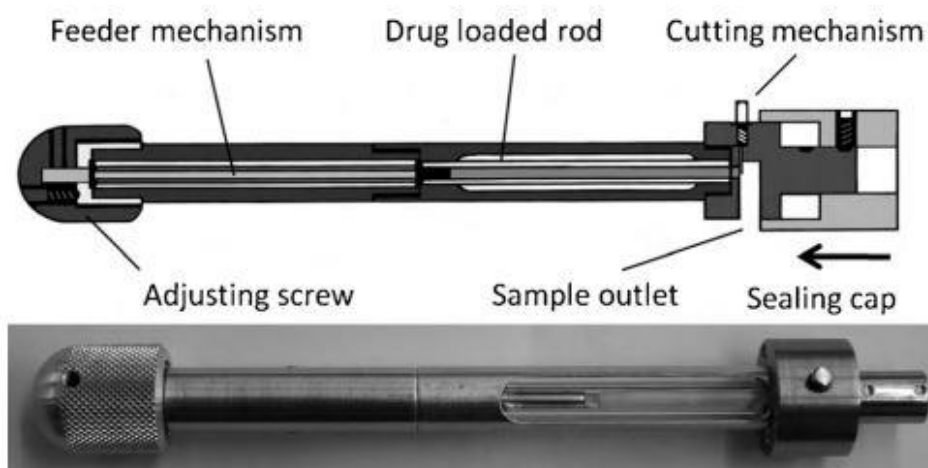


**Figure 4** - Novel cutting tool used by Wening *et al.*<sup>40</sup> (Total length 16.5 cm)



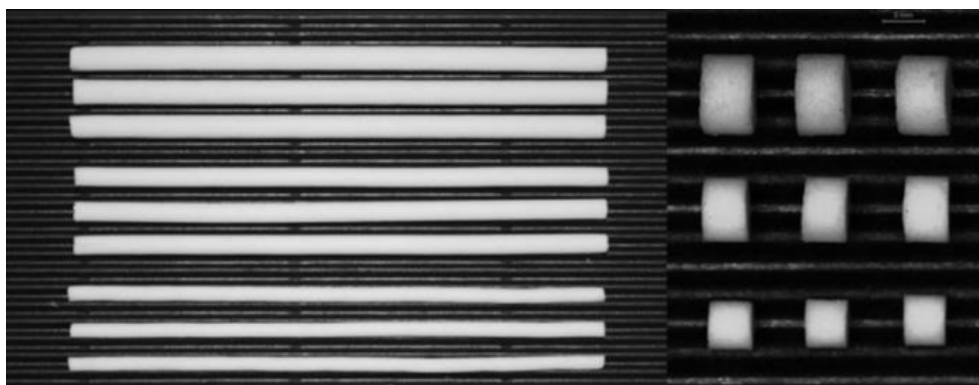


**Figure 5** - Extrudate prior to (left) and after (right) cutting.<sup>40</sup> Extrudates had a length of 10 cm and diameters of 4.5, 3.5 and 2.7 mm from top to bottom and were cut into segments of 2 mm in height.

The ability to vary both the diameters of the extrudate and the drug loading of the formulation allow for solid doses to be manufactured, which could potentially allow for greater variation and accuracy with dosing, when compared with splittable tablets. Although this suggests that dose alteration can only occur at the factory, it is possible to store the drug loaded ‘extrudate rods’ for cutting with the device at a later date, which means that specific doses can be selected directly by the doctor and administered immediately, rather than waiting for manufacture. The cutting device can also even be operated by the patients themselves as only forces of approximately 10-15 N are required for slicing the extrudate. This is less than the force required to operate insulin pens and means that even elderly patients should be able to operate the device, although if dosing is being determined by any patient (elderly or otherwise), cognitive function would still need to be assessed.

### 1.6.3 Inkjet Printing of Oral Dosage Forms

Inkjet printing has also been investigated as a potential method for accurately scaling doses, with the final dosage form being administered as an orodispersible film, or rolled and encapsulated within a gelatin capsule.<sup>47</sup> Several methods have been investigated, examples of which are discussed below:

#### 1.6.3.1 Electrohydrodynamic Drop-on-Demand Printing

Elele *et al.* have highlighted the delicate nature of pharmaceutical products and the requirement for them to be protected from environments where ‘chemical changes,

excessive heating and shear stress could occur.<sup>48</sup> As inkjet printing could typically expose the active pharmaceutical ingredient (API) to these conditions, Elele *et al.* have described a technique which overcomes these problems. They have demonstrated a method of producing varying pharmaceutical doses using electrohydrodynamic drop-on-demand (EHD DOD) printing of drugs, first using fenofibrate, aceclofenac and ibuprofen,<sup>48</sup> then continuing their research on ibuprofen and also including griseofulvin.<sup>49</sup> A method was developed to enable the printing of droplets of solutions, containing ibuprofen or griseofulvin onto freeze-dried porous polymer films. The dose can be tailored to individual patient needs by cutting or scoring, allowing flexibility in the dose, and can be administered in capsules or by folding the film and sealing it together. The printing method is shown schematically in Figure 6:

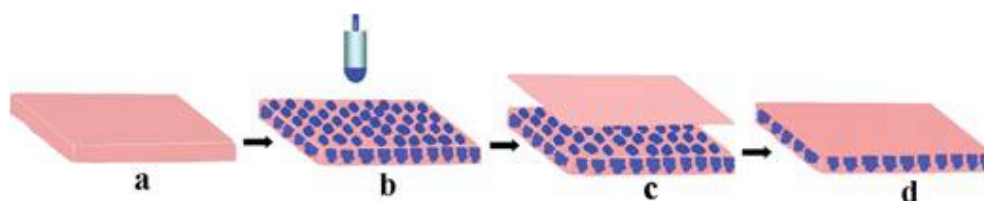


**Figure 6** - Electrohydrodynamic drop-on-demand encapsulation process.<sup>49</sup>

The process starts with the polymer film, a, and is then printed with a solution of the desired API in a specific pattern, b. This is then covered with a non-porous barrier film to produce the dosage unit, c and d. In their results, Elele *et al.* have demonstrated that this method provides a novel way of producing varying doses of a drug using a modified method similar to inkjet printing. Conventional ink-jet printers create an environment of high temperature and high shear, however this method overcomes the incompatibility and allows for the printing of solutions of poorly water soluble drugs that exceed the normal viscosity range of conventional inkjet print heads.

### 1.6.3.2 Thermal Inkjet Printing

Unlike the previous example, Sandler *et al.* make use of a conventional inkjet printer for thermal inkjet printing (TIJ) of dosage forms on porous substrates such as paper (Figure 7).<sup>50</sup>

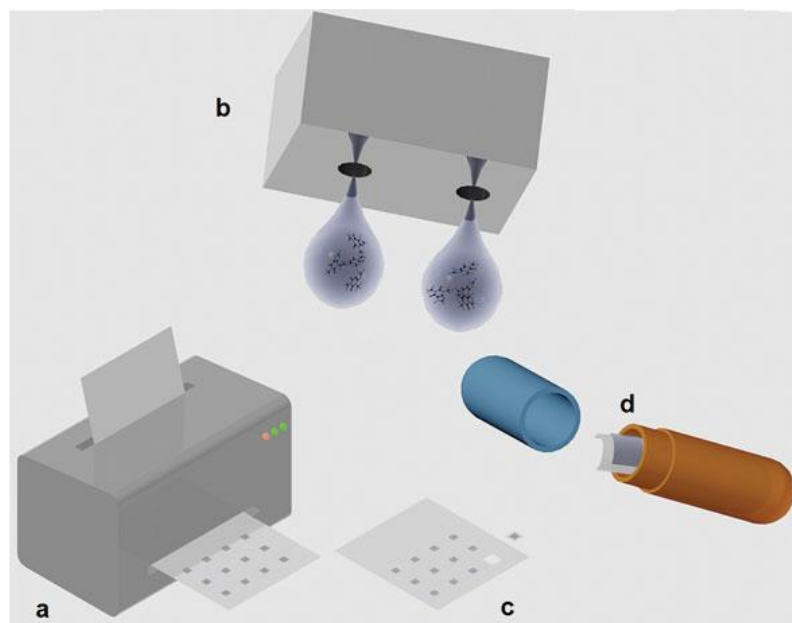


**Figure 7** - Conventional inkjet printing for oral dosage forms.<sup>50</sup>

The diagram shows an inkjet printer (a), accurate doses of drug substance exiting the nozzle of an inkjet printer (b), precise doses of drug printed on paper (c) and these doses being inserted into capsules as one method of fabricating the final dosage form (d).

Despite concerns being raised by Elele *et al.* over the operating conditions of inkjet printers,<sup>48,49</sup> it was reasoned that APIs could be ideal candidates for printing due to their structural similarity to the colorants used in inks.<sup>51</sup> TIJ has also been used in the aerosolisation of proteins,<sup>52</sup> which are known to denature at high temperatures. Analysis of a sample of protein before and after TIJ showed no significant changes, demonstrating that the high temperatures involved in TIJ have no detrimental effect on the protein.

In order to use an unmodified inkjet printer, it is essential that the drug solution has suitable properties (viscosity and surface tension). The viscosity cannot exceed  $20 \text{ mPa s}^{-1}$  and the surface tension should be in the range of  $25\text{-}45 \text{ mN m}^{-1}$  for successful printing to occur. Sandler *et al.*<sup>50</sup> used a propyleneglycol (PG)-water (30:70 vol%) solution, which had a viscosity value of  $3.1 \text{ mPa s}^{-1}$ , to produce formulations with optimal viscosity. An average surface tension for these solutions

was calculated as  $52.0 \pm 0.4 \text{ mN m}^{-1}$ , however printing was still successful despite this value being out with the desired operating conditions.

The aim of this piece of work was to demonstrate the printing of dosage forms onto porous substrates. Three different kinds of substrate were used: pigment-coated paper (porous substrate with low permeability), uncoated copy paper (porous substrate with high permeability) and polyethylene terephthalate (PET) film (nonporous substrate). Sandler *et al.* found that crystallisation behaviour of the drugs could be altered depending on the porosity of the substrate, meaning that the technique of thermal inkjet printing could provide better control over crystal growth. This could, in turn, lead to enhanced solubility of poorly soluble drugs and better design of drug delivery systems.

TIJ has also successfully been used by Gaisford and co-workers for the printing of salbutamol sulphate onto an oral film made of potato starch.<sup>53</sup> This drug was chosen by the group as it is prescribed for children under two years of age at  $100 \mu\text{g}$  per kg of body weight. As this could result in a child taking multiple tablets for the correct dose (not ideal for such a young person) this highlights the benefits of being able to develop a method of accurately scaling the dose of salbutamol sulphate.

As with Sandler and co-workers, Gaisford *et al.* adjusted their drug solutions to achieve optimum viscosity and surface tension for printing. Glycerine was added, in varying concentrations, to aqueous solutions of salbutamol sulphate in order to adjust the viscosity to an optimum value. This was achieved with concentrations of 10-20% v/v.

Salbutamol sulphate was then successfully printed onto a potato starch substrate in precise doses of  $38 \mu\text{g cm}^{-2}$ . In order to achieve the required dose for treatment either the printed area would need to be increased or multiple deposition on a smaller area would need to occur. As increased areas could be difficult to incorporate into dosage forms, investigation into dosage after multiple deposition was carried out. It was found that after one pass under the print head, the dosage obtained was within  $\pm 5\%$  of the theoretical dose, but multiple passes always resulted in lower doses that were out with the  $\pm 5\%$  range obtained after one pass. It was hypothesised that the lower dose was due to shearing forces eroding the dose already deposited on the substrate during

paper uptake by the printer. Despite these losses occurring, it was always predictable and variation of dose was always less than 5%. Further investigation into using a printer that operates slightly differently, to avoid shearing forces, along with more in-depth analysis of the drug product deposited on the substrate will lead to increased knowledge of this technique.

### 1.6.3.3 Piezoelectric Inkjet Printing

While thermal inkjet printing can be simple and relatively cheap to employ in the fabrication of dosage forms, piezoelectric inkjet printing can handle a wider range of liquids.<sup>54</sup> Genina *et al.* have used piezoelectric (PE) inkjet printing to investigate the production of personalised doses of loperamide, a low dose antidiarrheal drug with varying doses for adults and children, and caffeine.<sup>55</sup> Three different substrates were also investigated: a PET film, a hydroxypropylcellulose (HPC) film and a commercially available edible icing sheet. The composition of this icing sheet was as follows: corn starch, corn syrup (maltose and oligosaccharides), corn syrup solids (dextrose), cellulose, glycerine, sugar, vegetable oil, gum arabic (polysaccharides), polysorbate 80 (polyoxyethylene (20) sorbitan monooleate), vanilla (vanillin, piperonal), titanium dioxide and citric acid.

Preparation of flexible doses was carried out in two different ways, either by varying the drop spacing between printed droplets, or by varying the printing area of the dosage form. Figure 8 and Figure 9 show the drop spacing being varied for both model compounds in this piece of work.

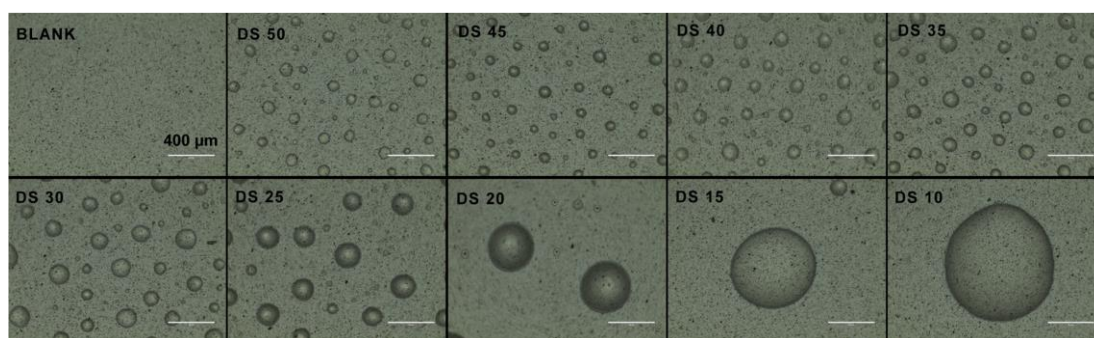


**Figure 8** - Optical microscopy of loperamide drug solution printed on PET film.<sup>55</sup>

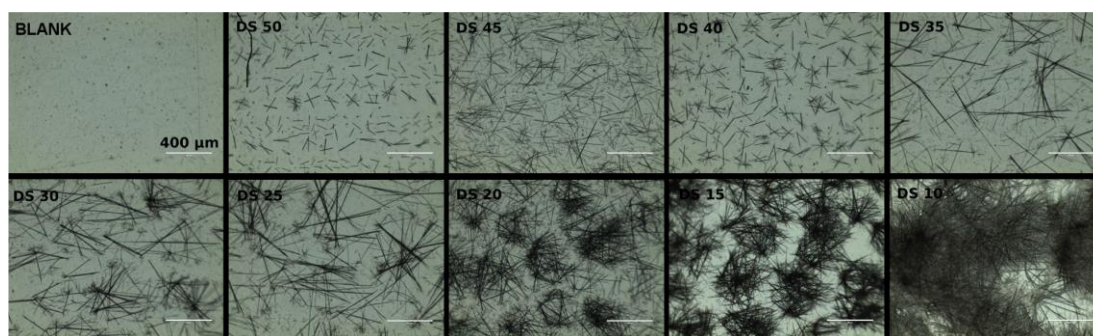


**Figure 9** - Optical microscopy of caffeine drug solution printed on PET film.<sup>55</sup>

As the drop spacing decreased, the content of drug increased as a power function for both loperamide and caffeine. No crystallisation occurred with the printed solution of loperamide, instead the drops coalesced and solidified in the shape of droplets on the surface of the PET film. This is likely due to the high content of PG in the ink formulation, which is known to inhibit the growth of crystals,<sup>56</sup> although this was not observed with caffeine. As the drop spacing decreased with the caffeine ink solution, the drops began to overlap more and recrystallisation was observed in the overlapping droplets (Figure 9). Decreasing the printed area would be expected to decrease the dose obtained in a linear fashion, although some deviation was observed. This has been attributed to either clogging of the nozzle or human factors during printing. Only the PET film was investigated as a substrate for the preparation of flexible doses. This is due to the other two substrates absorbing the inks, which would make analysis of the different factors being tested more difficult.

In summary, adjusting the doses of printed drugs was easily carried out by adjusting the distance between printed droplets, allowing for the production of flexible doses. Changing the area to be printed was deemed a less promising approach for tailoring the dose, presumably due to the possible production of very large oral doses which may cause difficulty for administration of the drug in the patient. Although flexible doses were not investigated on the edible substrates, it is envisioned that absorption of the inks would be beneficial as it minimizes losses of the API during subsequent transport steps during manufacturing.

### 1.6.3.4 Aerosol Jet Printing

As an additional method of inkjet printing, aerosol jet printing has been applied to the production of dosage forms which require the product to be amorphous for solubility enhancement.<sup>57</sup> A schematic of the equipment is shown in Figure 10:

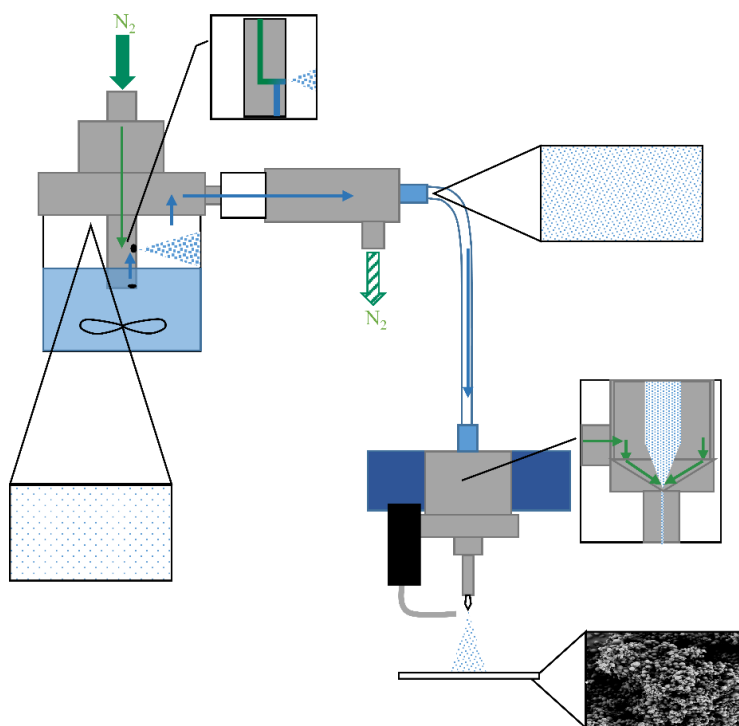


**Figure 10** - Aerosol Jet Printing of Pharmaceutical Dosage Forms.<sup>57</sup>

Doses of the model drug fenofibrate could be printed, in multiple layers and patterns, and scaled sufficiently without the need to change the starting ink formulation. Nozzle size of the final print head was also investigated as a means of scaling the resultant dosage form, but this was limited to a choice of four different nozzles.

While the aerosol jet printing technique itself is not sufficient to enhance the solubility of fenofibrate, as evidenced by the printing of fenofibrate alone resulting in a fully crystalline product, the addition of a polymer to the formulation alters the solid state considerably. On addition of polyvinylpyrrolidone (PVP) the crystallinity of fenofibrate was gradually reduced with increasing polymer content until a fully amorphous product was formed at 75% PVP or higher. This greatly increased the

dissolution properties of the API, resulting in a method of producing dosage forms with improved bioavailability over conventional dosage forms.

#### 1.6.4 Flexographic Printing

While inkjet printing has been shown to be a useful technique for scaling oral doses in the production of personalised medicine, there is often the requirement of another processing step, such as encapsulation, prior to administering to the patient. Genina *et al.* have addressed this extra processing step in the printing of controlled release oral dosage forms by combining both inkjet and flexographic printing.<sup>58</sup> A schematic drawing of the equipment is shown in Figure 11.

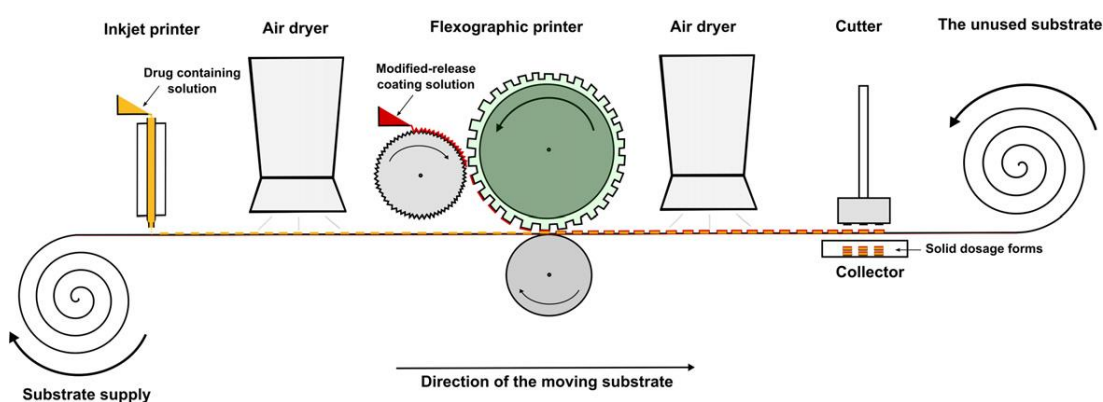


**Figure 11** - Schematic drawing of the combination of inkjet and flexographic printing.<sup>58</sup>

Flexographic printing is a rotary technique which allows for different inks to be printed on almost any substrate. Although it is not a very precise technique and cannot be used alone in the fabrication of dosage forms, the printing of highly viscous fluids is possible. Hence, the combination of both inkjet and flexographic printing allows the fabrication of precise doses (with inkjet printing) which can then be coated with a polymer (ethylcellulose (EC)) to tailor the release of the drug within the body.

Propranolol hydrochloride and riboflavin sodium phosphate were employed in this research, and both of these drugs were deposited onto three different types of substrate prior to being coated in EC polymer by flexographic printing. The three different paper substrates used were: A – alkyl ketene dimer-sized uncoated wood free paper,



B – triple-coated inkjet paper, C – double-coated sheet fed offset (SFO) paper. A PET film was also used as a reference substrate.

The results from this research showed that a combination of both inkjet and flexographic printing was successful in producing controlled release dosage forms only if a porous substrate is used for printing. When the non-porous PET substrate was used, flexographic coating removed part of the API solution due to the solution remaining on top of the substrate. With porous materials, the API solution is partially absorbed which ensures successful flexographic coating.

Successful application of this technique further enhances the possibilities achievable through manufacture of personalised medicines. Not only could controlled release dosage forms be created, but patient compliance could be increased by the polymeric coating masking the foul taste of some APIs.

While all the different techniques discussed up to now attempt to solve the issues associated with personalised dose manufacture, there is still some action required to create the final dosage form – e.g. dividing extrudate into segments, or cutting out a printed dot and placing inside a capsule. Additive manufacturing has the potential to eliminate this extra step, producing the final dosage form as a single tablet.

## **1.7 Additive Manufacturing and 3-Dimensional Printing (3DP)**

Additive manufacturing was not initially designed with the pharmaceutical industry in mind, instead its origins can be found in the 1980s as a rapid prototyping tool for the production of models and prototype parts.<sup>59</sup> Since then, the research area has grown enormously and covers a wide range of techniques such as: selective laser sintering<sup>60</sup> (SLS), stereolithography<sup>61</sup> (STL), fused deposition modelling<sup>62</sup> (FDM) and inkjet binder printing.<sup>63</sup> A schematic of these processes can be seen in Figure 12:

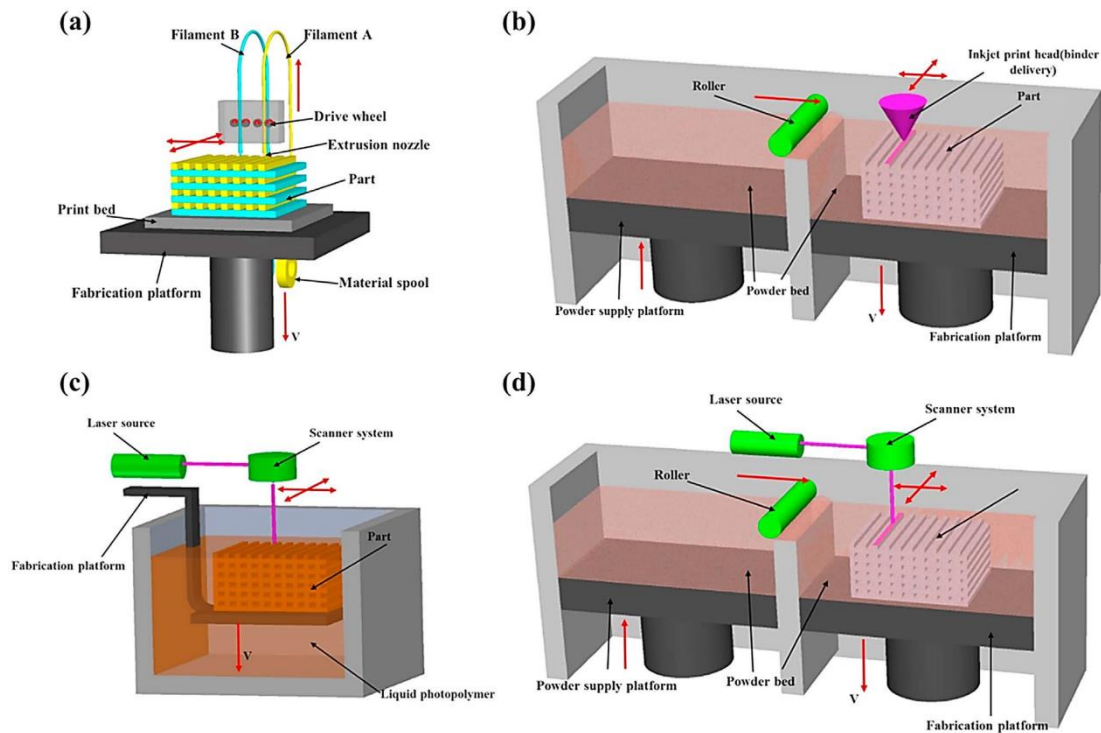


**Figure 12 - Variation in Additive Manufacturing (a) fused deposition modelling (b) inkjet binder printing (c) stereolithography (d) selective laser sintering.<sup>64</sup>**

Regardless of the technique used, the principle of additive manufacturing as a whole is that the final product is made by the addition of successive layers, with each layer being a very thin cross-section taken from an original 3D computer-aided design (CAD) created in compatible software. Each of these layers will have a certain thickness (a property of the individual process being used) and therefore the finished product is only an approximation of the original design (Figure 13), with thinner layers resulting in a more accurate representation.<sup>65</sup>

Different manufacturing techniques have the potential to improve this resolution by altering how the layers are created and bonded to each other, but not all techniques are suitable for every imagined creation, therefore careful consideration is required before addressing any 3D printing dilemma.



**Figure 13 - Top** - CAD drawing of a teacup **Bottom** - images showing printed teacup with differing layer thickness.<sup>65</sup>

Since the development of additive manufacturing and 3D printing technologies, a number of different industries now benefit from the implementation of these techniques. A selection of examples are discussed in the following sections.

### 1.7.1 Metals

Three dimensional printing (3DP) has been discussed and utilised in the production of metal and metal/ceramic composite parts as far back as the early nineties.<sup>66</sup> Originally, with regards to metals, this was in the construction of moulds that were later used for casting, but technology has improved such that metallic parts can be produced by direct metal laser sintering (DMLS) from a metal powder feedstock.<sup>67</sup> This process is essentially identical to the aforementioned SLS technique, with the only difference being a change to the feedstock material. Directed energy deposition (DED) is another additive manufacturing technique applied to the metal industry and involves melting wires or powder feedstock and building a structure layer by layer, although this is a less widespread technique due to inaccuracies and further post-

processing.<sup>68</sup> Metal parts made using this technology are of particular use to the aerospace, oil and gas, marine and automobile industries.<sup>68</sup>

### 1.7.2 Food

This area has gained a lot of interest for use in areas such as military and space missions, elderly food and the confectionery industry,<sup>69</sup> with some drivers in the field including: production of food which is shape stable throughout the cooking process, customisation of flavour and nutrition and the development of interesting and unique textures.<sup>70</sup> It is possible to build up different layers of ingredients on the same shape, as demonstrated with 3D printed pizza (Figure 14).

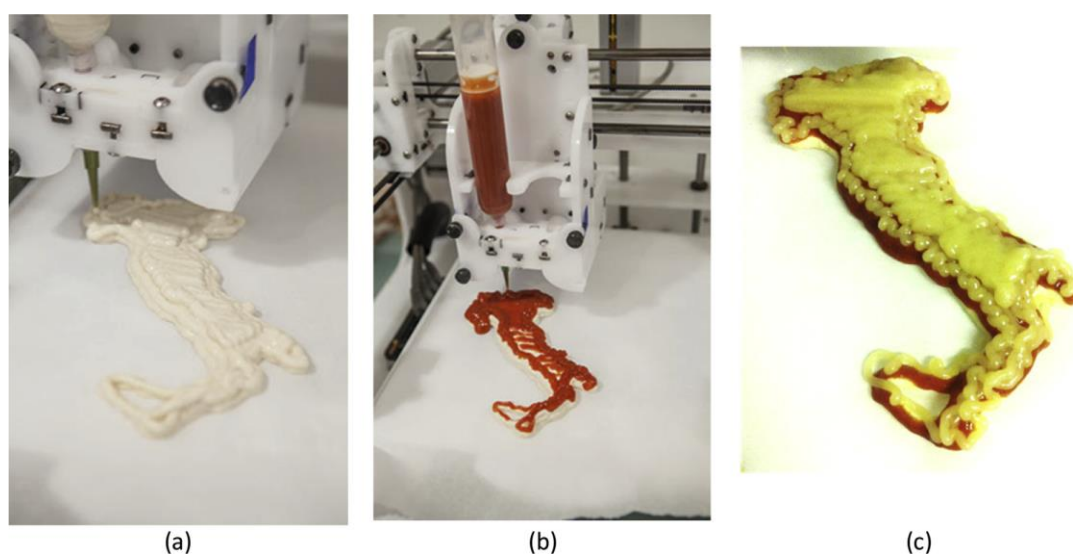


**Figure 14** - Pizza 3D printed from (a) dough, (b) sauce and (c) cheese.<sup>70</sup>

This demonstrates how well shape can be controlled during the printing process, allowing for intricate designs to be created.

Cookies have also been printed and are able to demonstrate the importance of ingredient ratios (specifically butter and yolk) on the stability of the final structure (Figure 15).<sup>70</sup> Increasing the butter concentration increases the ease of extrusion of the mixture, but results in lowered shape stability. Increasing the yolk concentration results in increased shape stability, however, too high a concentration results in restricting the height of the cookies. This demonstrates a narrow operating range for manufacture of acceptable product.

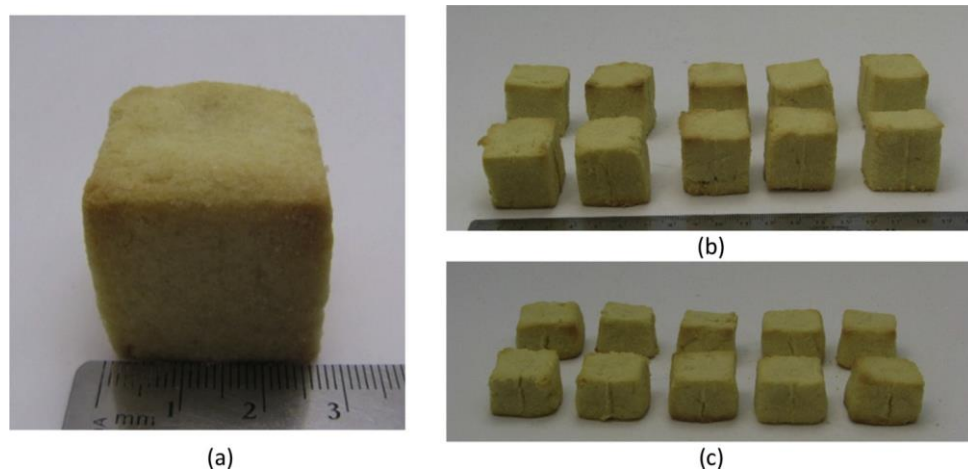


**Figure 15** - 3D printed cookies, (b) and (c) demonstrate how shape can vary with ingredient concentration.<sup>70</sup>

### 1.7.3 Medical Applications

3D Printing has also been utilised in the medical and pharmaceutical industries, which benefit from the unique and innovative designs which can be achieved. McAlpine *et al.* have reported the 3D printing of a bionic ear (Figure 16).<sup>71</sup>



**Figure 16** - 3D printed bionic ear.<sup>71</sup>

The complex structure of the human ear is difficult to construct via traditional tissue engineering approaches, therefore this presents a novel solution to the problem. Research, such as this, is of huge benefit in medicine, as it paves the way for manufacture of replacement body parts and organs, allowing for an alternative to waiting on the organ donation list for some patients.

3D printing is also utilised in the pharmaceutical industry for the production of drug eluting implants which inhibit bacterial growth in order to prevent infection.<sup>72</sup> Sandler *et al.* used hot-melt extrusion to produce a drug loaded strand that was then used as the feedstock for a 3D printer. Their model drug was nitrofurantoin, which they extruded along with poly(L-Lactic Acid) (PLA) in order to produce a suitable drug loaded filament for the 3D printer. This successfully inhibited the growth of bacteria and provides a ‘proof of concept’ study to aid in the future development of medical devices.

## 1.8 3D Printing of Solid Oral Dosage forms

With regards to dosage form production, this has successfully been achieved with the aforementioned inkjet binder printing, stereolithography, fused deposition modelling (also referred to as fused filament fabrication (FFF) in this context) and a further room temperature paste extrusion method, which is similar to FDM. Each are discussed separately in the numbered sections below:

### 1.8.1 Inkjet Binder 3D Printing of Dosage Forms

Katstra *et al.* have employed the inkjet binder 3D printing technique for the fabrication of oral dosage forms.<sup>73</sup> A schematic of the 3DP process is shown in Figure 17.

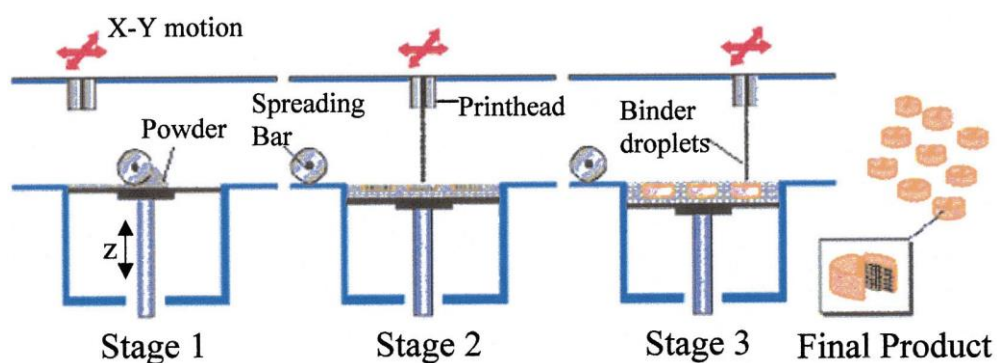


Figure 17 - 3DP process.<sup>73</sup>

The process begins by a thin layer of powder being spread over a stage. Binder solution is then deposited from an inkjet-like nozzle which can move in the X-Y plane as shown in the diagram. This binder solution causes the powder to stick together wherever it is deposited to form a two dimensional pattern. The stage is then lowered

in the Z direction, as shown in the diagram, and more powder is spread across the top of the printed pattern. Binder solution is then again applied to the powder, allowing multiple layers to be constructed. For this research, Avicel® PH301 was used as the pharmaceutical grade cellulose powder which was spread over the stage. Tablets that demonstrate either erosion or diffusion release mechanisms could be constructed with either Eudragit® E-100 or Eudragit® RLPO binder solutions respectively.

A further study by Rowe *et al.* has demonstrated the level of sophistication that can be employed using this technique.<sup>74</sup> Oral doses such as: immediate-extended, breakaway, enteric dual pulsatory and dual pulsatory can be fabricated by 3DP. Multiple sections can be engineered within the same tablet by using different binder solutions allowing for very complex release profiles to be achieved which would be otherwise difficult to obtain through conventional tablet manufacture.

Recently, this powder 3D printing technique was also utilised in the production of the first Food and Drug Administration (FDA) approved 3D printed tablet from pharmaceutical manufacturers, Aprelia.<sup>75</sup> Spritam® (levetiracetam), used for the treatment of seizures, is available in four different dose strengths (250 mg, 500 mg, 750 mg and 1000 mg) and utilises the patented ZipDose® technology, developed first by the Massachusetts Institute of Technology (MIT) and further enhanced by Aprelia, in order to deliver high dose pharmaceuticals to a wide range of patients. Using the powder based approach to 3D printing, products are designed to rapidly disintegrate on contact with a liquid and also have the ability to effectively taste mask the APIs.<sup>76</sup> Despite Spritam® still being the only drug on the market to utilise 3D printing technology, it provides a 'proof of concept' for this alternative form of manufacturing and could hopefully help to demonstrate the viability of this technique ahead of any future drug approvals.

While the inkjet binder 3D printing technique has been successfully used for the manufacture of commercial dosage forms, it is not without its limitations. The nature of the printing process lends itself to the production of tablets with low mechanical strength, which may be more friable than traditional tablets. The additional removal of any unbound powder material at the end of the process can also lead to a more

lengthy manufacturing time when compared traditional tablet manufacture, or even other 3D printing techniques.

### 1.8.2 Stereolithography (STL) Fabrication of Dosage Forms

Martinez *et al.* have successfully employed the stereolithography technique to produce drug loaded hydrogels with varying water content, which allowed for the tailoring of drug release from the final dosage forms.<sup>77</sup> Polyethylene glycol based resins were used along with the non-toxic photo-initiator, riboflavin, which catalysed the polymerisation of the resin, but still allowed the formulation to be pharmaceutically compatible. Ibuprofen was the drug tested and the resulting dosage forms are shown in Figure 18:

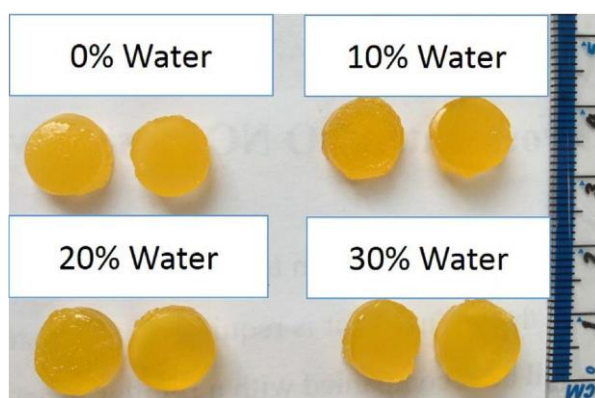


**Figure 18** - Dosage forms produced by stereolithography.<sup>77</sup>

While control over size and shape of printed tablets was achieved, variations in the mass increased with increasing water content. This was thought to be as a result of a decrease in the viscosity of the formulation prior to the printing process. Despite this, drug release profiles of the formulations indicated that the tablets exhibit delayed release, with the rate increasing as the water content of the dosage forms increased.

Similarly to inkjet binder 3D printing, the post-print removal of any unused resin can increase the manufacturing time, but care must also be taken to ensure the removal of any toxic components. Most examples of STL involve the use of expensive photoinitiators which are converted to reactive radicals during the printing process and



are only partially consumed, leading to relatively high levels being present in the final product.<sup>78</sup>

### 1.8.3 Room Temperature Paste Extrusion 3D Printing of Dosage Forms

Roberts *et al.* have demonstrated that the room temperature paste extrusion 3DP technique presents a novel, inexpensive method of formulation for controlled release bilayer tablets.<sup>79</sup> A feedstock paste is prepared, containing all the required excipients, which is then transferred to a syringe on the printer. The paste is then extruded onto a movable stage to build up multiple layers of a tablet containing a specified dose of the required drug. Figure 19 shows a schematic diagram and a photograph of the printer used in this research.

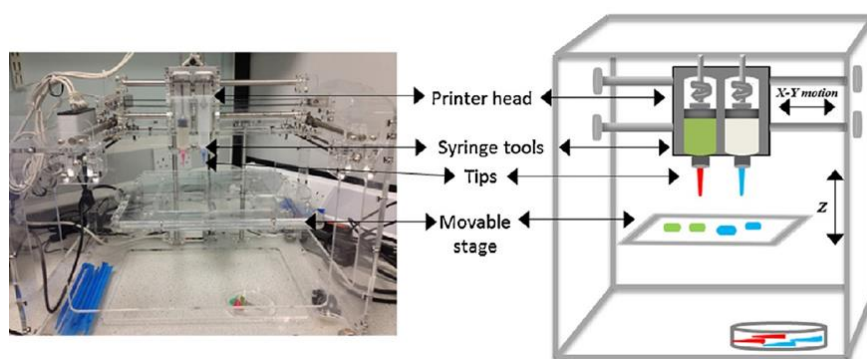


**Figure 19** - The 3D printer used by Roberts *et al.*<sup>79</sup>

Guaifenesin was used as a model compound in this research and printed as a bilayer formulation in order to compare the release with commercially available guaifenesin bilayer tablets. While tablets produced by new additive manufacturing technologies are unlikely to satisfy current pharmacopoeial tests (due to extreme differences in the manufacturing process as a whole), all tablets produced by this method were tested for uniformity of weight, thickness, hardness and friability and all satisfied the specifications listed in the U.S. Pharmacopoeia XXIV. The results obtained from this work showed that the printed tablets were comparable to commercially available guaifenesin bilayer tablets and highlights the benefits associated with optimisation of this technology, although the ability to vary the final dose of API was not fully investigated in terms of personalised medicine.

### 1.8.4 Fused Filament Fabrication of Dosage Forms

Fused filament fabrication (FFF) presents another potential area for manufacture, where the dose, in theory, can be easily scaled. While this method has the advantage of not requiring any lengthy post-processing treatments or clean-up, providing that the tablet design has not required any support material, manufacturing is often limited to thermally stable APIs. The feedstock is a polymer filament, which is heated up and extruded through the printer nozzle in successive layers to produce a 3D object. This feedstock is produced via either a solution loading or extrusion loading method, as discussed below:

#### 1.8.4.1 Solution Loading Process

Both Gaisford<sup>80</sup> and Alhnan<sup>81</sup> have successfully produced tablets using the FFF technique with polyvinyl alcohol (PVA), resulting in extended release tablets. Gaisford used fluorescein as the model drug and prepared the 3D printer feedstock by submerging filaments of PVA in an ethanolic solution of fluorescein for 24 hours. They used a MakerBot Replicator 2x Desktop 3D printer in order to print tablets of 10 mm diameter, with infill percentages of 0%, 10%, 25%, 50%, 90% and 100%, thus varying the dose.



**Figure 20** - Printed tablets with a view of cross-section.<sup>80</sup>

With varying the percentage infill of these tablets, varying the dissolution rate was also achieved. The drug was released much quicker with the 10% infill tablet, taking 6 hours for complete release, compared to the 50% and 90% infill tablets, which showed complete release after 15 and 20 hours respectively.

Alhnan and co-workers also prepared their drug loaded PVA filaments by submerging them in a saturated solution of their model drug for 24 hours. The drug chosen was prednisolone and the saturated solution was prepared in methanol. Alhnan *et al.* also used a MakerBot Replicator 2x Desktop 3D printer but, instead of varying the infill, they varied the size of printed tablet in order to demonstrate the feasibility of personalised dosing (Figure 21).

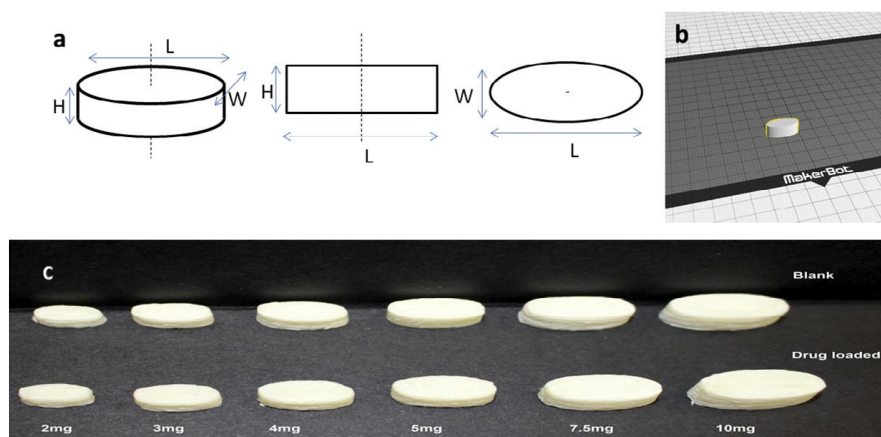


**Figure 21** - Alhnan *et al.* tablet design.<sup>81</sup>

The precision of dosing ranged between 88.7% and 107%, demonstrating some degree of control over the manufacturing process. X-Ray and thermal analysis also suggested that prednisolone remained in an amorphous state after printing, which could be highly beneficial when applied to poorly water soluble drugs.

While both of these methods achieve scalable dosing in tablets, the downfall arises when considering the maximum drug loading achieved in the filament feedstock – Gaisford achieved a final drug loading of 0.29% w/w and Alhnan a final drug loading of 1.9% w/w. This is very low and, while this could be a viable manufacturing route for a variety of low dose drugs, extrusion of the polymer feedstock in combination with API prior to printing could provide greater variation in drug loading and hence, scalability.

### 1.8.4.2 Extrusion Loading

Pietrzak *et al.* used both methacrylic based polymers (Eudragit® RL, RS and E) along with one cellulose based polymer (hydroxypropyl cellulose, HPC SSL) in order to extrude a 3D printer feedstock filament containing their model drug, theophylline, as shown in Figure 22.<sup>82</sup>

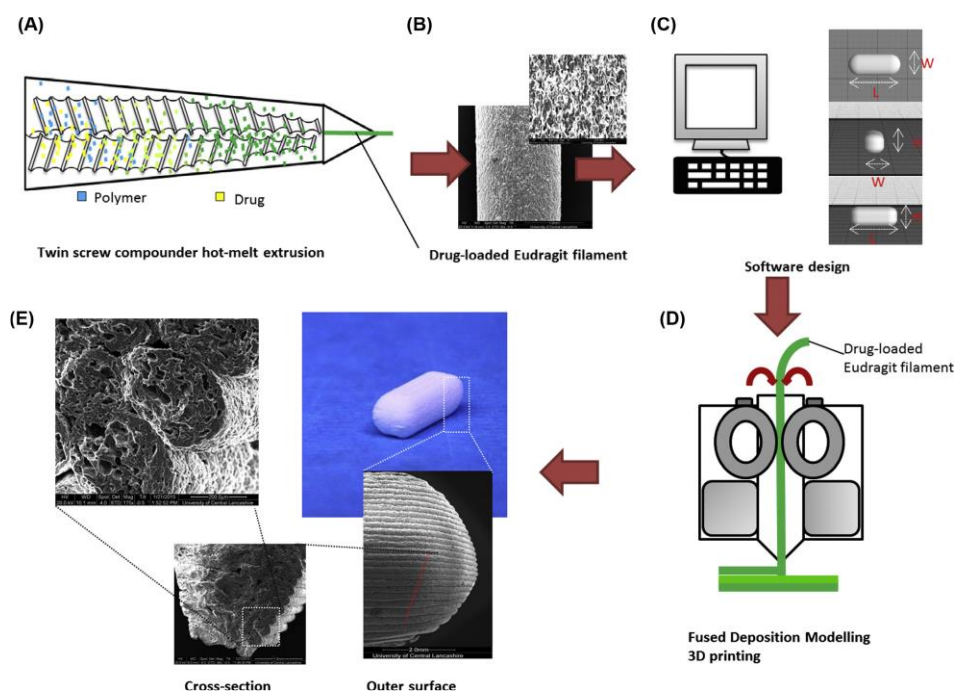


**Figure 22** - Schematic Illustration of the HME/FFF Process.<sup>82</sup>

As with their previous investigation into varying the size of prednisolone tablets, produced from solution loading of PVA, size was again the method of dosage control for this piece of work, with Eudragit® RL being used as the carrier polymer. A dose accuracy between 91-96% was achieved for tablets based on the desired dose and design which was input into the computer software. When using Eudragit® RL, this resulted in tablets which displayed sustained release characteristics, however substituting with Eudragit® E or HPC SSL allowed for tailoring towards immediate release tablets, although these released the API at a slower rate, compared to filament alone, presumably due to loss of surface area of the filament after fusion during manufacturing of the printed tablets.

Goyanes *et al.* have also utilised HME in the production of budesonide loaded 3D printed PVA tablets (Figure 23).<sup>83</sup> They also employed a coating technique in order to compare the release of API from their formulation with two commercial budesonide products already on the market - Cortiment® and Entocort®.

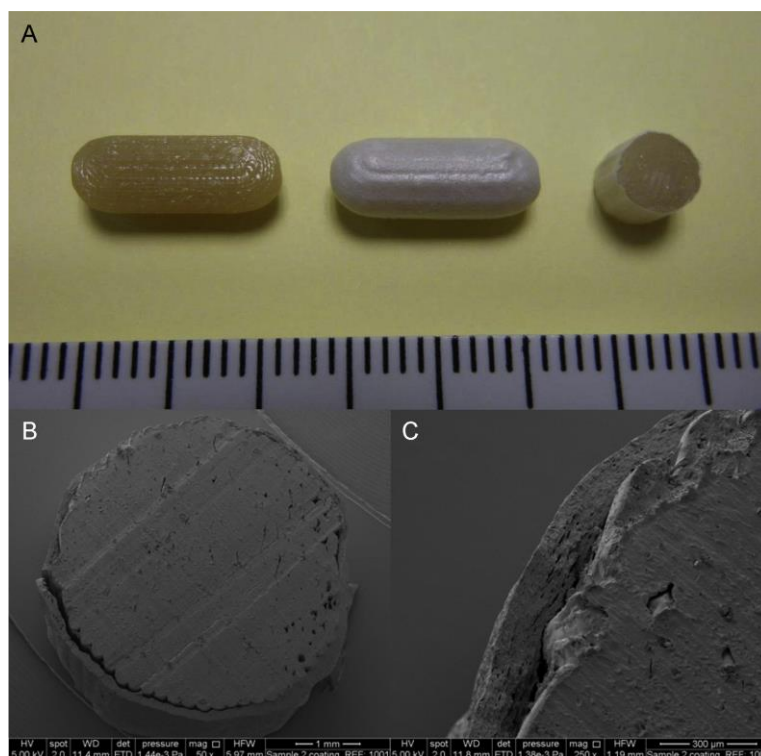


**Figure 23** - Images showing an uncoated, coated and cross section of coated tablet at the top, followed by SEM images of the cross section of coated tablet on bottom.<sup>83</sup>

Although production of tablets was successful, it was noted that the planned drug loading of 5% w/w was not achieved, with 4.14% w/w instead being the loading found in the filaments. Once dissolution analysis had been carried out on the 3D printed tablets and the commercially available products, a release profile with characteristics of both commercial products was demonstrated. This highlights the benefit for integration of 3D printing within traditional manufacture of dosage forms, although the speed of the process as a whole is unlikely to be able to compare with traditional manufacturing methods.

With these two examples of combining HME and 3D printing, manufacturing temperatures are in the range of approximately 200°C, which can be unfavourable with

some systems. Okwuosa *et al.* have demonstrated the production of immediate release tablets manufactured at temperatures as low as 110°C, using polyvinylpyrrolidone (PVP) as the carrier polymer (Figure 24).<sup>84</sup>

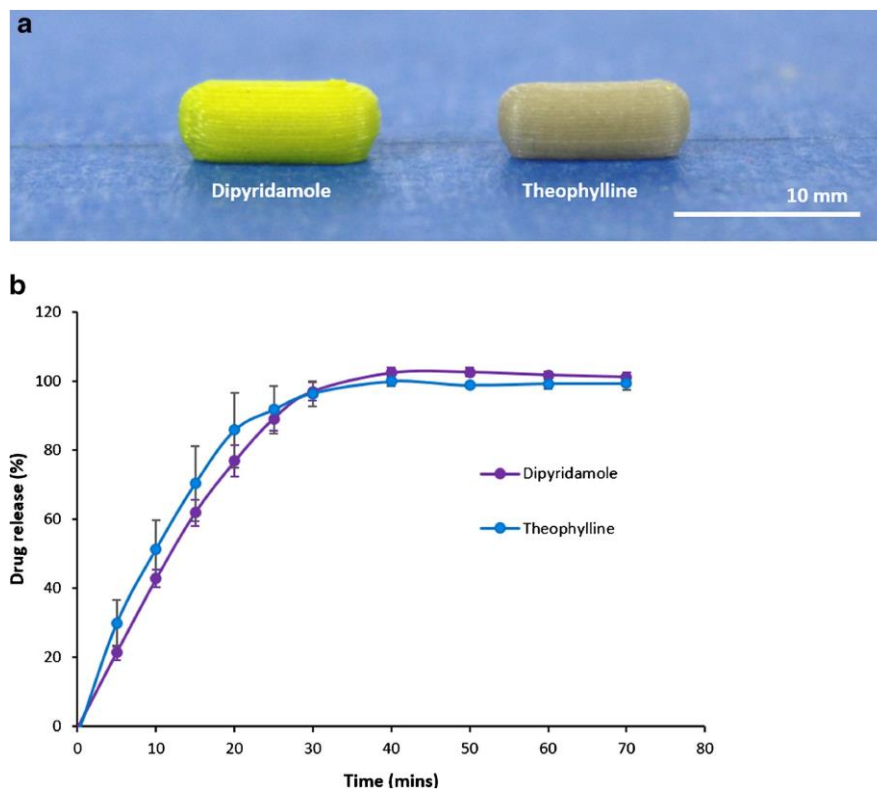


**Figure 24** - Tablets of dipyridamole and theophylline and their corresponding dissolution profiles.<sup>84</sup>

The model drugs under investigation (dipyridamole and theophylline) were successfully formulated with the PVP carrier polymer, producing tablets with a disintegration time of less than 15 minutes. As can be seen from the dissolution profiles, more than 85% of the API was released within the first 30 minutes of analysis for both model drugs under investigation, which is in contrast with the release observed in the previous examples.<sup>82,83</sup> This highlights the flexibility possible with the combination of both HME and 3D printing in tailoring the release profiles of dosage forms.

## 1.9 The Current Study

Although the techniques discussed so far demonstrate novel ways with which to address the scalability of dosage form manufacture, the overall research area is still in

its infancy and there is a need for further investigation into its overall viability in the pharmaceutical industry. There are still plenty of regulatory and quality control challenges to be overcome before adopting 3D printing as an alternative manufacturing technique and there is currently no universal set of guidelines to cover this, especially due to the number of different 3D printing techniques which can be applicable to manufacture of dosage forms.<sup>85</sup> While traditional pharmaceutical manufacturing is limited in many cases, there is still not enough evidence to encourage a complete shift towards a more modern and scalable method of producing dosage forms. The recent approval of Spritam® from Aprelia<sup>75</sup> has highlighted that additive manufacturing is a viable direction for this production shift, but other research examples are limited to a select number of APIs, with no real attempt to fully explore the design space and its limits within these techniques.

The current study aims to address some of these limitations and provide further evidence that printing technologies are a viable method for scaleable dosage form manufacture. As these technologies are relatively easy to use, future changes could potentially see them being installed within hospitals<sup>86</sup> and pharmacies, providing the relevant approval has been granted for such a venture, and allow a more ‘point of care’ approach to manufacture of personalised medicine in healthcare settings.

### **1.9.1 Method Selection**

After careful consideration of the numerous different additive manufacturing techniques discussed previously, FDM was selected as a potential area for further investigation due to the opportunities available for scaling the dose of the resulting tablet. On top of the variation in size or shape of the tablet, which is possible with any CAD compatible technology, infill of the tablet can also be varied, allowing for further investigation into scalability of the process.

Coupling this technique with either solution loading of existing filament feedstock, or extrusion of new feedstock with varying API/excipient compositions allows for a more comprehensive understanding of the technique and how different formulations may be applicable to this method of manufacture.

### 1.9.1.1 Printer Selection

While the variety and complexity of printers utilising FFF technology expanded rapidly throughout the duration of this research, there were only two potential candidates with which to initially investigate manufacture due to cost limitations. These two printers were either the MakerBot Replicator 2X or the Leapfrog Creatr HS (Figure 25):

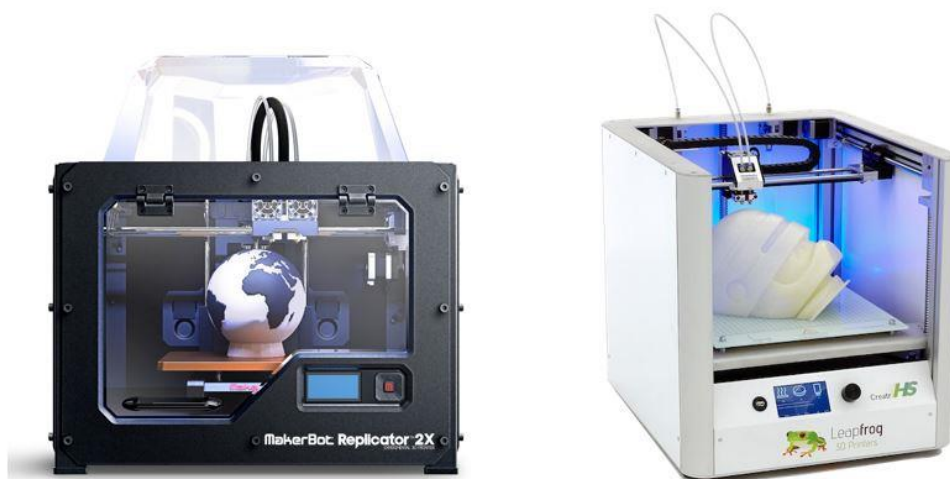


Figure 25 - MakerBot Replicator 2X (left) and Leapfrog Creatr HS (right)

Features and overall cost were comparable for both of these printers, but the Creatr HS presented easier access to gears and filament feeding mechanisms. This was deemed a benefit for investigation into new filaments, which are not typically used with these machines.

### 1.9.2 Polymer Selection

For solution loading experiments, the polymer feedstock was limited to pre-extruded Polyvinyl alcohol (PVA) as this was the only water soluble, biocompatible, commercially available filament that existed for use with the printer.

For extrusion loading experiments, there were theoretically many more polymers which could be investigated, but these were limited by lab availability and online availability at the beginning of experimentation. There was also very limited success



reported in the literature for transfer of extruded polymer filaments to a printer, so polymer selection was also influenced by success achieved by other colleagues within the department. For extrusion experiments to be comparable with solution loading experiments, PVA was selected as an initial polymer with which to begin investigation. This was followed up with investigation into the suitability of Affinisol™ LV15 as an alternative carrier polymer based on experiments carried out by colleagues.<sup>87</sup>

### **1.9.3 API Selection**

After looking through all the entries of drugs available in the British National Formulary (BNF),<sup>88</sup> a list of possible candidates was compiled and is presented in Table 1.

In order to initially narrow down possibilities and highlight where there may be a need for personalised medicine, the drugs were chosen based on there being more than four different doses available. For ease of operation when attempting to formulate these drugs, doses of less than 0.5 mg or more than 100 mg were also excluded due to the potential for inhomogeneity in the final dosage form – very low dose drugs may be difficult to detect, therefore difficult to prove homogeneous distribution, using the analytical techniques on offer, whereas high dose drugs may present difficulties with initial mixing of the drug and carrier polymer prior to extrusion.

Other factors must also be taken into consideration - the melting point of the API must be low enough to provide adequate miscibility within a chosen carrier polymer and also avoid any thermal degradation which may be experienced at higher processing temperatures.<sup>89</sup> It is also important to consider the safety of people working with these compounds - while some of these APIs are not considered to be hazardous substances, others can cause very serious health problems if the worker is exposed to them, even in small quantities e.g. warfarin.

Table 1 - Possible Candidate Drugs.

<b>Drug</b>	<b>Current Doses</b>	<b>Melting Point</b>	<b>BCS Classification</b>	<b>Hazard Information</b>
<i>Bisoprolol Fumarate</i>	1.25 mg	100°C	III	Harmful if swallowed
	2.5 mg			
	3.75 mg			
	5 mg			
	7.5 mg			
	10 mg			
<i>Carvedilol</i>	3.125 mg	113-117°C	II	Toxic to aquatic life
	6.25 mg			
	12.5 mg			
	25 mg			
<i>Prazosin</i>	0.5 mg	278-280°C	I	Toxic
	1 mg			
	2 mg			
	5 mg			
<i>Cilazapril</i>	0.5 mg	95-97°C	I	?
	1 mg			
	2.5 mg			
	5 mg			
<i>Enalapril Maleate</i>	2.5 mg	143-144°C	I	Not Hazardous
	5 mg			
	10 mg			
	20 mg			
<i>Lisinopril</i>	2.5 mg	148°C	III	Not Hazardous
	5 mg			
	10 mg			
	20 mg			
<i>Quinapril</i>	5 mg	120-130°C	II	Not Hazardous
	10 mg			
	20 mg			
	40 mg			
<i>Ramipril</i>	1.25 mg	109°C	I	Not Hazardous
	2.5 mg			
	5 mg			
	10 mg			

<i>Trandolapril</i>	0.5 mg	119-123°C	II	Not Hazardous
	1 mg			
	2 mg			
	4 mg			
<i>Warfarin Sodium</i>	0.5 mg	167-168°C	II	Toxic to humans and aquatic organisms
	1 mg			
	3 mg			
	5 mg			
<i>Atorvastatin</i>	10 mg	159.2-160.7°C	II	Not Hazardous
	20 mg			
	40 mg			
	80 mg			
<i>Rosuvastatin</i>	5 mg	122°C	III	?
	10 mg			
	20 mg			
	40 mg			
<i>Simvastatin</i>	10 mg	135-138°C	II	Not Hazardous
	20 mg			
	40 mg			
	80 mg			
<i>Haloperidol</i>	0.5 mg	147°C	II	Toxic
	1.5 mg			
	5 mg			
	10 mg			
<i>Aripiprazole</i>	5 mg	139-139.5°C	II	Not Hazardous
	10 mg			
	15 mg			
	30 mg			
<i>Olanzapine</i>	2.5 mg	195°C	II	Irritant and toxic to aquatic life
	5 mg			
	7.5 mg			
	10 mg			
	15 mg			
<i>Risperidone</i>	0.5 mg	170°C	I	Toxic if swallowed
	1 mg			

	2 mg			
	3 mg			
	4 mg			
	6 mg			
<i>Atomoxetine</i>	10 mg	167-169°C	I	?
	18 mg			
	25 mg			
	40 mg			
	60 mg			
	80 mg			
<i>Oxycodone Hydrochloride (OxyContin)</i>	5 mg	219°C	I	?
	10 mg			
	15 mg			
	20 mg			
	30 mg			
	40 mg			
	60 mg			
	80 mg			
	120 mg			
<i>Rivastigmine</i>	1.5 mg	123-125°C	I	Not Hazardous
	3 mg			
	4.5 mg			
	6 mg			
<i>Tadalafil</i>	2.5 mg	301-302°C	II	?
	5 mg			
	10 mg			
	20 mg			
<i>Glimepiride</i>	1 mg	207°C	II	Not Hazardous
	2 mg			
	3 mg			
	4 mg			
<i>Lenalidomide</i>	5 mg	269-271°C	IV	?
	10 mg			
	15 mg			
	20 mg			

---

Careful consideration was given to all of these APIs through examination of the pros and cons associated with using them for laboratory research. Although not a desirable criteria, cost also had to be examined as a factor when choosing a suitable API, as the infancy of the overall 3D printing technique, combined with the university PhD budget, limited the ability to test any expensive APIs within the scope of this research.

From the list of APIs in Table 1, carvedilol was selected for its relatively low melting point (compared to the others, Figure 26), its low human toxicity and the ease and cost with which it could be sourced from suppliers. Carvedilol is a non-selective  $\beta$ -blocker used to treat adults with heart failure, but there has also been investigation into its paediatric use,<sup>90,91</sup> although there is currently no suitable dose on the market for children. Paediatric doses are often based on weight and, given the earlier discussion surrounding the use of 3D printing as a technique for dose scaling, this choice presents an ideal candidate to begin manufacturing varying doses of a drug.

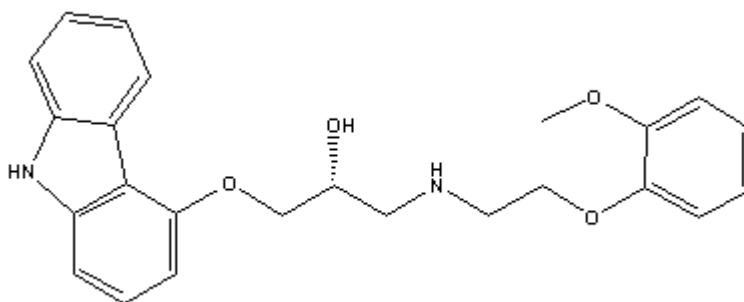


**Figure 26** - Carvedilol

Carvedilol is a basic, hydrophobic compound and is also categorised as a Class II drug in the biopharmaceutical classification system (BCS) meaning that it has poor solubility, but high intestinal permeability.<sup>92</sup> While this is not the area of primary focus for this research, hot-melt extrusion has been known to aid in the solubilisation of BCS class II drugs,<sup>93,94</sup> therefore its use as the primary step in the manufacture of scaleable doses could have wider potential than purely a personalised medicine perspective.

## **1.10 Aims and Objectives**

The main aim of this project is to develop a method for manufacturing solid oral dosage forms that allows for the potential to scale the dose and demonstrate an applicability for the use in personalised medicine.

An initial aim is to first prepare a drug loaded polymer feedstock that is suitable for transfer to a 3D printer. As mentioned in examples throughout this introduction section, this can be done either by loading a pre-extruded filament with API via a solution, or by extruding a combination of polymer and API, with the use of a hot melt extruder, to produce a filament with compatible size and mechanical properties for use with a 3D printer.<sup>95</sup> Drug loading of the extrudate can be increased or decreased, via either of these methods, allowing for dose variation at an early stage in formulation and linking back to the main aim of demonstrating applicability to personalised medicine.

A further aim of this research is the printing of tablets using drug loaded filaments prepared by the aforementioned loading techniques. Adjusting the dose of these tablets should be achievable by either varying the size and/or shape of the printed tablet, or by varying the percentage of the tablet that is filled in during printing, which again links back to the applicability of this technique in the field of personalised medicine. Altering the size or shape of a tablet is easily achieved by selecting a different tablet design, from a library of designs, drawn using compatible software. Varying the percentage of filled volume of the printed design is also a freely selectable parameter in the software of the 3D printer and the ease of this selection process means that different designs can be produced quickly and without the need for a specialist to operate the machinery.

A final overall aim of this research is to investigate the release of API from these 3D printed dosage forms and attempt to match the doses currently available on the market. Carvedilol is available as an immediate release formulation with a dose range of 3.125-25 mg and a controlled release formulation with a dose range of 10-80 mg, therefore being able to cover these ranges will allow for further applicability in the field of personalised medicine.

## **2 Materials and Methods**

### **2.1 Introduction**

This thesis aims to investigate scalable oral dose manufacture across three distinct chapters, the overall use of equipment and various techniques are very similar. These materials and methods are therefore collected within this stand-alone chapter in order to provide a more cohesive explanation of the experimental techniques used throughout the research.

### **2.2 Materials**

Polyvinyl alcohol (PVA) was obtained either as an extruded filament (1.75 mm diameter) from RoboSavvy (London, UK) or as a white powder in two different molecular weight ranges (13000-23000 and 89000-98000) from Sigma-Aldrich (Dorset, UK). Carvedilol was obtained as a white powder from Molekula (Newcastle, UK). Affinisol™ LV15 was obtained as an off-white powder from Dow Chemicals (Michigan, USA). The following additives to the formulations were obtained from different companies as follows: sodium chloride, glycine and mannitol from Sigma Aldrich (Dorset, UK), cellulose from Acros Organics (Geel, Belgium), hydroxypropylcellulose (Klucel ELF and Klucel HXF) from Ashland (Bradford, UK), erythritol and polyethylene glycol MWt 1000 (PEG 1000) from Alfa Aesar (Heysham, UK), polyethylene glycol MWt 4600 (PEG 4600) from Union Carbide Chemicals and Plastics (Houston, USA), sodium starch glycolate (Explotab® and VivaStar®) and crosscarmellose sodium (VivaSol®) from JRS Pharma (Cedar Rapids, USA). Solvents (1-butanol, 1-pentanol, 1-propanol, 2-butanol, 2-butanone, 2-methyl-1-propanol, 2-propanol, 3-methyl-1-butanol, methyl isobutyl ketone (MIBK), acetone, anisole, butyl acetate, dimethyl sulfoxide (DMSO), methanol, ethanol, heptane, isobutyl acetate and pentane) used were of analytical grade and purchased from either Sigma-Aldrich (Dorset, UK) or VWR International Ltd (UK). Sodium chloride (NaCl) and hydrochloric acid (HCl) for dissolution media were purchased from Sigma-Aldrich (Dorset, UK) and VWR International Ltd (UK) respectively.

### 2.3 Manufacture of 3D Printed Tablets

Tablets were produced using a Leapfrog Creatr HS desktop 3D printer (Leapfrog™ 3D Printers, The Netherlands). The tablets were designed using Auto CAD 2015 software, and further manipulated using Simplify3D software (v 3.0.1) on a Dell laptop with an Intel(R) Core(TM) i5-4300U CPU @ 1.90 GHz 2.50 GHz processor and a 64-bit operating system. The selected tablet design was cylindrical, with dimensions of  $x = 10$  mm,  $y = 10$  mm,  $z = 4$  mm, and the edges were rounded for 1 mm from either face, to avoid sharp edges (see Figure 27).

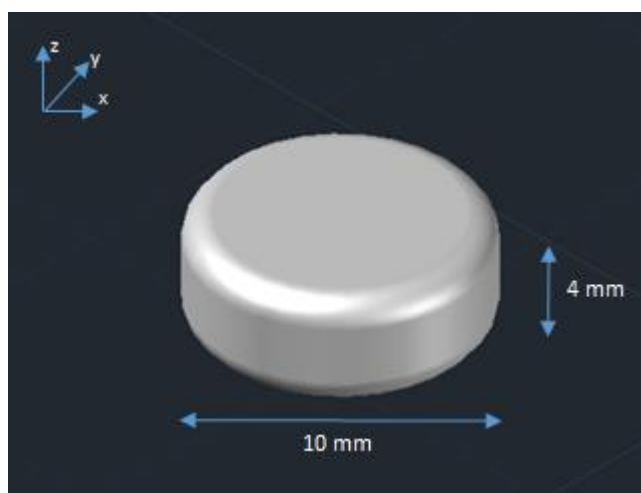


**Figure 27** - CAD Drawing of 3D Printed Tablet

For printing, the ‘rectilinear’ infill design was selected, and infill percentage varied according to experiment design. ‘Skirts’ were included, at an offset of 5 mm from the tablet, but the ‘raft’ option was not included in the design.

For experiments with PVA, temperature settings of 190°C for printing, with a bed temperature of 50°C, were used and combined with a default print speed of 200 mm/s. Optimisation of print settings when using Affinisol™ is discussed in more detail within the relevant results section, but generally, a print temperature of 195°C and a bed temperature of 50°C, were found to be the optimum temperature settings, again with a default print speed of 200 mm/s.



Two outer shells were included in the print design, along with three solid layers on the top and bottom of each tablet. Each tablet was printed with a standard infill of 30%, unless otherwise stated.

## 2.4 Extrusion of Polymer Filaments

All extrusion experiments were carried out using a process 11 twin-screw extruder (Thermo Fisher Scientific, Karlsruhe, Germany, Figure 28). For the specific screw configuration used in all extrusion experiments, see Appendix 7.1. The screw speed and die size were 60 rpm and 1.5 mm respectively unless otherwise stated.



Figure 28 - Process 11 Twin-Screw Extruder<sup>96</sup>

The extruder was equipped with eight different independently controlled temperature zones, which were set prior to commencement of extrusion and could be easily adjusted during the process if required. Materials were fed into an open barrel port using a small, single screw volumetric feeder equipped with a variable speed drive. The speed could be changed using arbitrary numbers on the feeder control panel, where settings increased from 1. For the purposes of this research, a setting of 5 was used for all extrusion experiments, unless otherwise stated. See Appendix 7.2 for corresponding feed rates in kg/h.

The required components for each formulation were individually weighed and combined in 40 g batches before being blended to ensure homogeneity prior to

extrusion. Each formulation (which contained more than just pure polymer) was blended for 15 minutes using a Bin Blender (PharmaTech AB-015, Coleshill, UK) with the blender rotating at 30 rpm, and an internal agitator speed of 400 rpm.

Each of the formulations from a specific batch of experiments were extruded one after another, discarding the initial material from each run in order to minimise cross contamination. Processing time was noted for each experimental batch by measuring the time taken from the first material entering the barrel at the feed port, to the emergence of material from the die block at the end.

## **2.5 Techniques Specific to Chapter 3 and Solution Loading of PVA Filaments**

### **2.5.1 Preparation of Drug Loaded Filaments**

Regardless of specific experimental condition under investigation, the process for loading the filaments with API is similar, with any changes discussed in the relevant section. The basic solution loading process, adapted from a literature method,<sup>80,81</sup> is as follows:

PVA filament was pre-dried (40°C for 16 hours), then immersed in the drug solution in a sealed vessel at room temperature for 24 hours in a fume cupboard. Post treatment, the filament was dried (40°C for a further 24 hours) and cuttings of approximately 50 mg taken, added to a volumetric flask and dissolved in water for HPLC analysis (see Section 2.8.1) to determine drug content.

### **2.5.2 Solvent Screening**

For testing the solubility of PVA in a solvent screen, the most suitable method was to cut a piece of filament, submerge in the selected solvent and leave for 24 hours, measuring the difference in weight before and after submersion. 18 different 2 cm pieces of PVA filament (one for each solvent under investigation) were cut and dried according to the generic solution loading method, before being weighed and added to a glass vial containing 10 mL of the selected solvent. These vials were then treated

as per the above method, before weighing and recording any observed difference in mass at the end of the experiment.

#### **2.5.2.1 Carvedilol Solubility Analysis**

The solubility of carvedilol was also screened, after excluding unsuitable solvents which either dissolved or partially dissolved PVA, as detailed in the results section. This was achieved by adding a few milligrams of API to the vials that had already been used for PVA solubility screening and shaking briefly before observing if any material remained.

#### **2.5.3 Varying the Loading with Solvent Evaporation Rate**

Three different sizes of vessels were chosen in order to vary the surface area of the solvent: 100 mL, 500 mL and 1 L. The surface area in each of these vessels was 17 cm<sup>2</sup>, 44 cm<sup>2</sup>, and 64 cm<sup>2</sup> respectively. These either remained sealed for the duration of the experiment, or open to the atmosphere, allowing for evaporation of solvent. A segment of PVA filament of approximately 3 cm in length, and weighing 0.10 g, was added to each vessel along with 50 mL of a 10 mg/mL carvedilol solution in ethanol. This was then stored and subsequently dried according to the generic loading method.

#### **2.5.4 Varying Concentration of Loading Solution**

Filaments were treated as per the generic solution loading method mentioned above, with the only change being the concentration of loading solution – either 10 mg/mL, 15 mg/mL or 20 mg/mL carvedilol in methanol.

#### **2.5.5 Varying Loading of Filaments With Time**

Different loading times were selected to investigate loading efficiency: 1, 2, 4, 8, 24 and 48 hours. 18 different 2 cm samples of PVA filament (3 per sample time) were treated as per the generic solution loading method, using a 20 mg/mL solution of carvedilol in methanol. Three of these samples were removed for analysis by HPLC (See Section 2.8.1) and TOF-SIMS (See Section 2.8.3.1) at each sample time point.

### 2.5.6 Varying Loading of Filaments with Varying Pressure

Three segments of PVA filament were selected as control samples and three were selected for high pressure analysis. For high pressure analysis, the segments were transferred to a PTFE loading tube, submerged in a methanolic solution of carvedilol (10 mg/ml) and sealed at both ends of this tube before being loaded into a large volume press, a schematic drawing of which is shown in Figure 29.<sup>97</sup> The internal bore of the loading cell is 10 mm in diameter and the pressure is applied to the cell via the use of a hydraulic press. The pressure is measured via an external gauge and, once the desired pressure is achieved, a retaining nut is rotated to lock the pressure within the loading cell. Once this is locked, the hydraulic press is released and the cell left for a desired length of time before checking the contents of the cell. For this experiment, an external pressure of 8 kbar (7 metric tonnes) was applied to the loading tube within the cell, and the equipment left at room temperature for 24 hours. The control samples of the experiment were also held in a PTFE loading tube, submerged in methanolic drug solution, but these remained at ambient temperature and pressure for 24 hours.

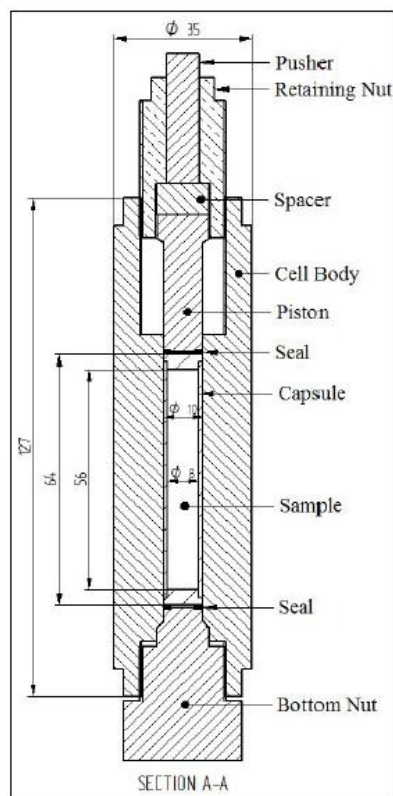


**Figure 29** - Schematic of Large Volume Press (measurements are in millimetres)

## 2.6 Techniques Specific to Chapter 4 and Extrusion Loading of PVA or Affinisol™

### 2.6.1 Milling of PVA Filament

PVA filament was first pelletised using an 11 mm hot-melt extruder strand pelletiser (Thermo Fisher Scientific, Karlsruhe, Germany) in order to obtain pellets approximately 2 mm in length. A Fitz-Quadro Hammer and Knife mill (Ontario, Canada) was then used to mill the pellets and was operated in the knife blade formation at 4500 rpm, with various gratings investigated. Powdered material was collected in a clear plastic bag rather than a metal collection vessel in order to observe the process while the mill was in operation.

### 2.6.2 Extrusion of PVA

Pelletised PVA filament was trialled within the extruder, in the absence of API, to demonstrate experimental conditions suitable for PVA alone. As this filament was originally intended for use in a 3D printer, extrusion temperature was based on the upper limit of the processing range when applied to 3D printing.<sup>98</sup> The extrusion settings are listed in Table 2:

**Table 2** - Extrusion Settings for Pelletised PVA Filament

<b>Trial</b>	<b>Barrel Temperature (°C)</b>	<b>Screw Speed (rpm)</b>	<b>Feeder Speed</b>
1	50°C at feed port, 200°C rest of barrel	100	2
2	50°C at feed port, 200°C rest of barrel	100	2
3	50°C at feed port, 200°C rest of barrel	100	2
4	50°C at feed port, 200°C rest of barrel	100	2
5	50°C at feed port, 200°C rest of barrel	120	2
6	50°C at feed port, 200°C rest of barrel	120	3

Investigation into the extrusion of powdered PVA was also carried out, again with no drug present. Settings used for high molecular weight PVA (89000-98000 MWt) are shown in Table 3:

**Table 3** - Extrusion Parameters for Powdered PVA (89000-98000 MWt)

<b>Trial</b>	<b>Barrel Temperature (°C)</b>	<b>Screw Speed (rpm)</b>	<b>Feeder Speed</b>
1	50°C at feed port, 190°C rest of barrel	100	3
2	50°C at feed port, 190°C rest of barrel	50	3
3	50°C at feed port, 190°C rest of barrel	30	3

When testing the extrusion of low molecular weight PVA (13000-23000 MWt), the die size also had to be varied according to the settings displayed in Table 4:

**Table 4** - Extrusion Parameters for Powdered PVA (13000-23000 MWt)

<b>Trial</b>	<b>Die Size (mm)</b>	<b>Barrel Temperature (°C)</b>	<b>Screw Speed (rpm)</b>	<b>Feeder Speed</b>
1	2	50°C at feed port, 220°C rest of barrel	50	3
2	2	50°C at feed port, 220°C rest of barrel	20	3
3	No Die	50°C at feed port, 170°C rest of barrel	300	3

### **2.6.3 DoE Approach to Extrusion of Affinisol™ with Disintegrants using MODDE Statistical Analysis**

Affinisol™ was selected as an alternative polymer to PVA, and formulated with carvedilol and a number of different disintegrants. For each disintegrant formulation included in the Design of Experiments (DoE) approach, MODDE software (version 11, Umetrics, Sweden) was used in order to determine the number of experiments and

levels of components which would give an overall idea of the experimental space under investigation.

Three factors were used for the design of experiments as follows:

1. API concentration (1% w/w, 10.5% w/w and 20% w/w corresponding to 'low', 'medium' and 'high')
2. Disintegrating agent (0% w/w, 5% w/w and 10% w/w corresponding again to 'low', 'medium' and 'high')
3. Type of disintegrating agent, salt (NaCl), small natural (glycine), large natural (cellulose), small synthetic (Klucel ELF) and large synthetic (Klucel HXF) for the first DoE and a selection of small natural molecules (erythritol, mannitol, PEG 100 and PEG 4600) for the second DoE.

The response factor was calculated as the percentage of filament remaining after one hour submerged and agitated in simulated gastric fluid (SGF) using a Charles Ischi AG disintegration bath (ED v.2. Zuchwil, Switzerland). A full factorial experimental design, with ten centre points for the first DoE and four centre points for the second DoE, was carried out and various plots populated in order to show the results.

#### **2.6.3.1 Extrusion of Affinisol™ with Carvedilol and Disintegrants**

For the purpose of fully investigating how each disintegrant affects a formulation containing carvedilol and Affinisol™, a design of experiments (DoE) approach was used, with an initial set-up of six different formulations investigated per disintegrant. These were carried out in order according to the following Table 5:

**Table 5** - Formulation Design for Disintegrant DoE

Formulation	API (% w/w)	Disintegrant (% w/w)	Polymer (% w/w)
1	1	0	99
2	20	0	80
3	1	10	89
4	20	10	70
5	10.5	5	84.5
6	10.5	5	84.5

These formulations were applied to the investigation of sodium chloride (NaCl), glycine, cellulose, Klucel ELF, Klucel HXF, erythritol, mannitol, PEG 1000 and PEG 4600. The individual powder blends for each formulation were made up in 40 g batches and the extrusion experiments were run as per the following settings: die size of 1.5 mm, barrel temperature of 50°C at feed port and 170°C for the rest of the barrel, screw speed of 60 rpm and a feeder speed of 5. A processing time of 7 minutes was recorded.

After an initial investigation into how formulations containing NaCl, glycine, cellulose, Klucel ELF and Klucel HXF extruded, formulation 6 was omitted from experiments containing erythritol, mannitol, PEG 1000 and PEG 4600 as results were only intended to be for screening purposes.

#### **2.6.4 Extrusion of Affinisol™ with Carvedilol and Varying Mannitol or PEG 4600**

For the purpose of investigating whether increasing the disintegrant concentration had any effect on the drug release from individual formulations, both mannitol and PEG 4600 were selected for further investigation. Again, six different formulations were investigated per disintegrant, along with a blank formulation containing no disintegrant, and were made up according to Table 6:



**Table 6** - Formulations for Further Investigation of Mannitol and PEG 4600 as Disintegrants

Formulation	API (%)	Disintegrant (%)	Polymer (%)
Blank	10.5	0	89.5
1	10.5	5	84.5
2	10.5	10	79.5
3	10.5	15	74.5
4	10.5	20	69.5
5	10.5	30	59.5
6	10.5	40	49.5

Each batch of extrusion experiments for the different disintegrants investigated were run as follows:

#### 2.6.4.1 Extrusion of Mannitol Formulations

The individual powder blends for each formulation were made up in 40 g batches and the extrusion experiments were run as per the following settings: die size of 1.5 mm, barrel temperature of 50°C at feed port and 170°C for the rest of the barrel, screw speed of 60 rpm and a feeder speed of 5. As the mannitol content increased, filament exiting the die became very soft, therefore the barrel temperature for formulations 5 and 6 was lowered to 165°C and 160°C respectively. A processing time of 7 minutes was recorded.

#### 2.6.4.2 Extrusion of PEG 4600 Formulations

Again, the individual powder blends for each formulation were made up in 40 g batches and the extrusion experiments were run as per the following settings: die size of 1.5 mm, barrel temperature of 50°C at feed port and 170°C for the rest of the barrel, screw speed of 60 rpm and a feeder speed of 5. A processing time of 7 minutes was recorded.

As observed with increasing mannitol content, increasing PEG 4600 content also resulted in very soft filament exiting the die. This time, the barrel temperature for formulations 4, 5 and 6 was lowered to 160°C, 145°C and 140°C respectively.

### 2.6.5 Extrusion of Affinisol™ with Carvedilol and Superdisintegrants

For the purpose of testing a selection of superdisintegrants – Explotab®, VivaStar® and VivaSol® – a range of different formulations were investigated. These were carried out with or without the inclusion of a constant concentration of mannitol in order to determine if there is any difference in the release of carvedilol from these formulations. These formulations were made up according to Table 7:

**Table 7 - Formulation Design for Superdisintegrant Investigation**

Formulation	API (%)	Superdisintegrant (%)	Mannitol (%)	Polymer (%)
1	10.5	1	0	88.5
2	10.5	2	0	87.5
3	10.5	3	0	86.5
4	10.5	4	0	85.5
5	1	10	0	89
6	20	10	0	70
7	10.5	5	0	84.5
Man 1	10.5	1	5	83.5
Man 2	10.5	2	5	82.5
Man 3	10.5	3	5	81.5
Man 4	10.5	4	5	80.5
Man 5	10.5	5	5	79.5
Man 6	10.5	10	5	74.5

The individual powder blends were made up in 40 g batches and the experimental conditions were kept constant for each formulation and run as per the optimised settings from previous extrusion experiments: die size of 1.5 mm, barrel temperature of 50°C for zone 2, 170°C for the rest of the barrel, screw speed of 60 rpm and a feed rate of 5. Processing times varied across the different formulations and are discussed further in Section 4.3.3.4.

### 2.6.6 Disintegration of Affinisol™/Carvedilol/Disintegrant Filaments

Disintegration was carried out using a Charles Ischi AG disintegration bath (ED v.2. Zuchwil, Switzerland). Six samples were analysed simultaneously, submerged in 1L

of simulated gastric fluid (SGF) and initially agitated for 15 minutes. As this apparatus is designed to handle tablets, the filaments were not ideally suited for this method and a further 45 minutes were added to the analysis time in order to get a better understanding of how each disintegrant affects the formulations. Samples were weighed before and after disintegration, and the percentage mass remaining calculated as a measure of the disintegrant's capabilities. Photographs were also taken of the samples, post-disintegration, in order to see how the filaments changed throughout the experiment.

## 2.7 Techniques Specific to Chapter 5 and the Population of a Ternary Phase Diagram

### 2.7.1 Population of a Ternary Phase Diagram

Based on experimental results gained from Chapter 4, construction of a ternary phase diagram, which included carvedilol, mannitol and Affinisol™, formed the basis for experiments carried out in Chapter 5 (Figure 30).

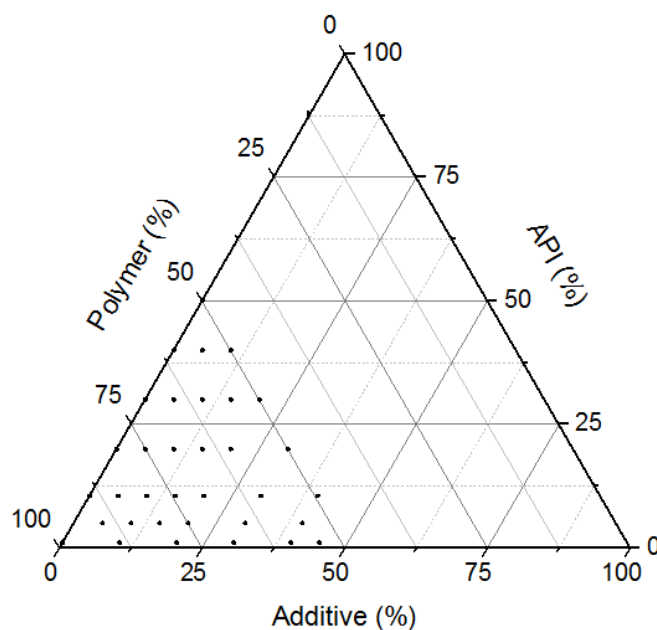


**Figure 30** - Ternary phase diagram for experiments containing carvedilol, mannitol and Affinisol™

Population of this space allowed for easier visualisation of the boundaries for 3D printing and experiments were planned according to the black dots visible on this diagram. The area surrounding large percentages of additive was excluded from investigations as it would limit the range of API doses possible, while still maintaining a level of polymer necessary for the extrusion process. Similarly, formulations containing high percentages of API were excluded due to the potential lack of stability within the extruder at lower polymer content. Therefore, formulations containing less than 50% Affinisol™ were initially excluded from this investigation, with three formulations at 45% Affinisol™ later added in order to demonstrate the boundaries of the space for printable formulations.

### 2.7.2 Extrusion of Formulations with 1% Carvedilol

The individual powder blends were made up in 40 g batches and the formulations designed according to Table 8:

**Table 8** – Design of Formulations Containing 1% API

Formulation	API (%)	Mannitol (%)	Polymer (%)
1	1	20	79
2	1	30	69
3	1	40	59
4	1	45	54

For formulations containing 1% API 0% mannitol and 1% API 10% mannitol, please refer to section 2.6.3.1 for the extrusion conditions as these experiments were not repeated for this section of work due to material already being available from previous experiments. Extrusion conditions remained constant, as per previous experiments, are detailed as follows: die size of 1.5 mm, barrel temperature of 50°C for the feed port and 170°C for the rest of the barrel, screw speed of 60 rpm and a feed rate of 5. A processing time of 4 minutes 30 seconds was recorded.

### 2.7.3 Extrusion of Formulations with 5% Carvedilol

The individual powder blends were made up in 40 g batches and the formulations designed according to Table 9:

**Table 9** – Design of Formulations Containing 5% API

Formulation	API (%)	Mannitol (%)	Polymer (%)
1	5	5	90
2	5	10	85
3	5	15	80
4	5	20	75
5	5	30	65
6	5	40	55

These powder blends were then extruded according to the previous settings of: die size of 1.5 mm, barrel temperature of 50°C for the feed port and 170°C for the rest of the barrel, screw speed of 60 rpm and a feed rate of 5. A processing time of 4 minutes 30 seconds was recorded.

### 2.7.4 Extrusion of Formulations with 10.5% Carvedilol

For formulation design and extrusion parameters, please refer to section 2.6.4 and section 2.6.4.1. These experiments were not repeated for this section of work as material was already available from previous experiments.

### 2.7.5 Extrusion of Formulations with 20% Carvedilol

The individual powder blends were made up in 40 g batches and the formulations designed according to Table 10:

**Table 10** – Design of Formulations Containing 20% API

<b>Formulation</b>	<b>API (%)</b>	<b>Mannitol (%)</b>	<b>Polymer (%)</b>
1	20	5	75
2	20	10	70
3	20	15	65
4	20	20	60
5	20	30	50

For formulations containing 20% API 0% mannitol, please refer to section 2.6.3.1 for the extrusion conditions, as this composition had already been prepared in previous experiments.

These powder blends were also extruded according to the previous settings of: die size of 1.5 mm, barrel temperature of 50°C for the feed port and 170°C for the rest of the barrel, screw speed of 60 rpm and a feed rate of 5. A processing time of 6 minutes was recorded.

### 2.7.6 Extrusion of Formulations with 30% Carvedilol

The individual powder blends were made up in 40 g batches and the formulations designed according to Table 11:

**Table 11** – Design of Formulations Containing 30% API

<b>Formulation</b>	<b>API (%)</b>	<b>Mannitol (%)</b>	<b>Polymer (%)</b>
1	30	0	70
2	30	5	65
3	30	10	60
4	30	15	55
5	30	20	50

While the previous settings of: die size of 1.5 mm, barrel temperature of 50°C for the feed port and 170°C for the rest of the barrel, screw speed of 60 rpm and a feed rate of 5, were applied to formulation 1, the barrel temperature was lowered for subsequent

formulations to accommodate the softer filaments exiting the die. A processing time of 7 minutes 50 seconds was recorded.

As the API content of the formulations increased, there were also problems encountered with flow of the powder blends into the feed port. As such, the feeder speed was increased in order to combat this (Table 12):

**Table 12** - Extrusion Conditions for Formulations Containing 30% API

Formulation	Die Size (mm)	Barrel Temperature (°C)	Screw Speed (rpm)	Feed Rate
1	1.5	50°C zone 2, 170°C rest of barrel	60	5
2	1.5	50°C zone 2, 160°C rest of barrel	60	5
3	1.5	50°C zone 2, 160°C rest of barrel	60	15
4	1.5	50°C zone 2, 150°C rest of barrel	60	15
5	1.5	50°C zone 2, 150°C rest of barrel	60	15

### 2.7.7 Extrusion of Formulations with 40-50% Carvedilol

The individual powder blends were made up in 40 g batches and the formulations designed according to Table 13:

**Table 13** – Design of Formulations Containing 40-50% API

Formulation	API (%)	Mannitol (%)	Polymer (%)
1	40	0	60
2	40	5	55
3	40	10	50
4	50	0	50

Based on observations of softer filaments and poor powder flow with increasing API content, these powder blends were then extruded according to the following settings:

die size of 1.5 mm, barrel temperature of 50°C for the feed port and 150°C for the rest of the barrel, screw speed of 60 rpm and a feed rate of 10. A processing time of 8 minutes was recorded.

### 2.7.8 Extrusion of Formulations with 45% Affinisol™

Due to printing being successful with 20% API and 30% mannitol, further extrusion experiments were required in order to reveal where the boundary for print failure of these formulations could be established. Three formulations were extruded which looked at varying the concentration of carvedilol and mannitol, while keeping the Affinisol™ concentration the same at 45% of the overall composition. This allowed for three points surrounding the 20% CAR 30% mannitol formulation to be investigated further (Table 14):

**Table 14-** Design of Formulations Containing 45% Affinisol™

Formulation	API (%)	Mannitol (%)	Polymer (%)
1	10	45	45
2	20	35	45
3	30	25	45

With the reduction in polymer content, similar problems with powder flow were encountered and the feeder speed was adjusted to 8 accordingly. Die size and screw speed were maintained at 1.5 mm and 60 rpm respectively, but the temperature of the barrel was lowered from 170°C to 165°C for formulation 3 on account of the higher drug content. A processing time of 8 minutes was recorded.

### 2.7.9 Direct Compression of Affinisol™/Carvedilol/Mannitol Formulations

In order to make a comparison with traditional tablet manufacture and hot-melt extrusion coupled with 3D printing, direct compression was selected as a tool to carry out this comparison. This was carried out in order to determine whether extrusion and subsequent printing provide any benefits over current manufacturing processes.



The following formulations were selected for investigation. These were made up in 500 g batches according to Table 15:

**Table 15** - Formulation Design for Direct Compression Experiments

Formulation	API (%)	Mannitol (%)	Polymer (%)
1	10.5	10	79.5
2	20	10	70
3	30	10	60

Similar to the preparation for extrusion experiments, each formulation was blended for 15 minutes using a Bin Blender (PharmaTech AB-015, Coleshill, UK) with the blender rotating at 30 rpm, and an internal agitator speed of 400 rpm. Each of the formulations were then further blended with 0.5 %w/w magnesium stearate (Parateck LUB MST, Merck Millipore, Merck Group, Massachusetts, USA) at 20 rpm for 60 seconds, to gently lubricate the blend. Each blend was then transferred to the hopper of a single punch tablet press (Korsch XP1, Korsch AG, Berlin, Germany) to produce flat-faced round tablets with a 0.80 mm bevel edge in a die with a 9 mm diameter at a rate of 10 per minute. The tablet press was calibrated for each experimental condition to produce tablets with different target weights in order to compare with the 3D printed tablets already produced.

Carvedilol is described in the literature as having poor flowability properties<sup>99,100</sup> and difficulty with filling the cavity of the tablet press was encountered at 20% and 30% drug loadings. As a result, individual tablets from each of the different formulations were manually filled into the press to produce tablets of approximately 300 mg weight. This was the maximum weight which was produced as it was again difficult when attempting to manually fill the cavity for any higher tablet weights.

Tablets obtained from each of the formulations are as follows:

### **10.5% Carvedilol**

Approx. 30 tablets at ~200 mg (automated tablet press), Approx. 30 tablets at ~300 mg (automated tablet press), Approx. 30 tablets at ~480 mg (automated tablet press) and 5 tablets at ~300 mg (manual filling of tablet punch).

### **20% Carvedilol**

Approx. 30 tablets at ~300 mg (automated tablet press) and 5 tablets at ~300 mg (manual filling of tablet punch).

### **30% Carvedilol**

3 tablets at ~180 mg (automated tablet press) and 5 tablets at ~300 mg (manual filling of tablet punch).

## **2.8 Analytical Techniques**

### **2.8.1 Determination of Carvedilol Concentration**

A known weight of filament or tablet was placed in a volumetric flask, dissolved in distilled water (for samples containing PVA) or acetonitrile (for samples containing Affinisol™) with the aid of sonication, made to volume and an aliquot transferred to HPLC vials for analysis. The concentration of drug was determined with HPLC (Agilent 1290 UPLC, Agilent Technologies, UK) using a method from literature.<sup>101</sup> The HPLC assay involved injecting 10 µL of samples for analysis into a mobile phase consisting of 10 mM ammonium formate in H<sub>2</sub>O (mobile phase A, pH 3) and 10 mM ammonium formate in ACN/H<sub>2</sub>O (9:1 v/v, mobile phase B, pH 3) in varying amounts according to the following gradient method: 0 minutes – 30% B, 3 minutes – 100% B, 4 minutes – 100% B, 4.5 minutes – 30% B. This was pumped through a Luna 5 µm C18 column, 150 x 4.6 mm, 100 Å (Phenomenex, UK) maintained at 60°C and at a flow rate of 1.5 mL/min. The sample was monitored using a DAD at wavelengths of 214, 254 and 291 nm, with 254 nm being selected as the most suitable for quantification. Carvedilol eluted at approximately 2.5 minutes and an example chromatogram is shown in Figure 31:

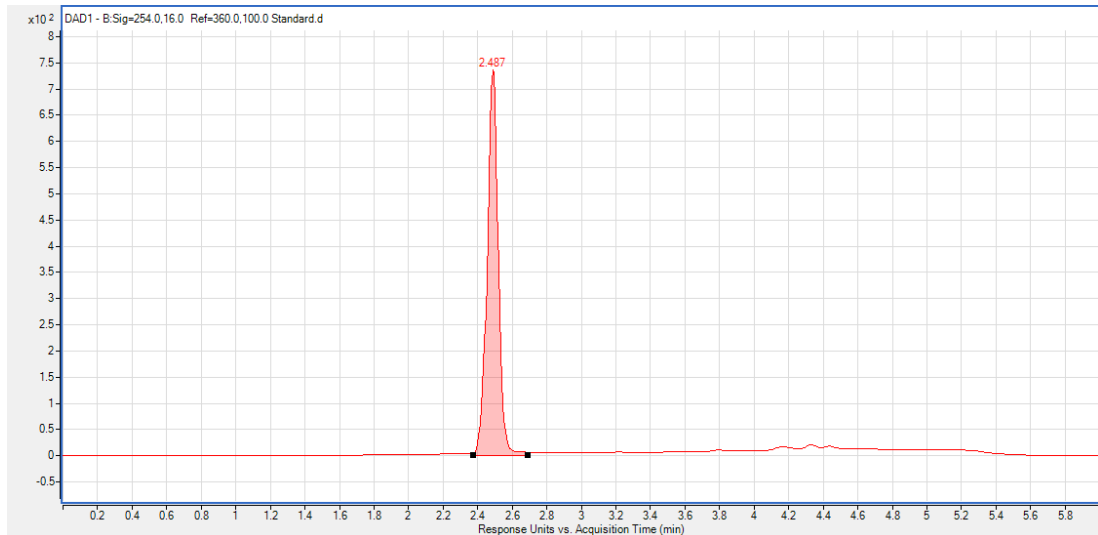


**Figure 31** - Carvedilol Peak at 2.5 minutes measured at 254 nm

Regular calibrations were carried out, with standard concentrations as follows: 0.0078125 mg/mL, 0.015625 mg/mL, 0.03125 mg/mL, 0.0625 mg/mL, 0.125 mg/mL, 0.25 mg/mL and 0.5 mg/mL. All these calibration standards were made up from an initial stock solution of 0.5 mg/mL and diluted by half each time, producing a calibration plot, similar to the following, whenever the system was re-calibrated:

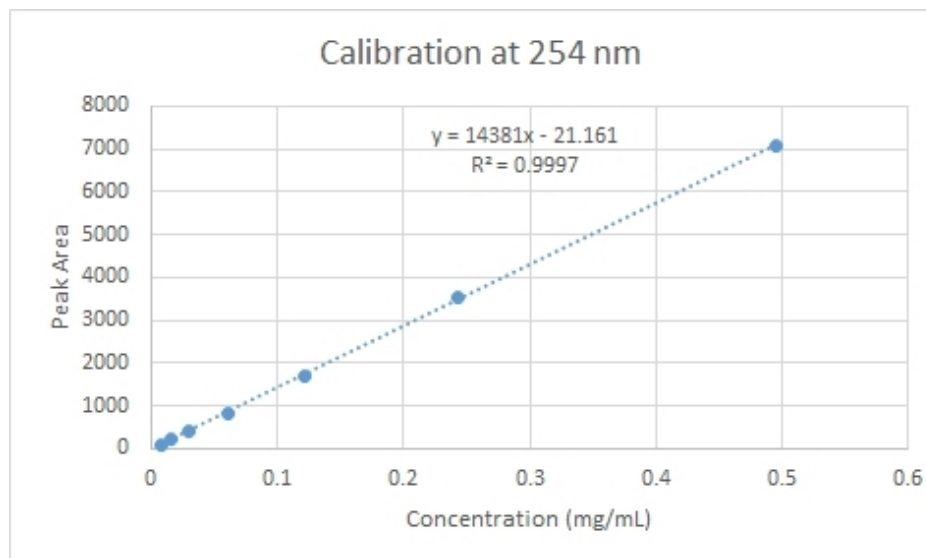


**Figure 32** - HPLC Calibration Plot

### **2.8.2 Dissolution Analysis**

Dissolution testing was carried out either using a USP 1 dissolution bath (Erweka D726) and a separate UV spectrophotometer (Carl Zeiss MCS600), equipped with a transmittance probe of 2 mm path length, or using a USP 1 ADT8 Dissolution bath, coupled with an ALS SP700 UV Spectrophotometer (Automated Lab Systems, Berkshire, UK) Paddles were equipped and a paddle speed of 50 rpm was set for every experiment. To investigate how tablets are likely to behave upon initial contact with the stomach environment, dissolution analysis was carried out at 37°C in triplicate, using 500 mL simulated gastric fluid (SGF) dissolution media at pH 1.2, with the pepsin omitted.<sup>12</sup> Samples were analysed at time points of 15 min, 30 min, 45 min, 60 min, 90 min, 120 min, 240 min and 360 min when using the separate UV spectrophotometer with transmittance probe, or at time points of 15 min, 30 min, 45 min, 60 min, 75 min, 90 min, 105 min, 120 min, 150 min, 180 min, 210 min, 240 min, 300 min and 360 min when using the combined automated system.

### **2.8.3 Analysis of Drug Distribution**

Three different techniques, listed below, were employed in an attempt to determine the location of carvedilol and the level of homogeneity within the tablets and filaments produced.

#### **2.8.3.1 Time of Flight Secondary Ion Mass Spectrometry (ToF-SIMS)**

ToF-SIMS was performed as a collaboration with Eleonora Paladino, another PhD student within the Centre for Continuous Manufacturing and Crystallisation. For the purpose of this research, it was used to assess the distribution of API within the polymer matrix, but this analysis provided complementary data to support Ms Paladino's research, which is still in the process of submission at the time of writing this thesis. The analyses were carried out with a TOF.SIMS 5 instrument (IONTOF GmbH, Münster, Germany), based at the Wolfson Foundation Pharmaceutical Surfaces Laboratory in the Technology and Innovation Centre, University of Strathclyde, and with a ToF-SIMS IV instrument (IONTOF GmbH, Münster, Germany), based at the National Physical Laboratory (NPL, Teddington, Middlesex

TW11 0LW, UK). Both instruments are equipped with a Bismuth Liquid Metal Ion Gun (LMIG) for analysis.

In order to prevent any charge build-up on the surface of individual samples, a low-energy electron (21 eV) flood gun was used to optimise the surface potential of each sample for analysis. The surface analysis conditions were selected and adjusted to keep the primary ion dose density below the static limit of  $1 \times 10^{13}$  primary ions/cm<sup>2</sup> to minimise surface damage during the analysis.

For obtaining macro images of filament slices, the following was applied: A 30 kV Bi<sub>3</sub><sup>+</sup> primary ion beam was employed to acquire high mass resolution macro images on cross-sections of the filaments. These were processed using SurfaceLab 6.7 software (ION-TOF, Münster, Germany). Each image of the raster has a size of 500 μm × 500 μm, and was acquired in the positive secondary ion polarity in the *m/z* range of 0-900 Da. The total area analysed was 2.5 mm × 2.5 mm. Mass resolution: 2300 *m/Δm* at *m/z* 407 (C<sub>24</sub>H<sub>27</sub>N<sub>2</sub>O<sub>4</sub><sup>+</sup> [M+H]<sup>+</sup> carvedilol).

A 30 kV Bi<sub>3</sub><sup>2+</sup> primary ion beam was selected to generate high lateral resolution secondary ion images of the external surface of the filament. These were collected over a surface area of 50 μm × 50 μm, with a resolution of 256 × 256 pixels (pixel width was circa 0.2 μm), in the positive secondary ion polarity. The images were then processed using SurfaceLab 6.7 software (ION-TOF, Münster, Germany). All the mass spectral information was recorded in the *m/z* range of 0–900 Da.

The TOF.SIMS 5 instrument was equipped with an argon gas cluster ion beam (GCIB) to sputter away surface layers of the sample and expose a new area for analysis. By alternating the use of the LMIG analysis beam and the GCIB sputter beam, 3D imaging and depth profiling of samples can be carried out. 3D analyses were carried out using a 30 kV Bi<sub>3</sub><sup>+</sup> primary ion beam for analysis (pulsed current 0.25 pA) and a 10kV Ar<sub>1500</sub><sup>+</sup> beam for sputtering (DC current 10 nA).

The argon sputter beam was rastered over an area of 300 μm × 300 μm to create a large crater. For the extrudates, the bismuth primary ion beam was used to analyse an area of 100 μm × 100 μm in the centre of the sputtered crater. A smaller area of

50  $\mu\text{m}$   $\times$  50  $\mu\text{m}$  was analysed for the tablet in order to deliver a higher dose and increase the secondary ion counts.

### **2.8.3.2 Raman Mapping**

Raman mapping was carried out using an mPAT 3D Raman Spectrometer (H2Optx, San Jose, California, USA), to assess the distribution of drug within the polymer filaments and tablets. Due to the instrument being located at Rutgers University, New Jersey, these analyses were carried out in collaboration with Sarahjane Wood, a PhD student within the Centre for Continuous Manufacturing and Crystallisation, while taking part in an exchange programme. Standard direct compression tablets can be sheared using this system to generate a 3D image of component distribution, however the tablets in this current study were too hard for this aspect of the technique and only a map of the surface could be produced. Reference spectra of carvedilol and PVA were collected by placing material of each component onto the sample window (enough to cover the entire window) and compressed to remove air. Using the manual tab, the microscope image was focused using the Olympus 50x objective and a raman spectrum obtained whilst subtracting background noise. A Class 3B laser was used (Innovative Photonics Solutions, New Jersey, USA) and the settings used were as follows: Laser current: 160 mA, Laser Power: 90 mW, Exposure Time: 10 s, Wavelength: 754 nm.

MetaScan (H2Optx program) was used for collecting spectra and maps of the drug loaded samples, tablets or filaments were glued to sample holders which were slotted into the sample holder of the mPAT system, exposing top surface to sample window. The 4 mm x 4 mm Raman map was acquired on the surface of the sample with 10  $\mu\text{m}$  steps along the x and y-axis to produce a 6x6 sample grid. The same laser settings and objective were used as when collecting the reference data.

Using H2Optx MetaAnalyser software, the Raman spectra were converted to black and white base maps using the powder reference spectra to assign peaks. These base maps were then converted into a colour system using Python coding (provided by C-SOPS, Rutgers University) – green for PVA and red for carvedilol. This allowed a

pixel value roughly corresponding to the concentration of each substance to be obtained.

### **2.8.3.3 X-Ray Nano-Computed Tomography (Nano-CT)**

Nano-CT was used in order to assess drug distribution and internal structure within samples. Both a placebo and drug loaded sample of filament, and a drug loaded printed tablet underwent analysis using a Bruker Skyscan 2211 X-Ray nanotomograph (Bruker, Belgium). The scanned images were reconstructed using the NRecon software (version 1.6.8.0, Bruker). To visualise and analyse the data, CTAn software (Version 1.16.4.1) and CTVox software (Version: 3.2.0) for surface rendering were used.

## **2.8.4 Determination of Crystallinity**

### **2.8.4.1 Powder X-Ray Diffraction (XRPD)**

The crystallinity of the raw components, drug loaded filaments and 3D printed tablets was determined via X-Ray diffraction using a D8 Advance II diffractometer (Bruker, Germany) with a Vantec 1D Detector with 2.5° Soller Slits. The operating voltage was 40 kV and had an operating current of 50 mA with an operating wavelength of 1.54 Å in the angular range of  $4^\circ < 2\theta < 35^\circ$  using a step scan mode (step width = 0.017°, counting time = 1 s/step).

### **2.8.4.2 Differential Scanning Calorimetry (DSC) Thermal Gravimetric Analysis (TGA)**

Samples were analysed using a DSC214 Polyma (Netzch Geratebau GmbH) using a heating profile of 20°C to 190°C and a heating rate of 5°C/min. Data was collected and analysed using Netzch Proteus Analysis software (Version 7.1.0). TA aluminium pans with pierced lids were used with an average sample mass of 4 mg and were analysed alongside an empty, pierced TA aluminium pan as a reference. Blank correction was carried out with empty pan under the same measurement conditions prior to sample analysis. The DSC was calibrated for both temperature and sensitivity

over the temperature range  $-93^{\circ}\text{C}$  to  $605^{\circ}\text{C}$ , at a heating rate of  $20^{\circ}\text{C}/\text{min}$ , using the following set of reference materials supplied by Netzsch: In, Sn, Bi, Zn.

For some powdered polymer samples, thermogravimetric analysis was also utilised and these were characterised with DSC and TGA using an STA 449 F1 Jupiter (Netzsch Geratebau GmbH) using a heating profile of  $20^{\circ}\text{C}$  to  $250^{\circ}\text{C}$  and a heating rate of  $5^{\circ}\text{C}/\text{min}$ . This was followed by an isothermal segment at  $250^{\circ}\text{C}$ . Data was collected and analysed using Netzsch Proteus Analysis software (Version 7.1.0). TA aluminium pans with pierced lids were used, again with an average sample mass of 4 mg, and analysed alongside an empty, pierced TA aluminium pan as reference. Prior to sample analysis, buoyancy correction was carried out with an empty pan run with the same method as used for sample analysis. The STA was calibrated for both temperature and sensitivity over the temperature range  $-200^{\circ}\text{C}$  to  $675^{\circ}\text{C}$ , at a heating rate of  $20^{\circ}\text{C}/\text{min}$ , using the following set of reference materials supplied by Netzsch: In, Sn, Bi, Zn, CsCl.

For analysis of samples in relation to the construction of the Affinisol<sup>TM</sup>/carvedilol/mannitol phase diagram, pelletised filament was analysed and a slightly different heating profile was used: samples of extrudate were characterised with DSC using a DSC214 Polyma (Netzsch Geratebau GmbH) at a heating rate of  $20^{\circ}\text{C}/\text{min}$ . Temperature was raised to  $190^{\circ}\text{C}$ , cooled to  $0^{\circ}\text{C}$  then followed by an isothermal segment for 2 minutes. The final step involved heating the samples to  $190^{\circ}\text{C}$  once more. Data was collected and analysed, as before, using Netzsch Proteus Analysis software (Version 7.1.0).

### **2.8.5 Surface Morphology**

In order to investigate if there are any structural discrepancies in either the filaments or the tablets, and whether the presence of carvedilol has any effect, the surface morphology of filaments and tablets were analysed using a Keysight 8500B SEM microscope. Samples were uncoated and added to aluminium stubs with conductive sticky carbon tabs and placed under vacuum for 2 minutes prior to transfer to SEM for analysis. The Keysight 8500B SEM was operated at a beam voltage of 20 kV and



with data collected in secondary electron mode at magnifications of approximately 1000x for the filament and 450x for the printed tablets.

### 2.8.6 3-Point Bend Testing

3-point bend testing was used in order to assess the mechanical properties of the filaments, and determine if print failure could have been predicted prior to attempting printing. By quantifying the maximum stress and strain values that each of the filaments can withstand, it is hoped that this can provide an indication of an acceptable range for these properties and allow for greater understanding of the experimental space under investigation. Method development of suitable test parameters for hot-melt extruded polymers was carried out, prior to this research, within the department.<sup>87</sup> Mechanical properties of filaments were tested on a Texture Analyser TA-XT (Stable Micro Systems, Godalming, UK) equipped with a mini 3 point bend rig. Filaments were cut to approximately 2 cm pieces, the length and diameter of the specimen measured using digital calipers, and balanced across two lower support beams which were situated at a distance of 0.8 cm from each other. The speed of the upper blade was set to 0.5 mm/s until a trigger force of 0.049 N was reached. Testing was then carried out using a blade speed of 0.02 mm/s and a total displacement of 4.5 mm. Data acquisition was performed with Exponent software (version 6,1,11,0) with a rate of 25 points per second and data analysis was also carried out using the same software. Stress-strain graphs were plotted based on the following relationships for stress and strain:

$$\sigma_f = FL/\pi R^3 \quad (\text{circular cross section})$$

where:  $\sigma_f$  is the flexural-stress, F is the applied force (N), L is the span (or gap) (mm), R is the radius of the specimen.

$$\varepsilon_f = 600sh/L^2 \%$$

where:  $\varepsilon_f$  is the flexural strain (expressed as percentage), s is the deflection (mm), h is the thickness of the test specimen (mm), L is the span (or gap) (mm).

The flexural modulus was determined as the slope of the linear region of the stress strain graph between 1 and 3% strain. Maximum stress and associated strain values were also derived from these obtained stress strain graphs. In case of product failure, the break point was determined by selecting the minimum on the second derivative of the stress strain graph. At the associated strain value, the stress value on the stress strain graph was reported as break stress. In addition the modulus of toughness was calculated as the area under the stress strain curve from 0 strain to break point, representing the energy in the system at break point.

### **2.8.7 ANOVA Statistical Analysis**

One-way or two-way ANOVA were employed using Minitab software (version 17) to analyse the difference in various results throughout this research. When carrying out an F-Test on differences in these results, the accompanying probability (P) value was used to determine if differences were considered significant. Values above probability level  $P > 0.05$  were considered not significant, whilst  $P < 0.05$  were considered significant. Tukey interaction plots were also employed to determine which of the parameters under investigation were most significant.

## **3 Producing Drug Loaded 3D Printed Tablets via Solution Loading of PVA**

### **3.1 Introduction**

When considering a suitable drug to begin investigation into the application of scaleable doses and personalised medicine, it makes logical sense to concentrate efforts on APIs which already have a range of doses on the market. Based on selection criteria discussed previously (Section 1.9.3), carvedilol was chosen as a suitable model compound with which to pursue further work.

Based on 3D printing work already carried out by other research groups,<sup>80,81</sup> solution loading of this API onto pre-existing PVA filaments was chosen as a suitable initial method for producing a range of different oral doses.

This chapter focuses on different methods of varying the drug loading in PVA filaments, prior to printing, with a view to understanding the doses achievable via this method. By using evaporative techniques, high pressure, differing concentrations of loading solution or simply by varying the experimental time, it is hoped that a range of doses, comparable to those currently on the market (3.125-25 mg immediate release, 10-80 mg extended release), can be produced which could provide suitable flexibility for patients.

### **3.2 Aim**

The overall aim for this chapter was to successfully develop a method for manufacture of varying doses of carvedilol tablets, intended for the oral route of administration. Control over dosing, with a target within the range currently available on the market, is intended to be achieved via initial loading of the filament, prior to printing, and by changes to the tablet design during manufacture of the tablets. Analytical techniques were applied in order to understand drug distribution and drug release from these non-conventional dosage forms.

### **3.3 Results and Discussion**

#### **3.3.1 Loading of PVA Filaments with Carvedilol**

In order to print pharmaceutically relevant tablets using a Leapfrog Creatr HS, suitable drug-loaded filament should be fabricated prior to feeding into the printer. As the PVA filaments for this work were acquired in a pre-extruded state, the API must first be incorporated into these via a solution loading process.<sup>80,81,102</sup> This involves the submersion of a PVA filament in a suitable solvent containing the API of choice (in this case, carvedilol), leaving for an allocated period of time and subsequently drying in an oven, to produce the required filaments for dose fabrication (Figure 33):



**Figure 33** - Solution Loading Process. Left - Commercially available filament. Middle - A solution containing the desired API. Right - Drug loaded filaments after drying.

Aside from any differences arising due selecting different APIs, investigation was carried out into the factors which could potentially influence the drug loading of filaments, such as solvent selection, API solution concentration, length of time for submersion etc. Results are discussed in the following sections.

##### **3.3.1.1 Solvent Selection for Optimum Solution Loading**

Given that solubility of compounds can vary greatly in different solvents, it is clear that solvent choice can have a significant effect on the concentration of drug within the polymer. Any chosen solvent must successfully dissolve carvedilol, without destroying the PVA filament, so initial investigation into the solubility of these filaments in a selection of available solvents was carried out.

For testing the solubility, the most suitable method was to cut a piece of filament, submerge in the chosen solvent and leave for 24 hours, measuring the difference in weight before and after submersion and drying. This provided replication of the

conditions for a regular drug loading experiment, and allowed for inspection of the filament in order to see if the structural integrity remained after being in contact with the solvent. Ideally, the filament should remain intact, with little or no changes to the overall surface. While a clean split down the length of filament upon swelling is unlikely to have much effect after drying and returning to its original size, any imperfections across the overall filament surface would result in inhomogeneity and potential issues when feeding through the gear wheels of the 3D printer at a later stage in manufacture.

The solvents examined are listed below, along with the results from the basic solvent screen:

**Table 16 - Results from Submersion of PVA in Various Solvents**

<b>Solvent</b>	<b>Start Weight of Filament (mg)</b>	<b>End Weight of Filament (mg)</b>	<b>% Change</b>	<b>Other Observations</b>
1-butanol	70.9	70.8	-0.1%	
1-pentanol	67.6	67.5	-0.1%	
1-propanol	70.4	71.9	+2.1%	
2-butanol	65.6	65.7	+0.2%	
2-butanone	66.5	65.9	-0.9%	Sticky Residue
2-methyl-1-propanol	68.8	68.4	-0.6%	
2-propanol	67.0	66.9	-0.1%	
3-methyl-1-butanol	65.4	65.6	+0.3%	
MIBK	68.5	67.7	-1.2%	Sticky Residue
acetone	68.9	67.3	-2.3%	Sticky Residue
anisole	69.5	71.4	+2.7%	Sticky Residue
butyl acetate	65.4	65.6	+0.3%	Sticky Residue
DMSO	68.9	0.0	-100%	Full dissolution
ethanol	63.7	66.1	+3.8%	
heptane	68.3	68.3	0%	
isobutyl acetate	67.2	67.3	+0.1%	Sticky Residue
water	67.4	0.0	-100%	Full dissolution
pentane	68.4	68.3	-0.1%	

PVA is reported to be soluble in both DMSO and water, which is shown in the results from this table, along with both ethylene glycol and N-methyl pyrrolidone,<sup>103</sup> which were not tested in this solvent screen. Except for DMSO and water, the weights after removal from solvent and drying remain within  $\pm 4\%$  of the starting weights, which can be explained by the sample still being slightly damp (in the case of a gain) or a small amount dissolving (in the case of a loss).

After removal from the oven, there was a small, sticky residue observed around the dry filament for the samples from 2-butanone, MIBK and acetone. Increasing amounts of this sticky residue was also observed around filaments which were submerged in anisole, butyl acetate and isobutyl acetate. These made it very difficult to remove the filament and were also accompanied by a strong solvent smell, indicating that they may not be completely dry and highlighting a possible reason for the observed weight gain. This sticky residue can be seen in the following pictures:



**Figure 34** - Left - anisole, middle - butyl acetate, right - isobutyl acetate after filament removal

Given the stickiness of these filaments and the strong solvent smell which accompanied them, all further investigation with these solvents was halted, as they would be unsuitable for any subsequent drug loading experiments. All remaining solvents, which did not appear to dissolve the PVA, are listed below:

**Table 17** - Suitable Solvents for Further Investigation

<b>Solvent</b>
1-butanol
1-pentanol
1-propanol
2-butanol
2-methyl-1-propanol
2-propanol
3-methyl-1-butanol
ethanol
heptane
pentane

Before proceeding with any printing experiments, a quick solubility test was carried out to see if carvedilol would dissolve in any of these remaining solvents, using the 5 mL vials from the PVA screen. Carvedilol has been shown to be soluble in various alcohols, with the solubility increasing as the carbon chain length of the alcohol decreases,<sup>104</sup> but there is no record of the solubility in alkanes. Carvedilol (50 mg) was added to each vial in order to achieve a solution concentration of 10 mg/mL. Results are shown in the Table 18:

**Table 18** - Solubility of Carvedilol in Selected Solvents

<b>Solvent</b>	<b>Observed Solubility (at ~10 mg/mL)</b>
1-butanol	almost full dissolution
1-pentanol	almost full dissolution
1-propanol	almost full dissolution
2-butanol	partially soluble, very cloudy
2-methyl-1-propanol	partially soluble, very cloudy
2-propanol	partially soluble, very cloudy
3-methyl-1-butanol	partially soluble, very cloudy
Ethanol	soluble, concentration increased to ~15 mg/mL with almost full dissolution
Heptane	insoluble
Pentane	insoluble

When ‘almost full dissolution’ is listed, this refers to the presence of only a small number of suspended particles remaining, with the majority of the API in solution.

The results from this initial solvent screen show that the most promising solvents with which to pursue further work are unbranched alcohols. Branched alcohols only result in partial solubility, and the alkanes investigated did not result in any dissolution of the API. Ethanol was the only solvent in which the solubility of carvedilol seemed to increase, with a maximum being achieved somewhere between 10 mg/mL and 15 mg/mL. Although not tested in this solvent screen, and given that a decrease in carbon chain length seems to result in higher solubility of the API, methanol may also be a potentially suitable loading solvent, allowing for further investigation using either methanol or ethanol as a suitable solvent.

### **3.3.1.2 Varying the Loading with Solvent Evaporation**

Based on results from the solvent screen, ethanol was selected as a solvent to trial in the solution loading of carvedilol, due to its ability to solubilise the API while keeping the PVA filament intact.

The conditions which were varied in this experiment were surface area of solvent and whether the vessel was open to the atmosphere or closed, with the theory being that vessels which were open to the atmosphere would slowly evaporate, increasing the solution concentration of carvedilol and, hence, driving an increase in the overall drug loading within the filament. The following conditions remained constant: filament mass, drug concentration, solvent volume and time.

At the end of the 24 hour experimental period, it was observed that all solution had evaporated from the open vessels, leaving partially or fully dissolved filaments behind. This was unexpected given the results from the solvent screening in Section 3.3.1.1. The closed vessels still contained solution along with slightly swollen pieces of filament. Each piece of filament was removed for drying, except in the case of the open 500 mL beaker, in which the filament had completely dissolved. The partially dissolved filaments were difficult to remove and had to be peeled off the bottom of the beakers, see picture below:





**Figure 35** – Filament from Open 100 mL Vessel

The remaining filaments either gained or lost mass according to whether they were in an open or closed vessel:

**Table 19** - Results of evaporative loading from a 10 mg/mL carvedilol in ethanol solution

<b>Filament</b>	<b>Mass gained or lost after drying (g)</b>
Open 100 mL	-0.036 (-36%)
Closed 100 mL	+0.014 (+14%)
Open 500 mL	No Filament to Measure
Closed 500 mL	+0.010 (+10%)
Open 1 L	-0.029 (-29%)
Closed 1 L	+0.010 (+10%)

In the case of the closed samples, it would normally be assumed that the gain in weight after drying was due to the drug, however the samples still had a strong smell of ethanol when removed from the oven. The filaments were also a lot easier to cut than a placebo sample of PVA, which had not been subjected to an ethanol solution, suggesting the samples may either still be slightly wet, that the polymer may have been slightly degraded by the solvent or that the combination of drug and solvent has potentially plasticised the polymer, making the filament more pliable.

Had this experiment been carried out with the intention of producing dosage forms, further drying would have been carried out, until samples weighed the same after two

consecutive time points. Given that this was, however, only a feasibility study of the evaporative method, further drying was not undertaken.

In order to gain a greater understanding of the suitability of ethanol as a loading solution, HPLC analysis was carried out on small pieces of filaments cut from samples in the closed vessels in order to determine drug loading.

**Table 20** - Drug Loading Achieved from Ethanol Solution

<b>Sample</b>	<b>Drug Loading</b>
100 mL Closed Vessel	0.50% w/w
500 mL Closed Vessel	0.51% w/w
1 L Closed Vessel	0.53% w/w

This is low when compared to methods such as hot melt extrusion,<sup>94,105</sup> (where higher drug loadings are achieved), but when compared to the results obtained by Goyanes *et al.*<sup>80</sup> (0.29% w/w fluorescein in PVA) who also used ethanol as a loading solution, this result is very similar.

Based on the decreased weight and poor structural integrity of the filaments from open vessels, it is unlikely that the evaporative method would be a successful way to drive an increased concentration of API within PVA filaments. The results from the open vessels also highlighted that ethanol could be altering the surface structure of the filaments, albeit at an accelerated rate, and may therefore only provide a short term manufacturing solution.

### **3.3.1.3 Varying Concentration of Loading Solution**

As the previous section demonstrates, a loading solution of 10 mg/mL carvedilol in ethanol results in a relatively low filament concentration of 0.51% w/w. Based on the suitability of alcohols, as determined in Section 3.3.1.1, coupled with the increased drug loading achieved by Skowrya *et al.*<sup>81</sup> with a methanolic solution of prednisolone (1.9% w/w), investigation into varying the drug loading using a methanolic solution was carried out.

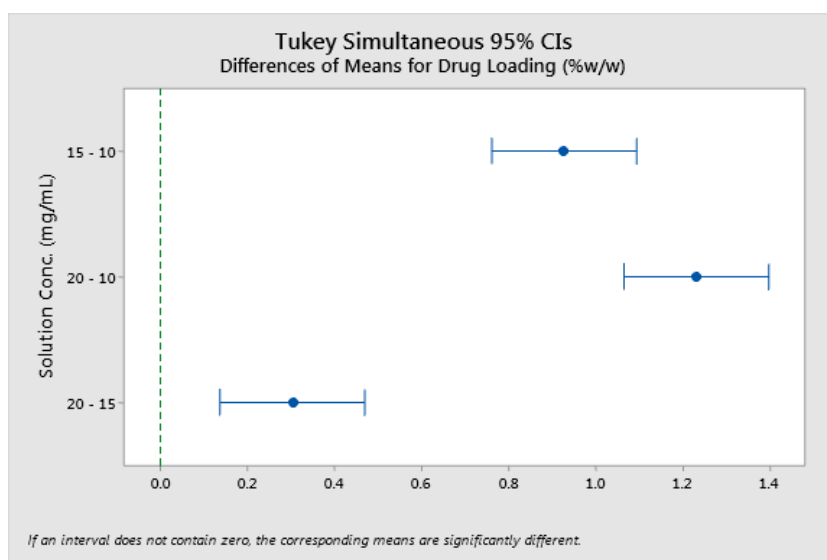
Three different solution concentrations were trialled: 20 mg/mL, 15 mg/mL and 10 mg/mL in order to investigate the effect this had on the drug loading of PVA filaments. The time for submersion was kept constant, and the samples were prepared as per the generic solution loading process outlined in Section 2.5.1. HPLC analysis was carried out in triplicate and an average drug loading calculated. The results are detailed in the table below:

**Table 21** - Filament Drug Loading Achieved from a Methanolic Solution of Carvedilol

Solution Concentration (mg/mL)	Average Drug Loading (% w/w)
10	2.35 ± 0.03
15	3.28 ± 0.10
20	3.58 ± 0.06

*n = 3, ± standard deviation*

It is clear that increasing the solution concentration of carvedilol in methanol does increase the drug loading of the resulting filament within the time period observed. An increase of 0.93% w/w was observed between 10 mg/mL and 15 mg/mL, and a smaller increase of 0.30% w/w was observed between 15 mg/mL and 20 mg/mL. Statistical analysis using a one-way ANOVA method was carried out to detect if these observed differences are statistically relevant and combined with Tukey analysis, to show which of these values show any differences from one another (Figure 36):



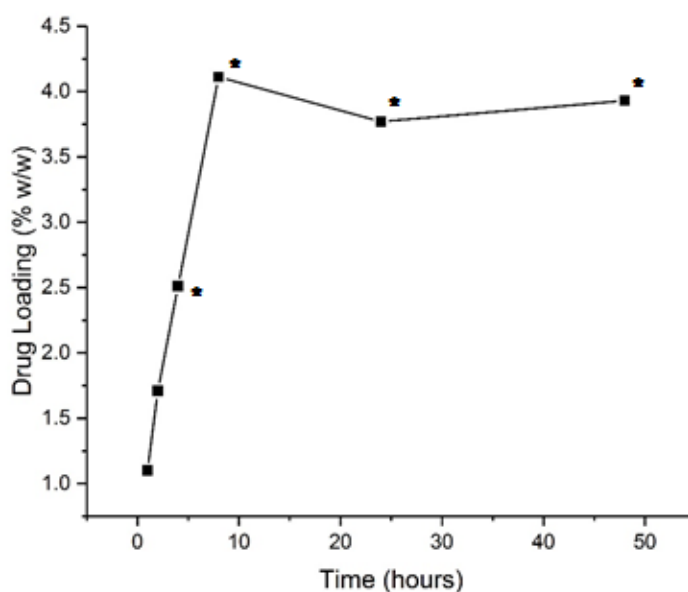
**Figure 36** - Tukey Analysis of Differences in Solution Concentration

Figure 36 is a visual comparison of the difference between the means under investigation at the 95% confidence interval. The y-axis shows which two means (in this case solution concentrations) are being compared and demonstrates how these differ from one another. As none of the intervals investigated contain zero, the drug loadings obtained from each of the different loading solutions are statistically different from one another. The diagram also shows there is less difference in the means of 15 mg/mL and 20 mg/mL, compared with the difference observed between 10 mg/mL and 15 mg/mL or 10 mg/mL and 20 mg/mL, and reiterates the findings mentioned above. Given that the increase observed between the latter two concentrations does not mirror that of the former two concentrations, there is little benefit to increasing the solution concentration further, as it would lead to large amounts of wasted material.

#### **3.3.1.4 Varying Loading With Time**

While adjusting the loading solvent concentration, and even the solvent itself, can affect the concentration of API within the polymer filament, the time allocated for solution loading may also result in various different concentrations of carvedilol within the PVA. By carrying out investigation into the drug loading at different time points, it is possible to pin-point an ‘ideal’ loading time using methanol.

Different loading times were selected (1, 2, 4, 8, 24 and 48 hours) in order to determine the loading efficiency. A 20 mg/mL methanolic solution of carvedilol was used, despite the smaller observed increase in concentration as determined in Section 3.3.1.3, in order to investigate the highest drug loading achievable at each time point. HPLC analysis of dried filaments from each time point is discussed below:



**Figure 37** - Variation in Drug Loading of PVA Filaments with Time. An asterisk (\*) is used to indicate filaments which failed to retain their structural integrity throughout the experiment.

The first two samples (after 1 and 2 hours) retained their structural integrity. The third sample (after 4 hours) contained a piece of filament which had split upon swelling, the other two retained their cylindrical structure. All other samples completely split after submerging for the allocated time, which will likely affect the depth the drug has penetrated into the filament. Those filaments which split are marked on the graph with an asterisk.

From the HPLC results, it is clear that there is not any added benefit from submerging the samples for any longer than 8 hours, as optimum drug loading is achieved after 8 hours. There is also an indication that maximum drug loading may only be achieved after enough swelling to result in splitting of the filaments, indicating that this may be an important mechanism in the drug loading process. This mechanism, however, has not been observed with any other solution loading of filaments in the literature<sup>80,81,106</sup> and therefore may only have prematurely increased the drug loading over that which would have been achieved through diffusion from the surface alone.

Based on these results, an optimum time length for solution loading can be selected, allowing for submersion of the filament at the start of the day, drying overnight, and printing the following day, saving time in the overall manufacturing process.

### **3.3.1.5 Varying Loading with Varying Pressure**

As a final effort to look at ways of altering/improving the solution loading process for filament production, high pressure was investigated. The specific aim of the experiment was to determine what effect the application of an external pressure of 8 kbar (7 metric tonnes) during the solution loading of carvedilol into PVA has on the filaments and the drug loading process as a whole. Previous work on metal-organic framework materials<sup>107</sup> and even organic systems<sup>108</sup> have indicated that pressure can enable solvent molecules to penetrate into the pores of a solid. As polymers are an inefficiently packed solid, it was reasoned that the application of high pressure may succeed in increasing the penetration of the API into the polymer. By using pressure both the solvent and solute are likely to penetrate the polymer. In addition to this there is the possibility that the solvent penetrates before the solute, thereby increasing the concentration gradient and inducing a driving force for the inclusion of the solute in the polymer. Through studies such as these, it is hoped that a better understanding of whether the overall drug loading can be improved, or loading time could be shortened can be gained, allowing for manufacture to become more efficient.

Three pieces of PVA filament were subjected to high pressure, while submerged in a 10 mg/mL methanolic solution of carvedilol. As a specific final drug loading of the filaments was not required, a lower concentration of loading solution was sufficient for the experiment. Three more pieces of PVA filament were used as a control sample and submerged in a 10 mg/mL solution at ambient pressure. Determination of drug loading was carried out by HPLC and results are discussed below:

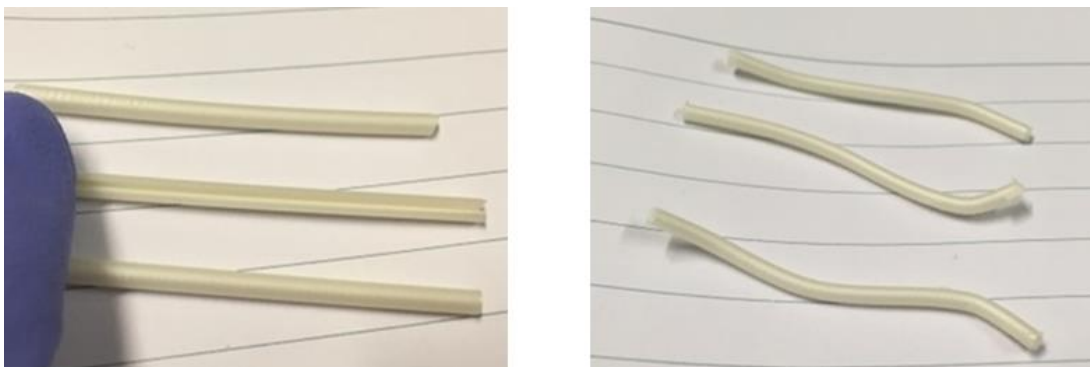


**Figure 38** – Left – Control Samples, Right – High Pressure Samples

Upon initial inspection of the filaments, there appeared to be some differences between the samples. The control samples had split and become very soft and flaccid, whereas the high pressure samples remained very rigid and had become curved in places. This is likely due to the high pressure preventing the filament from swelling and could result in limited drug loading.

HPLC analysis was carried out in order to determine drug loading in the different samples, resulting in average drug loadings of 1.63% w/w  $\pm$  0.10 (n = 3,  $\pm$  standard deviation) for the control samples and 0.41% w/w  $\pm$  0.19 (n = 3,  $\pm$  standard deviation) for the high pressure samples. It should be noted that the concentration observed for the high pressure samples fell out with the calibration range, and so is not accurate and can only provide a general idea of the drug loading for those samples.

The drug loading observed in the control samples was lower than expected for a loading solution of 10 mg/mL, in comparison to the previous drug loading of 2.35% w/w mentioned in Section 3.3.1.3. This could be due to the higher filament to solution ratio in the small loading tube used for the experiment, and brings about the question of whether the volume of loading solution can also have an effect on loading efficiency of PVA filaments, however no evidence of this effect was found in the literature and no further investigation was carried out into any effects caused by the volume of loading solution. Although the high pressure samples cannot be accurately quantified (as explained above), it is still possible to see that drug loadings are lower in filaments exposed to high pressure, regardless of the lower filament concentrations observed overall. It is likely that the high pressure inhibits the swelling of the

polymer, preventing adequate drug loading from taking place, and providing further evidence that the most important part of the drug loading mechanism is the swelling of the carrier polymer.

### **3.3.2 Production of 3D Printed Tablets**

#### **3.3.2.1 Production of Placebo PVA Tablets**

As mentioned in Section 2.3, circular tablets (diameter 10 mm, height 4 mm) were designed and employed in this research. Aside from varying the dosage by adjusting experimental conditions prior to printing, changing the infill of the tablet design provides an additional method for dose variation after the solution loading process.

The term ‘infill’ refers to the internal structure of the design itself, and can be adjusted between completely filled, and no fill, although larger designs require at least some infill in order to maintain structural integrity. The addition of ‘skirts’ is also an option, and allows for a small amount of material to be printed first, at a specified distance from the object, and surrounds the outline of the design being printed. This is useful for testing that the filament is feeding properly and exiting the nozzle correctly, prior to the commencement of the design printing. Three different infills are visible on the tablets shown in Figure 39, along with a skirt (positioned at an offset of 5 mm) surrounding the tablet itself, highlighting how the design changes with increasing infill percentage.

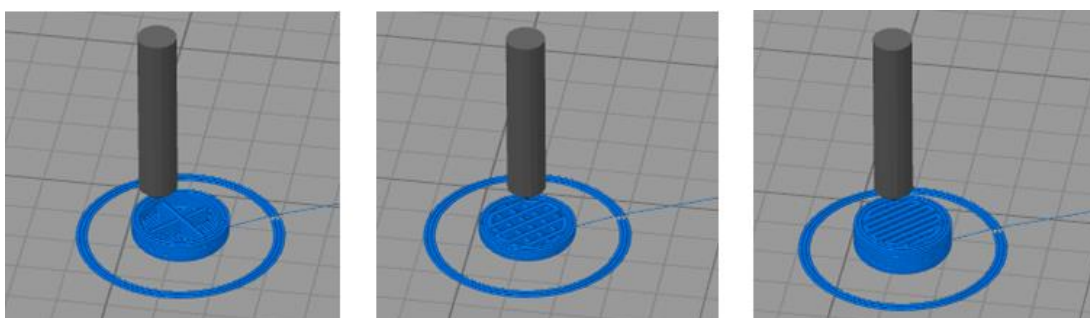


**Figure 39 - Left - 10% Infill Middle - 50% Infill Right - 90% Infill**

The recommended printing temperature for PVA is between 185°C-200°C,<sup>98</sup> although temperatures close to the upper limit of that range can result in clogging of the printer



nozzle with burned PVA residue as shown in Figure 40. Printing at 190°C was found to be the most suitable temperature and allowed for the feeding of filament and printing of tablets without any clogging.



**Figure 40** - Burned PVA removed from clogged printer nozzle

Other than issues with filament degradation, using PVA (as opposed to PLA or ABS which have a higher tolerance to heat<sup>109</sup>) presents problems with filament softness. This is especially evident when feeding PVA filament through the print head, as the Leapfrog Creatr HS is optimised for use with PLA and ABS and only typically employs the use of PVA as a support material rather than the primary polymer.

For the desired print designs to be pharmaceutically relevant, PVA is favoured over PLA and ABS due to its water solubility and biocompatibility. The sole use of PVA to produce tablets caused difficulties with feeding the filament into the extruder head and also resulted in jams around the gear wheels which feed the filament. This appeared to be a common problem when using soft filaments, but a solution in the form of a 'flex filament adaptor' had been designed by other 3D printer users, and submitted to 'thingiverse',<sup>110</sup> a publicly available online library of print designs:



**Figure 41** - 'Flex Filament Adaptor' design as found on Thingiverse

*Producing Drug Loaded 3D Printed Tablets via Solution Loading of PVA*

This adaptor was printed using PLA and a 2 mm wide hole was drilled down the middle in order for the filament to pass through. A 4 mm hole was made for the screw thread, the adaptor was then fitted and a tablet successfully printed (Figure 42 and Figure 43):



**Figure 42** - Flex Filament Adaptor Fitted at the Printer Gear Wheel

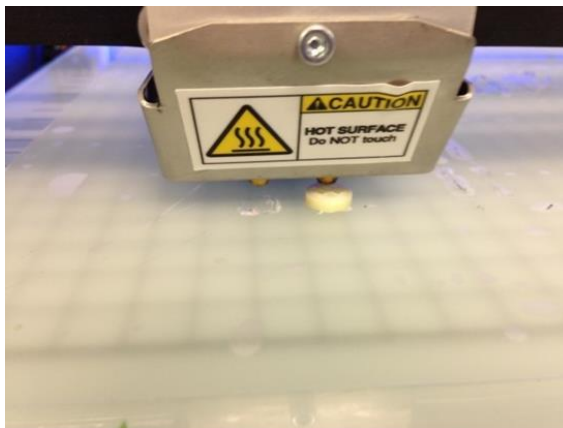


**Figure 43** - Blank PVA Tablet Print in Progress

This adaptor allowed for easy feeding of the filament, whereas prior to this, it was not even possible to load the filament properly. One tablet of PVA was printed and measured to see how closely the dimensions matched those in the design software, details shown in Table 22:

**Table 22** - Comparison of Blank PVA Tablet Dimensions

	<b>Software</b>	<b>Printed Tablet</b>
<b>Diameter</b>	10 mm	10 mm
<b>Height</b>	4 mm	3.5 mm

The discrepancy in height observed for the printed tablet would be unacceptable in the manufacture of pharmaceuticals, and it was also observed that there were problems with the PVA initially sticking to the print bed. The first couple of layers on the bottom of the tablet appeared to have not printed correctly, which explains the difference in height observed (Figure 44):



**Figure 44** - PVA Tablet with Bottom Layers Peeling Away

It is possible to see where the base appears to be peeling away slightly from the rest of the tablet (bottom left of Figure 44), which is not ideal and is likely to produce issues with incorrect dosing of tablets. When researching poor adhesion online, it appeared to be a common problem, with the solution being to raise the temperature of the build plate and enclose the printer (if possible) in order to retain the heat. Enclosing the printer was not practical in this instance, but the build plate temperature was raised from 40°C to 50°C in order to determine if this solved the ‘sticking’ problem.

Before printing again, the flex filament adaptor was examined to check for any abnormalities. Noting that the original adaptor did not fit smoothly into place, and the hole for the filament was slightly off centre, another adaptor was printed using PLA (Figure 45 and Figure 46):



**Figure 45** - New Flex Filament Adaptor with Correctly Positioned Hole



**Figure 46** - New Adaptor in Correct Position

Once in place, three placebo PVA tablets were printed side by side in order to test that the adaptor worked and to test if the printer could handle multiple designs at once. The results from this test can be seen in the image below:



**Figure 47** - PVA Placebo Tablets with 10% Infill

When printing with PVA, the filament often leaks out of the nozzle causing extra filament to be present when moving between structures. This causes extra deposits which disrupt the print design. While not particularly obvious in the first tablet (left) the second and third (middle and right) tablets did not retain their structural integrity and broke apart when removing from the build plate. Attempting multiple tablet printing again, using a higher infill setting in the design, may result in improved print quality, but given that the time saved to the overall manufacture would have been negligible in this instance, this was not investigated. There are articles available online from the Simplify3D® software company which provide advice on the simultaneous printing of multiple parts,<sup>111</sup> but the overall production of pharmaceutical designs via this method is still in its infancy and would likely require much more optimisation of other factors (e.g. nozzle temperature, print speed) before being able to confidently deliver larger batches of medication. The personalised nature of this manufacturing method and the target demographic for the final product would also be unlikely to benefit from large batches of the same dosage form, therefore research will be focussed on printing only one tablet at a time, with a view to optimising the manufacture of single tablets prior to any further larger scale production.

### **3.3.2.2 Production of Drug Loaded PVA Tablets**

Filament which had been soaked in a 20 mg/mL methanolic solution of carvedilol, and analysed by HPLC as having a drug loading of 3.58% w/w  $\pm$  0.06 (see Section 3.3.1.3) was used in the production of drug loaded tablets. Three tablets were printed with 30% infill and, based on the observations from printing blank tablets, each was printed one at a time before being weighed. The weight of each tablet was combined with the HPLC analysis of the filament, and used to estimate drug dosage in each tablet, as shown in Table 23:

**Table 23** - Variation in the observed and predicted tablet doses.

<b>Tablet Weight (mg)</b>	<b>Estimated Dose by Weight (mg)</b>	<b>Measured Dose by HPLC (mg)</b>
227.8	8.16	8.16
247.8	8.87	9.36
248.1	8.88	5.94

No specific target dose was selected, although a dose inbetween the current market range of 3.125 mg to 25 mg for immediate release was aimed for in order for the tablets to be pharmaceutically relevant. The latter two tablets were very close in weight, but the former weighed a little less. This was caused by inadequate sticking to the build plate of the first printed layer of the tablet, causing a slight reduction in weight. While the structural integrity of the tablet remained intact in this instance, care must always be taken to ensure layers are printing correctly in order to minimise weight discrepancies.

When HPLC analysis was carried out in order to measure the actual drug loading in each tablet, the first two tablets were within 0.5 mg of the expected dose. The last tablet, however, was almost 3 mg less than expected. Given the very cloudy nature of the solution when dissolving the tablet, it was very difficult to ascertain if full dissolution had been achieved, although further inspection, after HPLC analysis, showed that the tablet had not fully dissolved in the flask, so this provides an indication as to why there is a lower drug loading in the sample.

Given the destructive nature of HPLC as an analytical technique, any further analysis on printed tablets would require assumptions to be made about the dosage of tablets from HPLC analysis of the filament loading prior to printing. Given that the actual dose was within 0.5 mg of the expected dose, these loading values, combined with tablet weight, provide adequate means of dosage calculation without the need to analyse, and will therefore be the method of dose calculation for future experiments.

### 3.3.2.3 Dissolution of Carvedilol Loaded PVA Tablets

In order to determine the effect that changing the infill percentage had on the achievable dose and subsequent release of API from the dosage forms, tablets were manufactured at different infill percentages (Table 24):

**Table 24** - Variation of Dose by Infill Percentage

Infill Percentage	Tablet Weight (mg)	Estimated Dose by Weight (mg)
10% <sup>a</sup>	203.3	6.32
	204.7	6.37
	204.4	6.36
30% <sup>b</sup>	258.0	9.24
	235.0	8.41
	249.0	8.91
50% <sup>a</sup>	297.0	9.24
	296.0	9.21
	286.6	8.91
90% <sup>a</sup>	351.7	10.94
	349.7	10.88
	347.2	10.80

<sup>a</sup>Tablets produced from a filament with drug loading 3.11% w/w

<sup>b</sup>Tablets produced from a filament with drug loading 3.58% w/w

As expected, the weight and estimated dose gradually increase with increasing infill percentage, except when increasing from 30% to 50%. The similar estimated doses across these tablets are as a result of filament drug loading prior to printing, but any difference to drug release arising from changes to the infill percentage can still be monitored during dissolution analysis.

All tablets were subjected to dissolution analysis according to the method described in Section 2.8.2 (separate UV spectrophotometer with transfectance probe). The following release profiles were obtained (Figure 48):

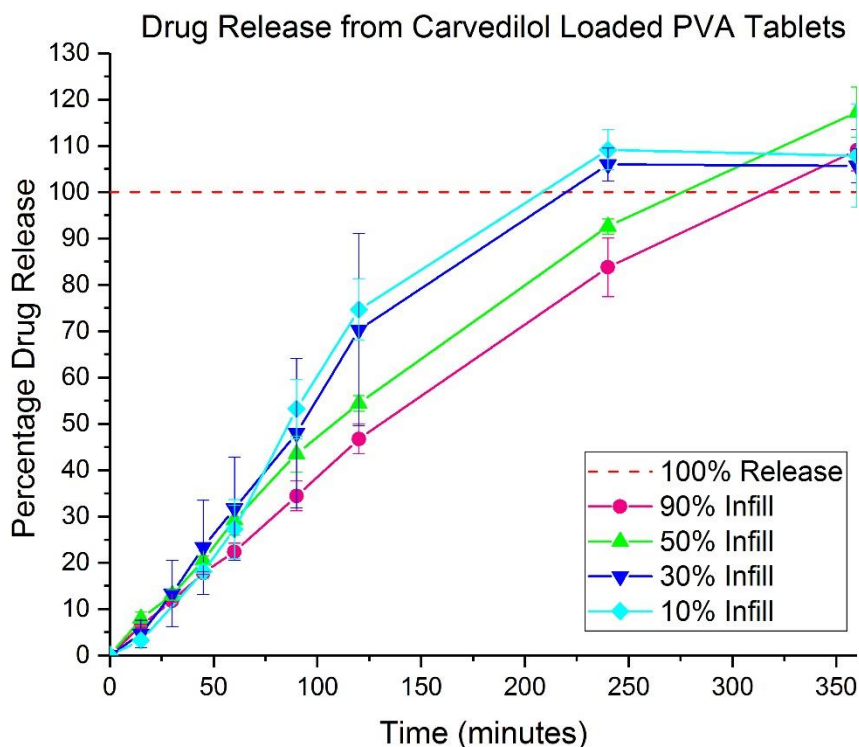


**Figure 48** - Drug Release from Carvedilol Loaded PVA Tablets (n=3) with a theoretical 100% release based on calculated drug content from filament loading and tablet weight.

From this data, it can be seen that all dissolution is complete after 360 minutes (6 hours), with dissolution complete after 240 minutes (4 hours) for both the 10% and 30% infill samples. There is no further increase in absorbance after this time point, indicating that there is no further increase in concentration. Ideally, the experiment would have been extended to include another few data points in order to confirm that no further increase in absorbance was detected, but lab time was limited and automatic sampling was not available when carrying out this experiment. It should be noted, however, that all tablets had completely dissolved by the end of the 6 hours, so no further increase in absorbance would be expected after this time point.

It can also be seen that each of the different formulations appears to have a different final level of release, all of which are over the theoretical 100% release, indicating that there is some degree of content variability within the polymer filaments prior to printing, making it difficult to estimate drug loading within the final dosage form. It



was noted in Section 3.3.2.2 that the variation in actual drug loading of a tablet, compared to that calculated from the filament, could vary by 0.5 mg, although this was only noted from a sample size of n=2. The variation between the calculated tablet drug loadings and those calculated from the six hour time point are therefore tabulated below in Table 25:

**Table 25** - Variation in Drug Loading between Filament and Tablet (n=3, ± standard deviation)

<b>Infill Percentage</b>	<b>Estimated Dose from Tablet Weight (mg)</b>	<b>Calculated Dose from Dissolution (mg)</b>	<b>Difference from Calculated (%)</b>
10% <sup>a</sup>	6.35 ± 0.03	6.85 ± 0.72	+ 7.87%
30% <sup>b</sup>	8.85 ± 0.42	9.35 ± 0.36	+ 5.65%
50% <sup>a</sup>	9.12 ± 0.18	10.70 ± 0.63	+ 17.32%
90% <sup>a</sup>	10.87 ± 0.07	11.85 ± 0.49	+ 9.02%

<sup>a</sup>Tablets produced from a filament with drug loading 3.11% w/w

<sup>b</sup>Tablets produced from a filament with drug loading 3.58% w/w

The difference in doses for the tablets with 10% infill are within the calculated standard deviation, and are therefore not different from one another. All other tablets have increased calculated doses compared to those estimated from the drug loading of the filament prior to printing. This would suggest that there is difficulty in controlling the dose within the filament, from which the dose is estimated, using this technique and the number of HPLC samples would need to be increased in order to provide more accurate estimates of filament drug loading. Methods of detecting drug distribution within these filaments and tablets would also be beneficial for confirming location of carvedilol in these formulations.

### **3.3.2.4 Analysis of Drug Distribution**

#### **3.3.2.4.1 Time of Flight Secondary Ion Mass Spectrometry (ToF-SIMS) Analysis**

In order to understand the distribution of API within the dosage forms, time of flight secondary ion mass spectrometry (ToF-SIMS) was used to detect differences on, and slightly below, the surface of carvedilol loaded PVA filaments and tablets. This has proved a successful method in the analysis of inkjet and 3D printed formulations from other groups,<sup>112,113</sup> therefore should apply to this work also.

Three different samples were analysed: the surface of a drug loaded filament, a cross-section of filament after 1 hour of submersion in drug solution, and the surface of a 3D printed tablet. This allows for comparison of drug distribution prior to and after printing, and highlights any changes which may occur as a result of the manufacturing process.

For the surface of the filament, extracted ion images were normalised against a total ion image, where the total ion intensity for a given pixel is calculated by the sum of all the ion intensities detected at that pixel. This is carried out in order to minimise any topographical effects.

Figure 49 shows these extracted ion images for PVA peaks corresponding to the polymeric repeating unit  $C_2H_4O^+$  and  $C_2H_5O^+$ , and the carvedilol molecular ion  $C_{24}H_{27}N_2O_4^+ [M+H]^+$ . The attached colour bars indicate the scale of relative ion intensity for each extracted ion image. Figure 49 also includes an overlaid image to compare ion distribution across the target area, with PVA shown in orange and carvedilol in blue:

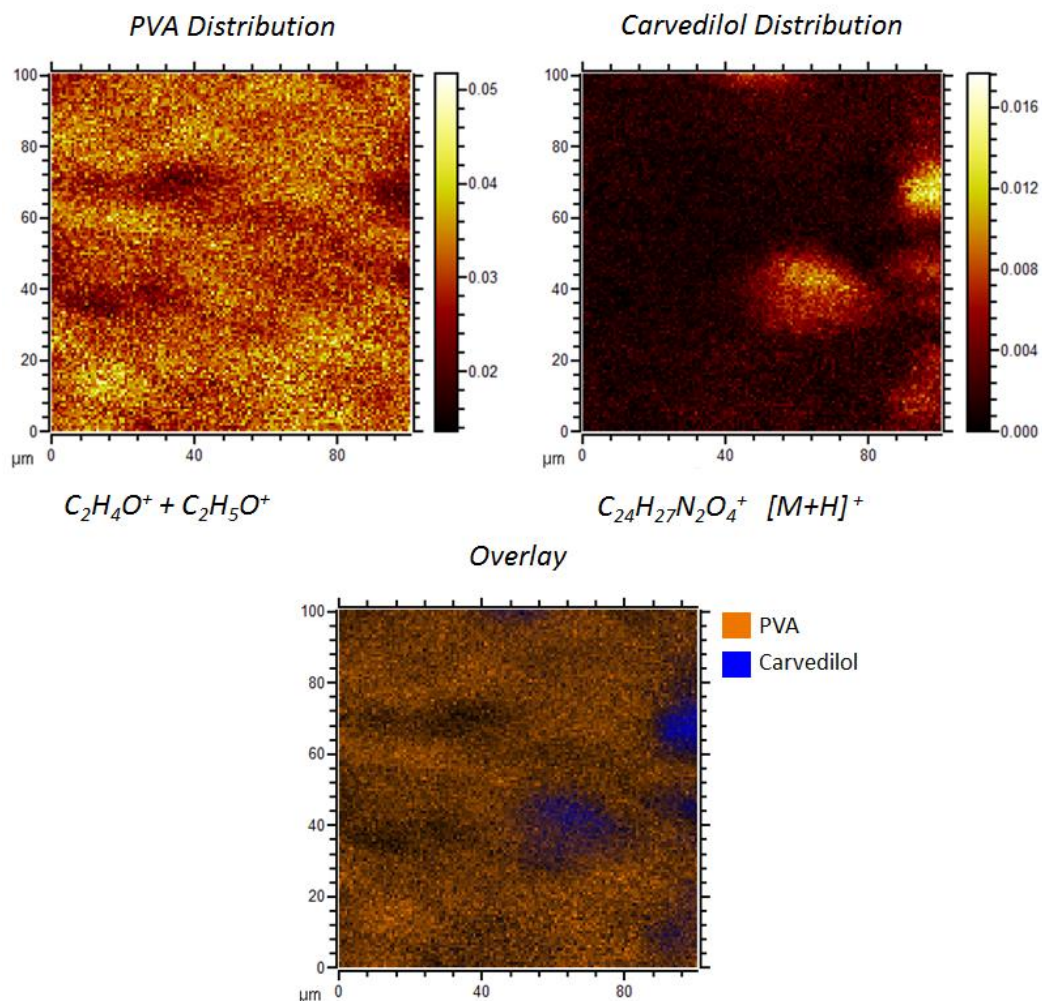


**Figure 49 - Top** - extracted ion images of PVA and carvedilol. **Bottom** - overlay of both components.

From these images, it is clear that the carvedilol is not well distributed across the surface of the filament and can be found in varying concentrations. This is also evident when looking at the results of depth profiling on this 100  $\mu\text{m}$  by 100  $\mu\text{m}$  area of filament. By using an argon cluster beam to remove surface layers of material from the sample, it is possible to see how the carvedilol content changes beneath the surface of the filament. Figure 50 shows a 3D overlay of carvedilol (blue) and PVA (orange) over the area under investigation. Figure 51 shows various slices of this 3D area, along with a graph showing the gradual decline of carvedilol the deeper into the filament the analysis is carried out. In both figures, the depth analysed is the same, and is represented as a cube in Figure 51 or as the more accurate flat image in Figure 50. To quantify the true depth under investigation, AFM analysis would be required.

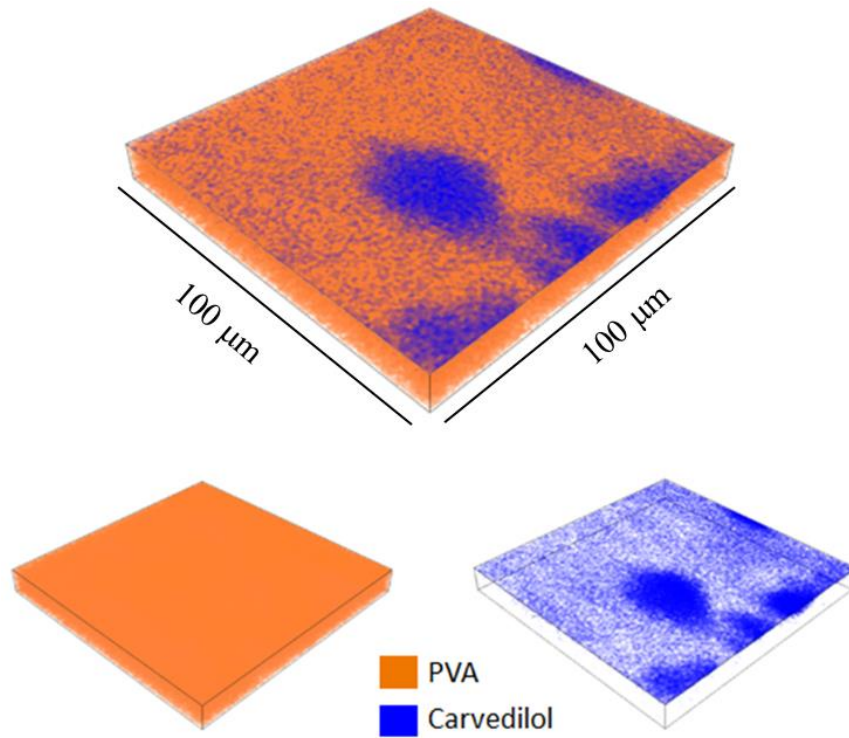


Figure 50 – 3D image of area under investigation

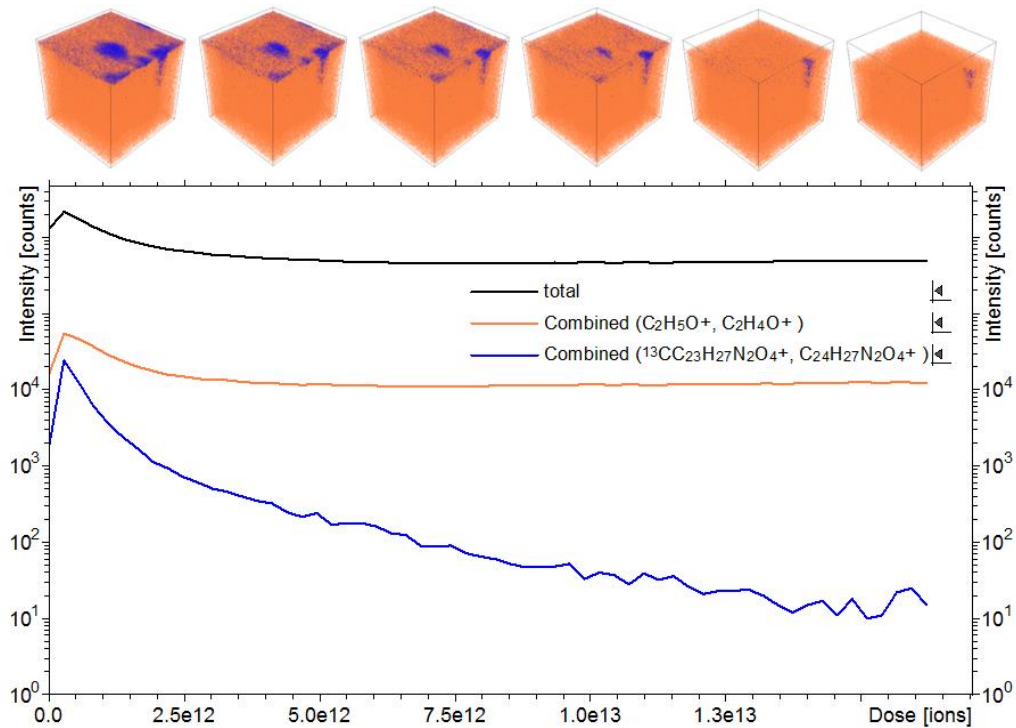
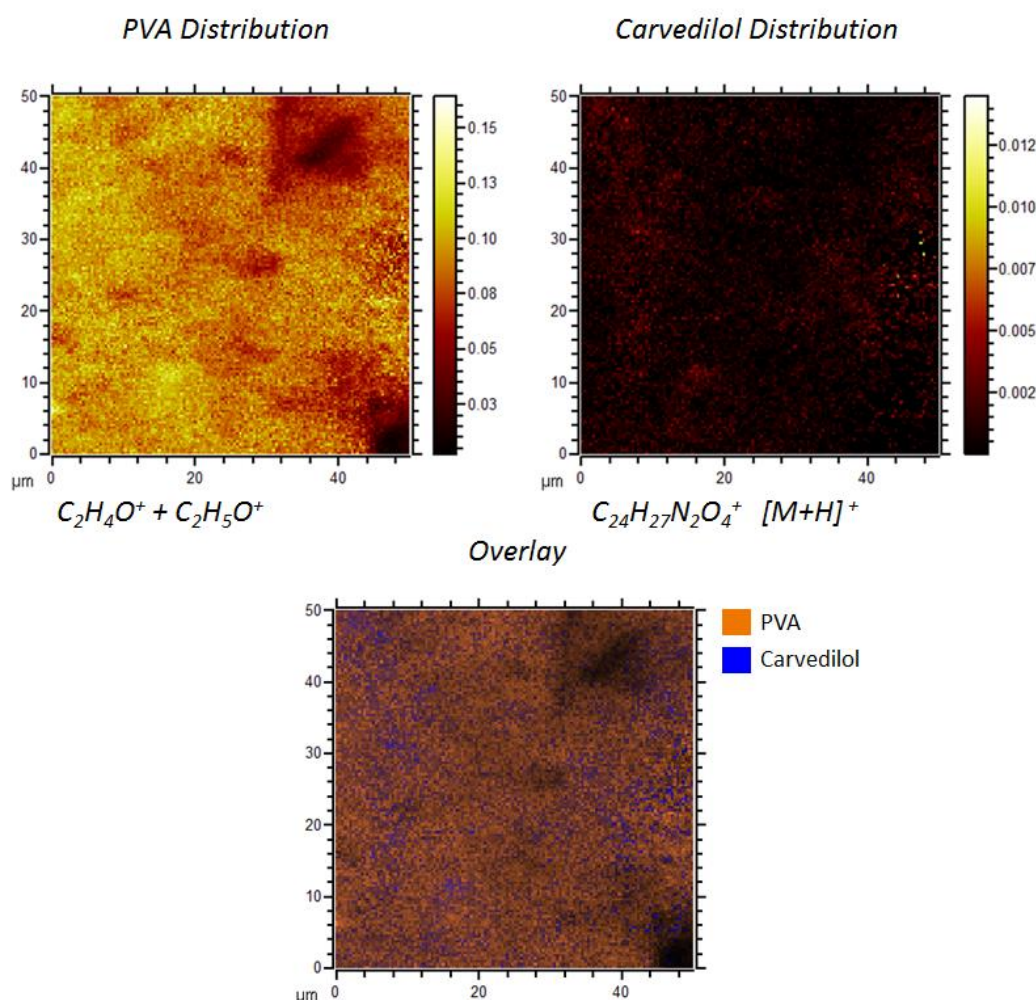


Figure 51 - Graph and images showing gradual drop in intensity of carvedilol across the entire surface as depth profiling analysis progresses.

Although it is not possible to quantify the exact depth analysed with just the ToF-SIMS, it is still possible to see that the API is mainly detected on the surface of the filament, which is to be expected given the nature of the loading process. The depth profiling also shows channels through which there is greater penetration of carvedilol, which could be due to defects in the surface of the polymer. This highlights the potential variation in drug loading throughout the filament and supports the HPLC and UV data discussed in Section 3.3.2.3.

As with the surface of the filament, the same analysis was carried out on the surface of the tablet, although over a smaller area of 50  $\mu\text{m}$  by 50  $\mu\text{m}$ . This was in order to deliver a higher dose of ions and increase the secondary ion counts for ease of detection. Extracted ion images, along with an overlay, are shown in Figure 52.



**Figure 52 - Top** - extracted ion images of PVA and carvedilol. **Bottom** - overlay of both components.

From these extracted ion images, it is clear that the carvedilol is much more evenly distributed in a tablet, than it is in the filament prior to printing. The carvedilol extracted ion image shows a relatively even distribution of the API and may suggest that there could be homogeneous distribution throughout the tablet itself, although it must be remembered that this is only over a  $50\ \mu\text{m} \times 50\ \mu\text{m}$  area, and not necessarily representative of the whole tablet.

Similarly with the filament, depth profiling was also carried out on the tablet over the  $50\ \mu\text{m} \times 50\ \mu\text{m}$  area under investigation. Figure 53 shows the flatter 3D image of the area undergoing depth profiling and Figure 54 shows this area represented in a cubic form, along with a graph showing the intensity of the components across this whole area as the profiling progresses.

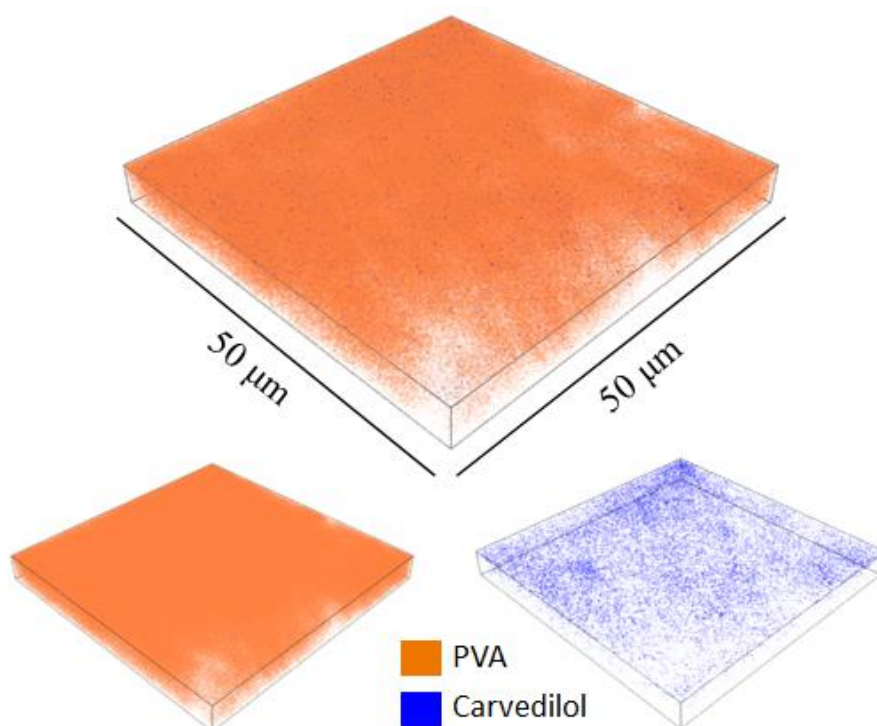


**Figure 53** – 3D image of area under investigation

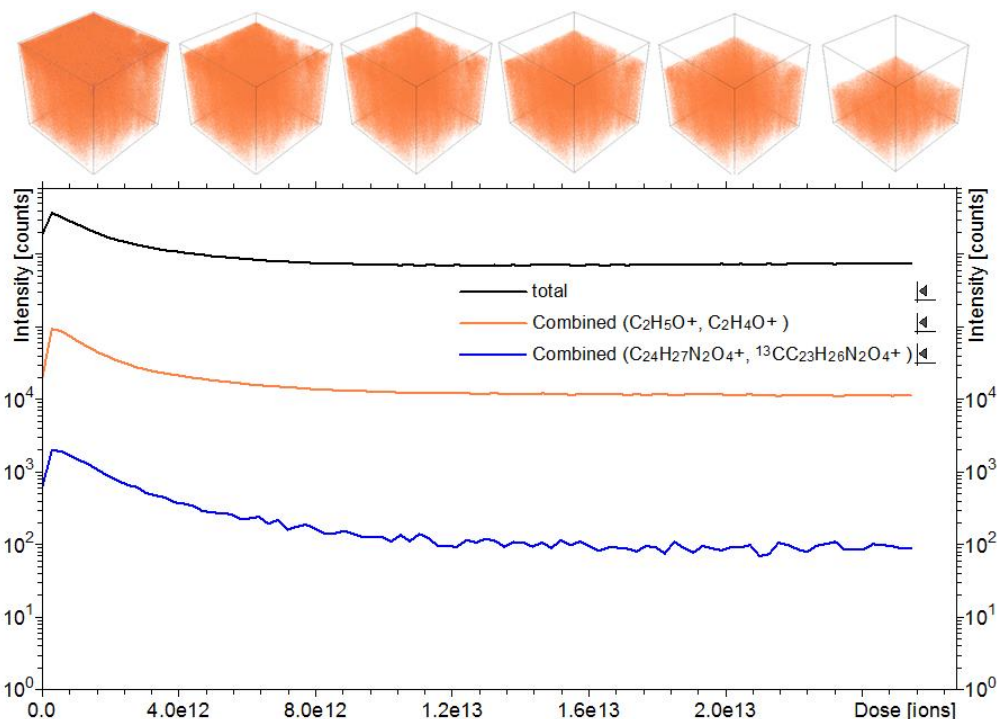


**Figure 54** - Graph and images showing intensity of carvedilol across the entire surface throughout depth profiling analysis.

From the graph, it would appear, at first, that the components are decreasing, but after normalisation with the total ion count (the black line), this is not the case. The flat 3D images show what appears to be an overall homogeneous distribution of API within the area analysed, but the drug loading was low (approximately 3%) and therefore difficult to visualise in the depth profiling images. It is also not possible to quantify the depth of the analysis without further investigation with a technique such as AFM, in order to determine the depth of the crater. Despite these limitations however, differences are observed between the filament and the tablet, and it can be concluded that homogeneity is not essential in the filament, as the re-melting during printing solves the distribution problem and demonstrates a homogeneous distribution of API within the tablet.

A cross section of filament from the 1 hour time point, described in Section 3.3.1.4, was also analysed in order to provide insight into how the drug penetrates the surface and why there may be variation in drug loading throughout the filaments. The images are a composite of smaller images, which build up the overall filament cross-section.

Producing Drug Loaded 3D Printed Tablets via Solution Loading of PVA

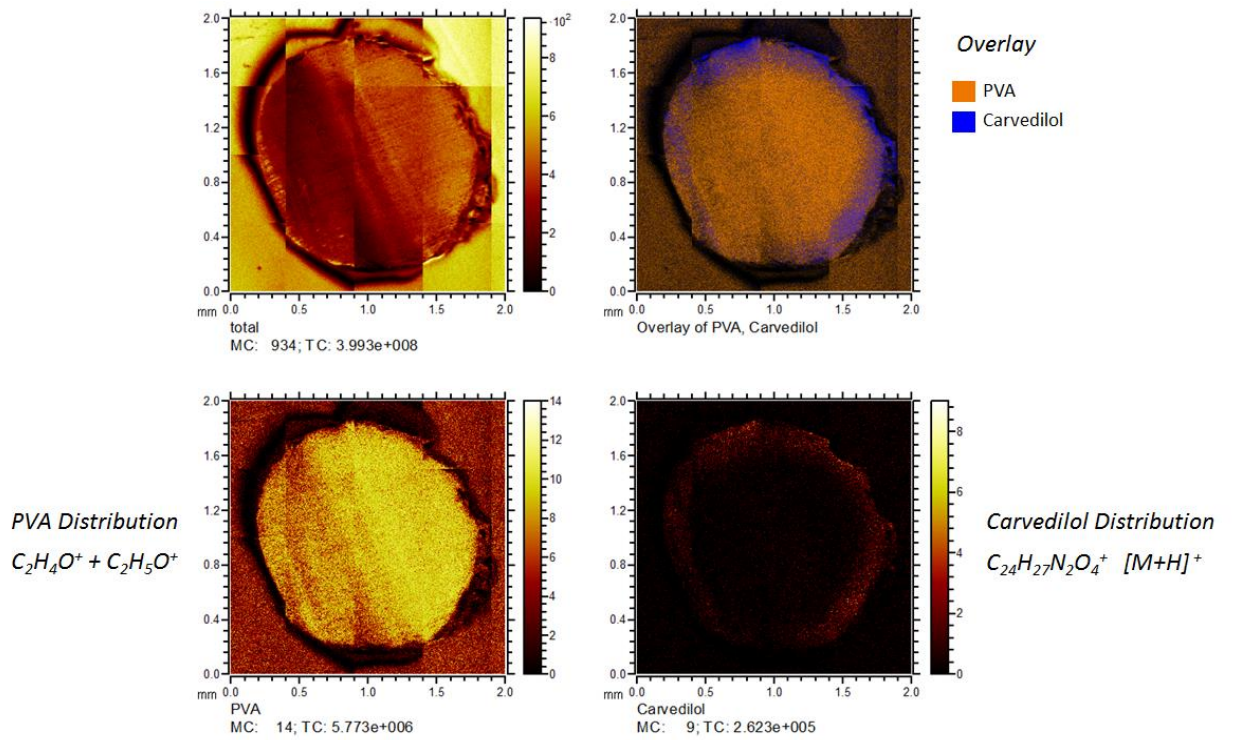


Figure 55 - Top left - total ion image Top right - Overlay of extracted ion images Bottom left - PVA extracted ion image Bottom Right - carvedilol extracted ion image

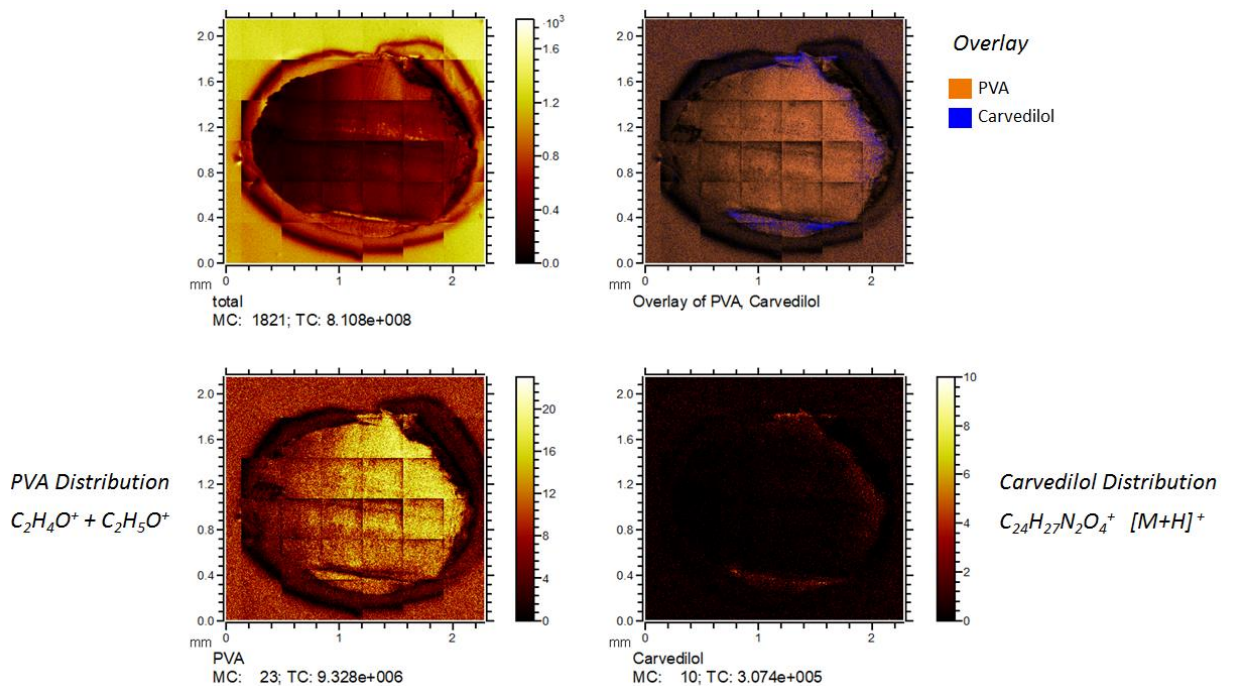


Figure 56 - Top left - total ion image Top right - Overlay of extracted ion images Bottom left - PVA extracted ion image Bottom Right - carvedilol extracted ion image



Figure 55 shows the distribution of drug across one cross-sectional area and Figure 56 shows the distribution over a second cross-sectional area. From these extracted ion images, it is clear that the carvedilol is not well distributed throughout the strand, and can be found mostly surrounding the outer edge of the filament. This is to be expected as the sample under investigation had only been submerged in a loading solution for 1 hour prior to the analysis being carried out. In both slices (most easily seen in the combined single ion images), there appears to be a greater concentration of carvedilol on one side of the filament, compared to the opposite side. This could be a result of the way in which the filament is resting in the flask during solution loading, and could demonstrate that drug diffusion is further hindered by contact with surfaces. Given that this analysis was from such an early time point, it is unsure whether the distribution of drug is 'corrected' the longer the filament is submerged in the loading solution, although analysis of the printed tablet suggests that distribution in the filament does not appear to affect homogeneity of drug distribution in the finished printed tablet. Depth profiling was not carried out on this sample, given that the cross-section itself gives a better idea of the drug penetration from the surface of the filament. No other 3D printed systems of this type have been analysed in this way and ToF-SIMS has been able to provide a novel insight into the drug distribution within solution loaded 3D printed dosage forms.

#### ***3.3.2.4.2 Raman Mapping for Analysis of Drug Distribution***

Given the small areas investigated when using TOF-SIMS ( $100\ \mu\text{m}^2$  for a filament and  $50\ \mu\text{m}^2$  for a tablet), Raman mapping was also used to assess drug distribution due to the increased area available for analysis ( $4\ \text{mm}^2$ ). Successful use of this technique has also been employed by Goyanes *et al.*<sup>114</sup> but this was in order to demonstrate separation of distinct areas designed to contain different drugs, rather than to investigate homogeneity of a single drug within a formulation.

Samples of a drug loaded filament and a printed tablet were both analysed, and black and white maps produced for both carvedilol and PVA, indicating where these individual components were located. Colour maps were then produced which combined the black and white maps, and allowed for visualisation of areas with high

or low drug loading. Results from the drug loaded filament are shown in Figure 57 (larger images available in Appendix 7.3.1 for easier visualisation), with PVA represented by green and carvedilol represented by red:

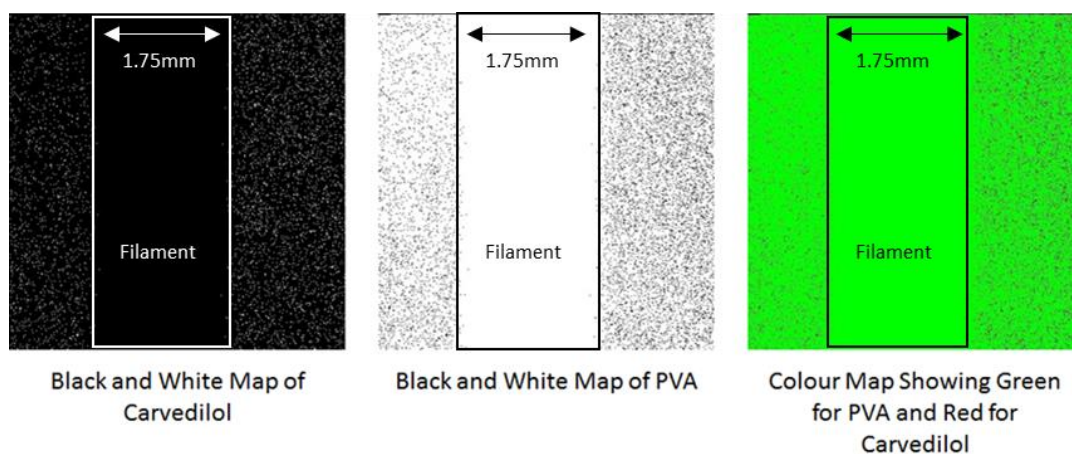


**Figure 57** - Raman maps of Carvedilol Loaded PVA Filament over a 4 mm x 4 mm area, with readings taken at 10  $\mu\text{m}$  intervals along the x and y axes.

The theoretical concentrations of PVA and carvedilol in both the filament and tablet were calculated as 97% w/w and 3% w/w respectively according to HPLC analysis, rounded to the nearest whole number. However, the measured concentrations calculated using the Raman map were 94% w/w and 3% w/w for the filament respectively. As can be seen from both the black and white, and the colour image, there seems to be some difficulty with actually analysing the filament. Not only does the measured concentration of PVA seem less, but the instrument also seems to be detecting drug out with the filament, rather than actually on the filament, where it should be. Given that the filament was so thin that there was obviously going to be void space on either side, which could be presenting difficulties with assigning Raman peaks, along with the nature of the curved filament surface impacting on the light scattering. Another limitation of this technique is the fact that it assigns a colour to a pixel based on whether the Raman peak referring to the analysed compound is either present or absent, rather than the concentration of the compound. Therefore from visual analysis of the filament map images, it would appear that there was drug scattered over the glass slide, which was not the case for these experimental set ups.

This effect has been observed previously in fenofibrate and PVP K30 samples produced by aerosol jet printing.<sup>57</sup>

Results from the analysis of a drug loaded PVA tablet are shown in Figure 58 (larger images available in Appendix 7.3.2 for easier visualisation) with PVA again represented by green and carvedilol by red:

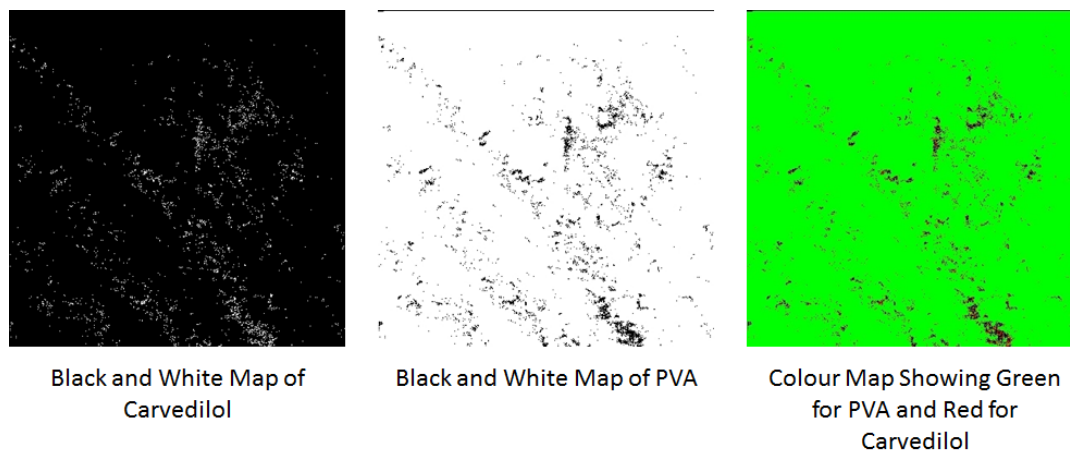


**Figure 58** – Raman maps of Carvedilol Loaded PVA Tablet over a 4mm x 4 mm area, with readings taken at 10  $\mu$ m intervals along the x and y axes.

With the analysis of the printed tablet, the measured concentrations of the components calculated using the Raman map were 97% w/w for PVA and 2% w/w for carvedilol. This was improved over the filament measurement as the tablet fit within the area under analysis and therefore did not incorporate any void space. The carvedilol content measures slightly less than expected, but this could again be due to the difficulty in assigning pixels mentioned above. It has also been shown that this technique struggles to identify amorphous material,<sup>57</sup> but this is difficult to determine in this case due to the lack of amorphous carvedilol standard prior to analysis.

Analysis would also have been improved if the tablets could have been sheared using the attached LAB-Pillerator, as this would have allowed for the visualisation of a 3D distribution of API within the printed tablet and would have given a better idea of overall drug distribution and whether this distribution is homogeneous. Unfortunately, this technique is better suited to tablets produced via compression as the 3D printed tablets appeared too hard for the instrument to slice. Meng *et al.*<sup>115</sup>

have successfully applied this shearing and 3D mapping technique to the visualisation of paracetamol in polyvinylpyrrolidone (PVP) tablets produced via continuous granulation and direct compression, and were able to show the variation in distribution of components throughout their system.

Regardless of the lack of 3D visualisation, analysis of the tablet does however show that there is a pattern to the drug distribution, which is not seen on the smaller scale used for TOF-SIMS analysis. Due to the method of manufacture for 3D printed tablets produced by fused filament fabrication, which creates parallel lines and leads to a surface which is not completely flat, it is unclear whether the map shows a completely accurate representation of drug distribution. Areas which dip slightly on the surface may be presenting as areas which don't contain any drug, but this is difficult to investigate further without the ability to shear this uneven surface away. Overall, TOF-SIMS would suggest a homogenous drug distribution over a 50  $\mu\text{m}$  by 50  $\mu\text{m}$  area, but when zooming out to the 4 mm by 4 mm area measured here, a less than homogenous distribution is observed, with the drug mainly concentrated along the lines created by tablet manufacture.

### **3.3.2.5 Analysis of Filament and Tablet Structure**

Both filament and 3D printed tablet were analysed to provide greater detail on their overall structure using X-Ray nano-computed tomography (nano-CT). Nano-CT analysis detects subtle differences in the density of samples due to differences in attenuation of the X-Ray beam, and these differences in attenuation allow for the detection of voids within these samples, making this a useful tool for analysing porosity within filaments and tablets. If subtle differences in density also correspond to differences in drug loading, this tool could provide complimentary analysis to that obtained by ToF-SIMS and Raman mapping.

A drug loaded sample of filament, and a placebo PVA filament underwent analysis by securing each inside a plastic straw, which prevented any movement of the filament, and the results are shown below in Figure 59.

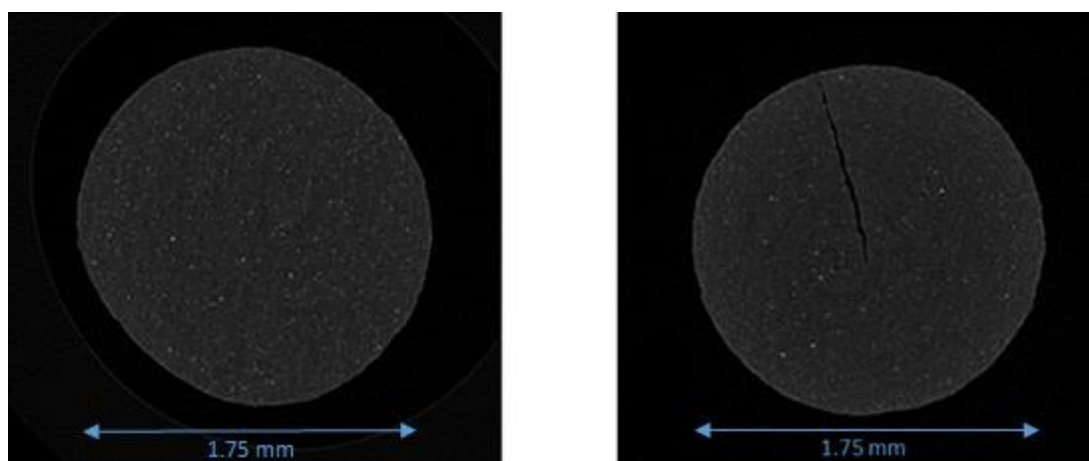


**Figure 59 - Left - Placebo PVA Filament Right - Drug Loaded PVA Filament**

From the image, you can clearly see where the filament split during the loading process. After drying, this split was difficult to see again with the naked eye, but is easily identified using this technique. The images also show areas of high and low density (light and dark areas respectively), which could indicate areas of high and low drug loading, however these are present in both the blank and drug loaded samples, as was observed by Alhijaj *et al.* in similar research.<sup>116</sup> This suggests that the differences in density are not due to drug particles, and may instead be caused by metal inorganic contaminants in the PVA filament.<sup>117</sup>

It was therefore reasoned that while nano-CT has the ability to provide visualisation of defects that would be difficult to detect with the naked eye, it is not a useful technique for analysing drug distribution for this manufacturing process. It was also thought that a lack of crystallinity, which can be confirmed using XRPD and DSC analysis, coupled with similarity in density of the organic materials analysed, means that any differences that may arise due to drug distribution would be too small to significantly contrast against the bulk material. The use of a heavier/inorganic compound in the loading process, to substitute the presence of drug particles, may provide insights into the distribution of compounds after using the solution loading manufacturing procedure, but this would not be representative of the API under investigation and would not necessarily demonstrate any further understanding than that obtained for the cross-sectional TOF-SIMS analysis.

Despite this inability to detect differences in drug loading, Nano-CT is a useful technique for the internal visualisation of samples, as can be seen with the split in the drug loaded filament (Figure 59) and with printed tablets (Figure 60):

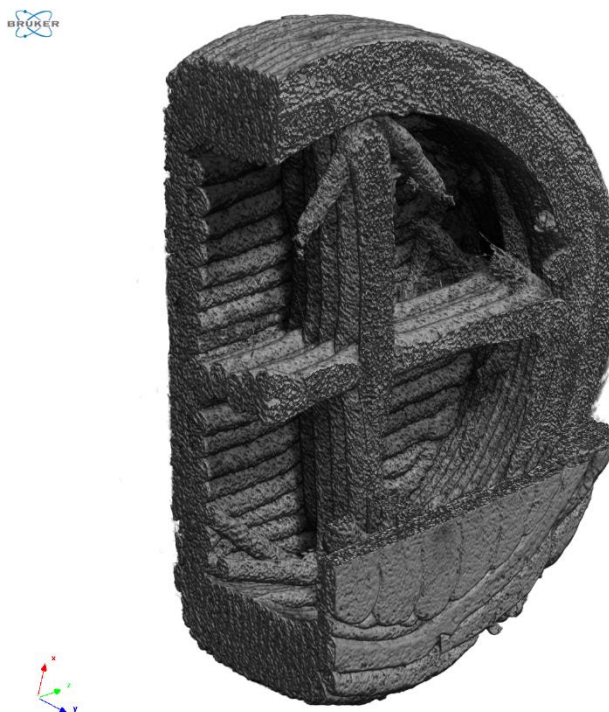


**Figure 60** - Nano-CT analysis of 3D Printed Tablet with 10% Infill

The internal ‘rectilinear’ design is clearly visible, but it is also possible to distinguish areas which stray from this design, and can therefore be used as a way to detect imperfections in the finished printed tablets. This could be used to help explain any discrepancies in the calculated drug loading of tablets (Section 3.3.2.3), although, as drug loadings are usually within 0.5 mg of the expected dose, it is likely that this technique may only serve to aid in quality control aspects of manufacture.

### **3.3.2.6 Determination of Crystallinity**

#### **3.3.2.6.1 X-Ray Powder Diffraction (XRPD)**

In order to determine the level of crystallinity of the API within the printed tablets, XRPD analysis was carried out on samples of pure drug, blank polymer filament, drug

loaded polymer filament and a drug loaded printed tablet. Results from this analysis are shown below (Figure 61):

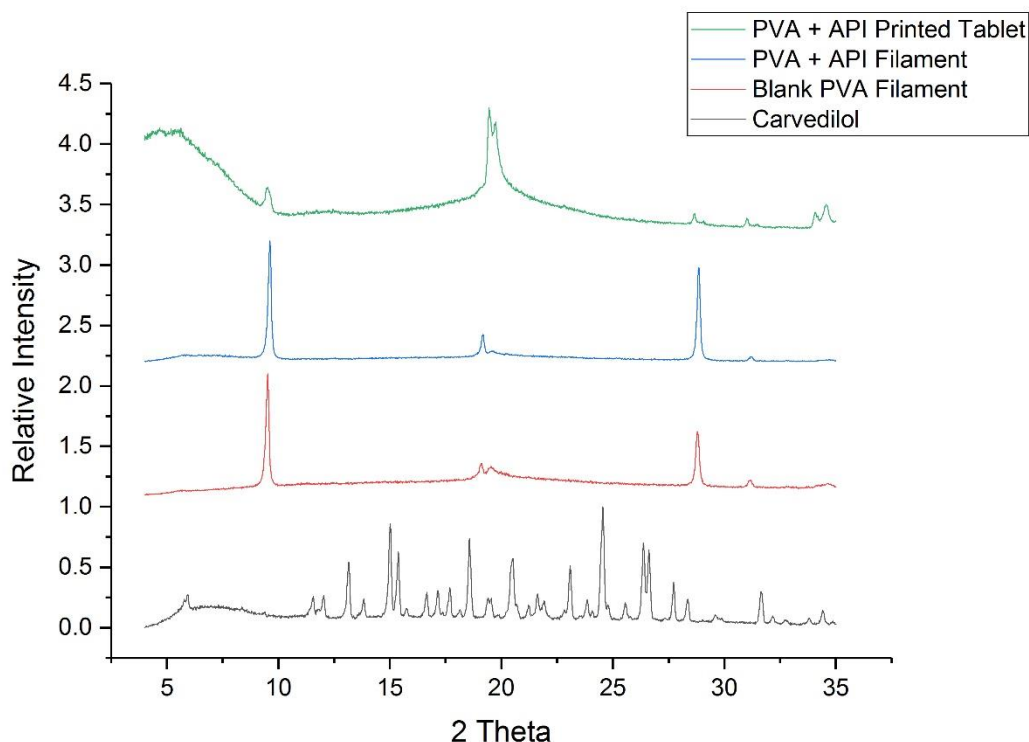


**Figure 61** - XRPD Analysis from Solution Loading of PVA Filament

It is not possible to clearly see any peaks corresponding to carvedilol in any of the drug loaded samples, but some features common to PVA are still present. This could either mean that the drug is present in an amorphous form, nanocrystalline form, or that there is not enough drug present in either sample to display crystalline peaks. Analysis with a technique such as high-energy X-ray total scattering coupled with pair distribution function analysis could be used to further investigate any amorphous or nanocrystalline material present,<sup>118</sup> but this was not carried out on any of these samples in favour of using DSC for complimentary analysis instead.

### 3.3.2.6.2 *Differential Scanning Calorimetry (DSC)*

DSC analysis was also carried out on samples of pure drug, blank polymer filament, drug loaded polymer filament and material that had passed through the extruder head of the printer. It is impossible to grind up a full tablet for analysis, but material which

has been passed through the print head, but not printed, will have been exposed to the same conditions as a printed tablet. Results are shown below:

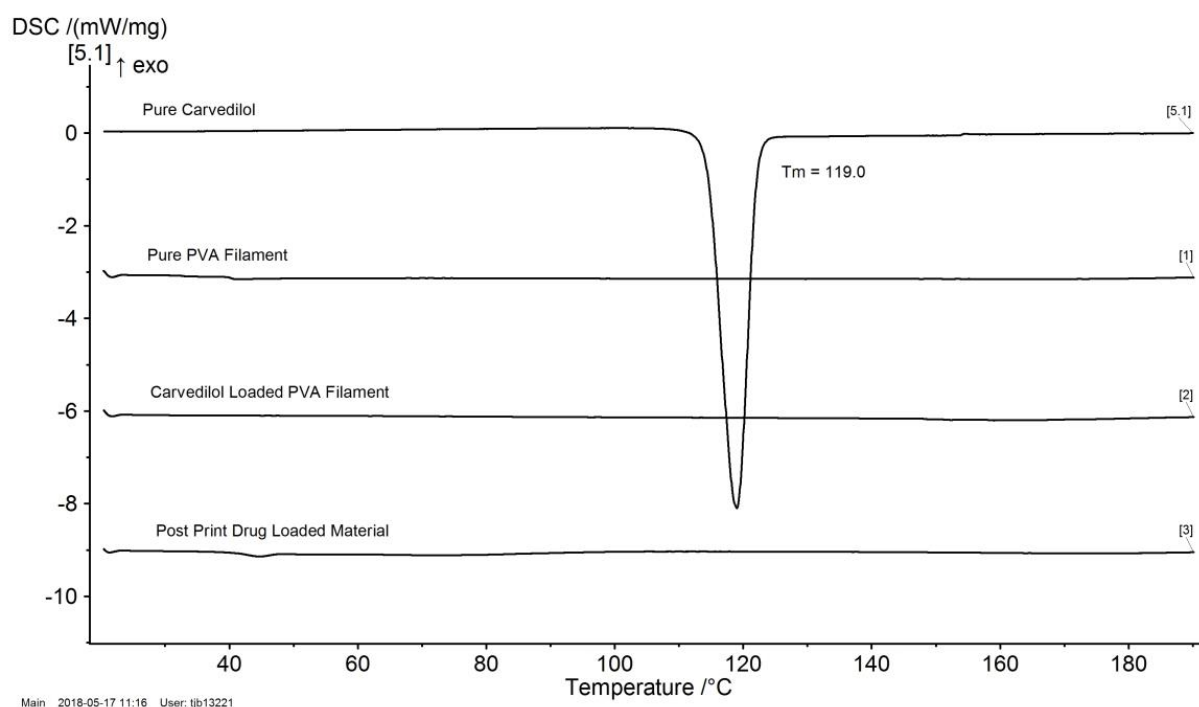


**Figure 62** - DSC Analysis from Solution Loading of PVA

In the DSC trace for pure carvedilol, one sharp melting peak is observed at 119°C, which corresponds to the melting of carvedilol form II.<sup>119</sup> No peak corresponding to carvedilol is present in either the drug loaded filament or the post-print material, suggesting that the drug may be present in an amorphous form. This matches the literature for the solution loading of PVA filaments with either prednisolone<sup>81</sup> or aminosaliclylate<sup>102</sup> where the model drug, in both cases, was not detected by DSC after loading of a PVA filament.

### **3.3.2.7 Surface Morphology**

In order to investigate surface morphology of the samples, scanning electron microscopy was used to obtain images of both filament and tablet. Results are discussed below (Figure 63):



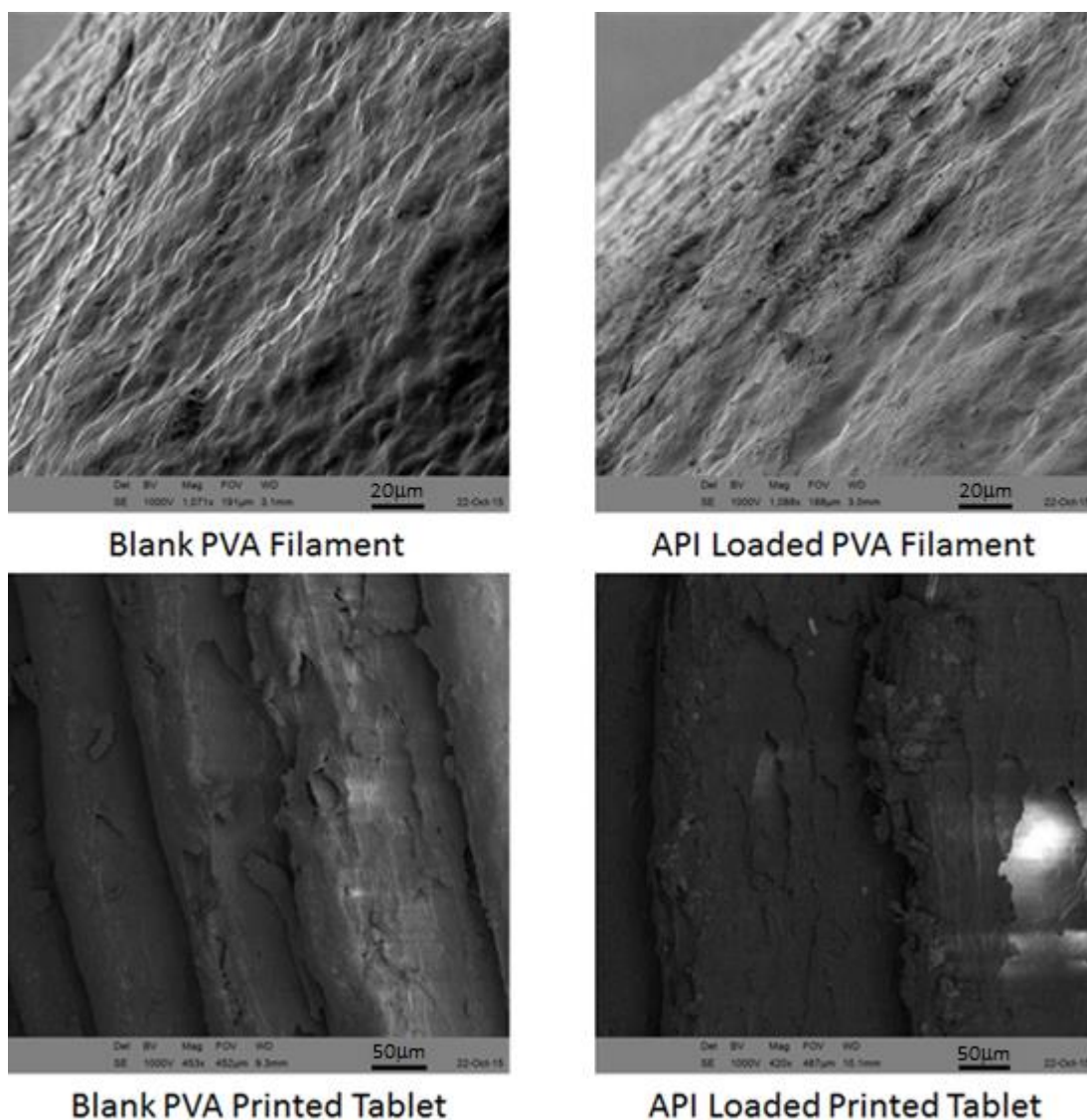


**Figure 63** - SEM Analysis of Filaments and Printed Tablets

When comparing the filament samples, there doesn't appear to be a huge amount of difference between the blank and drug loaded filaments. Both have relatively smooth surfaces, albeit with small bumps distributed across the surface. When comparing printed tablets, again, both samples appear very similar, but subtle differences can be observed. At the edges of the printed tablets, it is possible to see different printed layers due to the slightly curved edge of the tablet design. These appear much smoother in the blank tablet when compared to the drug loaded tablet. This is likely due to residual solvent present in the drug loaded sample, which has rapidly evaporated on printing. Residual solvent is also the likely cause of a 'popping' noise heard during

printing, and also the much softer nature of the drug loaded filament when compared to the blank PVA filament. Further care should be taken during the loading process to ensure that the filament is as dry as possible, in order to minimise any damage which could occur as a result of rapid evaporation of residual solvent.

### **3.4 Conclusions and Next Steps**

The work carried out in this chapter has facilitated, for the first time, the manufacture of a 3D printed carvedilol tablet produced via a solution loading method. From the various experiments carried out to investigate drug loading of filaments, tablets and overall scalability of a solution loading drug printing method, this research has provided several conclusions. With regards to specific experimental conditions, when considering the initial loading aspect of manufacture, the following conclusions can be made:

1. Increasing drug loading by evaporation, a technique that has not been previously investigated in the literature, is not a viable method and is far too difficult to control. The damage inflicted on filaments loaded under evaporative conditions results in non-viable materials for further manufacture and halts the process before printing can even occur.
2. Varying the concentration of the loading solution can allow for selection of different drug loadings, but becomes more limited as the solution concentration increases. The optimal length of time for solution loading is 8 hours in a 20 mg/mL methanolic solution of carvedilol, further than this, no increase in filament drug loading is observed.
3. Methanol is the most suitable loading solvent from those investigated for this system, but it should be noted that any residual methanol could have an impact on approval for this manufacturing method given that the permitted daily exposure (PDE) limit for methanol is 30 mg/day.<sup>120</sup>
4. For the first time, the use of high pressure was investigated as a way to increase drug loading, but was found to not offer any added benefit to the process. Instead, high

pressure hinders the overall drug loading as a whole, with results suggesting that the mechanism of incorporation of drug within the filament is by swelling of the polymer, a process that is restricted within the high pressure environment.

When considering the use of these filaments in the production of final dosage forms, these further conclusions can also be made:

1. When printing with filaments such as PVA, a 'flex filament adaptor' is required in order for the filaments to be successfully fed through the gear wheels of the printer. This is due to the soft nature of these filaments, which are easily misshapen by the feeding mechanisms prior to extrusion through the print head.
2. Due to oozing from the print head, only one tablet should be printed at a time in order to preserve its internal structure, meaning that there is an impact to the speed and efficiency of this manufacturing process as a whole.
3. When using methanol as a loading solution, an estimated dose range of between 7-12 mg can be achieved, which is within the marketed dose range of 3.125 mg and 25 mg for immediate release carvedilol formulations, but does not cover the upper or lower limits of this range. When considering if this could be applicable to other APIs, solution loading results in quite a narrow dose range and would be unsuitable for very high or very low dose drugs currently on the market.
4. Sustained release is the overall mechanism of release for these formulations, with dissolution complete after 4 hours for tablets with 10% or 30% infill, and after 6 hours for tablets with 50% or 90% infill. This means that the dose range of 7-12 mg previously mentioned as being within that required for immediate release formulations is almost outwith the controlled release range of 10-80 mg, and only covers the lowest of carvedilol's controlled release marketed doses.
5. Drug distribution within the filament itself was found to be non-homogeneous and concentrated mostly on the surface, or occasionally deeper within through defects on the surface, making accurate dose prediction of tablets very difficult. While the printing process appears to 'smooth' this effect, with homogeneity observed on a small

scale in the tablets, the API seems to be concentrated in distinct patterns following deposition of material during printing when observed on a larger scale.

6. Crystallinity appears to be removed through the processing involved in this technique, but further work would be required to determine the limits of detection, given the low drug loadings observed, and whether this impacts the dissolution and observed release of API from these tablets.

Overall, the solution loading method of manufacturing 3D printed tablets presents a way by which different doses of medication can be manufactured, although it does have its limitations with dose range and associated release mechanism to cover that small range. The low drug loadings obtained using this method would be ideal to match some of the doses available for immediate release formulations, but the observed dissolution profiles, when using PVA as the carrier polymer, result in sustained release only. The flexibility of being able to adjust print settings and infill percentage however, allows for the last minute selection of different tablet doses from the same starting material, a property which could be useful in the application of point of care manufacture, should approval of this manufacturing process be granted.

Future work will focus on extrusion as an alternative method for loading API, which would potentially allow for greater dose flexibility, and the option for additives which aid dissolution also to be included in the filament. This will likely produce a greater dose range and lead to a more viable route of manufacture for scaleable oral dose formulations.

## **4 Drug Loading of Polymer Filaments via Hot-Melt Extrusion**

### **4.1 Introduction**

While chapter 3 introduced the manufacture of varying doses of carvedilol via the solution loading and 3D printing of PVA based tablets, this was limited to a sustained release mechanism with a lack of dose variation which only achieved the lower end of the 10-80 mg range required for such a release.

Hot-melt extrusion has the ability to increase the drug loading of API within the polymer matrix,<sup>87,121</sup> which could therefore increase the amount of potential dose variation. Extrusion also allows for the inclusion of various other additives which may aid the disintegration, dissolution or ‘printability’ of the formulations themselves, which could provide access to immediate release formulations, rather than being limited to the sustained release observed from solution loaded formulations. There is also a greater range of polymers available for formulation, rather than being limited to off-the-shelf PVA filaments produced prior to solution loading experiments.<sup>116,122</sup>

This chapter investigates the manufacture of carvedilol loaded hydroxypropyl methylcellulose (HPMC, Affinisol™ 15LV) tablets, and various attempts to alter the release rate of these formulations from sustained to immediate release.

### **4.2 Aim**

The overall aim for this chapter was to successfully develop a method for manufacture of varying doses of carvedilol tablets, similar to the previous chapter, but with increased drug loading variation, which could match the dose ranges available on the market, and provide access to immediate release formulations in addition to the sustained release observed in Chapter 3. Control over dosing was intended to be achieved via careful blending of polymer/API/additive mixtures prior to hot-melt extrusion to produce a filament, and further changes to the tablet design during manufacture. Analytical techniques were applied in order to understand drug distribution and drug release from these non-conventional dosage forms.

## **4.3 Results and Discussion**

### **4.3.1 Extrusion and Milling of PVA**

In order to provide a link between extrusion experiments, and the work carried out with solution loading experiments, PVA was selected as a suitable polymer with which to begin investigation. Although this would likely not change the release mechanism from the sustained release observed in the previous chapter, larger drug loadings could potentially be achieved, with the possibility of also including additives to improve the release rate further.

PVA filament, suitable for use with a variety of 3D printers, was pelletised and fed into an 11 mm hot-melt extruder. This was carried out without the presence of any API in order to determine suitable extrusion parameters for the polymer alone. After six successive trials at various experimental conditions (Section 2.6.2), a filament with diameter ranging from 1.6-1.7 mm was produced (Figure 64).

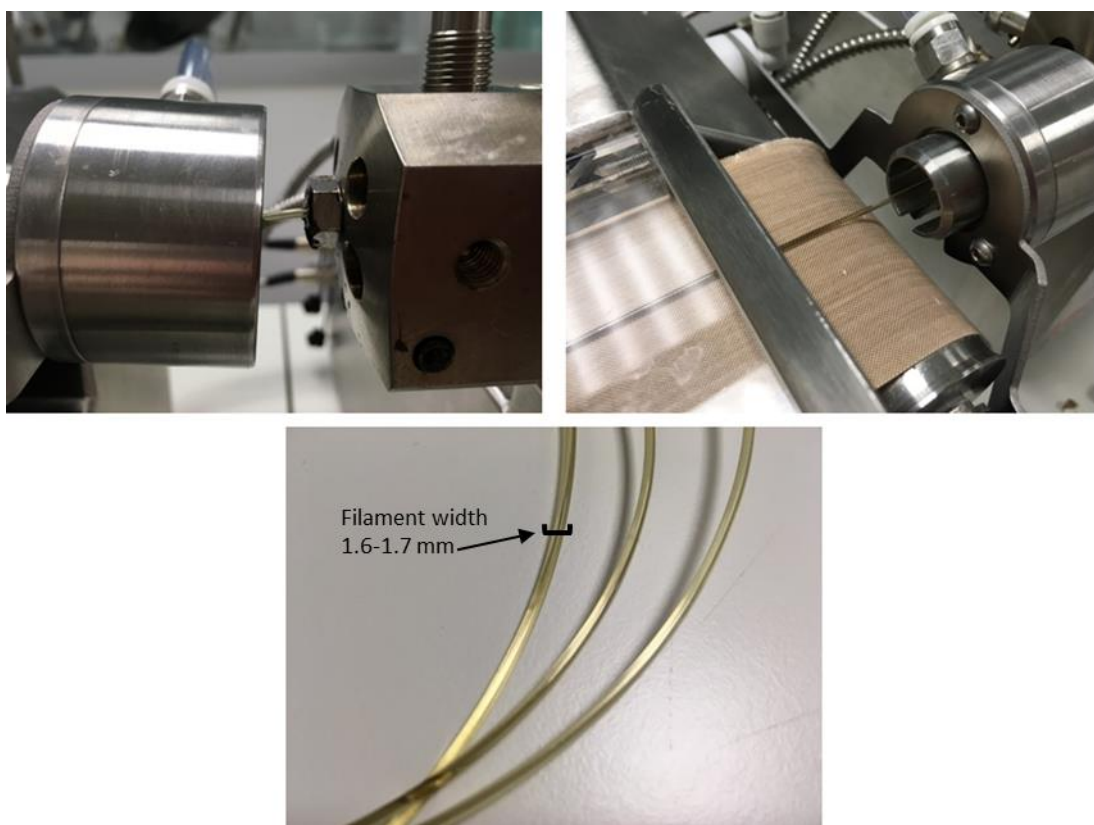


**Figure 64-** Extrusion of Pelletised PVA Filament

Despite the apparent success of this extrusion experiment, only a small amount of filament could be collected before the feeding port of the extruder became blocked with material. Upon inspection, it appeared that the size of the pellets was limiting the ability of the screws to carry material into the extruder barrel at a consistent rate for a filament with homogeneous diameter to emerge from the die. As the PVA feedstock had already been pelletised at the smallest limit for the pelletiser's capability, milling was investigated as a method to further reduce the size of these pellets and achieve an overall smaller feedstock particle size.

Given that the approximate size of PVA pellets were 2 mm, a grating with circular holes of 1.65 mm diameter was initially trialled for particle size reduction. The material produced is shown in Figure 65.

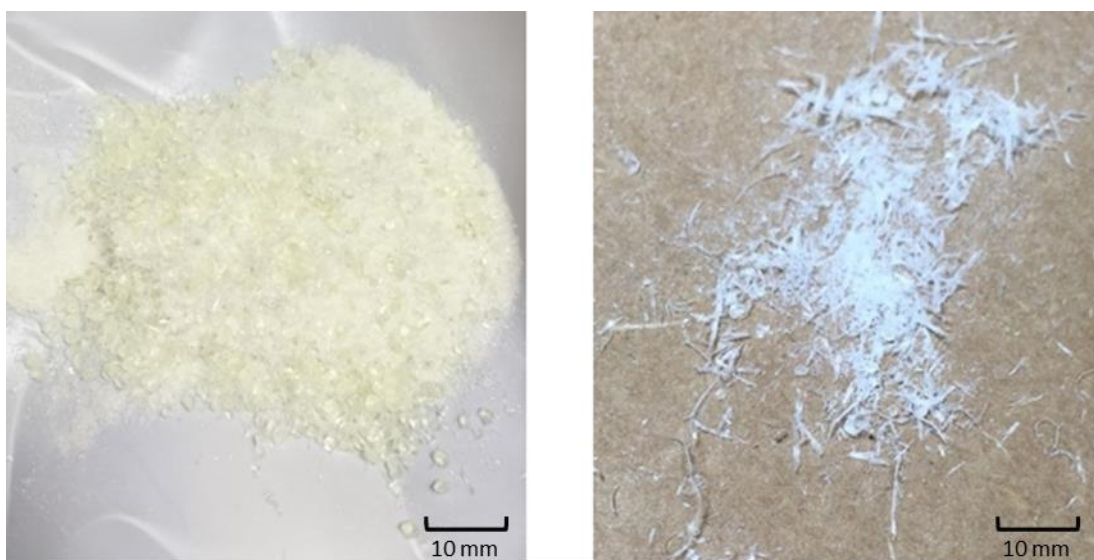


**Figure 65** – **Left** - Partially Milled PVA Pellets and Fines **Right** – Flakes of PVA.

Only a small amount of powdered material was produced and this was either partially milled, flakes or fines. Of the actual pellets produced, these only had a minimal size reduction and, given the time taken to produce this small amount of material coupled the quantity required for extrusion, repeated milling of pellets would not be in the best interests of the process overall.

In order to try and increase the size reduction, a rasping screen with a hole diameter of 1 mm was trialled. This screen works in a similar way to a cheese grater, but proved

completely unsuitable for the milling of PVA. The equipment immediately seized and the PVA melted due to the high temperatures caused by friction within the equipment.

Returning to a circular hole grating, holes of larger diameter (2 mm) were investigated in order to see what effect these had on the PVA pellets. This resulted in, as expected, even less size reduction than that observed with 1.65mm holes (Figure 66):



**Figure 66 - Left - pelletised starting material Right - milled PVA using 2 mm holes**

In order to try and increase the throughput, more material was added to the equipment, in the hope that attrition would provide further size reduction in the PVA, but this only resulted in increasing the temperature of the mill, so further investigation was abandoned so as not to melt the remaining PVA.

Given the difficulties associated with milling PVA filament, and the wide availability of powdered PVA in different molecular weights from various suppliers, powdered PVA was investigated as an alternative means to achieve higher drug loadings within a filament, while also reducing the number of steps in the manufacturing method.

A molecular weight range of 89000-98000 was initially investigated and, after varying screw speed and temperature slightly (see Section 2.6.2), a very brittle filament with a diameter range of 1.65-1.75 mm was produced (Figure 67):



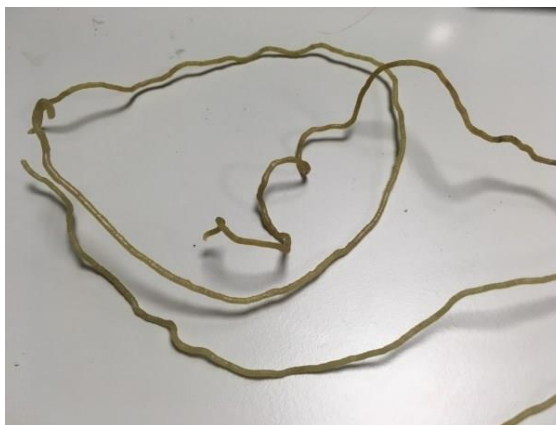


**Figure 67** - Extruded PVA Filament (89000-98000 MWt)

Only one extrusion was possible before the extruder blocked, but on closer inspection of the screws from the interior of the equipment, it is not clear if the polymer was melting correctly. In order to avoid straying too far from the recommended printer processing temperature for PVA,<sup>98</sup> further investigation was attempted using lower molecular weights.

When using PVA with a molecular weight range of 13000-23000, multiple issues were encountered. High torque was observed, despite lowering the extruder screw speed to 20 rpm in an attempt to counteract this. The temperature was increased to 220°C, but given the recommended processing temperature for PVA on Leapfrog printers should not exceed 200°C<sup>98</sup>, and TGA of the powdered PVA indicated loss of mass (potentially degradation) when held at temperatures above 230°C (Figure 68 – The green line is the TGA trace, the blue line is the DSC thermogram and the temperature is shown as the red line), the extrusion temperature was lowered to 170°C and the die removed entirely (Figure 69).

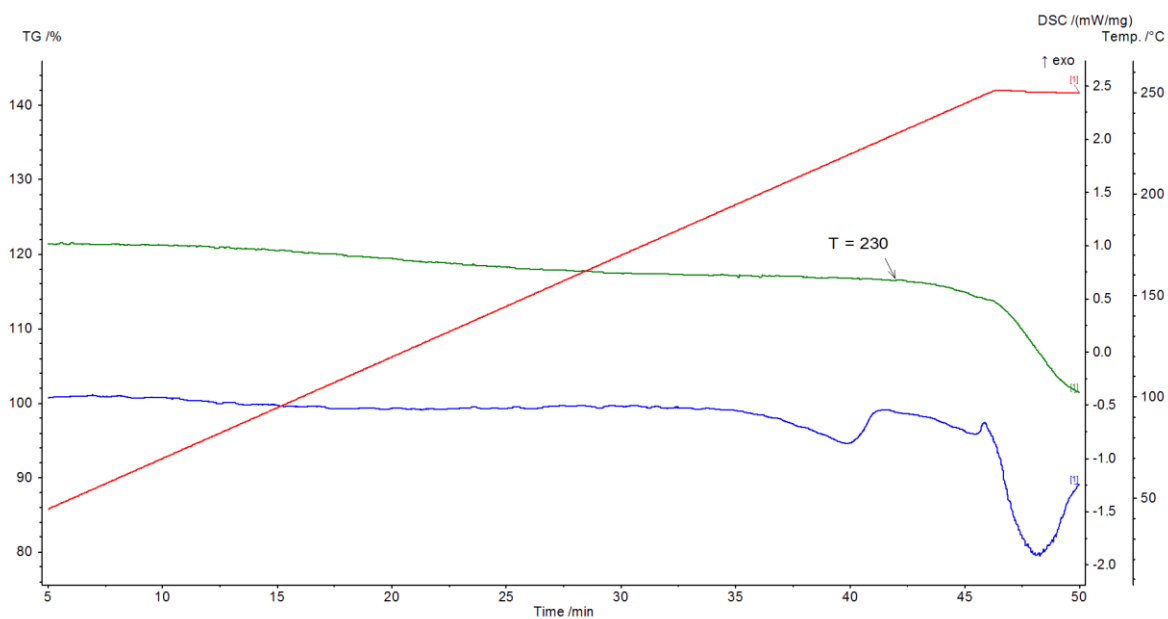


**Figure 68** - DSC and TGA of 13000 MWt PVA. (Red – temperature, Green – TGA, Blue – DSC)



**Figure 69** - Extrusion of Powdered PVA (13000-23000 MWt)

This obviously produced extrudate with a very thick diameter which was completely unsuitable for 3D printing, but was the only way to avoid experiencing high levels of torque within the extruder barrel.

When considering extrusion experiments of PVA, even when extrusion was initially successful with 89000-98000 MWt, the resulting extrudates were very brittle, and more investigation would be required to suitably plasticise the material for further use. As these grades of PVA appear unsuitable for extrusion, and no improvement could

be made to the method of pelletising commercial PVA filaments, all further experiments were abandoned in favour of trying a different polymer.

#### **4.3.2 DoE Approach to Extrusion of Affinisol™ with Disintegrants**

After the success experienced by colleagues within the group, using hydroxypropyl methyl cellulose (HPMC, Affinisol™ LV 15) for extrusion and subsequent 3D printing of paracetamol formulations,<sup>87</sup> attention was focused on this polymer as a potential candidate for 3D printing of carvedilol formulations.

Given the tendency of Affinisol™ formulations to produce sustained release 3D printed dosage forms,<sup>123</sup> attention was immediately focused on the inclusion of additives to act as disintegrants in order to aid the release of API from any tablets which may be produced. It should be noted however that while disintegration usually refers to the breaking apart of tablets in order for the drug to be released, when formulations are produced using the extrusion method, the result is API distributed within a solidified polymer strand, obtained by melting. The resulting formulation, obtained after subsequent 3D printing, will therefore be unlikely to behave as a conventional tablet would, and will instead follow more of an erosion method of disintegration.<sup>124</sup> As such, the 'disintegrants' mentioned in this piece of work are intended to act as dissolution aids, rather than true disintegrants.

In order to determine a suitable disintegrant with which to pursue further investigation, a three factor design of experiments was planned. The factors under investigation were: API content (1% w/w, 10.5% w/w and 20% w/w, corresponding to low, medium and high), disintegrant content (0% w/w, 5% w/w and 10% w/w, again corresponding to low, medium and high) and type of disintegrant – in this case salt, small natural molecule, large natural molecule, small synthetic molecule and large synthetic molecule.

Six different formulations were used, according to Table 26, which varied the API and disintegrant content, and these were repeated for each of the five disintegrants under investigation.































**Table 26** - Experimental Design for Investigation of Disintegrants

<b>Formulation</b>	<b>API (%)</b>	<b>Disintegrant (%)</b>	<b>Polymer (%)</b>
1	1	0	99
2	20	0	80
3	1	10	89
4	20	10	70
5	10.5	5	84.5
6	10.5	5	84.5

Sodium Chloride (salt), glycine (small natural molecule), cellulose (large natural molecule), Klucel ELF (hydroxypropylcellulose with small molecular weight - synthetic polymer) and Klucel HXF (hydroxypropylcellulose with large molecular weight - synthetic polymer) were chosen as disintegrants for this investigation. Cellulose and cellulose derivatives have been used as additives to aid disintegration of conventional tablets.<sup>125,126</sup> Although less common, glycine has also proven useful in the formulation of rapidly disintegrating tablets.<sup>127</sup> As an alternative method of action, sodium chloride was investigated due to its high aqueous solubility and the idea that any holes formed in the tablet due to NaCl dissolution may also permit the ingress of water and help with the overall disintegration of the tablets. Performance of each of these disintegrants was measured by calculating the mass remaining after subjecting the extruded filaments to an hour long disintegration test. Samples were weighed before and after this test, and the percentage mass remaining calculated as a measure of the disintegrant's capabilities.

Prior to carrying out any disintegration, it was clear that some formulations had extruded better than others. This was obvious even just from the physical appearance of the filaments, as shown in Table 27:

**Table 27** - Extruded Filaments from Disintegration DoE

Formulation Number	NaCl	Glycine	Cellulose	Klucel ELF	Klucel HXF
1					
2					
3					
4					
5					
6					

All of the filaments for NaCl visually appear incredibly dark, as do some of the Glycine filaments, whereas the other filaments approach a much more golden colour. While the dark colour alone is unlikely to have an effect on printing and is more likely an indication of some polymer degradation, some of the filaments from NaCl, glycine and

cellulose formulations exhibit surface roughness, which is more likely to impact successful printing, but this is less so than experienced with PVA extrusion (Section 4.3.1). Despite this observed roughness, all filaments have enough flexibility to be coiled and stored without snapping.

When subjecting the formulations to 1 hour of agitation in SGF, it is possible to see if any of the disintegrants improve the overall disintegration behaviour when compared to polymer/API formulations alone, listed as formulations 1 and 2 (Table 28):

**Table 28** - Percentage Mass Remaining After 1 Hour Disintegration

<b>Formulation</b>	<b>NaCl</b>	<b>Glycine</b>	<b>Cellulose</b>	<b>Klucel ELF</b>	<b>Klucel HXF</b>
1	8	17	20	9	14
2	59	58	51	62	53
3	10	0	51	0	50
4	54	0	55	46	68
5	47	0	32	45	58
6	41	0	45	37	62

All formulations containing glycine had completely dissolved after the hour long disintegration time, whereas the presence of Klucel HXF only seemed to further hinder the process. It also appeared that formulations with lower drug loading seemed to have less mass remaining at the end of the disintegration experiment, than those containing higher amounts of drug, which may be as a result of carvedilol being a BSC Class II drug, and hence exhibiting poor aqueous solubility.<sup>128</sup> It has however been reported that carvedilol has a solubility of 0.879 mg/mL in acidic aqueous media,<sup>129</sup> therefore as the mass of carvedilol present at any one time within the disintegration apparatus was less than this maximum solubility, the amount of carvedilol itself shouldn't have had an impact on this disintegration experiment alone. It could be that interactions between drug and polymer may be having some effect on the disintegration, although further investigation would be required to confirm this.

There is also some variation within the results, although formulations 1 and 2 should be almost identical across the different disintegrants, as these formulations are purely

just high and low concentrations of API within the polymer. These small differences could be attributed to variation in drug loading throughout the filament therefore, in order to confirm drug concentration, HPLC analysis was carried out on samples from each of the different formulations (Table 29).

**Table 29** - Average Drug Loading (%) per Formulation (n=3)

<b>Formulation</b>	<b>NaCl</b>	<b>Glycine</b>	<b>Cellulose</b>	<b>Klucel ELF</b>	<b>Klucel HXF</b>
1	0.4	0.4	0.5	0.5	0.6
2	17.4	18.3	9.8	17.1	15.2
3	2.8	2.8	15.5	2.4	6.6
4	18.1	14.6	17.3	16.6	17.0
5	11.8	14.9	12.0	12.3	12.7
6	11.4	11.8	10.9	11.1	11.4

According to the values selected at the start of this DoE, the expected drug loadings were as follows: 1% for formulations 1 and 3, 20% for formulations 2 and 4 and 10.5% for formulations 5 and 6. On a whole, formulations 1 and 6 appear to be closest to the expected values, but some level of variation is seen between expected and observed values for the other formulations. As this DoE was only intended to be a screening tool, extrusion experiments were performed 'back to back' as the increased processing control obtained through repeated cleaning was not deemed necessary. Dismantling and cleaning the extruder after processing every formulation would also result in lengthy delays to the progression of this research, so efforts were instead concentrated on finding suitable types of additives to investigate further. The variation in the results obtained for this initial screening experiment highlight that material may still remain in the barrel from extrusion of the previous formulation, therefore greater care will be taken when measuring processing time and selecting sampling areas of filaments in future experiments to ensure material analysed is representative of its corresponding formulation.

Compiling the data obtained from disintegration of the filaments, the following plot of disintegration coefficients was obtained from MODDE (Figure 70):

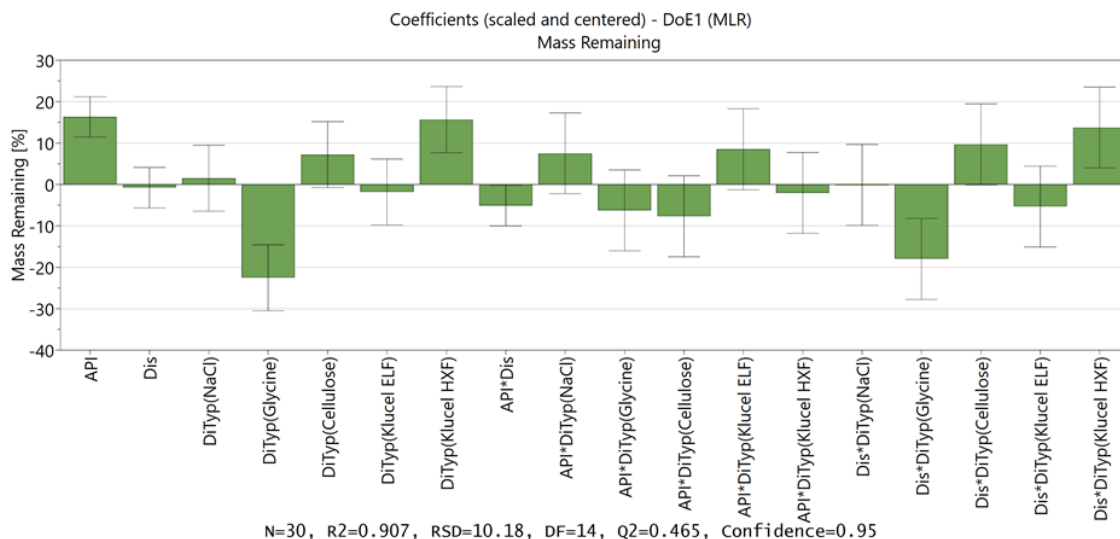


**Figure 70 - DoE Model Coefficients**

As the mass remaining is the term on the y-axis, all factors are displayed in relation to how they affect the overall mass remaining at the end of the experiment. When looking at this data, the magnitude of the bars indicate the overall importance of a factor with positive bars relating to increased mass remaining and negative bars relating to a decrease in mass remaining. The error bars are based on a statistical calculation of variance in the data, after being scaled and centred, and are an indication of whether a term is statistically relevant – i.e. for API concentration, this is a statistically relevant term because the error bars do not cross 0, whereas the overall disintegrant concentration does not display any statistical relevance as the error bars lie directly over the 0 value.

From this data, it can be seen that the concentration of API dominates the results, with increased concentration having a negative effect on the overall disintegration, as mentioned above. NaCl, cellulose and Klucel ELF display no statistically relevant effect on the overall mass remaining, whereas increased quantities of both glycine and Klucel HXF do affect the formulations, albeit with opposite outcomes – glycine decreases the mass remaining and Klucel HXF increases the mass remaining.

The API and disintegrant cross term (API\*Dis) shows how these two factors interact with one-another and shows that the combined result does appear to be favourable on the overall mass remaining, but this is only a small effect. The cross terms of



API\*DisTyp show no benefit to any of the disintegrants tested when the API is at high levels, but the cross terms of Dis\*DisTyp further reinforce that at high levels of disintegrant, glycine reduces the mass remaining and Klucel HXF increases the mass remaining. A possible explanation for this difference is that addition of glycine provides discrete pockets of material throughout the filament which disrupt the polymeric chain structure of the Affinisol™ and allow for easier disintegration, whereas the polymeric chain structure of Klucel HXF allows the molecule to more easily align with the molecular structure of the carrier Affinisol™ and therefore hinders the overall disintegration process.

These results can also be displayed in contour plots for each of the different disintegrants (Figure 71):

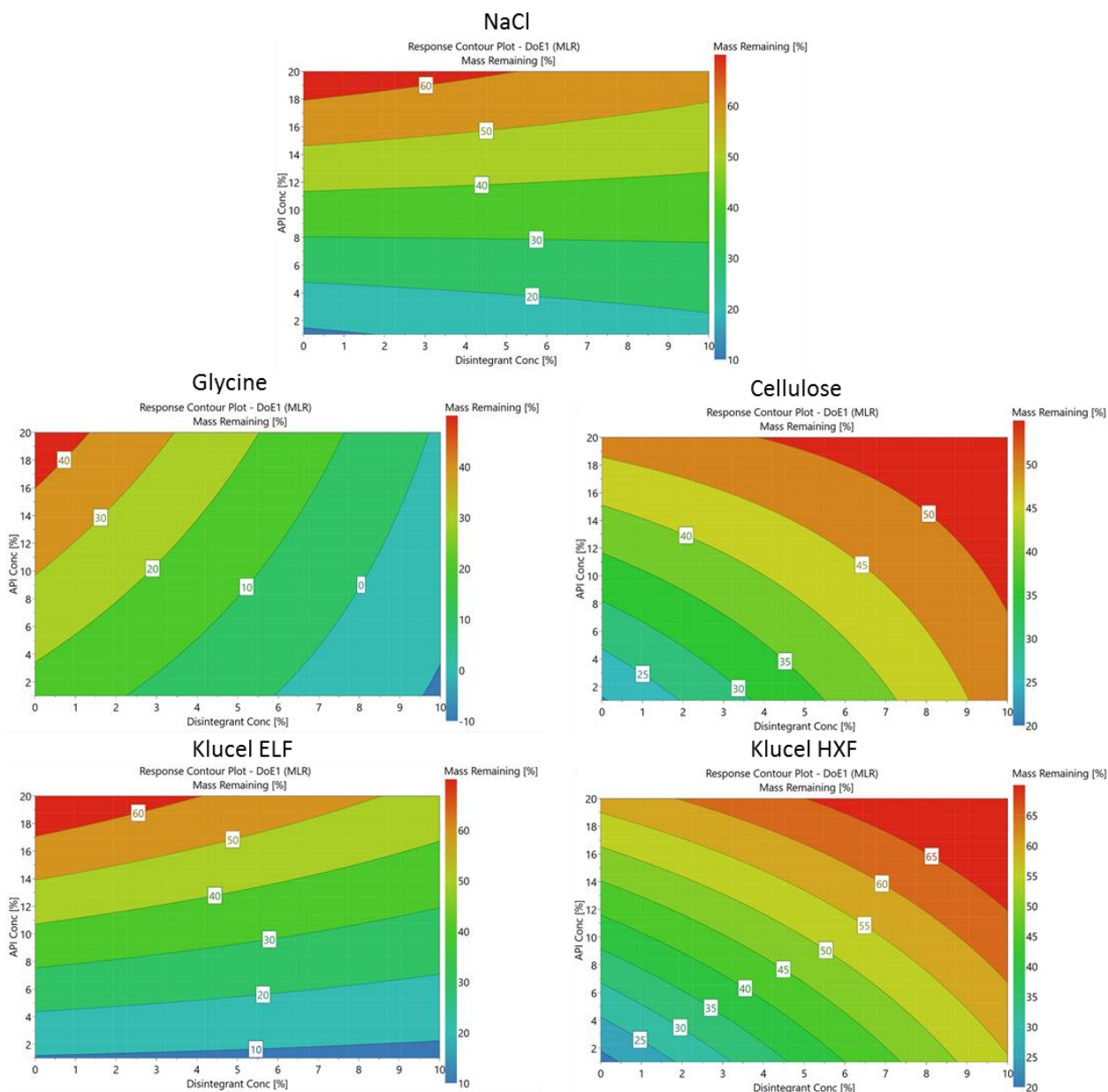


**Figure 71** - Contour Plots of Mass Remaining for each Disintegrant.

x-axis - Disintegrant concentration, y-axis – API concentration. Colour Coding: Red – high mass remaining, Blue – low mass remaining.

In each of these contour plots, the disintegrant concentration is displayed along the x-axis and the API concentration is displayed along the y-axis. The colour coding relates to the percentage mass remaining after 1 hour disintegration time, with red corresponding to high mass remaining and blue corresponding to low mass remaining. For glycine and Klucel ELF, the contour plots indicate that increasing the disintegrant concentration has a favourable effect and results in less mass remaining, although

higher concentrations are likely to be required at higher drug loading. In contrast, the contour plots for cellulose and Klucel HXF suggest the opposite - increasing the disintegrant concentration results in more mass remaining at the end of the experiment, especially at higher drug loadings. NaCl shows mostly horizontal banding, indicating that it has very little effect on the formulations overall.

In general, when pooling these results together, the following statements can be made:

- Increased API Concentration results in increased mass remaining (poorer disintegration), therefore higher disintegrant concentrations are likely to be required at high drug loadings.
- High molecular weight disintegrants do not aid the process, and instead make the overall disintegration worse for the drug loadings investigated (potentially due to the long chains of the molecules becoming entangled with Affinisol™ molecules during extrusion).
- Small molecular weight compounds aid disintegration, but only small natural disintegrants are statistically relevant for further investigation.
- NaCl has almost no effect on disintegration of the formulations, and visual inspection of the filaments would suggest some degradation due to their darker appearance.

From the disintegrants trialed in this experiment, glycine would seem like the most obvious choice to continue further research, however, as the end aim is to produce printed tablets, it is not possible to use glycine due to the rough nature of the extruded filament. Instead, another DoE was implemented in order to investigate other natural small molecular weight compounds that are commonly used in the pharmaceutical industry, such as sugar alcohols<sup>130</sup> or poly-ethylene glycols.<sup>131</sup>

The same three factor design of experiments was employed, looking at the API content, disintegrant content and type of disintegrant under investigation. This time, erythritol, mannitol, PEG 1000 and PEG 4600 were investigated as potential disintegrants for this process.





















The same levels of both API and disintegrant content were investigated, but the sixth formulation was excluded as, since this was a screening process, it was not critical to include a repeat of the medium concentrations for each of the disintegrants (Table 30):

**Table 30** – Experimental Design for Further Investigation of Disintegrants

<b>Formulation</b>	<b>API (%)</b>	<b>Disintegrant (%)</b>	<b>Polymer (%)</b>
1	1	0	99
2	20	0	80
3	1	10	89
4	20	10	70
5	10.5	5	84.5

Again, performance of each disintegrant was measured by calculating the mass remaining after subjecting the extruded filaments to an hour long disintegration test. The filaments, prior to any disintegration, are shown in Table 31:

**Table 31** - Extruded Filaments from Further Disintegration DoE

Formulation Number	Erythritol	Mannitol	PEG 1000	PEG 4600
1				
2				
3				
4				
5				

This time, all formulations 1 and 2 are consistent in colour, which makes sense given that there is no disintegrant present in any of these formulations. In contrast, both erythritol and mannitol formulations 3-5 exhibit darkening of the filaments, which could indicate some level of degradation, although it has been reported that both erythritol and mannitol both have high thermal stability and do not take part in Maillard browning reactions.<sup>132</sup> The colour is darkest in formulation 3, where only a low concentration of API is present, and gradually gets lighter as the API concentration increases. It could be that both these components are interacting with the polymer

itself, and as the polymer concentration decreases (with increasing drug content) there is less Affinisol™ for either erythritol or mannitol to interact with, which therefore produces a lighter colour.

Overall mass remaining after subjecting the formulations to 1 hour of agitation in SGF was again recorded, with formulations 1 and 2 being those that contained either a high or low concentration of API with no disintegrant (Table 32):

**Table 32 - Percentage Mass Remaining After 1 Hour Disintegration**

<b>Formulation</b>	<b>Erythritol</b>	<b>Mannitol</b>	<b>PEG 1000</b>	<b>PEG 4600</b>
1	11	7	2	10
2	67	67	61	61
3	7	7	11	22
4	42	53	58	32
5	44	37	34	42

As with the previous DoE, the filaments with lower drug loading had less mass remaining at the end of the hour long disintegration experiment, than those containing higher drug loading. This is likely due to the lower aqueous solubility observed with all BCS Class II drugs, as mentioned earlier. When comparing all the results to formulations 1 and 2 (which contain no disintegrant), it is possible to draw the initial conclusion that each of these 'dissolution aids' does seem to have a favourable effect on the disintegration. While this effect is not really evident at low drug loadings, at high drug loadings the overall disintegration appears to be improved. Confirmation of drug loading, as determined by HPLC, is shown in Table 33:

**Table 33 - Average Drug Loading (%) per Formulation (n=3)**

<b>Formulation</b>	<b>Erythritol</b>	<b>Mannitol</b>	<b>PEG 1000</b>	<b>PEG 4600</b>
1	0.5	0.8	0.6	0.7
2	18.8	20.6	18.6	18.4
3	1.2	2.9	2.6	2.6
4	20.6	21.4	18.8	18.9
5	11.6	11.1	11.8	10.0

Unlike the previous DoE, there were no numbers which indicated drug loadings different to what was expected, which would suggest that the formulations did not become mixed during the extrusion process. The numbers for formulation 3 are only slightly higher than expected and are likely due to a high drug loading formulation being extruded immediately beforehand. Regardless of this fact, the values still represent low, medium and high drug loadings and are therefore still able to provide information on how formulations with these component ratios behave.

Again, after compiling the data obtained from disintegration of the filaments, the following plot of disintegration coefficients was obtained from MODDE (Figure 72):

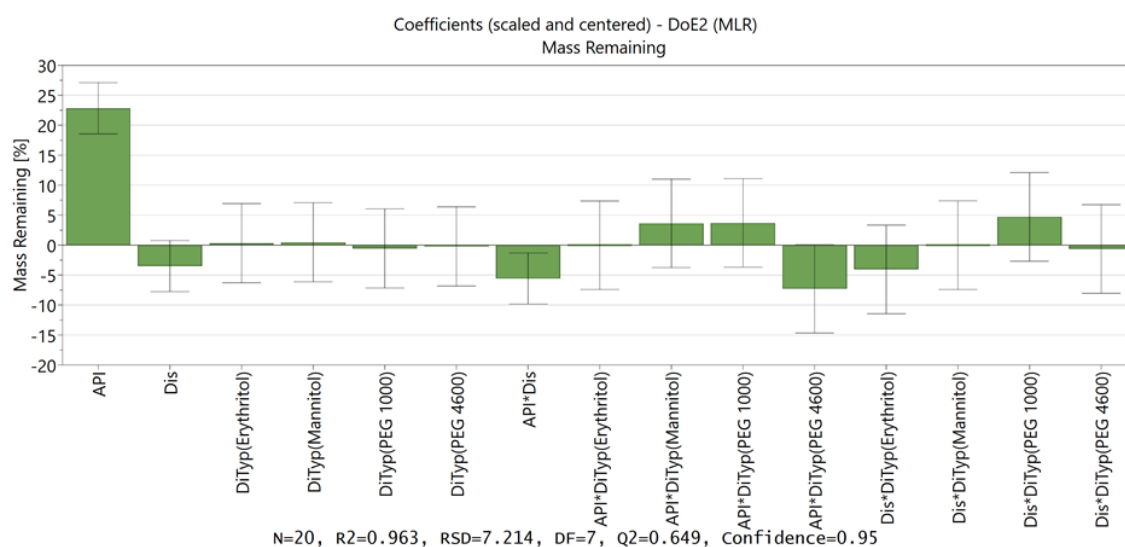


Figure 72 - Further DoE Model Coefficients

From this data, it can again be seen that the concentration of API dominates the results, with increased concentration having a negative effect on the overall disintegration. None of the disintegrants investigated appear to have any statistically relevant effect on the mass remaining at the end of a one hour disintegration experiment, with bars that remain very close to zero across each type.

The API and disintegrant cross term (API\*Dis), similarly to the first DoE, shows that the combined result does appear to be favourable on the overall mass remaining, but this is, again, only a small effect. The cross terms of API\*DisTyp show no benefit to any of the first three disintegrants tested, but when the API is at high levels, high levels

of PEG 4600 may improve dissolution. The cross terms of Dis\*DisTyp all have error bars which cross the zero mark and indicate that none of the disintegrants really provide any benefits to the formulations.

Relating this data to contour plots for each of the different disintegrants (Figure 73):

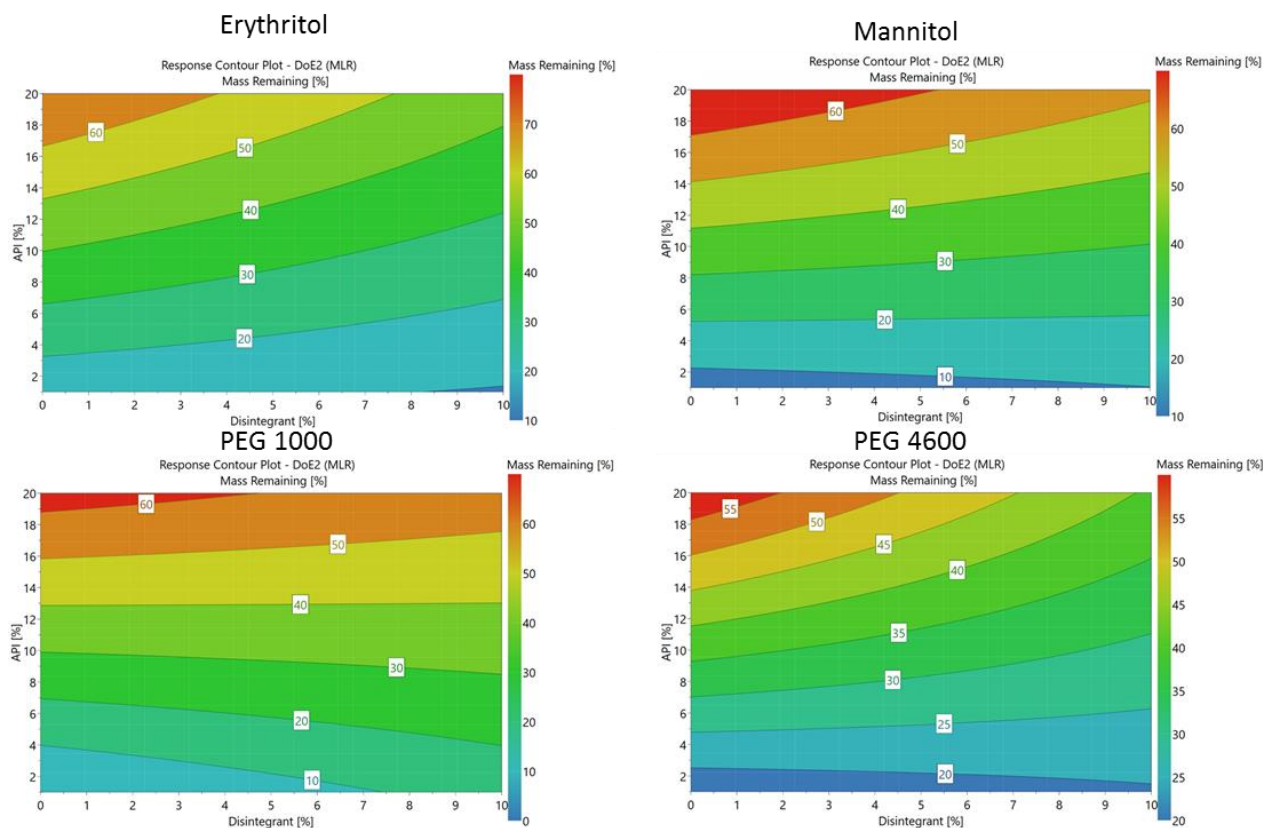


**Figure 73** - Contour Plots of Mass Remaining for each Disintegrant.

x-axis - Disintegrant concentration, y-axis – API concentration. Colour Coding: Red – high mass remaining, Blue – low mass remaining.

In each of these contour plots, the disintegrant concentration is again displayed along the x-axis and API concentration displayed along the y-axis, with red corresponding to high mass remaining and blue corresponding to low mass remaining.

Except with PEG 1000, which appears very similar to the result obtained from NaCl in the previous DoE, the contour plots indicate that increasing the disintegrant concentration has a favourable effect on the mass remaining, with perhaps the most pronounced effect being seen with higher drug loadings for PEG 4600.



When considering all the results gained from this DoE and investigation into the use of disintegrants for drug loaded Affinisol™ filaments, for the first time the following statements can be made:

- With regards to the use of carvedilol, increased API concentration results in increased mass remaining (poorer disintegration).
- Overall disintegrant concentration does not change the results either way.
- There is no obvious 'better' disintegrant from those selected, and further investigation into 'printability' would be required in order to select a suitable dissolution aid.

Bearing all this in mind, the next step was to investigate whether any of the formulations containing 'small natural' molecules could be successfully transferred to the 3D printer.

### **4.3.3 3D Printing of Affinisol™ Formulations**

#### **4.3.3.1 3D Printing of Pure Affinisol™**

Prior to printing any drug loaded formulations, printing of pure Affinisol™ was investigated in order to establish suitable print settings. Extruded filaments of pure Affinisol™ were loaded into a Leapfrog Creatr HS 3D printer and successfully fed using the gear mechanism at the rear. A test print of a 10 mm diameter tablet (height 4 mm) was selected with an infill percentage of 30%. An initial printing temperature of 160°C was selected (build plate 50°C) with results shown in Figure 74:



**Figure 74** - Pure Affinisol™ Printed at 160°C

As can be seen from the image, only the initial print layers were successfully printed. The filament was feeding into the print head perfectly fine, but the polymer was not sticking to layers already deposited on the build plate. The print temperature was increased to 180°C in the hope that the filament would stick together better (Figure 75):



**Figure 75** - Pure Affinisol™ Printed at 180°C

While increasing the print temperature to slightly above the extrusion temperature (170°C) seemed to improve the printing process, still only a couple of layers were printed before the filament again stopped sticking to layers already deposited. In a final attempt, the print temperature was increased to 190°C (Figure 76):



**Figure 76** - Pure Affinisol™ Printed at 190°C

At 190°C (build plate 50°C), full tablets could be printed, which matches the conditions used by Prasad *et al.*<sup>87</sup> in similar printing experiments, albeit with drug loaded Affinisol™, rather than pure Affinisol™. The layers stuck together adequately

enough during printing for the full 3D object to be produced, but subsequently broke apart upon removal from the build plate. On further inspection, it was revealed that the layers could be unravelled into single strands of polymer again.

While increasing the temperature initially resulted in better quality printed tablets, further temperature increases are unfavourable and are likely to degrade to polymer.<sup>133</sup> Further investigation into pure Affinisol™ was suspended after reasoning that the presence of carvedilol could plasticise the polymer, as observed with Prasad *et al.* and the use of paracetamol,<sup>87</sup> which could potentially allow for the creation of better quality prints without increasing the print temperature further.

#### **4.3.3.2 Printing of Affinisol™ Formulations Containing Erythritol, Mannitol, PEG 1000 and PEG 4600**

With a general idea of suitable print settings, it was possible to investigate if any filaments from the second disintegrant DoE could be printed as tablets. With formulations 1 and 2 intended to be identical across the range of different additives trialled – as both contained 0% disintegrant – these were only investigated for printing once from all the DoE samples.

Print temperatures of 170°C, 180°C, 190°C and 195°C were investigated, with 195°C offering the best results, but none of these settings resulted in complete tablets being produced (Figure 77 and Figure 78):



**Figure 77** - Printing of DoE Formulation 1 (1% CAR 99% Affinisol™) 195°C print temperature.








**Figure 78** - Printing of DoE Formulation 2 (20% CAR 80% Affinisol™) 195°C print temperature.

It was reasoned that the presence of API alone was not enough to suitably plasticise the filament, and the inclusion of further additives may produce more suitable formulations for printing.

Formulations 3, 4 and 5 were tested across all different disintegrants and the results are displayed in Table 34:

**Table 34** - Results of DoE Printing at 195°C.

Formulation	Erythritol	Mannitol	PEG 1000	PEG 4600
3 (1% API, 10% Disintegrant)	No Tablets	No Tablets	No Tablets	No Tablets
4 (20% API, 10% Disintegrant)	No Tablets		No Tablets	No Tablets
5 (10.5% API, 5% Disintegrant)				

As can be seen, tablets were produced for all formulations when the the API and disintegrant were present at levels of 10.5% and 5% respectively. Additionally, when mannitol was used as the disintegrant, tablets could also be produced from a formulation containing 20% API and 10% disintegrant. In the case of formulation 3 (1% API, 10% disintegrant) material could be passed through the print head for both erythritol and mannitol, but the material did not adequately stick together enough to build successive layers of the design. For formulation 4 of erythritol, the filament

snapped continually when attempting to feed through the gear mechanisms of the printer, either due to sample brittleness or issues with consistent filament diameter. For both PEG 1000 and PEG 4600, failure of printing of formulations 3 and 4 seemed due to the soft nature of the filaments, possibly due to increased plasticisation provided by the increased disintegrant concentration. Further physical analysis of the filaments may provide insight into why print success or failure has occurred.

#### 4.3.3.2.1 Analysis of Filament Mechanical Properties

As a method of investigating the mechanical properties of printer filaments, 3-point bend testing has the potential to quantify the maximum stress and strain required for a filament to be suitable for printing.<sup>87,121</sup>

Five different filament samples were taken from formulations 1 and 2, along with five different filament samples from formulations 3, 4 and 5 for each of the individual disintegrants, and these were subjected to 3-point bend testing using a texture analyser. Results are displayed in Stress (MPa) versus Strain (%) graphs for each of the disintegrants investigated (Figure 79, Figure 80, Figure 81 and Figure 82):

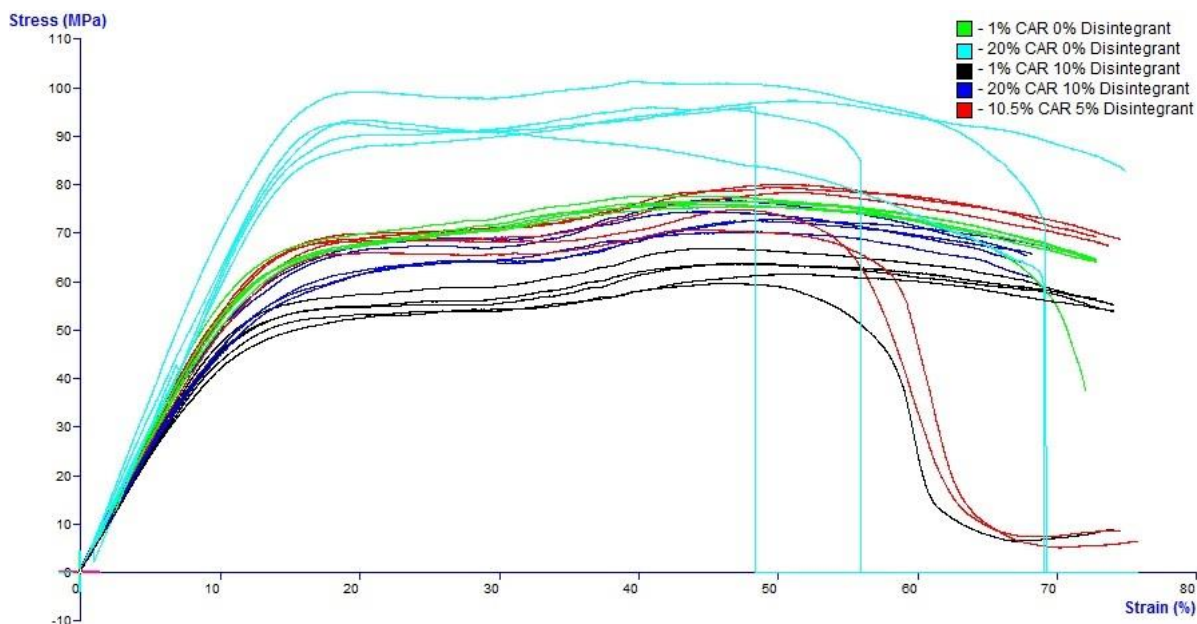
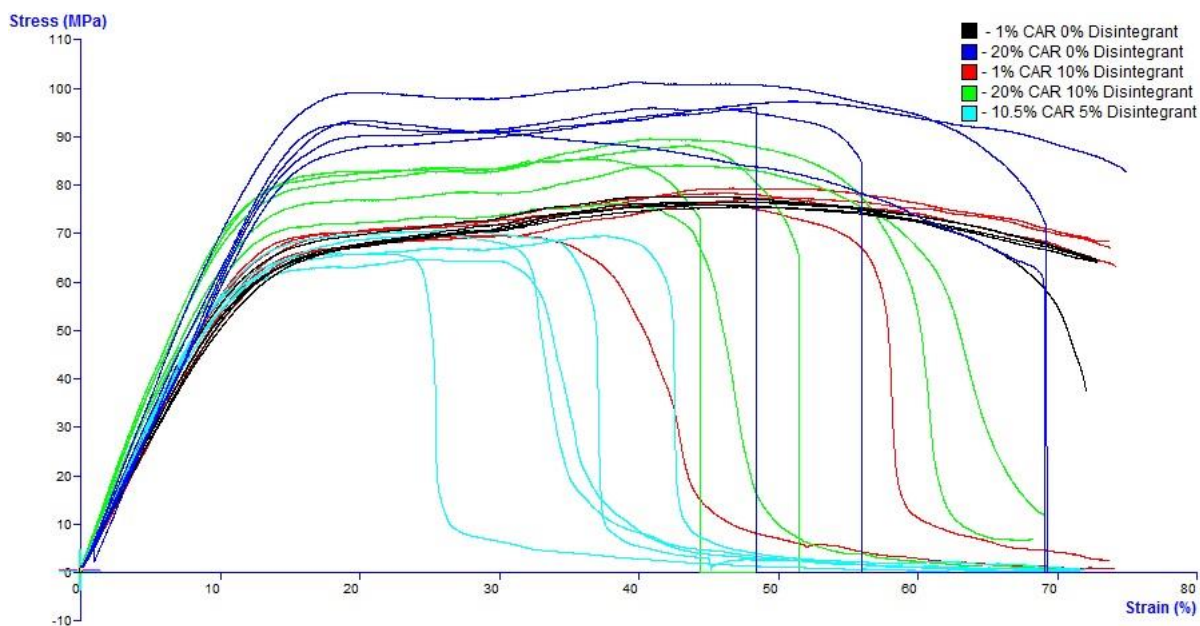


Figure 79 - Stress vs Strain Graph for Erythritol Formulations

In stress versus strain graphs, the linear portion of the data (approximately 0-15% strain in this case) relates to the 'elastic region' of the material in question, meaning that any changes undergone by the material in this region are reversible. All further portions of the graph are an indication of 'plastic deformation' and are non-reversible. Sharp drops in the data to 0 usually indicate a break in the filament, however this can also correspond to the filament slipping off the stage of the equipment, which was the case in all the sharp drops observed for formulation 2 (20% CAR, 0% erythritol). A gradual drop towards zero, as observed in some of the data from formulations 3 and 5 (1% CAR, 10% erythritol and 10.5% CAR, 5% erythritol), also relates to a break in the filament, but is an indication that the break was not caused by the material being brittle. High values for stress are an indication of how strong the filaments are, with changes observed across the filaments a potential indication of the level of plasticisation within the filaments.

For erythritol, results appear quite similar across the different formulations, with the exception of formulation 2 (20% CAR, 0% erythritol), which appears stronger than all the rest. The addition of erythritol to a 20% formulation of carvedilol (formulation 4, 20% CAR, 10% erythritol) lowers the maximum stress which can be applied before plastic deformation is observed, which lowers the overall strength of the filament, and is an indication that erythritol plasticises the formulation. This effect is also observed to a lesser extent in formulations containing 1% carvedilol.



**Figure 80** - Stress vs Strain Graph for Mannitol Formulations

For formulations containing mannitol, a lot more breakage of the filaments is observed, but this does not seem to necessarily correlate with ‘printability’ in this instance. In a similar manner to the results obtained for erythritol, the addition of mannitol to a 20% carvedilol formulation results in lowering the maximum stress which can be applied, although to a lesser extent than is seen with erythritol. This effect is not evident when comparing formulations containing 1% carvedilol, which would indicate that mannitol does not plasticise these formulations to the same extent as erythritol.

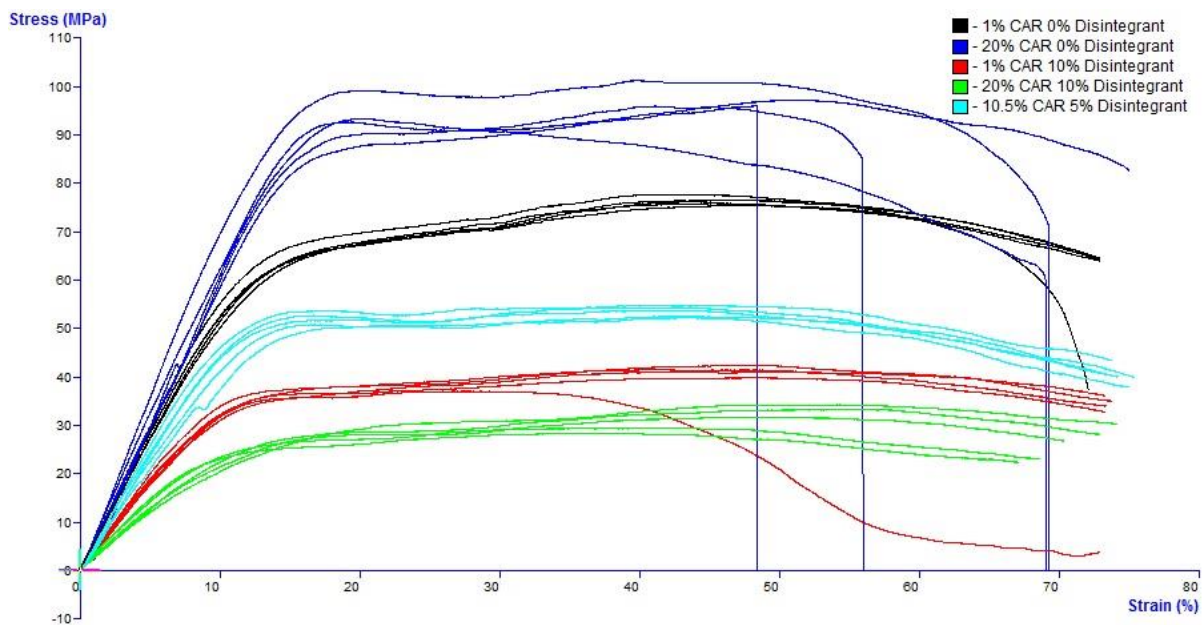


**Figure 81** - Stress vs Strain Graph for PEG 1000 Formulations

Formulations containing PEG 1000 show distinct variation in the values for maximum stress, indicating that the presence of PEG 1000, carvedilol or a combination of both result in different degrees of plasticisation throughout the filaments. In the absence of disintegrant, increasing the level of carvedilol in the filament increases the strength, whereas when PEG 1000 is included in the formulation, a combination of high drug loading and high disintegrant loading result in a filament that appears very soft. Given that both formulations 3 and 4 (1% CAR, 10% PEG 1000 and 20% CAR, 10% PEG 1000 respectively) failed to print due to filament softness, it would appear that a ‘threshold’ maximum stress must be reached for a filament to be suitable for printing, which seems to be above approximately 40 MPa in the case of this DoE. This is similar to what was observed with Prasad *et al.* and the printing of paracetamol containing formulations,<sup>87</sup> although the threshold maximum stress recorded in their research was approximately 30 MPa, which is lower than observed for this DoE.



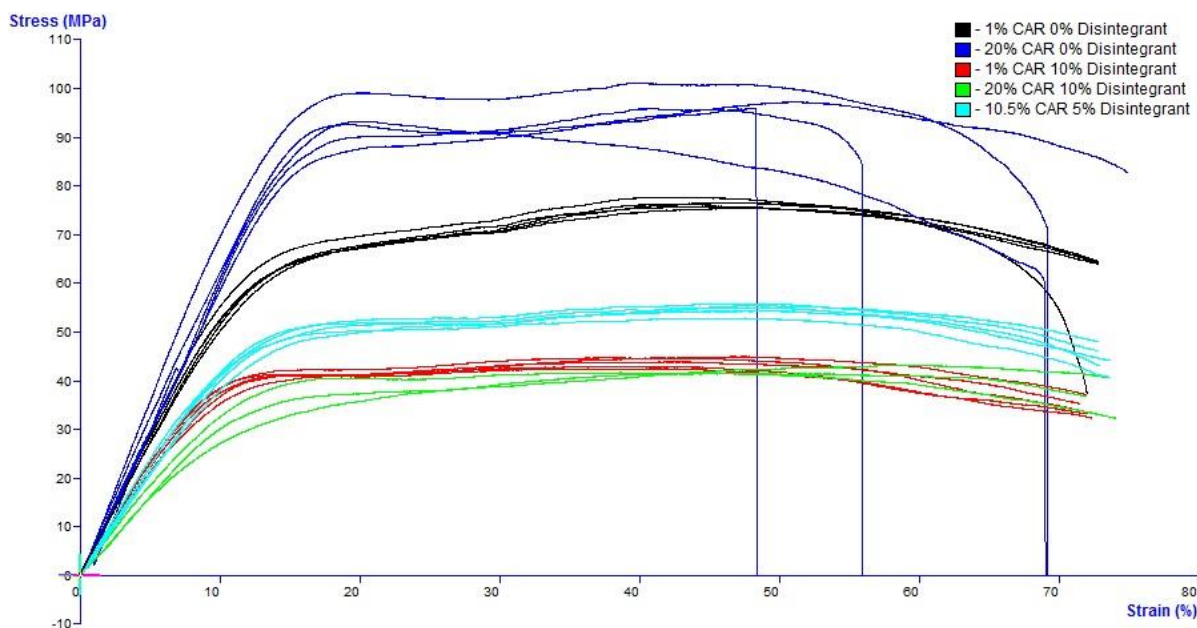


**Figure 82** - Stress vs Strain Graph for PEG 4600 Formulations

Formulations containing PEG 4600 are very similar to those containing PEG 1000, although those with the high disintegrant loading (10% disintegrant) have slightly stronger filaments in the case of PEG 4600. As mentioned above, print failure was experienced due to filament softness in formulations with high levels of PEG 4600, which further reinforces the theory that a ‘threshold’ maximum stress of above 40 MPa must be reached for printing to be viable in the case of the materials used for this DoE.

For ease of visualisation, the maximum stress for each disintegrant under investigation has been plotted in Figure 83 along with the flexural modulus, which is determined from the slope of the linear region of the stress/strain graphs presented. Both these features have been compared by Prasad *et al.* when describing their similar system using paracetamol,<sup>87</sup> and could together provide information on which systems are likely to be printable.

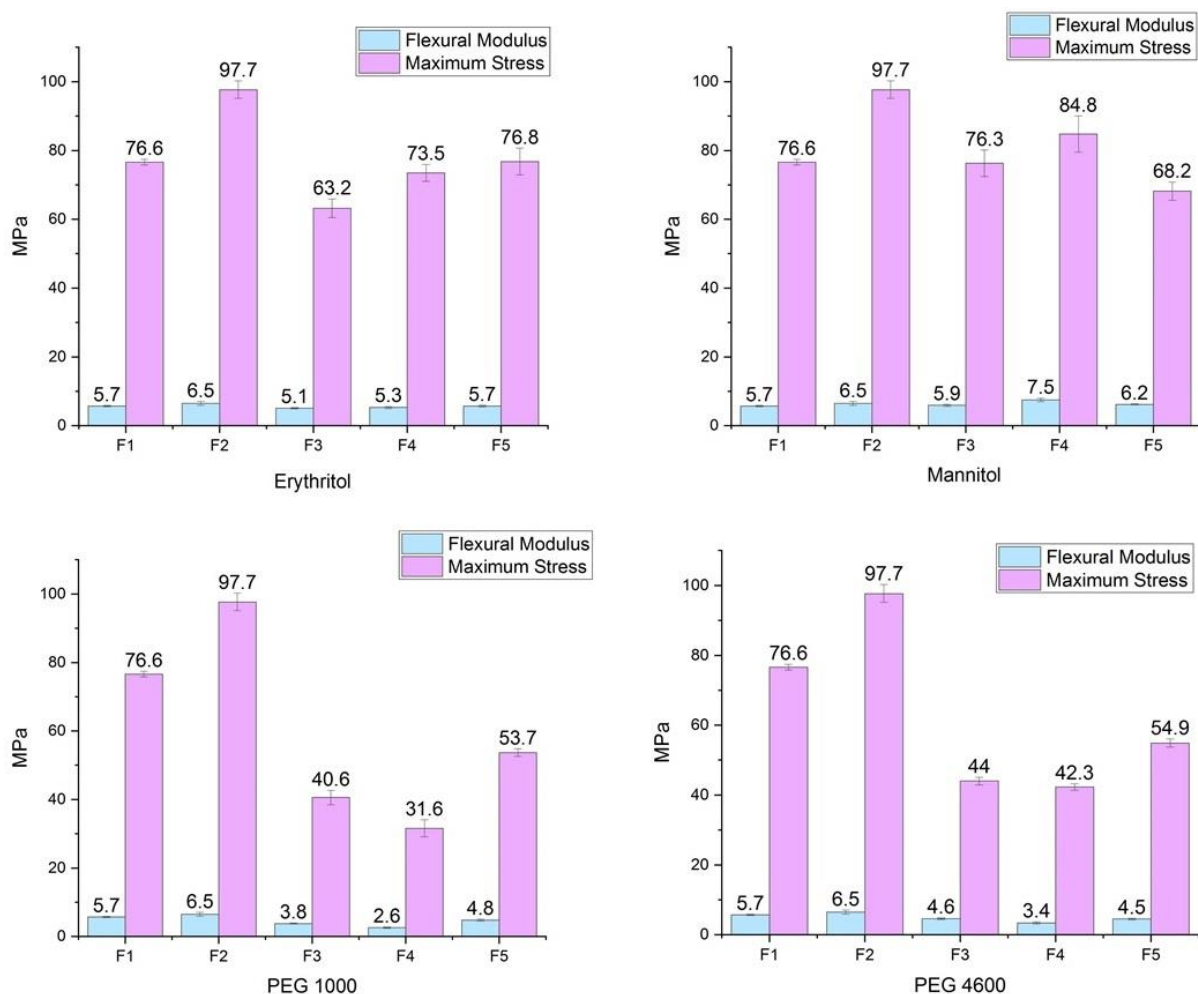


**Figure 83** - Flexural Modulus and Maximum Stress for each Disintegrant (n=5 ± standard deviation)

In the work described by Prasad *et al.* printing was successful with filaments that had a flexural modulus in the range of 3.1-4.4 MPa and failure to print was seen with filaments with a flexural modulus in the range of 0.2-1.2 MPa. In the work described within this thesis, filaments exhibiting print failure due to softness had a flexural modulus in the range of 2.6-4.6 MPa, however the lowest flexural modulus observed with a successful print was 4.5 MPa, which would indicate that more than flexural modulus alone is required to predict print success. When considering the maximum stress observed for each of the different formulations, it is difficult to predict print failure unless the resulting filaments are very soft. Successful printing was observed with maximum stress in the range of 53.7-84.8 MPa, but (with the exception of previously discussed soft filaments) failure was also seen within this range. The only

outlier in terms of an upward threshold for maximum stress is the value observed for formulation 2 (20% CAR, 0% disintegrant), which was 97.7 MPa, but further investigation into upward limits would be required in order to more accurately apply this as an acceptable stress range.

Overall, 3-point bend testing only seems to provide an indication of print failure in the case of very soft filaments. With regards to failure from filaments which don't appear too soft, analysis of the mechanical properties does not provide a sufficient reason for this print failure. An increased amount of breakage is observed in formulations containing mannitol, but these formulations resulted in greater print success and therefore filament breakage cannot be used as an indication of print suitability for any of these formulations. Investigation in to levels of crystallinity may provide further insight to printing viability.

#### ***4.3.3.2 Crystallinity Determination of Filaments***

In order to assess the crystallinity of the components within the extruded filaments, XRPD analysis was carried out on pelletised filament. In order to determine how the formulations behave without any disintegrants, formulations 1 and 2 were analysed and compared to the Affinisol™ and carvedilol starting materials (Figure 84):

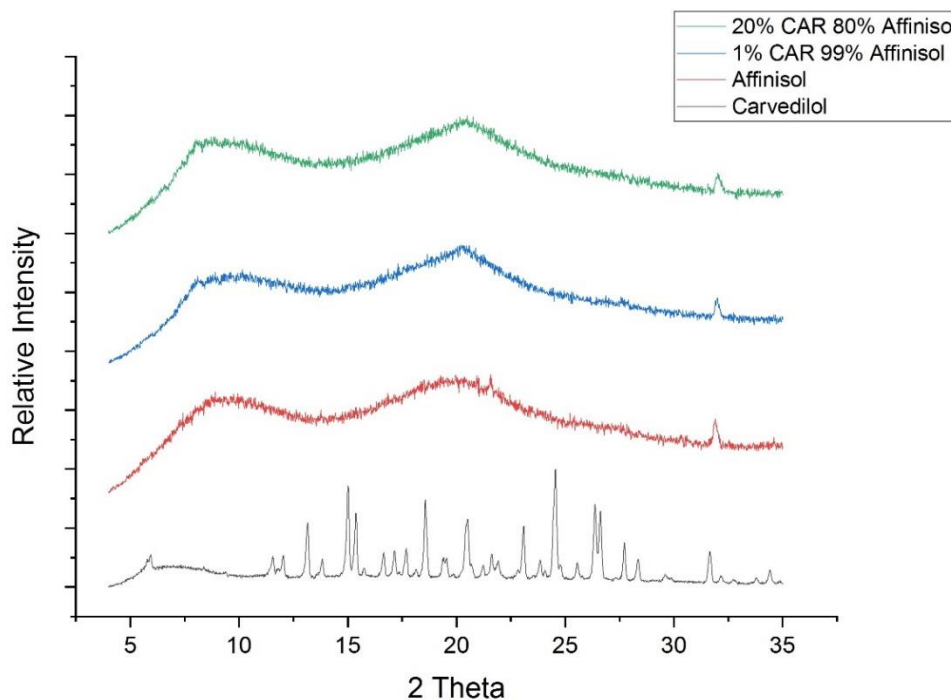


**Figure 84** - XRPD of formulation 1 (1% CAR, 99% Affinisol™) and 2 (20% CAR, 80% Affinisol™).

The absence of any additional peaks in the filament pellets of formulations 1 and 2 suggest that the carvedilol remains amorphous in these formulations, and throughout the extrusion process. The clear peak observed in Affinisol™ alone is due to a sodium chloride impurity, which has been reported in the literature<sup>87,134</sup> and is present in all Affinisol™ containing samples. Based on the lack of crystallinity observed in the absence of disintegrants, any further peaks detected in formulations 3, 4 and 5 are therefore not caused by either carvedilol or Affinisol™. XRPD analysis of each of the disintegrant formulations is shown in the following graphs (Figure 85, Figure 86, Figure 87 and Figure 88):

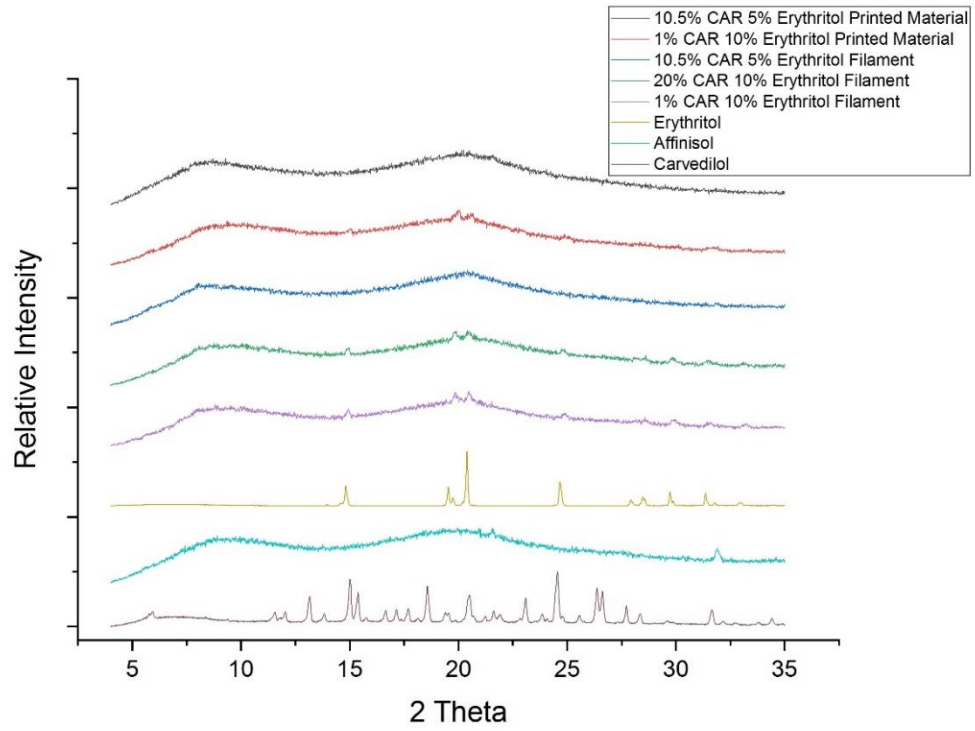


Figure 85 - XRPD Analysis of Erythritol Formulations

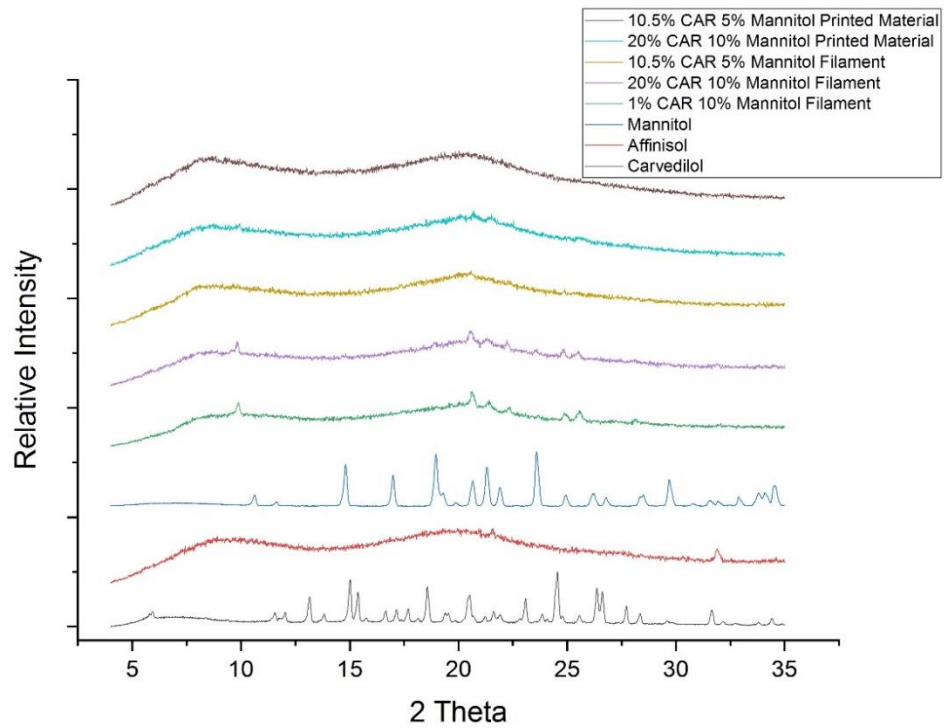


Figure 86 - XRPD Analysis of Mannitol Formulations

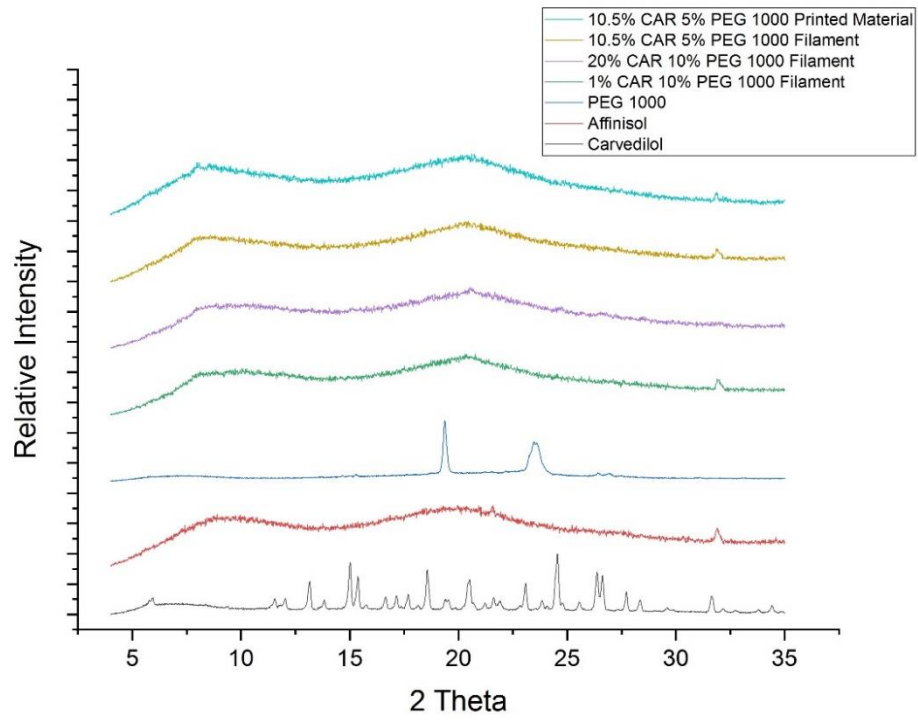


Figure 87 - XRPD Analysis of PEG 1000 Formulations

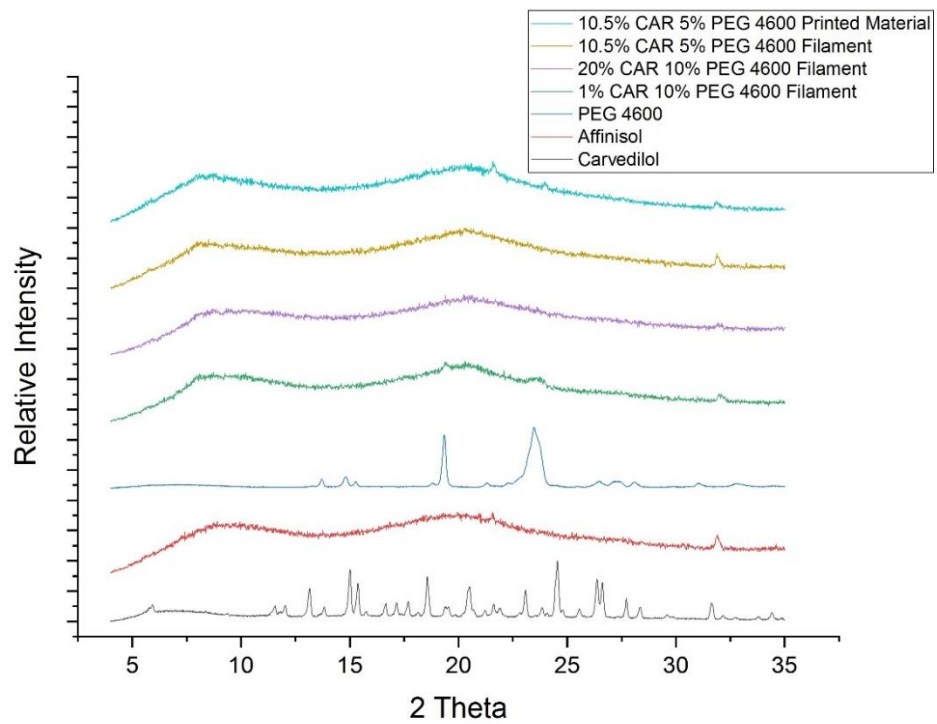


Figure 88 - XRPD Analysis of PEG 4600 Formulations

In formulations containing PEG 1000, there is no evidence of peaks, suggesting that the reason for print failure was purely attributed to filament softness, as measured by 3-point bend testing. When looking at filament pellets and printed material of erythritol and mannitol containing formulations however, and comparing them to the raw starting materials, it is clear there are some peaks observed in material from formulations 3 and 4. This is also seen to a lesser extent with formulations containing PEG 4600. Based on the lack of peaks observed in formulations 1 and 2, these peaks are consistent with being from the disintegrants themselves. In both formulations 3 and 4, the concentration of erythritol is double that of formulation 5 (10% versus 5%), therefore it is likely that this increase has caused the presence of peaks in these formulations.

While this presence of crystallinity indicates that HME is not sufficient for completely processing the components of these formulations at a molecular level, it is still difficult to determine print failure based on the detection of crystalline material. Formulations 3 and 4 of erythritol both display crystalline material and both fail to print, whereas mannitol also displays crystallinity in these formulations but print failure is only observed in formulation 3. It should also be noted that crystallinity is still observed in printed material from these formulations, indicating that the printing process does not aid any further distribution of the components at a molecular level.

#### ***4.3.3.2.3 Dissolution of Printed Tablets***

In order to determine which, if any, of these disintegrants improved the dissolution and release of API from the formulations, all tablets which could be printed were subjected to dissolution analysis using a USP 1 dissolution test. Samples were run for six hours and the following release profiles were obtained (Figure 89):

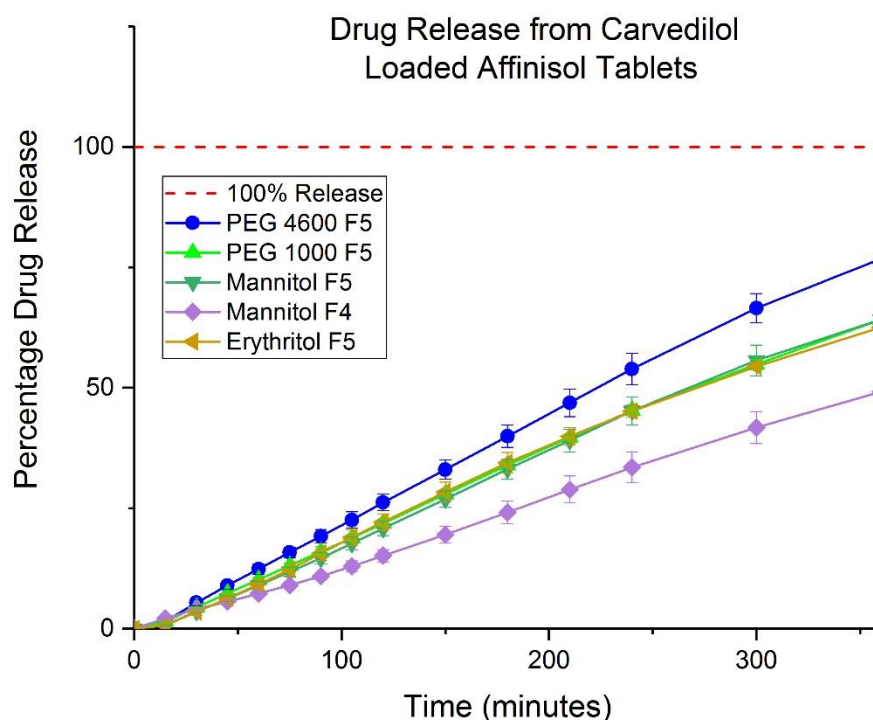


**Figure 89** - Dissolution of 3D Printed Tablets with Various Disintegrants ( $n=3 \pm$  standard deviation)  
F4=20% CAR, 10% disintegrant, F5=10.5% CAR, 5% disintegrant.

As can be seen from the dashed line marking 100% release, none of the disintegrants result in a formulation with immediate release properties. As mannitol is the only additive which resulted in the printing of more than one formulation, it is difficult to determine if increasing the levels of disintegrant, while keeping the drug loading constant, results in any improvement to the overall release of carvedilol, and this should be investigated further. When comparing formulations of the same drug loading, but different disintegrant, PEG 4600 is the only disintegrant which improves the API release relative to the other formulations.

By the nature of the FFF 3D printing technique itself, the resulting tablets are highly compacted and, as mentioned above, result in an erosion based method of dissolution. As such the addition of disintegrants, which would usually aid in tablet fragmentation, do not offer results which would suggest immediate release in this instance. The use of additives has however been successful in improving dissolution when the paste



extrusion 3D printing method has been employed, with the addition of either croscarmellose sodium<sup>135</sup> or hydroxypropyl- $\beta$ -cyclodextrin<sup>136</sup> resulting in immediate release formulations of paracetamol or carbamazepine respectively.

Based on the success of printing with mannitol containing formulations, coupled with the slight improvement to release rate when using PEG 4600, further investigation into varying these disintegrant loadings may provide access to immediate release formulations.

#### **4.3.3.3 Printing of Formulations Containing Increased Mannitol or PEG 4600**

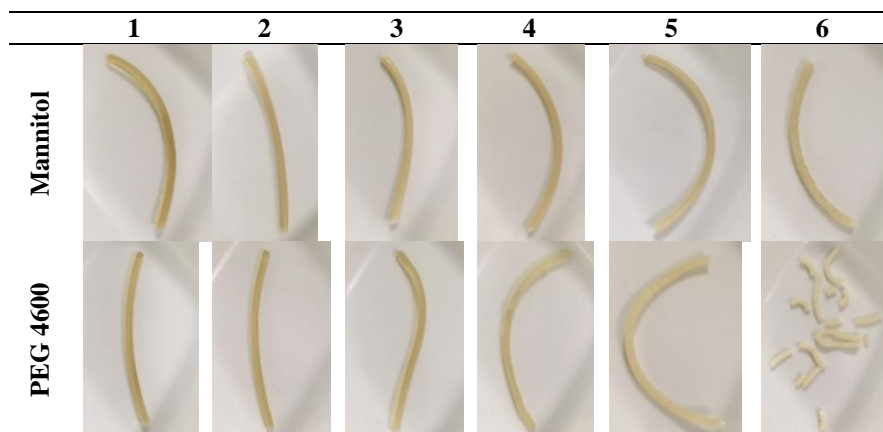
In order to investigate what effect increasing the concentration of the chosen disintegrants, mannitol and PEG 4600, has on the release of API, extrusion of a range of formulations was carried out according to Table 35:

**Table 35** - Extrusion of Mannitol and PEG 4600 Formulations

<b>Formulation</b>	<b>API (%)</b>	<b>Disintegrant (%)</b>	<b>Polymer (%)</b>
Blank	10.5	0	89.5
1	10.5	5	84.5
2	10.5	10	79.5
3	10.5	15	74.5
4	10.5	20	69.5
5	10.5	30	59.5
6	10.5	40	49.5

In each case material was successfully extruded, with the exception of PEG 4600 formulation 6, which was unsuccessful in forming a filament. The extrusion of a blank formulation was also successful, producing a glassy, golden filament with an average diameter of 1.77 mm. Results from these extrusion experiments are seen in Table 36:

**Table 36** - Filaments from Extrusion of Various Mannitol and PEG 4600 Formulations









For mannitol, formulation 1 starts out as a glassy golden filament, and gradually becomes paler and more opaque as the concentration of mannitol increases. All filaments retained structural integrity until formulation 6, where the filament became very brittle and snapped under very little pressure.

Similarly for PEG 4600, formulation 1 starts out as a golden, glassy filament, gradually becoming paler and more opaque as the concentration of PEG 4600 increases, but a very brittle filament is encountered at formulation 5, with formulation 6 completely crumbling into fragments.

With regards to printing, no tablets could be produced for the blank formulation, which further supports the theory that API alone is not enough to plasticise the filament. All other results are displayed in Table 37:

**Table 37** - Results of Increased Levels of Mannitol and PEG 4600 Printing

<b>Formulation</b>	<b>Mannitol</b>	<b>PEG 4600</b>
1 (10.5% API, 5% Disintegrant)		
2 (10.5% API, 10% Disintegrant)		No Tablets
3 (10.5% API, 15% Disintegrant)		No Tablets
4 (10.5% API, 20% Disintegrant)		No Tablets
5 (10.5% API, 30% Disintegrant)		No Tablets
6 (10.5% API, 40% Disintegrant)	No Tablets	No Tablets

Printing success was achieved with all mannitol formulations, with the exception of formulation 6, but success was only achieved with formulation 1 for PEG 4600 – the same composition as was manufactured in the DoE. Quality of finished tablets also seemed to decline as mannitol concentration increased, indicating that even if the disintegration is improved, this may come at a price of consistent tablet manufacture. Given that increasing PEG 4600 content resulted in softer filaments, as observed in the disintegration DoE, analysis of filament mechanical properties may provide a definitive answer as to why these formulations were unsuitable for printing.

**4.3.3.3.1 Analysis of Filament Mechanical Properties**

As with the filaments from the DoE (Section 4.3.3.2.1), five samples from each formulation were subjected to 3-point bend testing using a texture analyser. Results

are displayed in Stress (MPa) versus Strain (%) graphs for both mannitol and PEG 4600 and are shown in Figure 90 and Figure 91:

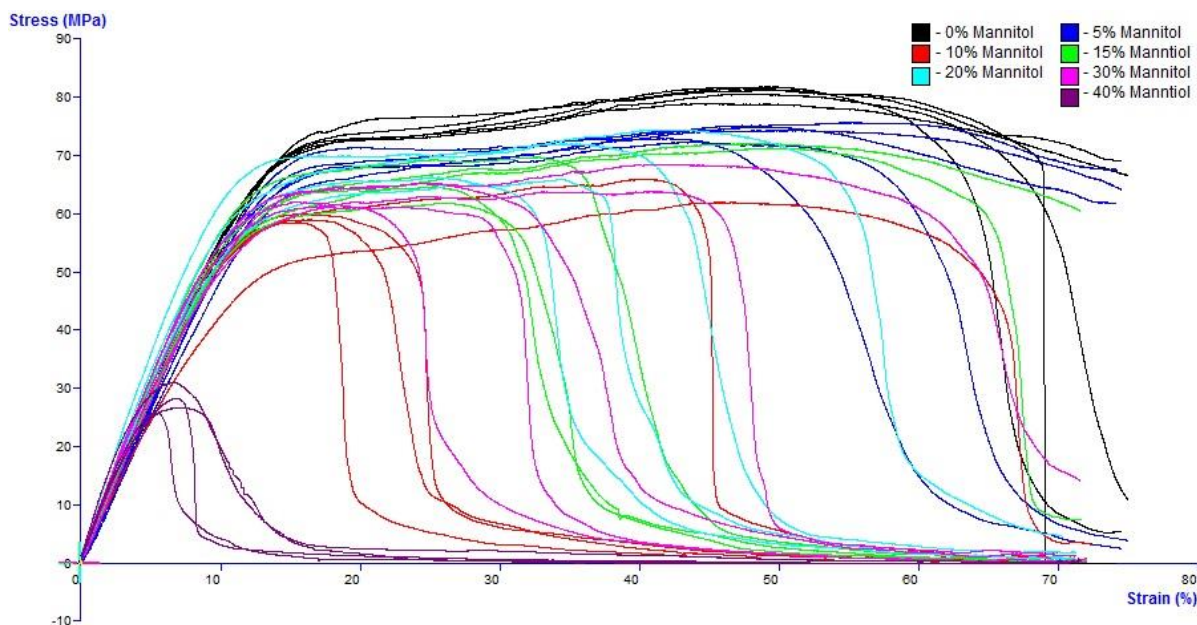


**Figure 90** - Stress vs Strain Graph for Mannitol Formulations

As observed with the different mannitol formulations in the previous DoE, there appears to be a lot of filament breakage, but this does not seem to correlate with printability of the formulations - all of these formulations could be printed, with the exception of 0% mannitol (black) and 40% mannitol (purple). Although textural analysis does not indicate a clear reason for failure in the case of 0% mannitol, there is a distinct difference observed in the maximum stress which could be applied to filaments containing 40% mannitol. These filaments can only be subjected to a stress of approximately 30 MPa, which is lower than the 40 MPa threshold discussed in Section 4.3.3.2.1, and they also break at a strain of approximately 10% which would indicate that the filaments are also fairly brittle. The brittle nature of these filaments could potentially be due to a lack of Affinisol™ coupled with high levels of crystallinity.

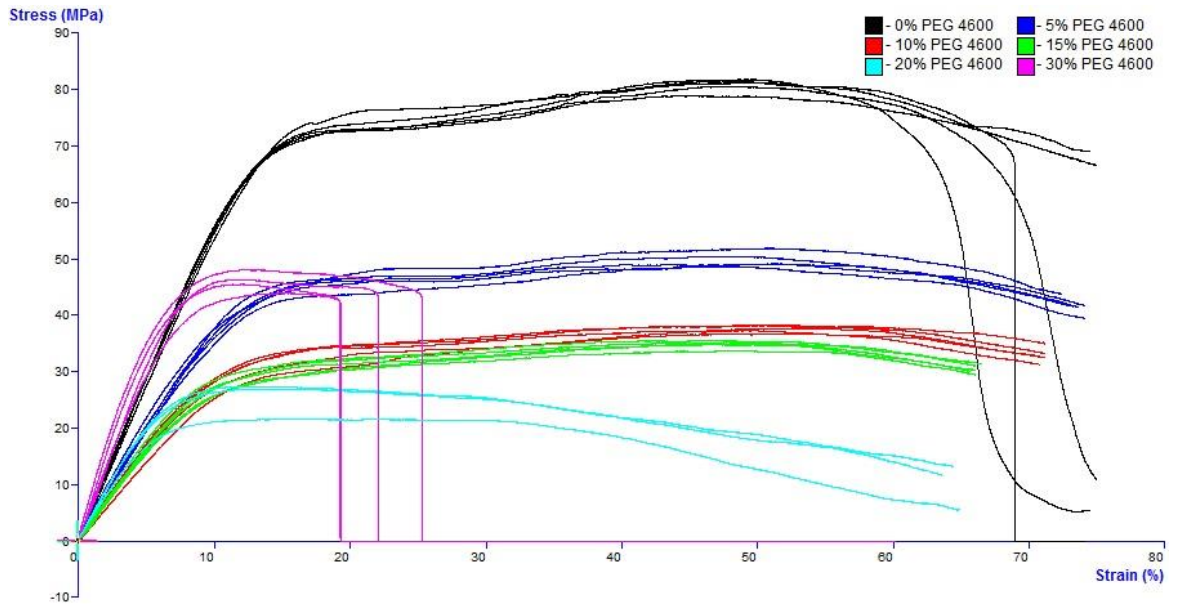


**Figure 91** - Stress vs Strain Graph for PEG 4600 Formulations

For the formulations containing PEG 4600, similar observations to that of the DoE can be made. Addition of PEG 4600 results in an increase in plasticisation of the formulations up until a level of 30% is reached. This plasticisation lowers the maximum stress which can be applied below the threshold level of 40 MPa and results in filaments which are too soft for printing. As with the results of mechanical testing in Section 4.3.3.2.1, the flexural modulus and maximum stress can be plotted for easier visualisation of these ‘threshold’ values (Figure 92):

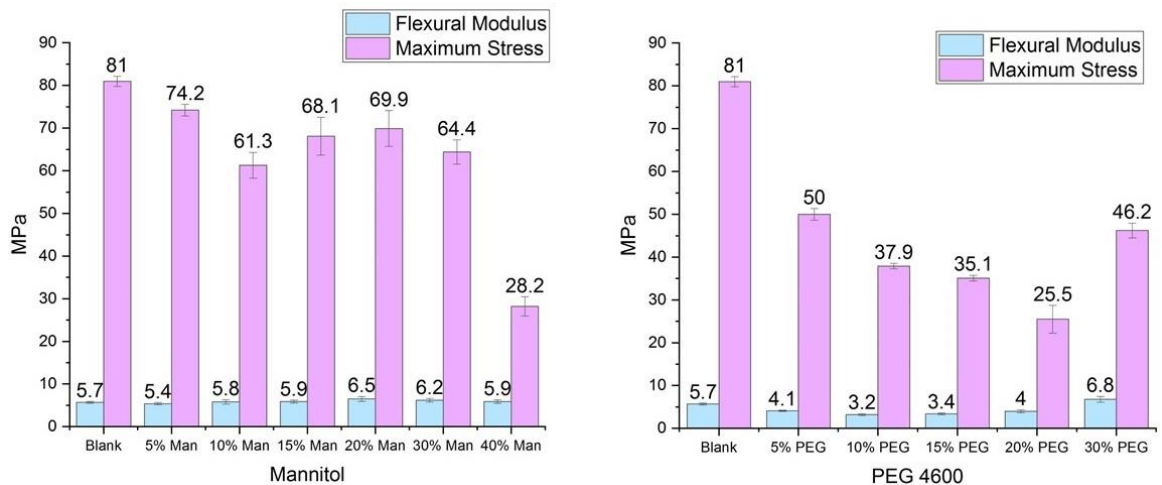


**Figure 92** - Flexural Modulus and Maximum Stress for Mannitol and PEG 4600 Formulations (n=5 ± standard deviation)

Looking at the flexural modulus, this remains fairly consistent across the mannitol formulations, providing no insight into printability, and remains above 4.5 MPa which was the lowest flexural modulus observed in a printable formulation in Section 4.3.3.2.1. With regards to formulations containing PEG 4600, all those with less than 30% PEG 4600 (with the exception of the blank) are lower than 4.5 MPa and could provide an indication that these filaments are too soft for printing, however print success was observed for 5% PEG 4600, therefore the lowest printable flexural modulus would need to be adjusted to 4.1 MPa. This is within the range observed by Prasad *et al.* for printable formulations containing paracetamol<sup>87</sup> and would indicate that careful comparison of both flexural modulus and maximum stress are required to determine printability due to filament softness. When comparing values for maximum stress with the mannitol formulations, all are within the printable range described in Section 4.3.3.2.1, with the exception of those containing 40% mannitol. The blank formulation displays the highest value observed for maximum stress (81 MPa), but this would not necessarily indicate that it should fail to print, given that a higher value of 84.8 MPa was observed in a formulation containing 20% CAR and 10% mannitol in Section 4.3.3.2.1. For the formulations containing PEG 4600, maximum stress can more much easily predict print failure due to the soft filaments obtained. In formulations containing higher than 5% PEG 4600, both the flexural modulus and maximum stress suggest that these formulations should not be printable, given that the lowest observed maximum stress for successful printing is 50 MPa. At levels of 30% PEG 4600 and above, brittle filaments were observed which either crumbled, or snapped under very little pressure. When comparing this to the results obtained from textural analysis, a maximum strain threshold of 15-25% can also be loosely applied, which could be another indicator used for prediction of print suitability. This strain threshold is also applicable to the filaments containing 40% mannitol, which all break at approximately 10% strain.

While increased plasticisation is sufficient explanation for print failure in formulations 2 to 4 of PEG 4600, another explanation is required for failure of formulation 5, although, given the lack of printing success overall, no further investigation into PEG

4600 formulations was carried out. Analysis of filament crystallinity for mannitol may indicate the limits of operation for formulations containing these components.

#### **4.3.3.3.2 Crystallinity Determination of Filaments**

As with filaments from the DoE, crystallinity was assessed for each of the formulations using XRPD analysis. Results are shown in Figure 93:

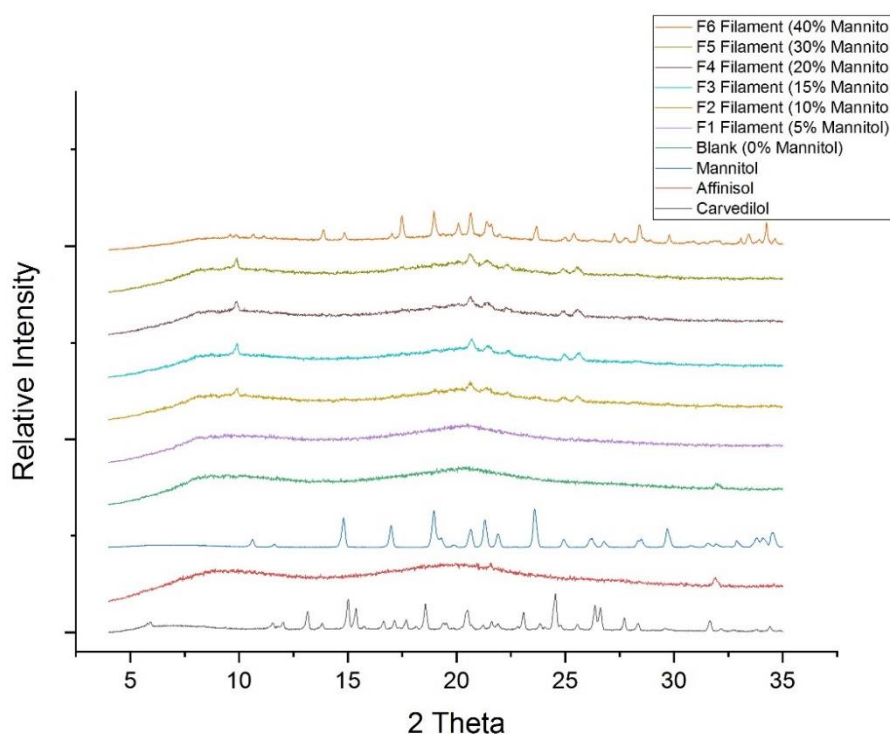


**Figure 93** - XRPD Analysis of Filaments from Further Mannitol Extrusion

As can be seen from the data, no peaks are observed in the blank formulation, or in formulation 1 (5% mannitol), but the appearance of peaks corresponding to mannitol are observed in formulations 2, 3, 4 and 5 (10%, 15%, 20% and 30% mannitol respectively). These peaks do not signal a failure in printing, instead, tablets could still be produced up until formulation 6 (40% mannitol), where printing eventually failed.

Formulation 6 shows mostly crystalline material, which also seems to be distinctly different from both the carvedilol and mannitol starting material, suggesting that (as it is a high concentration of mannitol) a different polymorph of mannitol has

recrystallised in the filament after extrusion. Mannitol is known to have three distinct polymorphs: alpha,<sup>137</sup> beta<sup>138</sup> and delta,<sup>139</sup> and comparison of literature XRPD data with XRPD data from the mannitol used in this research confirmed that the starting material was the beta form. Comparison of all three of these powder patterns with that of formulation 6 is shown in Figure 94:

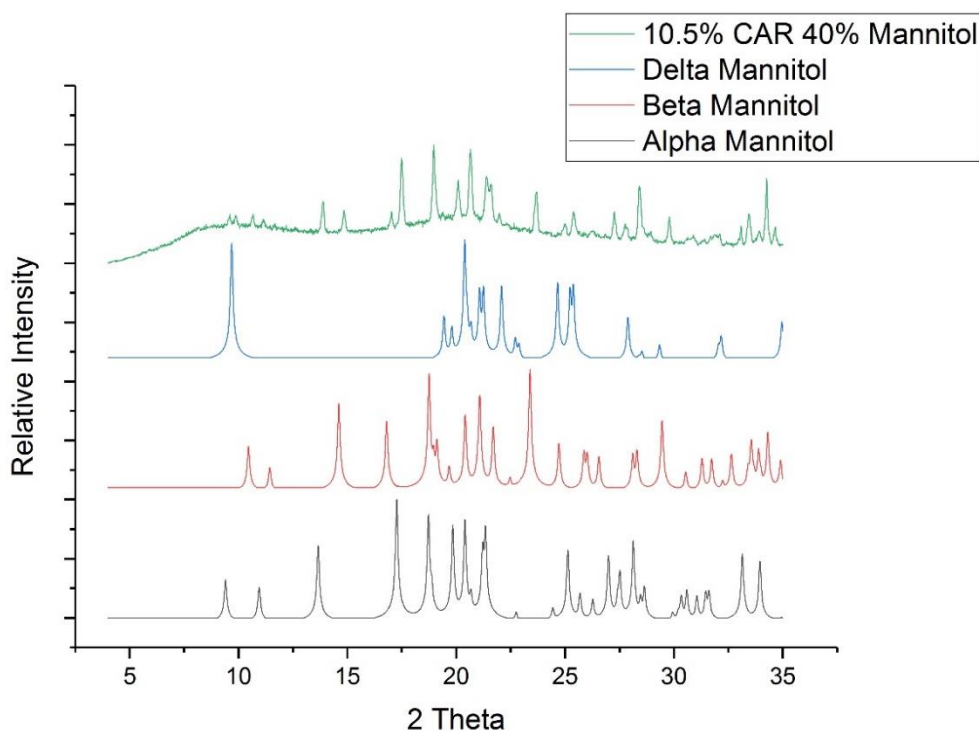


**Figure 94** - Comparison of Formulation 6 (10.5% CAR, 40% Mannitol) with alpha, beta and delta Mannitol Polymorphs

It is difficult to differentiate the peaks fully, but by looking at the intensity of the peaks, it seems that a mixture of both the alpha and beta polymorphs are present in formulation 6, with perhaps even a little of the delta polymorph present, although in smaller quantities.

Overall, these results demonstrate that, while small amounts of crystalline material do not seem to hinder printing of mannitol formulations, large amounts of crystallinity result in a non viable filament for printing. XRPD also highlights that processing of mannitol with these components using HME results in polymorphic changes which may also then be present in the final dosage form, post-printing.



#### 4.3.3.3 Dissolution of Printed Tablets

As printing was only successful for the PEG 4600 formulation with the same composition as was investigated in the DoE, this was excluded from further dissolution testing.

In order to determine if increasing the mannitol content improved the dissolution and release of API from the formulations, all tablets which could be printed were subjected to dissolution analysis using a USP 1 dissolution test. Samples were run for six hours and the following release profiles were obtained (Figure 95):

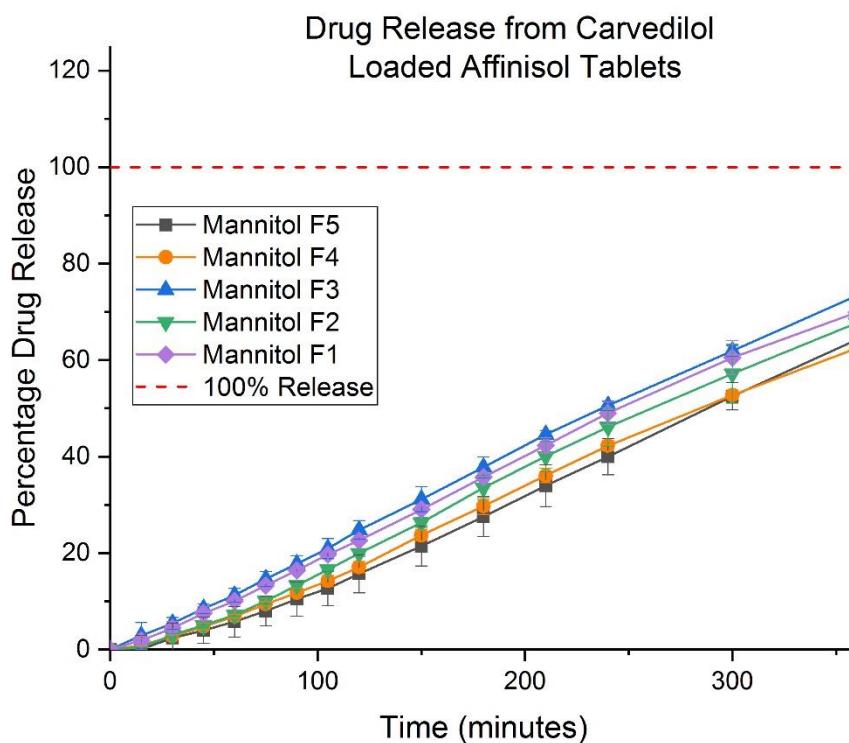


**Figure 95** - Dissolution of Formulations with Increased Mannitol Content (n=3, ± standard deviation)

As can be seen from the dashed line marking 100% release, none of these formulations result in complete release of the API from the tablets. As the error bars also overlap with each other, it can be concluded that increasing the mannitol content does not improve the overall release of carvedilol from these formulations, although this is discussed in greater detail in Chapter 5, Section 5.3.1.4.

Despite these results, mannitol does have the benefit of enabling printing when compared to 'blank' formulations, which could not be successfully printed. Therefore, investigation into combining carvedilol/mannitol/Affinisol™ formulations with alternative additives may result in formulations that have improved dissolution properties.

#### **4.3.3.4 Printing of Formulations Containing Superdisintegrants**

Superdisintegrants are additives included in tablet manufacture with the function of improving the dosage form disintegration to allow rapid dissolution of the API from the tablet matrix.<sup>140</sup> Several different types have been used for this purpose such as: sodium starch glycolate, cross povidone, alginates, cellulose derivatives, microcrystalline cellulose, chitin, indion 414 and modified polysaccharides.

In this research, two sodium starch glycolate compounds (Explotab® and VivaStar®), and one cellulose derivative (crosscarmellose sodium, VivaSol®), were investigated to determine if any could improve the disintegration and drug release from 3D printed tablets. The following different formulations were investigated for each of the superdisintegrants (Table 38):













**Table 38** - Formulations Design for Superdisintegrant Investigation

<b>Formulation</b>	<b>API (%)</b>	<b>Superdisintegrant (%)</b>	<b>Mannitol (%)</b>	<b>Polymer (%)</b>
1	10.5	1	0	88.5
2	10.5	2	0	87.5
3	10.5	3	0	86.5
4	10.5	4	0	85.5
5	1	10	0	89
6	20	10	0	70
7	10.5	5	0	84.5
Man 1	10.5	1	5	83.5
Man 2	10.5	2	5	82.5
Man 3	10.5	3	5	81.5
Man 4	10.5	4	5	80.5
Man 5	10.5	5	5	79.5
Man 6	10.5	10	5	74.5

Extrusion was successful for all formulations, with no indication of any degradation, as evidenced by an observed golden filament colour. This colour did not change across all the various formulations, therefore pictures of the filaments have been omitted from this discussion. Filaments appeared mostly smooth and flexible, with only those of high superdisintegrant concentration displaying any surface roughness. Slight variation in processing time was noted across different formulations, with a time of 7 minutes being recorded for those without mannitol which contained 5% and 10% of the superdisintegrants. This processing time then decreased when the concentration of superdisintegrant was at 4% and below, with times of either 5 minutes 30 seconds being noted for formulations containing Explotab® and 5 minutes 40 seconds for those containing VivaStar® or VivaSol®. The addition of mannitol to all of these formulations then reduced the processing time further and resulted in a time of 5 minutes being recored for each of the superdisintegrants under investigation.

All formulations without mannitol failed to print, which was expected given the seeming requirement for inclusion based on previous mannitol experiments. Results for formulations which included mannitol are shown in Table 39:

**Table 39 - Results of Superdisintegrant Printing**

<b>Formulation</b>	<b>Explotab®</b>	<b>VivaStar®</b>	<b>VivaSol®</b>
Man 1 (1% Superdis.)			
Man 2 (2% Superdis.)			
Man 3 (3% Superdis.)			
Man 4 (4% Superdis.)			No Tablets
Man 5 (5% Superdis.)		No Tablets	No Tablets
Man 6 (10% Superdis.)	No Tablets	No Tablets	No Tablets

Printing success was achieved with formulations 1-5 for Explotab®, 1-4 for VivaStar® and 1-3 for VivaSol®. With the exclusion of mannitol, printing was unsuccessful therefore it is likely that the superdisintegrants provide no plasticisation effect on the formulations. When mannitol was included, the formulations were printable, but only at low superdisintegrant loading, with increasing levels hindering the formulations to different degrees.

#### 4.3.3.4.1 Analysis of Filament Mechanical Properties

3-point bend testing was again used as a method of investigating the mechanical properties of printer filaments. Given the large amount of different formulations, and the seeming requirement for mannitol to be present for successful printing, only samples containing mannitol were investigated further. Five samples from each formulation were analysed and results are displayed in Stress (MPa) versus Strain (%) graphs for each of the superdisintegrants investigated (Figure 96, Figure 97 and Figure 98):

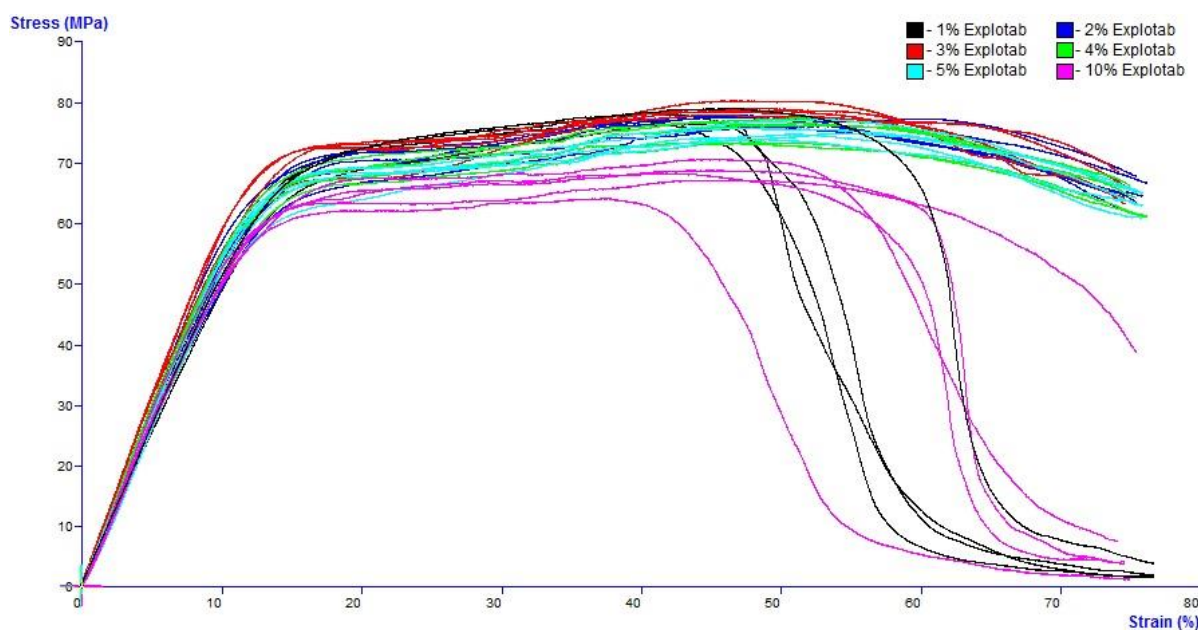


Figure 96 - Stress vs Strain Graph for Mannitol/Explotab® Formulations

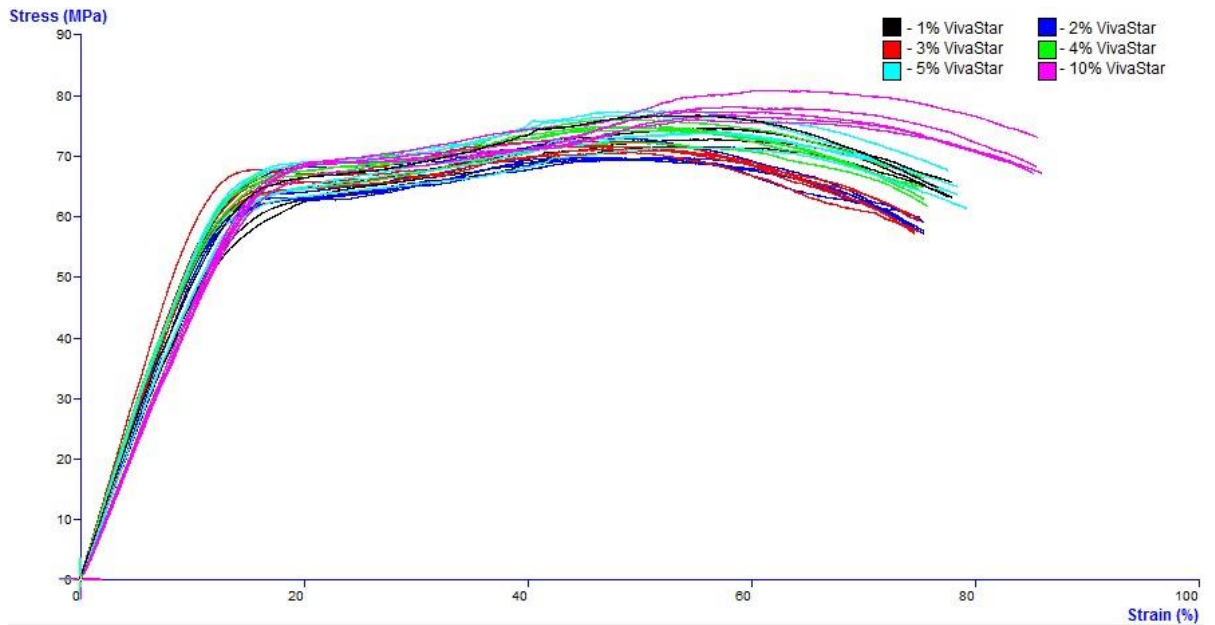


Figure 97 - Stress vs Strain Graph for Mannitol/VivaStar® Formulations

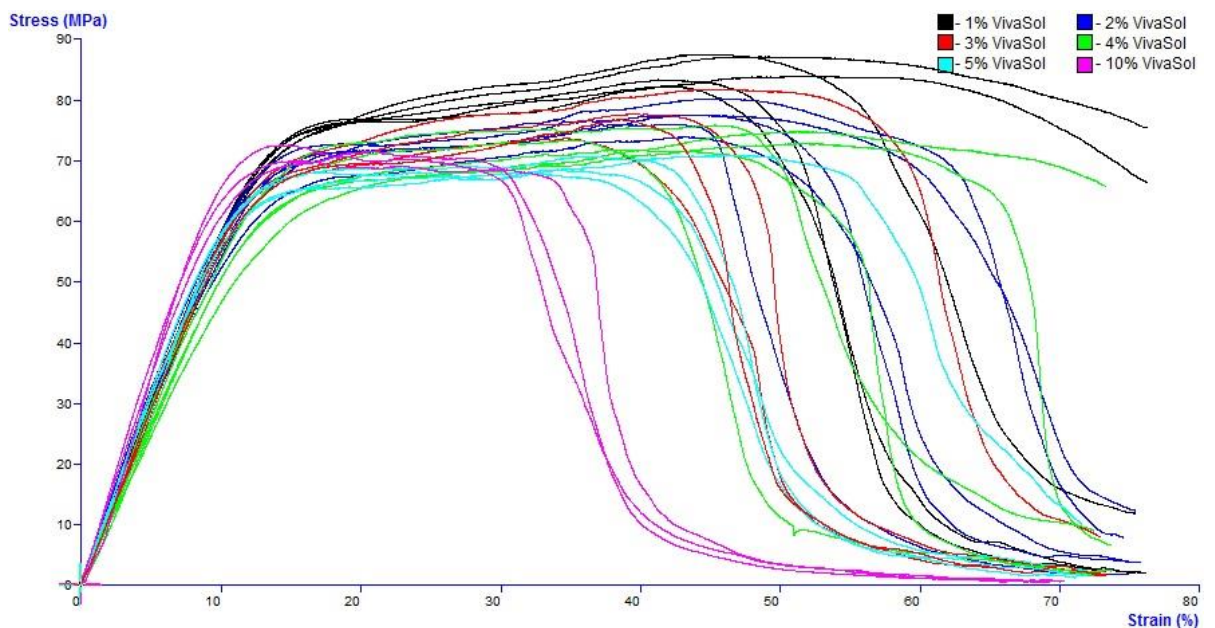
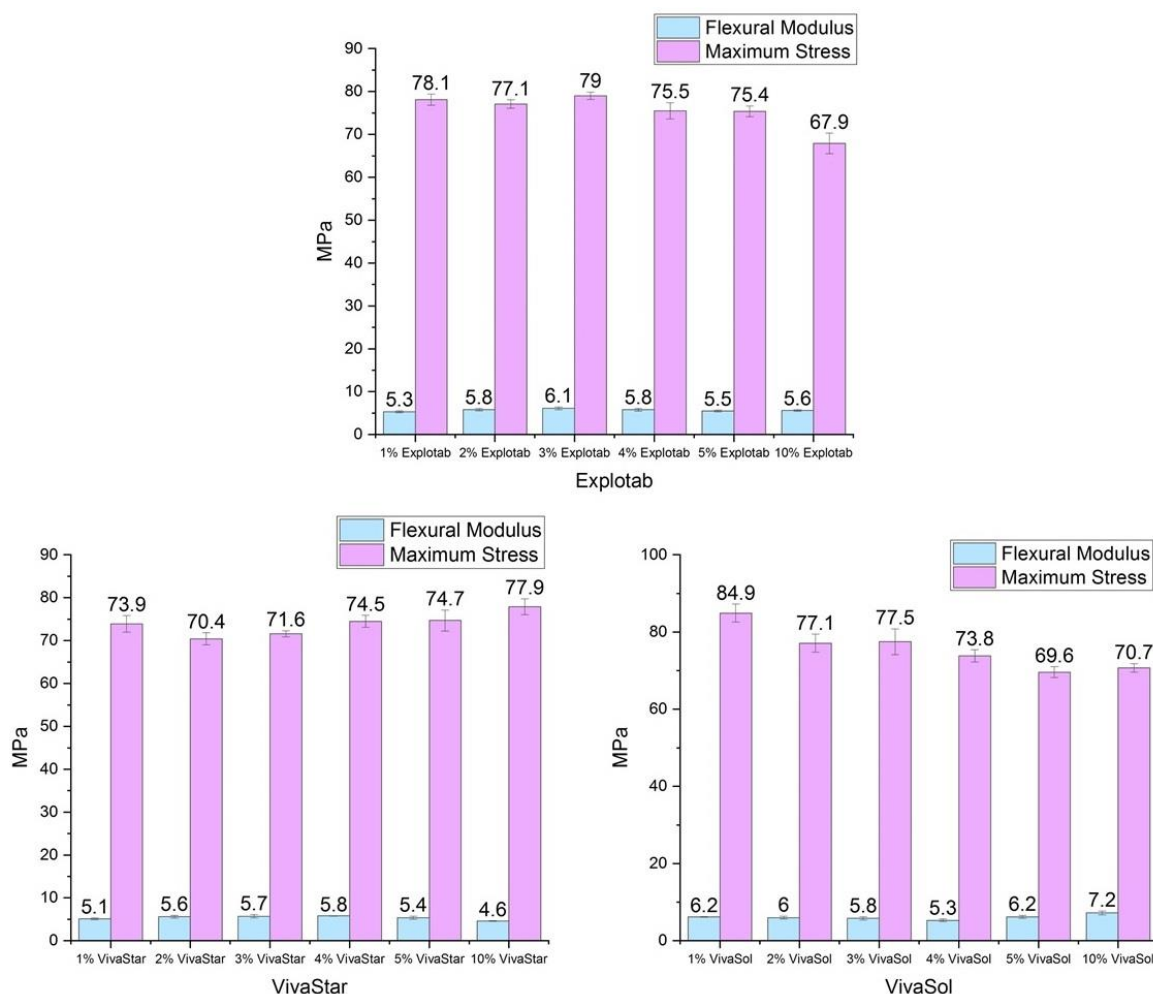


Figure 98 - Stress vs Strain Graph for Mannitol/VivaSol® Formulations

Overall, results for textural analysis across all of these formulations show very similar values for maximum stress observed, with only small variations in this number across all the various formulations investigated. There are differences observed in the maximum strain values that each of the formulations can withstand, with VivaStar® showing no filament breakage and both Explotab® and VivaSol® showing differing

amounts of breakage depending on the superdisintegrant concentration. Again, for ease of visualisation, the flexural modulus and maximum stress for each of the superdisintegrant formulations is displayed in Figure 99:



**Figure 99** - Flexural Modulus and Maximum Stress Observed for Superdisintegrant Formulations (n=5 ± standard deviation)

All these formulations show fairly consistent results for flexural modulus across the different superdisintegrants investigated. Coupled with results observed for maximum stress, all formulations display values above the 40 MPa threshold previously discussed, meaning that it is difficult to explain print failure from these values alone. A further increase to the upper limit for maximum stress is also observed with 1% VivaSol® at 84.9 MPa, which is just above the 84.8 MPa observed with formulation 4 of mannitol (20% CAR, 10% mannitol) in Section 4.3.3.2.1. When

considering any observed breakages, these all occur well above the strain threshold of 25% also previously discussed in Section 4.3.3.3.1, again making it difficult to determine an explanation for print failure. A greater degree of variation is seen in the results from mannitol/VivaSol® formulations, which would indicate that the filaments themselves have not been processed consistently. This in itself may provide some explanation why printing was less successful for these formulations. Based on previous analysis of mannitol containing formulations, showing that there should be no crystallinity associated with mannitol at the concentration used, any observed crystallinity should be due to superdisintegrant only, providing that the addition of a new component to the formulation has not resulted changes to how mannitol interacts within the overall formulation. XRPD analysis could potentially indicate a reason for print failure in these formulations.

#### **4.3.3.4.2 Crystallinity Determination of Filaments**

As with previous experiments, each of the formulations were assessed for filament crystallinity using XRPD. Results are shown in Figure 100, Figure 101 and Figure 102:

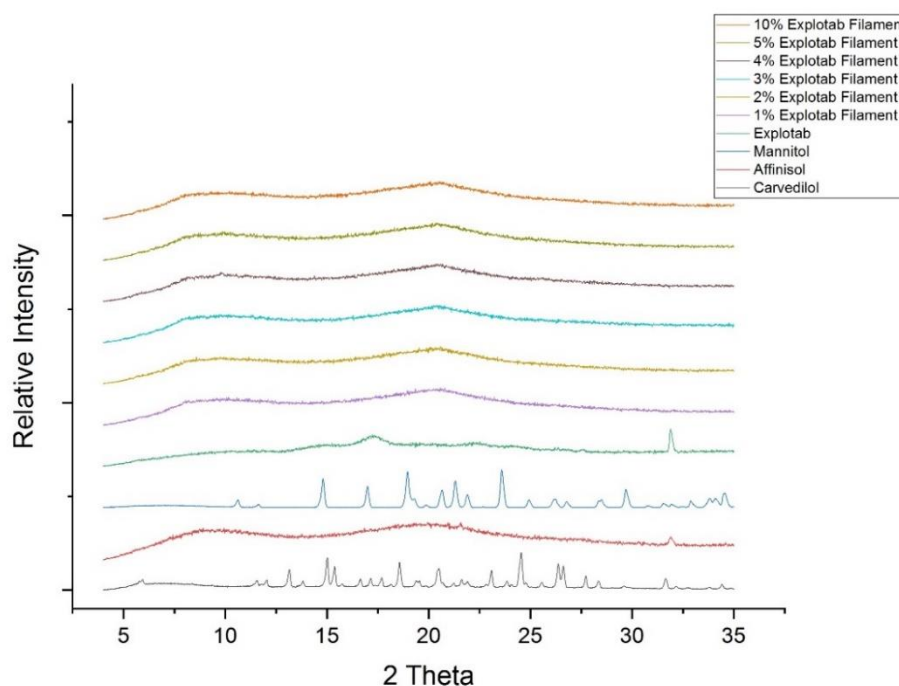


**Figure 100 - XRPD Analysis of Explotab® Filaments**

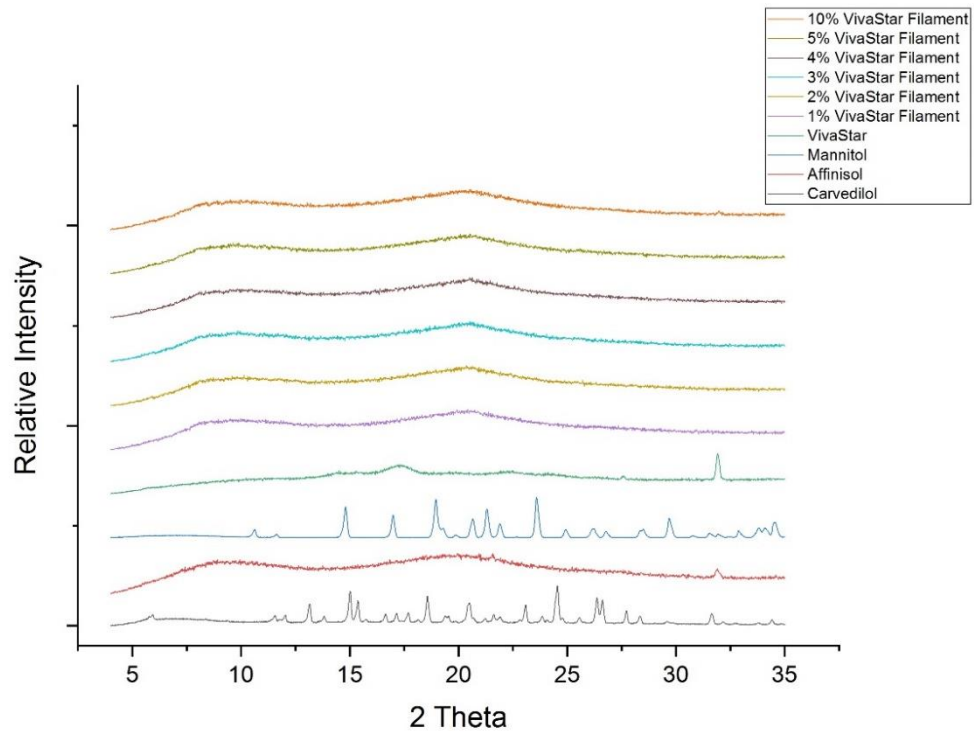


Figure 101 - XRPD Analysis of VivaStar® Filaments

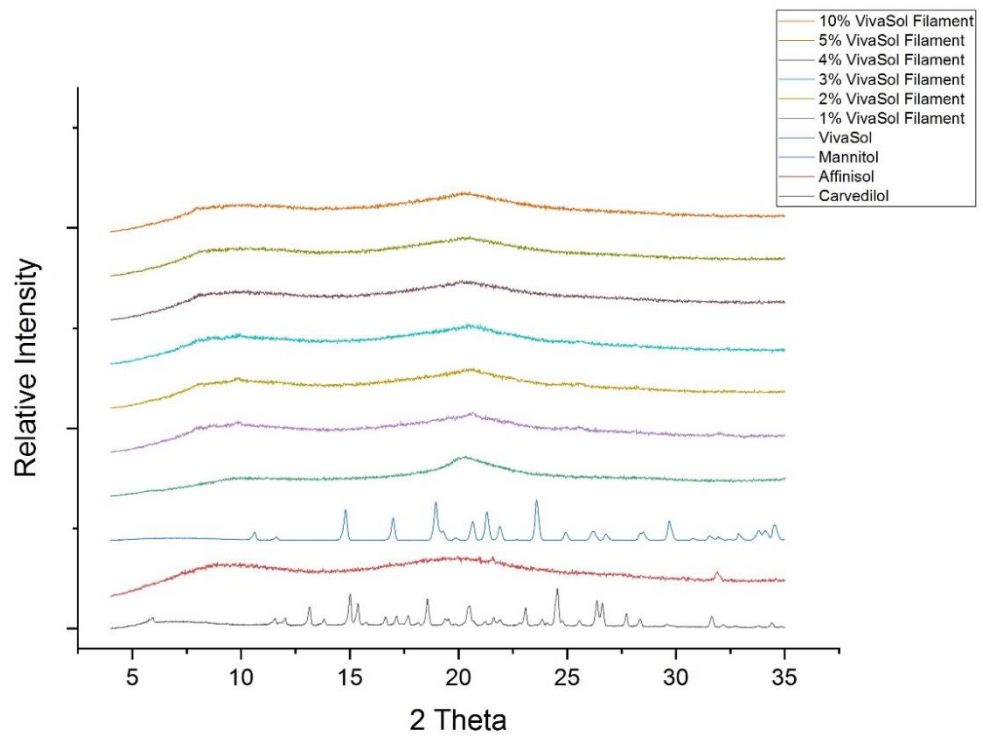


Figure 102 - XRPD Analysis of VivaSol® Filaments



When looking at filaments and comparing them to the raw starting materials, it is clear that there are no peaks corresponding to any of the starting materials observed in any of the formulations produced. This is likely due to the low level of crystallinity observed in the superdisintegrants themselves, combined with the low concentration of mannitol (5%) present in the formulations. As shown in experiments with increasing mannitol concentration, peaks attributed to mannitol begin to appear once levels reach 10% mannitol, therefore the level of mannitol here is likely in an amorphous state, or too low to be detected by XRPD.

#### 4.3.3.4.3 Dissolution of Printed Tablets

Given that the purpose of including superdisintegrants in the formulations was to improve the release of API from the printed tablets, all tablets which could be printed were again subjected to dissolution analysis using a USP 1 dissolution test. Samples were run for six hours and the following release profiles were obtained (Figure 103):

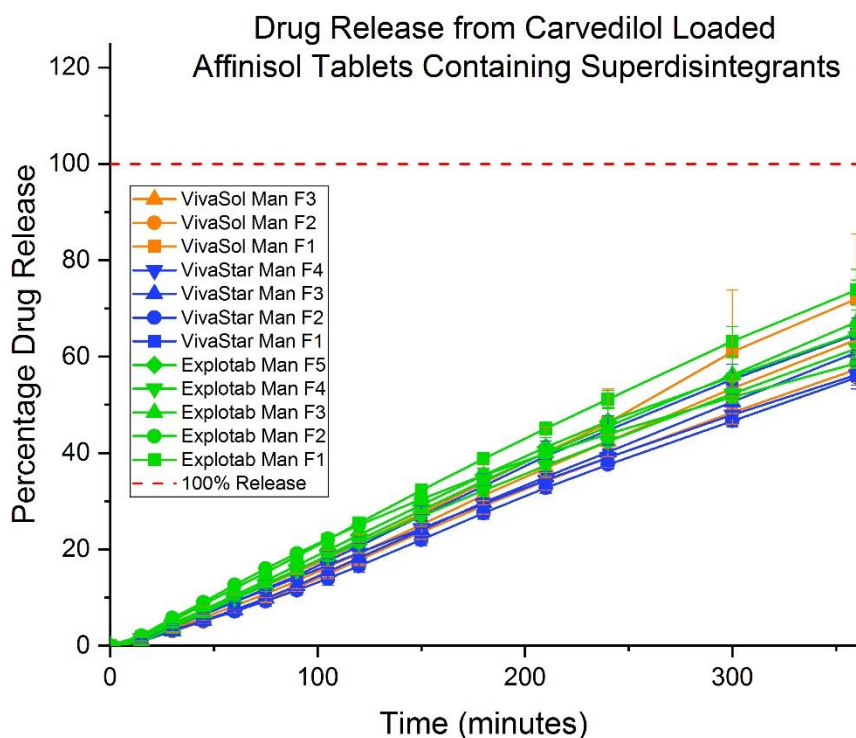
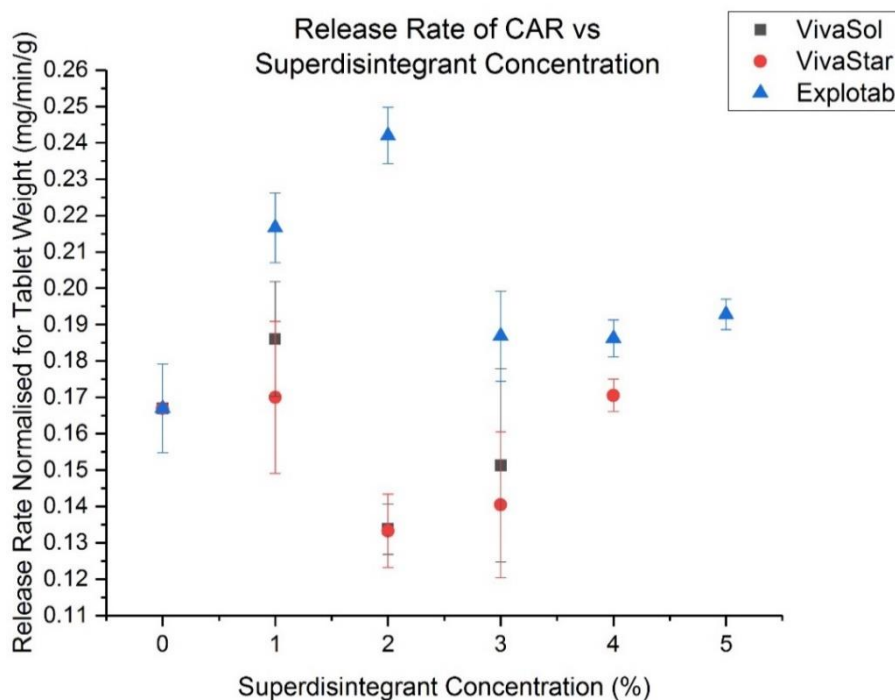


Figure 103 - Dissolution of Formulations Containing Superdisintegrants (n=3, ± standard deviation)

Given that the dissolution profiles remain fairly linear, release rate can be estimated by obtaining the gradient of the straight line. Due to the internal structure of the printed tablets, dissolution is not consistent once the inner cavity of the tablet has been breached due to erosion by the dissolution media, so to avoid any effects which may occur due to tablet fragmentation later on, release rate was only measured over the first hour of dissolution. Plots of concentration vs time for the first 60 minutes were obtained for each of the formulations, and a linear trend line fitted to the data for each of the tablets analysed. Points were then taken from each of these lines, and the release rate calculated according to the following equation, where  $m$  is the gradient of the line:

$$m = (y_2 - y_1) / (x_2 - x_1)$$

From each of the formulations, release rates (mg/min) were calculated according to the volume of the dissolution media, in this case 500 mL, and were normalised for weight (mg/min/g) to account for any discrepancies in weight between individual tablets. These rates were then plotted in the following graph (Figure 104), to illustrate how the rates change with different formulations and superdisintegrants:



**Figure 104** - release rate of carvedilol vs superdisintegrant concentration (n=3, ± standard deviation)

When looking at the information displayed in the above graph, it is difficult to determine if any of the superdisintegrants have a favourable effect on the overall dissolution rate. Carrying out Tukey analysis of these results using an ANOVA method can highlight any statistical differences between the results (Figure 105 and Figure 106):

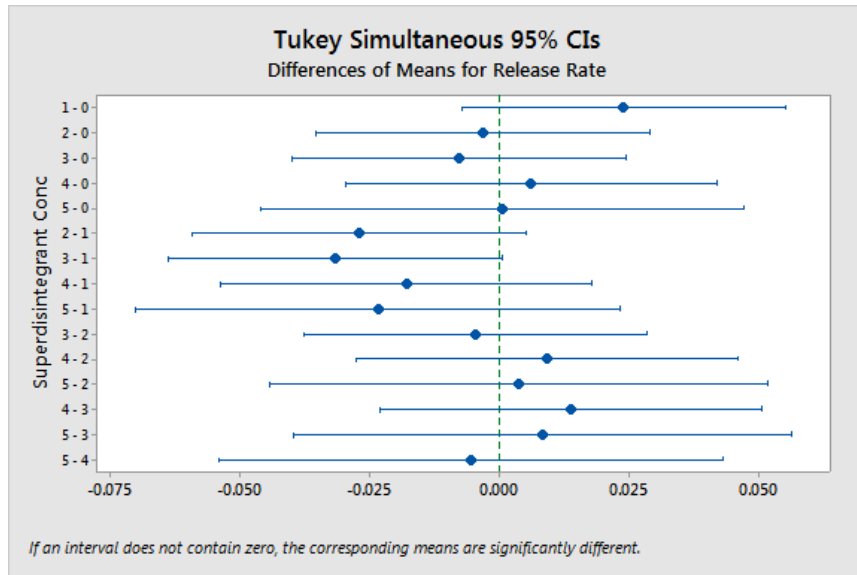


**Figure 105** - Tukey Analysis of Superdisintegrant Concentration

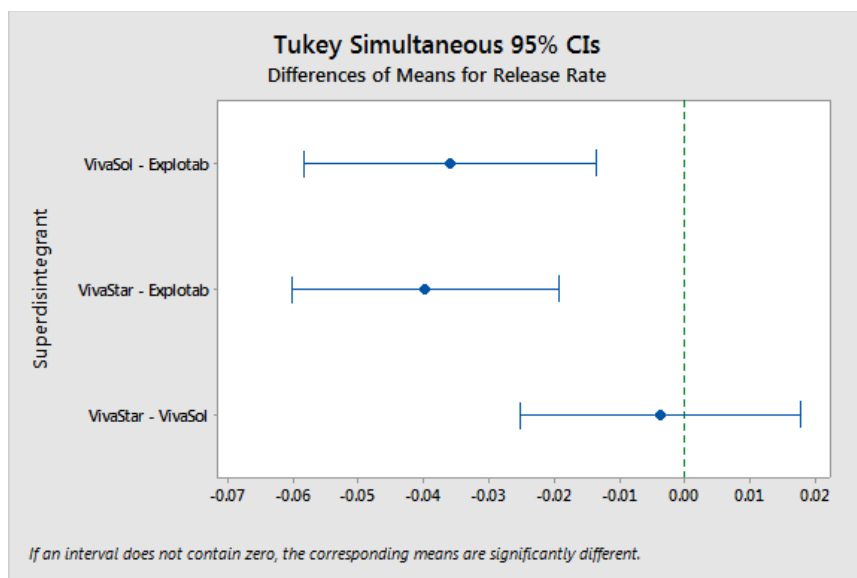


**Figure 106** - Tukey Analysis of Superdisintegrant Type

As stated in the images, 'if an interval does not contain zero, the corresponding means are significantly different.' Therefore, when looking at the percentage of superdisintegrant in the different formulations, there is no statistical difference observed in any of the different concentrations. It's only when comparing the different types of superdisintegrant, that statistical differences arise - while Explotab® is statistically different from both VivaStar® and VivaSol®, there is no statistical difference between VivaStar® and VivaSol® when compared with each other.

If we consider the absence of superdisintegrant as a type of disintegrant with the label 'None', the differences between superdisintegrants become clearer (Figure 107):

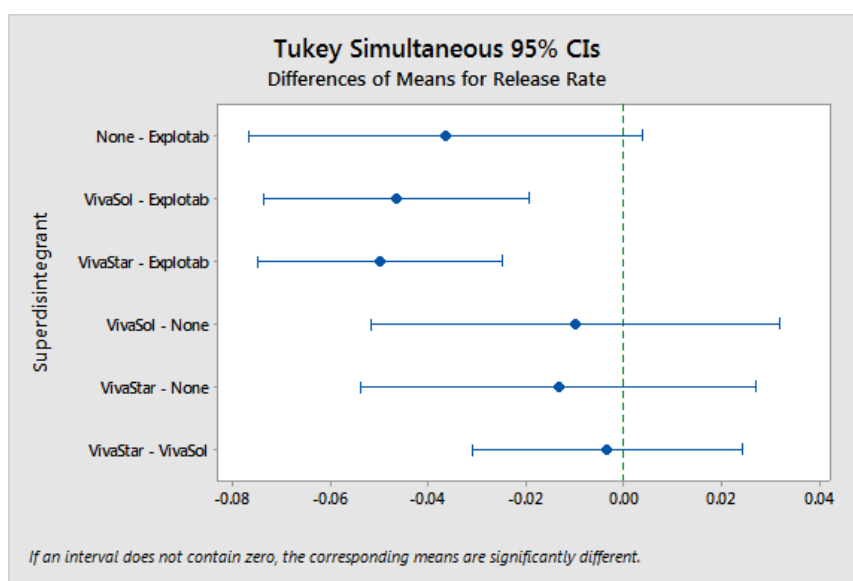


**Figure 107** - Further Tukey Analysis of Superdisintegrant Type

Visually, these results show more clearly that there is no statistical difference between the absence and presence of any of the superdisintegrants tested, but there is a clear difference between Explotab® and both VivaStar® and VivaSol®. Overall, there is no improvement of the dissolution rate with the addition of any of these components, compared to that which was observed when testing disintegrants from the DoE, and this is likely due to the erosion method of dissolution common to all tablets produced by FFF.

Although not fully comparable to FFF, which incorporates these components within the formulations at a molecular level, croscarmellose sodium and sodium starch glycolate have however been used within the paste extrusion 3D printing method as either a component of a joining layer in a multiple component tablet<sup>141</sup> or as the disintegrant in an immediate release formulation of paracetamol,<sup>135</sup> but the levels of these components were not varied during the experiments, so it's unclear if higher levels of superdisintegrant have any effect on the dissolution of 3D printed tablets overall.

#### **4.3.3.5 Changing Surface to Volume Ratio of Printed Tablets**

Based on observations made by Goyanes *et al.* on the differences in dissolution rate of 3D printed tablets in relation to their surface area to volume ratios,<sup>142</sup> investigation was carried out to determine what effect, if any, the surface area/volume ratio has on the dissolution of Affinisol™ loaded 3D printed tablets of constant width, length and height, with varying numbers of holes (hence different surface area and volume) throughout their structure.

Four different tablet designs were chosen (Figure 108), and these were compared to a blank tablet, with no holes, with each design being printed at 100% infill. As increasing mannitol content had no effect on improving the dissolution, a formulation containing 5% mannitol and 10.5% API was selected for investigation, with these concentrations remaining constant throughout the experiment.

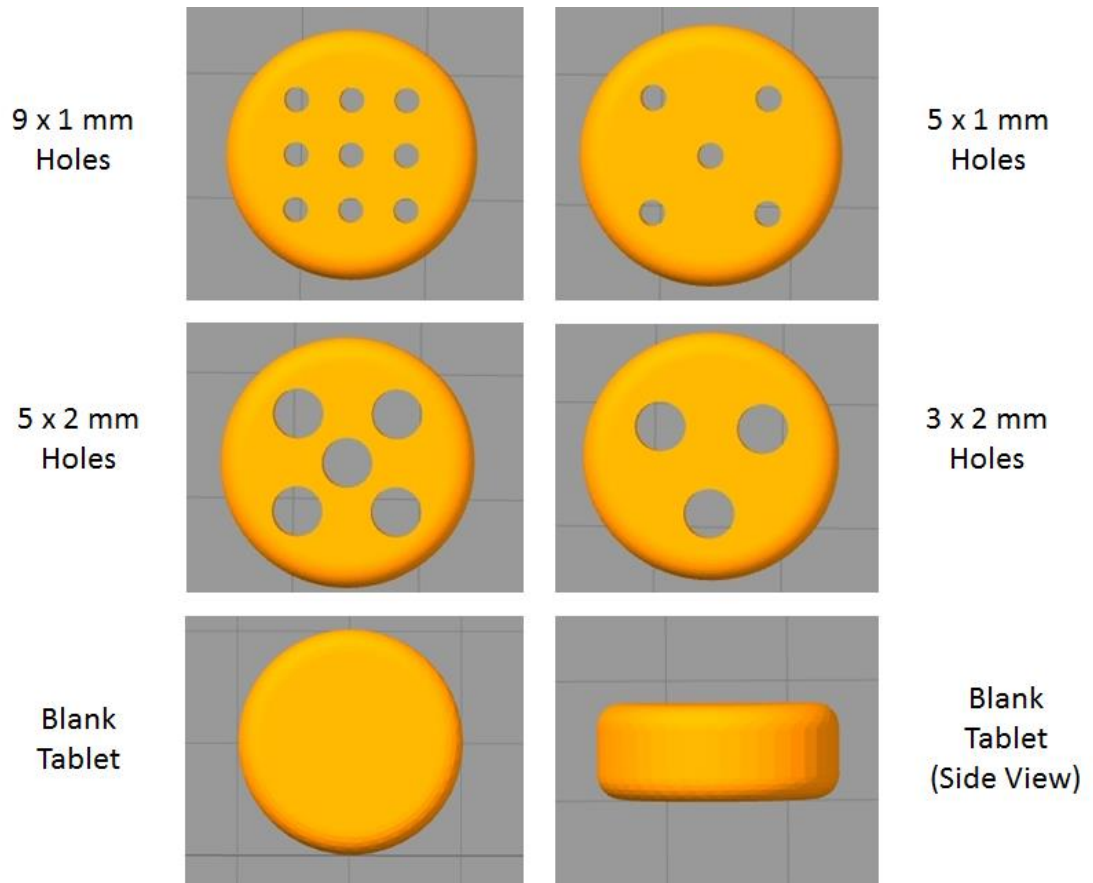


**Figure 108** - Tablet Designs for Surface Area/Volume Ratio Investigation

Tablets were successfully printed for each of the designs under investigation and are shown in Figure 109:



**Figure 109** - Printed Tablets with Varying Holes Incorporated into the Design

The different surface areas and volumes are given in the following Table 40 along with the average weight of printed tablet (n=3) and the theoretical drug content based on a filament containing 10.5% carvedilol and 5% mannitol:

**Table 40** – Surface Area/Volume Ratio of Different Tablet Designs

<b>Design</b>	<b>Surface Area (mm<sup>2</sup>)</b>	<b>Volume (mm<sup>3</sup>)</b>	<b>SA/V Ratio</b>	<b>Average Tablet Weight (mg)<sup>a</sup></b>	<b>Theoretical Drug Loading (mg)<sup>b</sup></b>
Blank	255	301	0.85	293	28.4
9 x 1 mm	354	273	1.30	193	18.7
5 x 1 mm	310	286	1.08	265	25.7
5 x 2 mm	349	238	1.47	169	16.4
3 x 2 mm	311	264	1.18	229	22.2

<sup>a</sup>n=3, <sup>b</sup>hplc analysis confirms filament drug content as 9.7% w/w

Results of printing show that, while the Blank (no holes) tablet design appeared finished to a good standard, once holes were introduced to the tablet design, defects began to appear on the surface of the tablets. This was most prominent on the 9 x 1 mm and 5 x 2 mm tablets, where the design meant that holes were closer together, with less space in between for a surface to be consistently printed. This led to some gaps appearing on the surface, and throughout the infill of the tablet. Oozing at the base of tablet designs with 1 mm holes was also noted, which caused some of the holes to close up restricting the space through which the dissolution medium could pass. Dissolution analysis will provide information on how these designs affect the release of API from the tablet matrix.

#### **4.3.3.5.1 Dissolution of 3D Printed Tablets**

All tablets were subjected to dissolution analysis using a USP 1 dissolution test and the following release profiles were obtained (Figure 110):



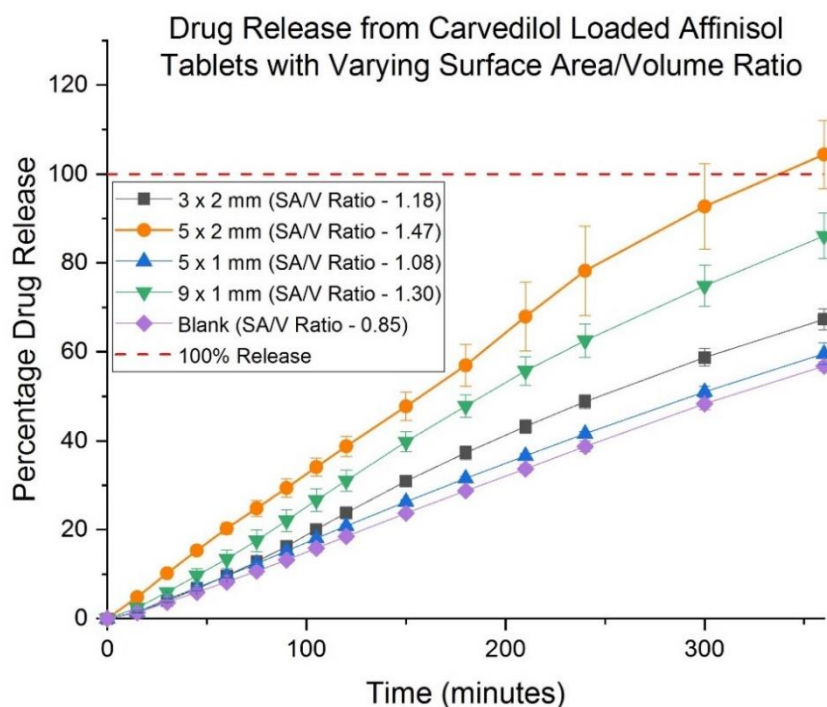


**Figure 110** – Dissolution of Tablets with Varying SA/V Ratios (n=3, ± standard deviation)

As can be seen from these results, the Blank tablet sets the baseline, with all other designs improving the dissolution in the following order:

$$5 \times 1 \text{ mm} < 3 \times 2 \text{ mm} < 9 \times 1 \text{ mm} < 5 \times 2 \text{ mm}$$

This corresponds directly to the Surface Area/Volume ratio, where higher values correspond to improved dissolution, consistent with the findings from Goyanes *et al.*<sup>142</sup> This also corresponds to the change in density across the formulations, with decreasing tablet density resulting in more percentage drug being released within the timeframe of the experiment.

This seems logical, as the tablets of higher density would have more carvedilol present within the overall dosage form, and tablets of lower density would have less carvedilol present. A closer look at the overall release rate for these different designs, normalised for tablet weight, could show if there is any improvement to the overall dissolution.

Like with investigation into superdisintegrant concentration, plots of release rate versus surface area to volume ratio were obtained based on simple linear regression analysis of concentration vs time for the first 60 minutes of dissolution.

From each of the formulations, release rates (mg/min) were calculated based on 500 mL of dissolution media and normalised for weight (mg/min/g) to account for any discrepancies in weight between individual tablets. These rates are plotted in the following graph (Figure 111), to illustrate how these change with different tablet designs:

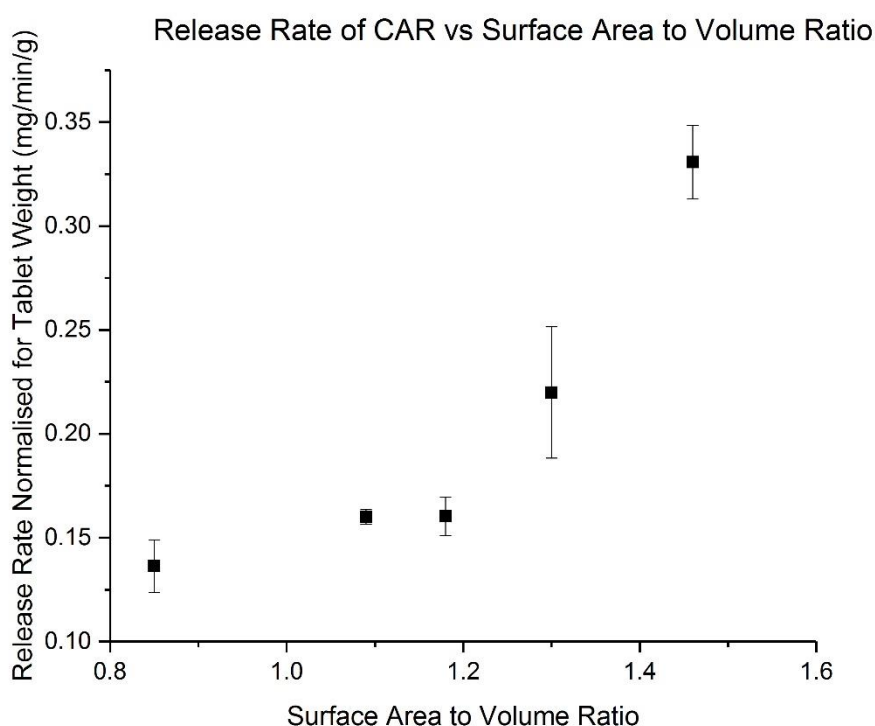


**Figure 111** - Release Rate of Carvedilol vs Surface Area to Volume Ratio (n=3,  $\pm$  standard deviation)

When looking at release rate plotted against surface area to volume ratio, the earlier statement of rates increasing as the surface area to volume ratio increases seems to be supported. Even though this data supports an earlier conclusion, the error bars from the first three data points are very close, or overlap entirely with each other. Statistical analysis using ANOVA calculations provides information on whether the release rates are statistically different or not, as shown in the Tukey plot below (Figure 112):

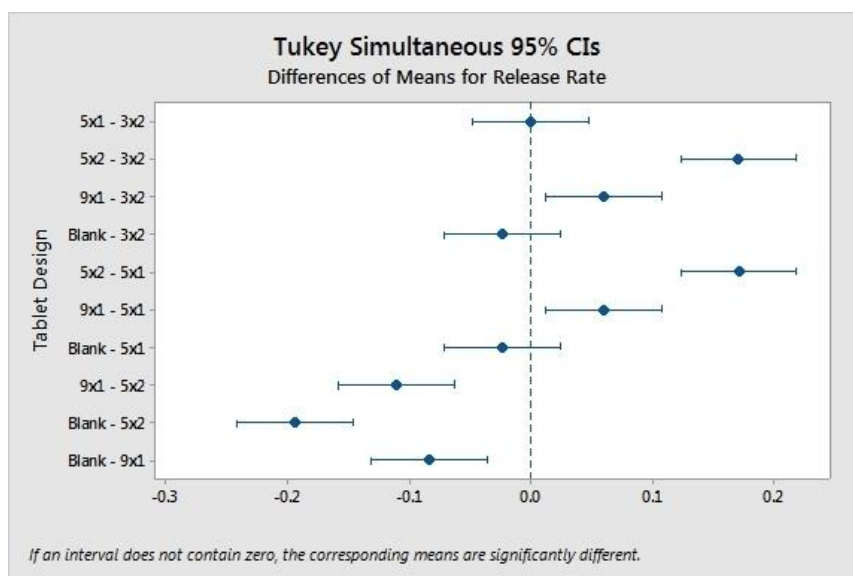


**Figure 112** - Tukey Analysis of Difference in Tablet Designs

When looking at the different tablet designs, there is no statistical difference observed between the blank, 5 x 1 mm or 3 x 2 mm tablets, which are the first three data points mentioned earlier. The other two tablet designs (9 x 1 mm and 5 x 2 mm) are however statistically different from both each other, and the individual first three tablet designs.

This data therefore suggests that while there may not be any observed difference in release rate from small increases in the surface to volume ratio, increasing this value to 1.30 and above (when compared to the initial value of 0.85 for the blank tablet) seems to offer the benefit of improving the rate of dissolution.

Based on the observed erosion mechanism of dissolution for tablets produced by FFF, altering the tablet geometry is a method employed by a number of different groups in order to alter the dissolution rate of 3D printed tablets. While the research of Goyanes *et al.*<sup>142</sup> has already been discussed, changes in geometry have also been investigated by Gültekin *et al.* with the addition of various holes to tablets of pramipexole dihydrochloride monohydrate in Eudragit® EPO and low molecular weight poly-ethylene oxide formulations.<sup>143</sup> This resulted in faster dissolution for tablets with more holes (hence increased surface area), with the drug release completion time of some tablets being reduced to as little as 5 minutes.

Changes in geometry have also been investigated by Arafat *et al.* with a much more complex design which incorporates various different sizes of gaps and bridges into a tablet of theophylline in hydroxypropyl cellulose produced by FFF.<sup>144</sup> A gap spacing of at least 1 mm was required in the tablet design in order to produce tablets which fulfilled the necessary requirements for an immediate release formulation.

Although immediate release has not been achieved with carvedilol and Affinisol™ in this research, it is clear that further investigation into altering tablet geometry could lead to more advances in understanding the release properties of these formulations.

#### **4.3.3.6 Varying Infill Percentage of Printed Tablets**

As was seen in section 3.3.2.3, variation is observed in the release of carvedilol from PVA tablets according to differences in the infill percentage of the dosage forms. This has also been demonstrated by Goyanes *et al.* in the dissolution of other 3D printed dosage forms.<sup>80</sup> Based on these results, attempts were made to alter the dissolution behaviour of Affinisol™ tablets, loaded with carvedilol, by changing the infill percentage of tablets produced from formulations of different carvedilol drug loadings.

Based on the requirement for mannitol to be present in order to achieve successful printing, a mannitol concentration of 5% was included in each formulation and kept constant throughout the experiment. Drug loading was investigated at three different levels: 10.5%, 20% and 30%, and the infill percentage at each of these drug loadings was varied at 10%, 30%, 50% and 100%, while keeping the outer dimensions of the tablets constant at 10 mm diameter and 4 mm height.

##### **4.3.3.6.1 Dissolution of 3D Printed Tablets**

All tablets were subjected to dissolution analysis using a USP 1 dissolution test, with samples being run for a total of six hours. Figure 113 presents the dissolution data obtained as a traditional release profile, where release of carvedilol is plotted as a percentage of the overall drug content of each tablet under investigation.

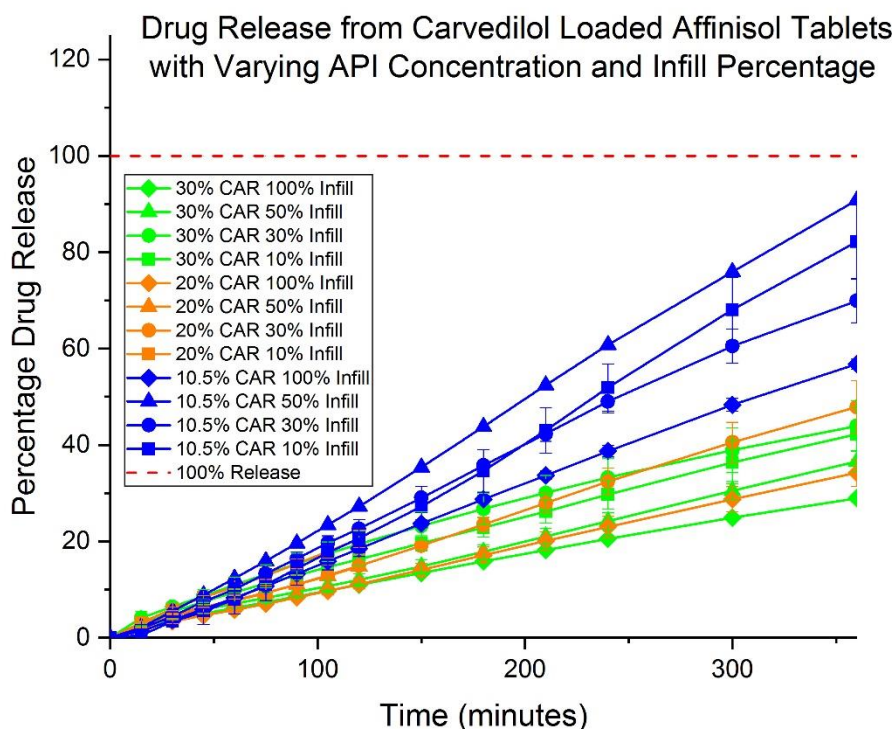


**Figure 113** - Dissolution of Tablets with Varying API Concentration and Infill Percentage (n=3,  $\pm$  standard deviation) - Analysis of 20% carvedilol tablets with both 10% and 50% infill were only analysed for two hours due an unexpected fault with the dissolution equipment and a lack of material to repeat the experiment.

Considering differences between infill percentage and drug content separately, these results seem to suggest that there is not a huge difference in release rate for different infill percentages at higher drug loadings, but the rate varies more widely for tablets with a drug loading of 10.5%. With regards to overall drug content, tablets with a drug loading of 10.5% appear to have faster release rates than those produced at 20% and 30% drug loadings, with the latter two having similar release rates.

It should be noted that the traditional way of presenting this data as 'percentage drug release' was usually intended for systems where each tablet has the same drug content, therefore when applied to this system, it does not take account of the varying carvedilol content of each tablet at the start of the experiment. Figure 114 and Table 41 show the carvedilol content of each tablet under investigation.

**Table 41** - Variation in Carvedilol Content per Tablet (mg) with Different Infill Percentages

Infill	10%	30%	50%	100%
<b>10.5% CAR</b>	16.8	20.5	22.9	28.4
<b>20% CAR</b>	32.9	39.7	47.3	60.7
<b>30% CAR</b>	47.5	57.9	64.7	79.6

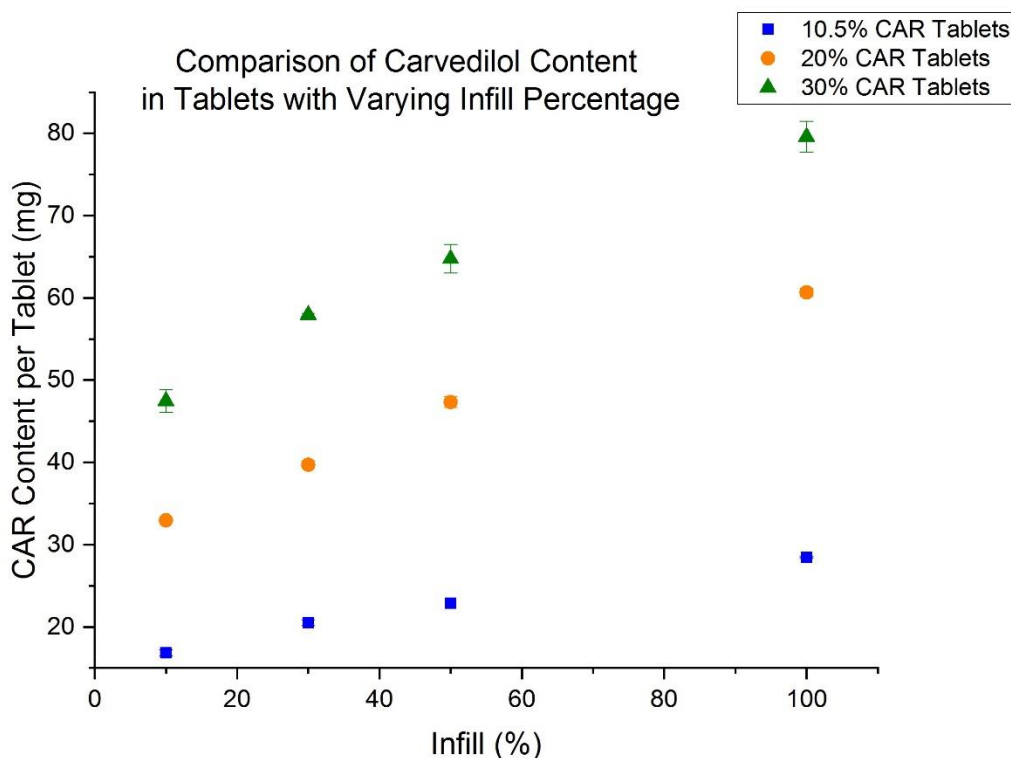


**Figure 114** - Comparison of Carvedilol Content in Tablets with varying Infill Percentage (n=3,  $\pm$  standard deviation)

The variance in carvedilol content, as shown in Figure 114 and Table 41 highlights the difficulty in determining differences in release rate from the dissolution data shown in Figure 113. Instead the data shows that lower drug loadings are releasing more of their overall drug content within the timeframe of the experiment, meaning that formulations with lower drug loading may well achieve full release quicker than those

with higher drug loading. Once again, a closer look at the overall release rates, normalised for tablet weight, may provide further insight into the data.

Simple linear regression analysis was carried out on plots of concentration vs time for the first 60 minutes of dissolution, with the following release rates (mg/min) again calculated based on 500 mL of dissolution media and normalised for tablet weight (mg/min/g). Results are plotted in the following graph (Figure 115), and illustrate how these rates change with different infill percentages:

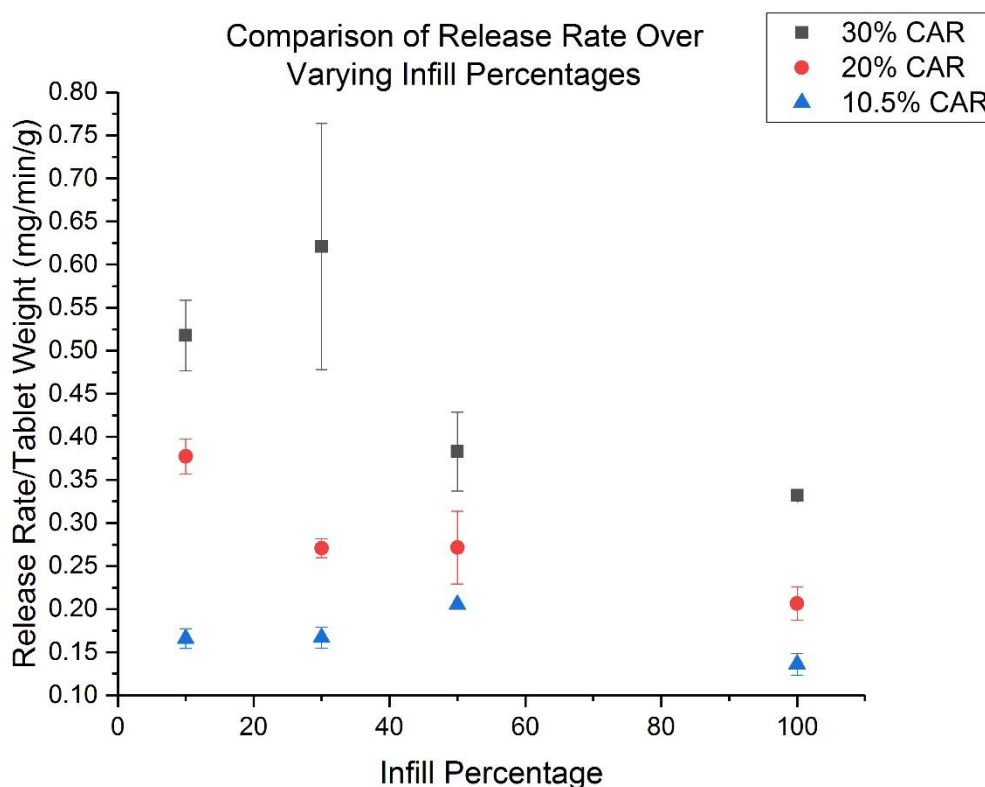


**Figure 115** - Release Rate across Varying Tablet Infill Percentages (n=3,  $\pm$  standard deviation)

When looking at release rate plotted against infill percentage, the most obvious trend seems to be the higher the drug loading, the faster the release rate. While there does appear to be a slight decrease in rate as the infill percentage increases, further statistical analysis, using ANOVA calculations, was carried out in order to determine if the results are different or not. Tukey plots for this analysis are shown below (Figure 116 and Figure 117):

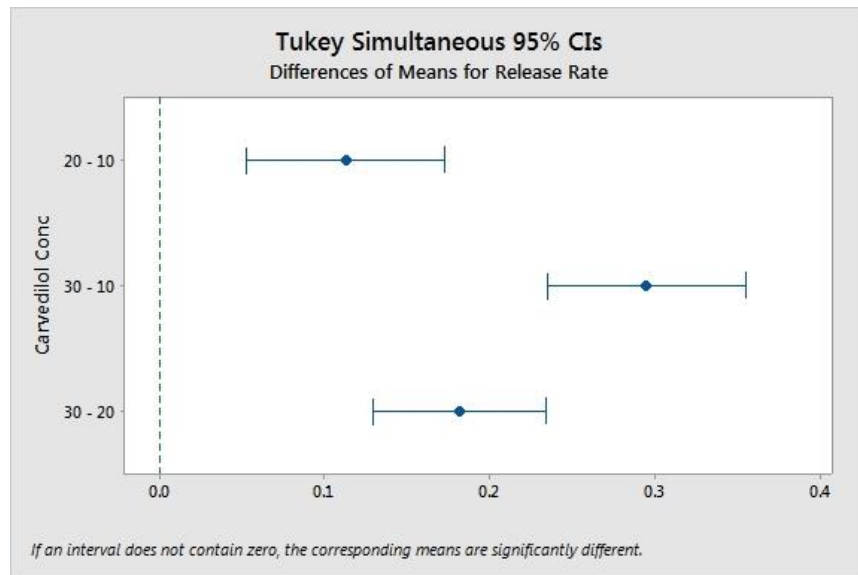


**Figure 116** - Tukey Analysis of Difference in Carvedilol Concentration

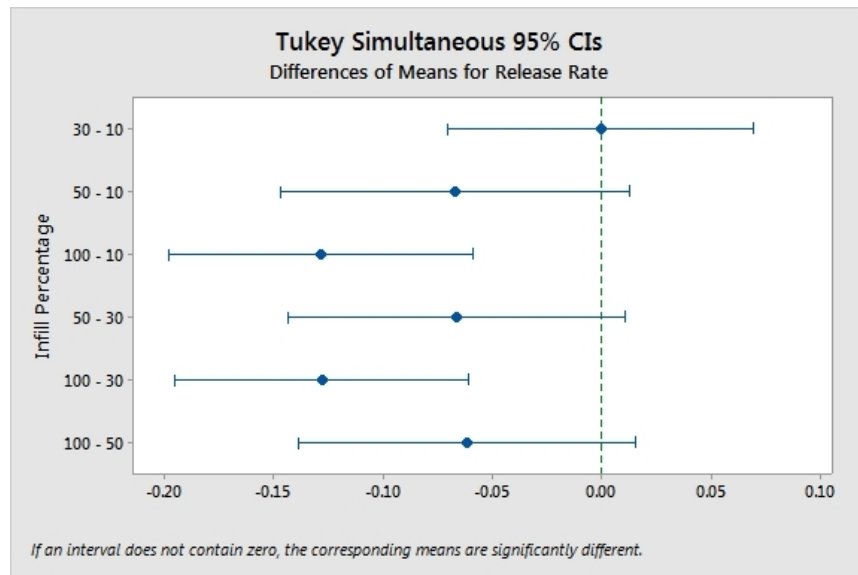


**Figure 117** - Tukey Analysis of Differences in Infill Percentage

When looking at the different drug loadings, it can clearly be seen that the differences observed between 10.5%, 20% and 30% are statistically relevant, and the conclusion that the rate increases with increasing drug loading is correct.

With regards to the different infill percentages, there is no statistical difference between 10% and 30% infill, 10% and 50% infill, 30% and 50% infill and 50% and 100% infill. Differences only seem to emerge between the extremes of 10% and 100%



and 30% and 100% infill. This means that while a tentative conclusion of increasing the infill percentage, decreases the release rate can be applied, this is only really evident when increasing from 10% or 30% up to 100% infill. No real improvements would be seen with smaller variations in infill percentage, therefore choosing a tablet design with either 10% or 30% infill would provide the most favourable release, although this would exclude doses higher than 60 mg from being manufactured. Release rate could still be tweaked using variations in infill percentage, but this is difficult to control and, as none of these formulations achieve 100% release in the six hour time frame, increasing the infill too much could lead to situations where the release rate becomes too slow to be clinically relevant.

#### **4.4 Conclusions and Next Steps**

In general, a method for producing sustained release dosage forms of carvedilol in Affinisol™, with control over the release rate in a 6 hour window has been achieved through the work carried out in this chapter. Steps towards the creation of flexible doses has begun by altering the drug loading of the feedstock filaments and the infill percentage of the printed tablets.

Extrusion of PVA, whether pelletised from existing printer filament, or purchased in powder form, does not present as a suitable polymer for extrusion. Affinisol™ is much more suited for extrusion and 3D printing, but usually results in sustained release formulations.

When examining the sustained release characteristics of drug loaded Affinisol™ tablets, it appears that the release is linear and hence controlled exclusively by erosion of the polymer matrix of the tablet. This is therefore an example of zero-order release kinetics, and is highly desirable due to the enhanced control this offers for controlled release formulations.<sup>145</sup>

Additives, in the form of disintegrants, were included in drug loaded Affinisol™ formulations, and although small molecule natural products, such as sugar alcohols and polyethylene glycols were found to have a favourable effect on disintegration of filaments, these still resulted in sustained release properties for the dosage forms. It

was also found that these additives were required for any successful printing, as filaments of drug and polymer alone failed to print.

When considering increasing the concentration of these disintegrants within the formulations, polyethylene glycols resulted in filaments which were too soft to print. The inclusion of higher loadings of mannitol resulted in successful printing, up to 30% loading, with failure encountered afterwards due to high levels of crystallinity. Despite these higher levels, however, increasing the mannitol content did not improve the dissolution or release of API from the dosage forms.

The superdisintegrants Explotab®, VivaStar® and VivaSol® were also investigated, but none improved release of API, and could not be printed at levels higher than 5% loading.

When changing tablet structures in order to vary surface area to volume ratio, or infill percentage, small improvements could be made, but sustained release was still the overall mechanism of release for the dosage forms produced.

Overall, a method has been found for slightly improving the dissolution rate of carvedilol loaded Affinisol™ tablets, but, based on all the work carried out in this chapter, a combination of techniques may be required in order to approach anything which resembles immediate release. Further work could potentially focus on some different additives, perhaps in the superdisintegrant category, or on understanding filament suitability through the use of rheology, but investigation into the boundaries of operation for sustained release alternatives presents the most viable route for continuing this research.

## **5 Population of a Ternary Phase Diagram to better understand Formulations for 3D Printing**

### **5.1 Introduction**

While chapter 3 introduced the manufacture of varying carvedilol doses via solution loading and 3D printing of PVA tablets, chapter 4 focused on ways of improving this method with the use of hot-melt extrusion. Due to various difficulties, the carrier polymer was substituted with Affinisol™ and, while this had the potential to allow for greater dose variation within the dosage forms, the sustained release mechanism was still the only method of API release achieved from the 3D printed tablets.

Given that carvedilol is marketed in a sustained release form, with doses which range from 10-80 mg,<sup>146</sup> 3D printed tablets with sustained release properties still provide a useful route with which to pursue research, but the overall goal, regardless of release mechanism, is to demonstrate flexible dosage and control over the system discussed.

This chapter focuses on investigating a full and comprehensive range of different carvedilol doses in an Affinisol™ polymer matrix, with the addition of mannitol as an additive to aid the printing process. This builds on the results from the previous chapters and tests the ultimate boundaries of failure for such formulations. Various analytical techniques were employed to provide a better understanding of the process as a whole.

### **5.2 Aim**

The overall aim for this chapter was to provide further insight into the manufacture of formulations containing carvedilol, mannitol and Affinisol™. Building on results from previous chapters, a full understanding of the design space for these formulations was attempted, with the aim of providing access to all the doses currently available on the market for sustained release formulations. Again, control over dosing was intended to be achieved via careful blending of polymer/API/additive mixtures prior to hot-melt extrusion to produce a filament, and analytical techniques were applied in

























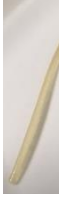









order to understand drug distribution and drug release from these dosage forms produced from a non-conventional manufacturing procedure.

### **5.3 Results and Discussion**

#### **5.3.1 Production of a Ternary Phase Diagram**

In order to fully investigate the experimental space for three component formulations containing carvedilol (CAR), mannitol (MAN) and Affinisol™, population of a ternary phase diagram was planned and carried out according to various experimental results such as: extrusion/printing success, variation of extrusion parameters, variation in expected drug loading and variation in filament mechanical properties. This aimed to provide a better understanding of formulations containing these components, with a view to providing a window of operation with which to manufacture scaleable oral doses of carvedilol. Extrusion of varying concentrations of mannitol and carvedilol within an Affinisol™ polymer matrix was successful for all different compositions under investigation. Golden filaments were produced for each formulation, which appeared more glassy and transparent the less mannitol was present in the formulation. This is shown in Table 42, where N/A represents compositions which were not tested:














**Table 42 - Results of Extrusion of Varying Mannitol and Carvedilol Formulations**

Formulation	0% MAN	5% MAN	10% MAN	15% MAN	20% MAN	30% MAN	40% MAN	45% MAN
1% CAR		N/A		N/A				
5% CAR	N/A							N/A
10.5% CAR								N/A
20% CAR							N/A	N/A
30% CAR						N/A	N/A	N/A
40% CAR				N/A	N/A	N/A	N/A	N/A
50% CAR		N/A	N/A	N/A	N/A	N/A	N/A	N/A

*Population of a Ternary Phase Diagram to better understand Formulations for  
3D Printing*

From all of these different extrusion experiments, tablets were produced as follows (Table 43):

**Table 43 - Results of Printing Varying Formulations**

	0% MAN	5% MAN	10% MAN	15% MAN	20% MAN	30% MAN	40% MAN	45% MAN
1% CAR	Fail	N/A	Fail	N/A	Fail	Fail	Fail	Fail
5% CAR	N/A	Fail	Fail	Fail	Fail	Fail	Fail	N/A
10.5% CAR	Fail						Fail	N/A
20% CAR	Fail						N/A	N/A
30% CAR				Fail	Fail	N/A	N/A	N/A
40% CAR	Fail	Fail	Fail	N/A	N/A	N/A	N/A	N/A
50% CAR	Fail	N/A	N/A	N/A	N/A	N/A	N/A	N/A

Taking the results from these extrusion and printing experiments, it was possible to construct a ternary phase diagram, allowing for easier visualisation of the experimental space under investigation (Figure 118):

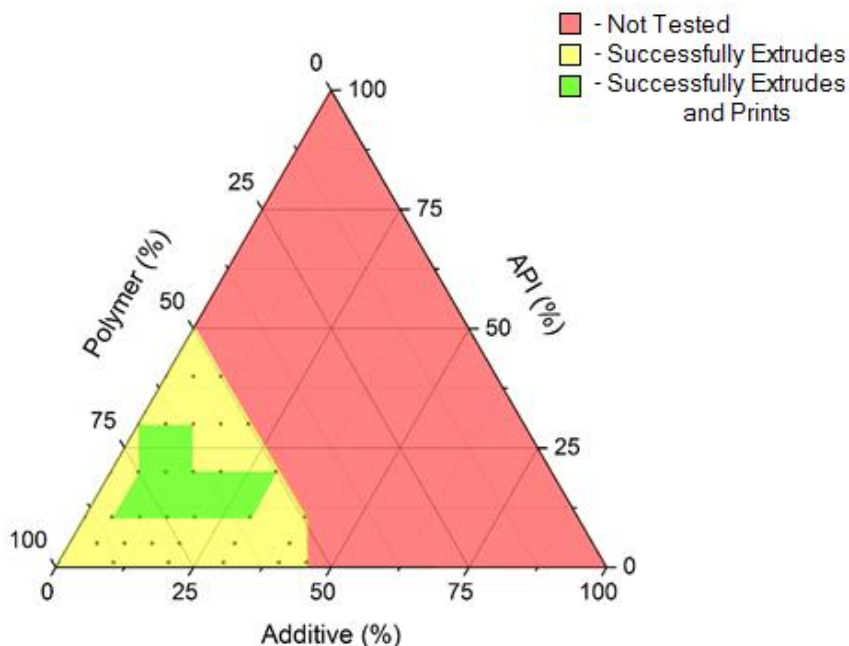


**Figure 118** - Ternary phase diagram showing boundaries of successful extrusion and printing based on results shown in Table 42 and Table 43. Data points indicate compositions which have corresponding experimental data.

The red area represents design space which was not investigated due to the reduction of the carrier polymer (necessary for the extrusion process) to levels below 50% w/w of the overall composition. While the points in the red area cover compositions that were not extruded, it should be noted that this in itself is not an indication of extrusion failure, rather an indication that these compositions were not investigated for this research. The yellow area represents successful extrusion experiments, but failed printing experiments, and the green area represents success in both extrusion and printing.

As can be seen from these results, there is a limited 'window' for manufacture of pharmaceutical tablets by 3D printing, using these three materials. By looking at the results from various analytical techniques across the different experiments, it may be possible to explain why the boundaries of failure are in these positions and what could be causing failure of the printing process.

*Population of a Ternary Phase Diagram to better understand Formulations for 3D Printing*

Before comparing these different results, the experimental boundary surrounding 20% w/w carvedilol 30% w/w mannitol was extended slightly due to the ability of this formulation to be printed. A set of extrusion experiments was carried out, which looked at varying the concentration of carvedilol and mannitol, while keeping the Affinisol™ concentration the same at 45% w/w of the overall composition. This allowed for three points surrounding the 20% CAR 30% mannitol formulation to be investigated further. The three compositions to be investigated were:

10% w/w CAR - 45% w/w mannitol - 45% w/w Affinisol™

20% w/w CAR - 35% w/w mannitol - 45% w/w Affinisol™

30% w/w CAR - 25% w/w mannitol - 45% w/w Affinisol™

All of these formulations could be extruded, but none could be successfully printed, thereby confirming the boundaries of the successful extrusion/printing zone and allowing for the ternary phase diagram to be updated accordingly (Figure 119):

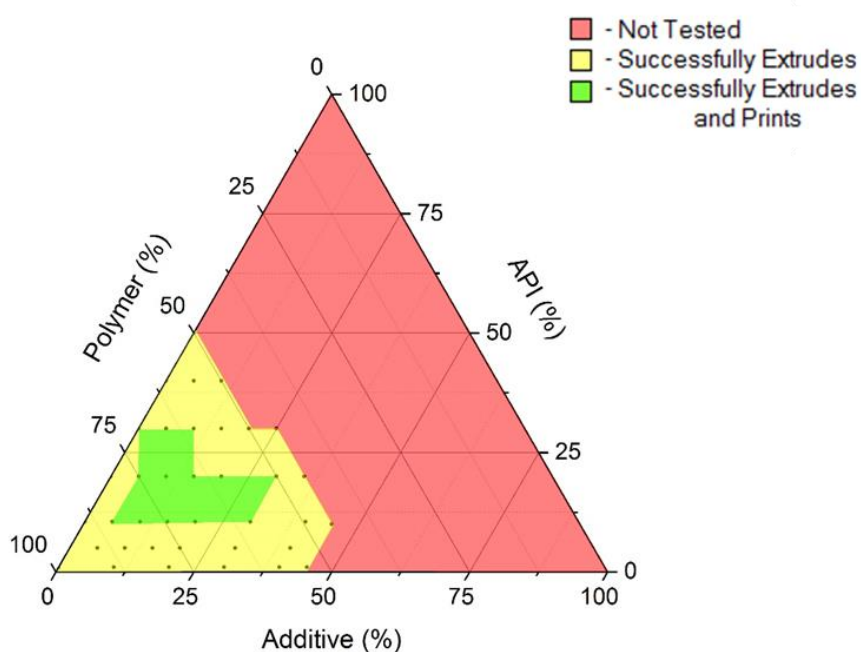


**Figure 119** - Updated Ternary Phase Diagram Showing Successful Extrusion and Printing



As can be seen, the boundaries of the successful printing zone have been fully investigated, and show the edges of failure for processing these materials.

Extrusion parameters, although intended to be kept constant throughout, have varied as drug content increased. The initial settings were as follows: extrusion temperature - 170°C, feed rate – 5, screw speed – 60 rpm. While these settings can potentially be adjusted without altering the nature of the drug or polymer within the matrix, which have melting points and glass transition temperatures ( $T_g$ ) of 119°C<sup>119</sup> and 115°C<sup>147</sup> respectively, the melting point of  $\beta$  mannitol is 166.7°C and therefore any drop in extrusion temperature below this level may mean that the mannitol is not fully melted and hence, not distributed at a molecular level, leading to discrete ‘pockets’ of crystalline material throughout the resulting filament.

Increasing the drug content of the formulations also had the effect of reducing the flowability of the pre-extruded powder blends, which then required adjustments of the feed rate to compensate for this. Even with an increase in the feed rate, the blend entered the extruder in clumps, rather than as a steady flow of material. This therefore presents another issue which could cause the individual components of the formulations to be poorly mixed within the resulting filaments.

Another ternary phase diagram can be constructed to illustrate this, where extrusion using the original settings remain in green, and any variance in these settings are colour coded appropriately. A drop in extrusion temperature anywhere between 1°C and 10°C is colour coded yellow. A drop in extrusion temperature anywhere between 11°C and 20°C is colour coded orange. Similarly, as maintaining steady flow from the feeder became difficult, an increase in feed rate anywhere between 5 and 10 is colour coded yellow, and between 11 and 15 is colour coded orange. The remaining experimental space that has not been investigated with extrusion remains red (Figure 120):

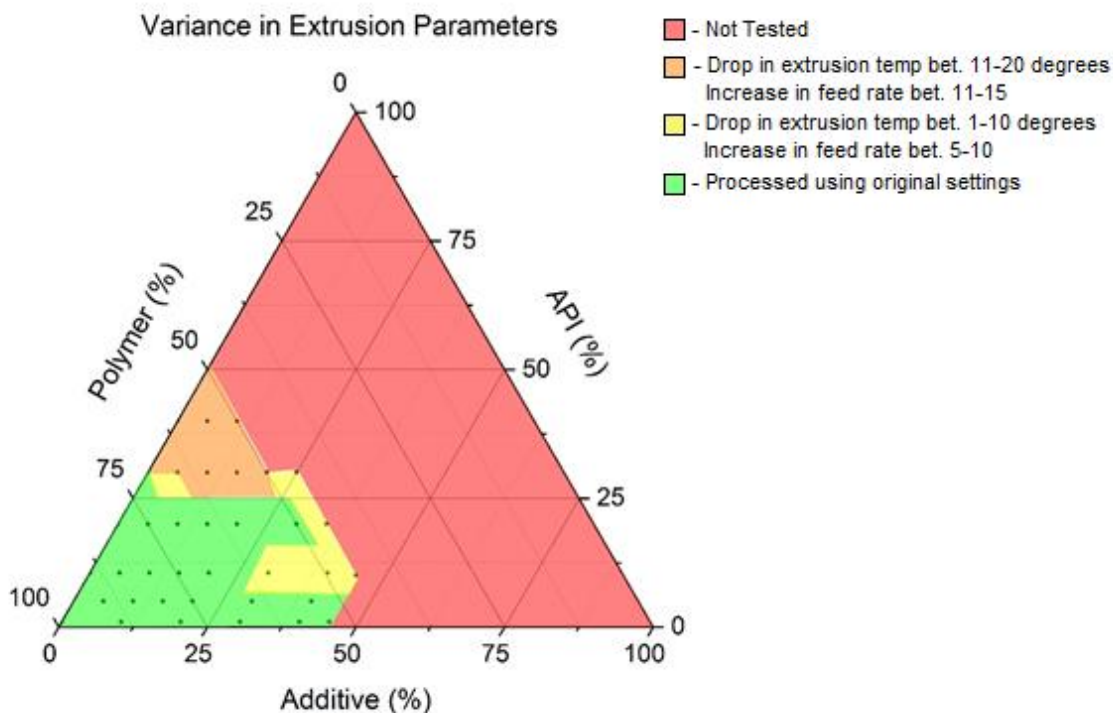


**Figure 120** - Ternary Phase Diagram Showing Variance in Extrusion Parameters

Knowing which formulations could actually be printed, this further reduces the ideal manufacturing space available for these materials, with the majority of formulations containing 30% carvedilol arising from undesirable extrusion conditions.

### 5.3.1.1 Analysis of Drug Loading Within the Formulations

Looking at the HPLC data, for the analysis of drug loading within the formulations, also gives an idea of which of these formulations can be processed well. Any variance in the actual drug loading, compared to what was expected, gives an indication of the processing limits of these materials. In order to apply this to the drug loadings observed in the individual formulations, a range of 'acceptable' drug loadings were applied. These were based on traditional pharmaceutical analysis approaches and are detailed as follows:

- Within 5% of expected values is coded green
- Within 10% of expected values is coded yellow

- Outwith 10% of expected values is coded red

The drug loadings obtained from the different formulations investigated, as determined from HPLC, are shown in Table 44, where N/A represents compositions which were not investigated:

**Table 44 - Drug Loading (by HPLC) of Carvedilol/Mannitol/Affinisol™ Formulations**

API (%)	Mannitol (%)									
	0	5	10	15	20	25	30	35	40	45
1	0.8	N/A	2.9	N/A	1.1	N/A	1.3	N/A	1.5	1.6
5	N/A	5.3	5.3	5.6	6.1	N/A	6.9	N/A	7.8	N/A
10.5	10.6	9.7	9.5	10.9	11.6	N/A	13.2	N/A	13.7	18.0
20	20.6	21.5	21.9	23.1	24.3	N/A	26.8	30.7	N/A	N/A
30	33.2	33.0	33.9	32.3	32.2	38.5	N/A	N/A	N/A	N/A
40	42.3	42.9	43.4	N/A	N/A	N/A	N/A	N/A	N/A	N/A
50	53.4	N/A	N/A	N/A	N/A	N/A	N/A	N/A	N/A	N/A

This can then be further represented in another ternary phase diagram, with the same colour coding applied (Figure 121):

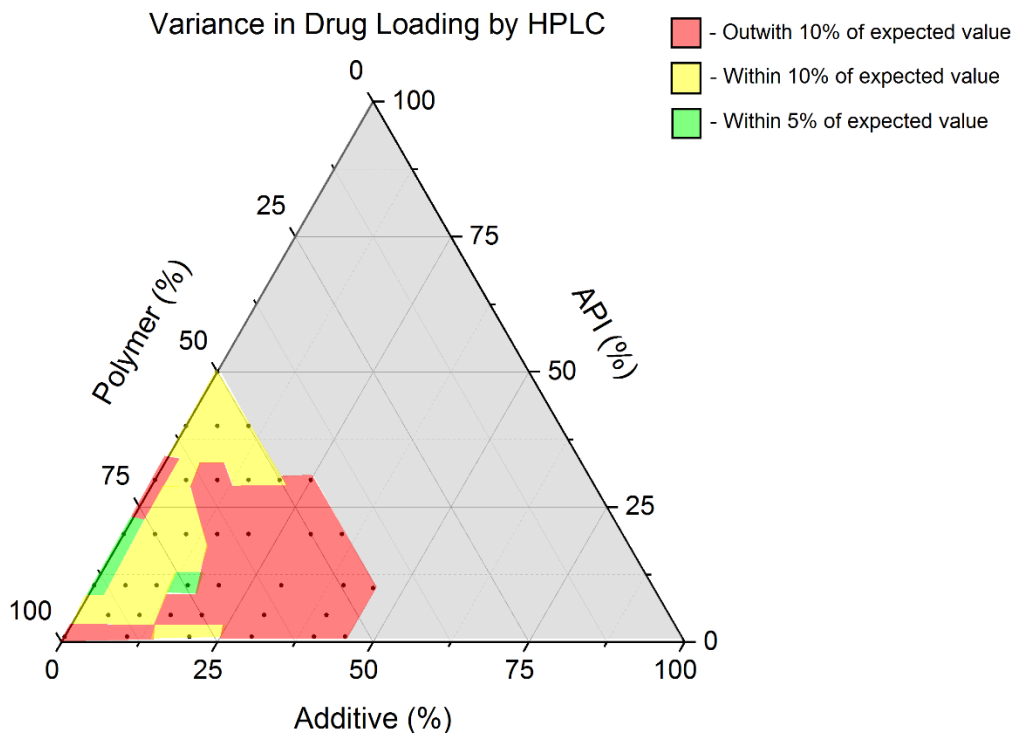


**Figure 121** - Variance in Drug Loading as Determined by HPLC Analysis

Similar to when examining the extrusion parameters, using HPLC data further reduces the suitable manufacturing space for these formulations. It should be noted though, in the interests of time, that the formulations from each of the different drug loadings were processed through the extruder 'back-to-back' in order of increasing mannitol content. This could result in carry over of the drug between the formulations, artificially increasing the drug loadings as the experiments progressed. It is therefore highly likely that one selected formulation, when processed alone, may result in an acceptable drug loading, providing the desired concentration is below 30% w/w carvedilol, as indicated from the analysis of the extrusion parameters. At the time of carrying out these experiments, in-line monitoring with process analytical technology was not available, but future application of these techniques could lead to more accurate measurements of drug loading in filaments, and easier selection of filaments with the desired composition.

### **5.3.1.2 Analysis of Filament Mechanical Properties**

3-point bend testing was again used as a method of investigating the mechanical properties of printer filaments. Five different filament samples were taken from each of the formulations and subjected to 3-point bend testing using a texture analyser. The maximum flexural stress and strain was again obtained from plots of stress versus strain for each of the different formulations and these can be found in Appendix 7.4 for each of the different drug loadings of carvedilol. As these graphs show the how the stress and strain vary with different mannitol content, a comparison of different carvedilol drug loadings at 0% w/w mannitol is also included in the appendix.

In an attempt to explain why print failure occurs in some filaments, and not others, results from all three point bend testing, across all experiments (regardless of whether they were investigating mannitol content or not), were compared in order to investigate if any trends arose. A commercial filament of Polylactic Acid (PLA) was also analysed and included for comparison as the Leapfrog Creatr HS printer was optimised for use with this filament. This resulted in a flexural modulus range of 4.1-8.1 MPa for successful printing and a maximum stress range of 50-84.9 MPa for successful printing. The upper limits of these ranges should be treated with care however, as there was only one sample which failed to print above this maximum stress threshold and no examples of the flexural modulus range being exceeded. A similar strain threshold of 10% can also be applied, based on results from Section 4.3.3.3.1, below which filaments are too brittle for successful printing.

All values for flexural modulus and maximum stress are tabulated in Appendix 7.5, however for a visual representation of how results of 3-point bend testing relate to the formulations in this experiment, another ternary phase diagram can be constructed where green indicates formulations which should print and red indicates formulations which may be problematic for printing (Figure 122):

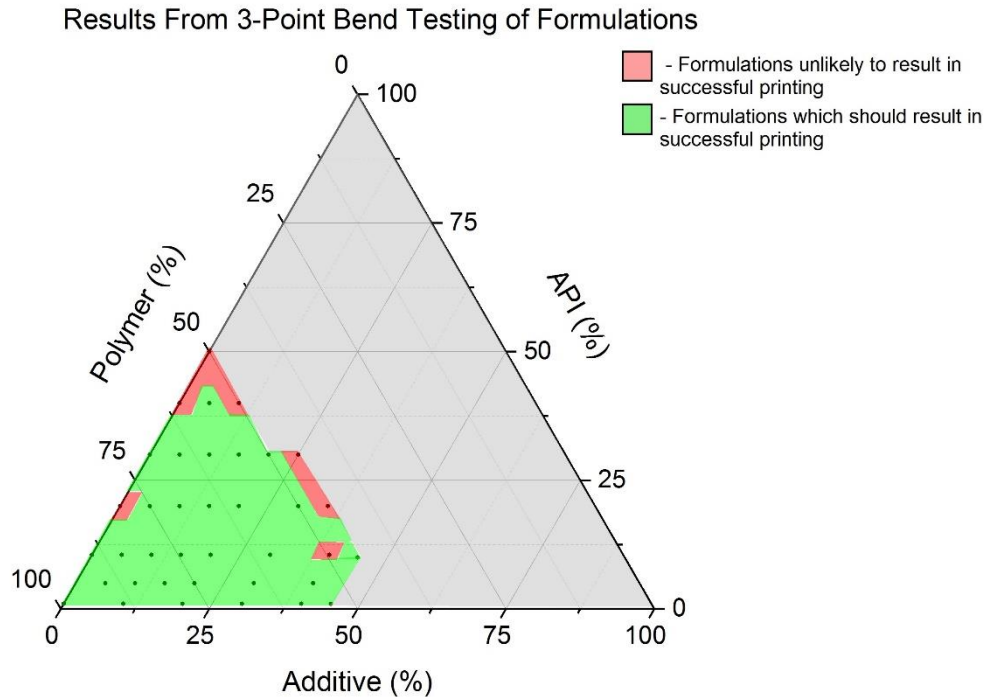


Figure 122 - Prediction of Print Success Based on 3-Point Bend Testing Alone

It is clear from this diagram that more factors, than just filament softness or brittleness, are contributing to whether successful printing will occur with these formulations, as it suggests that printing should be successful in almost all instances, with the exception of some extremes of the experimental space.

While 3-point bend testing does provide an excellent screening tool for exclusion of filaments which are far too soft or brittle for printing, it only has limited use when used as the only screening tool for testing filaments. There have been many filaments tested, across a range of different experiments, which did not print, but had values within the ranges specified above. From the literature, it appears that combining 3-point bend testing with elongation experiments, which look at axial filament stiffness, may have further success at screening suitable filaments,<sup>95</sup> but this was not available at the time of carrying out these experiments.

### 5.3.1.3 Crystallinity Determination of Filaments

#### 5.3.1.3.1 X-Ray Powder Diffraction (XRPD)

Based on the XRPD data observed from individual experiments which feed into this work (Sections 4.3.3.2.2 and 4.3.3.3.2), crystallinity seemed to increase with increasing mannitol content, with no evidence of any crystalline carvedilol present in any formulations. In order to determine which of the three known forms of mannitol were present, the highest mannitol content from each different drug loading was compared against XRPD patterns of the different mannitol polymorphs: alpha,<sup>137</sup> beta<sup>138</sup> and delta<sup>139</sup> (Figure 123, Figure 124, Figure 125, Figure 126, Figure 127, Figure 128):

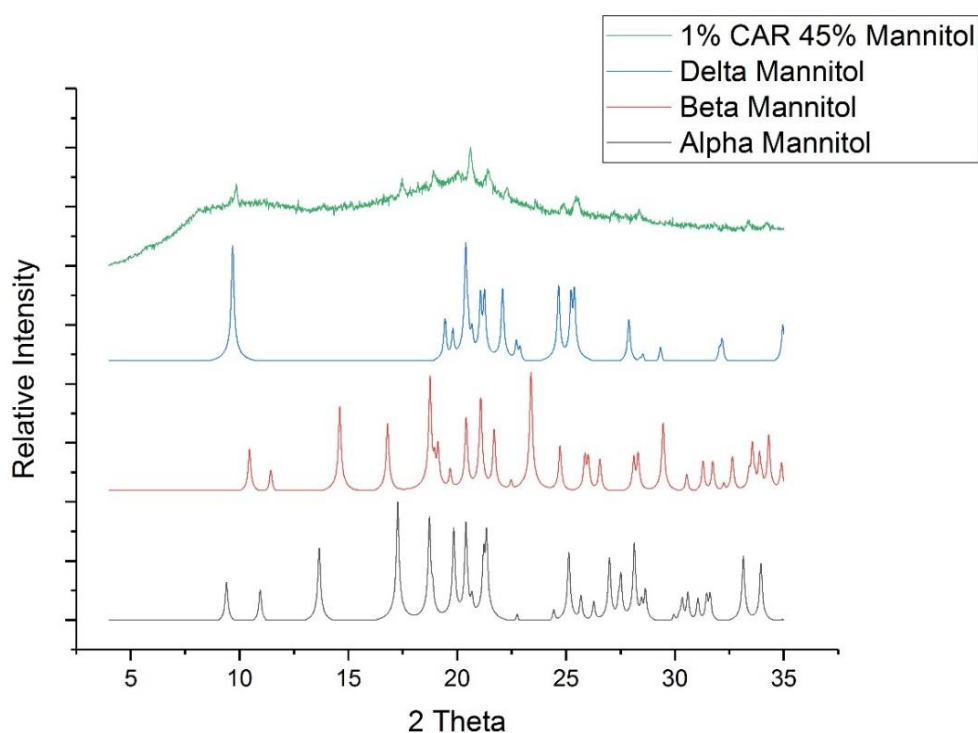


**Figure 123** - 1% Carvedilol with Comparison of Mannitol Polymorphs

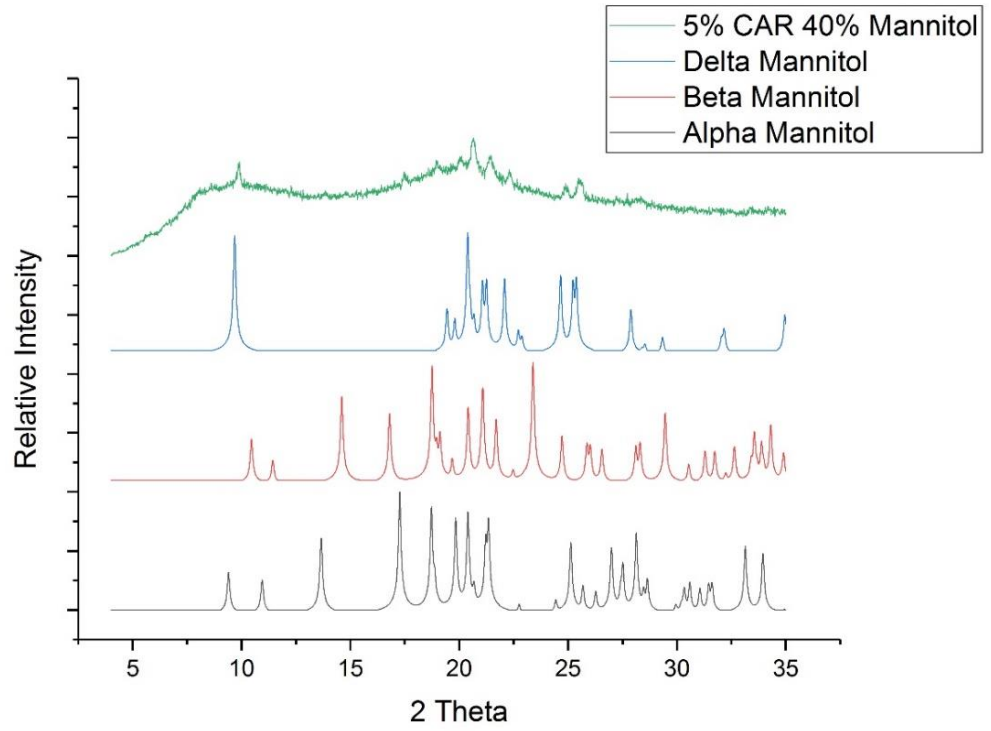


Figure 124 - 5% Carvedilol with Comparison of Mannitol Polymorphs

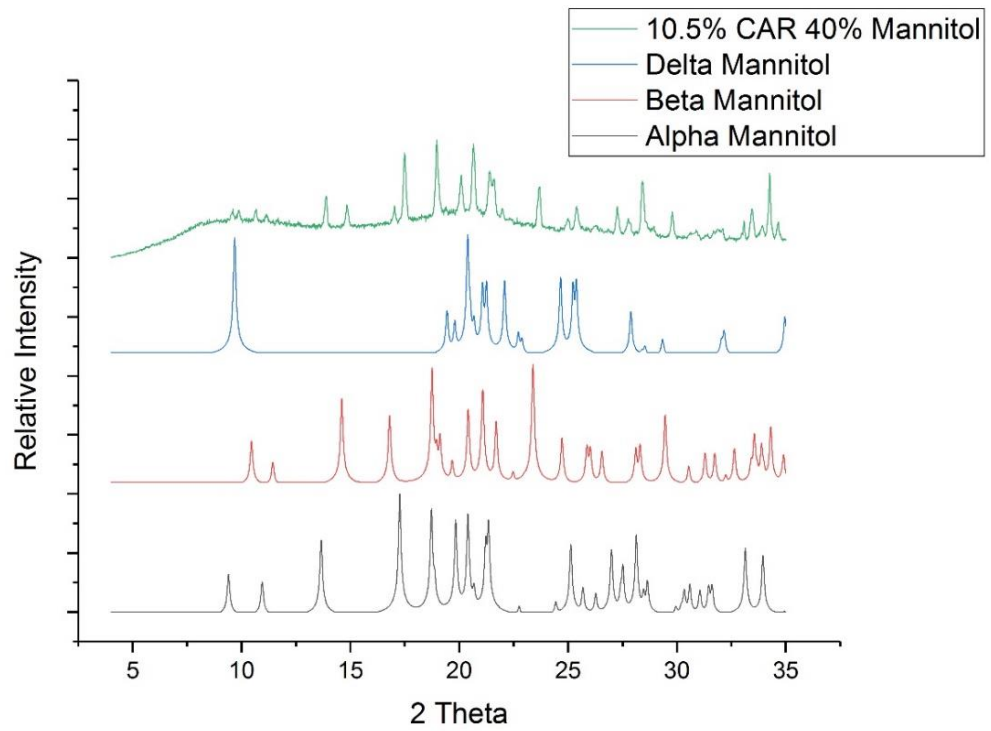


Figure 125 - 10.5% Carvedilol with Comparison of Mannitol Polymorphs



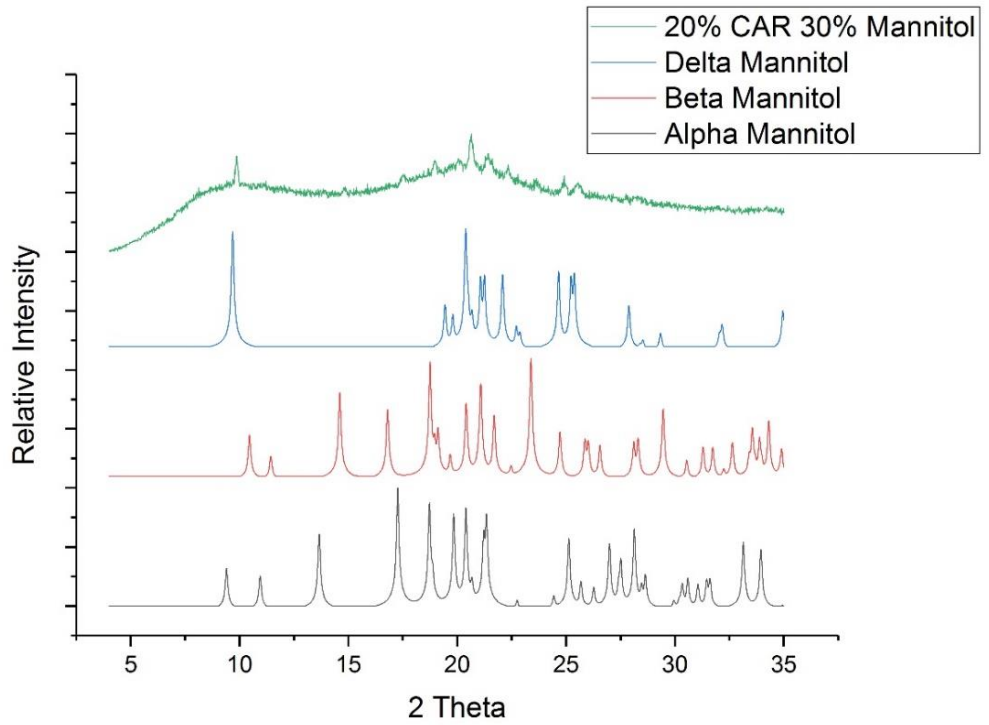


Figure 126 - 20% Carvedilol with Comparison of Mannitol Polymorphs

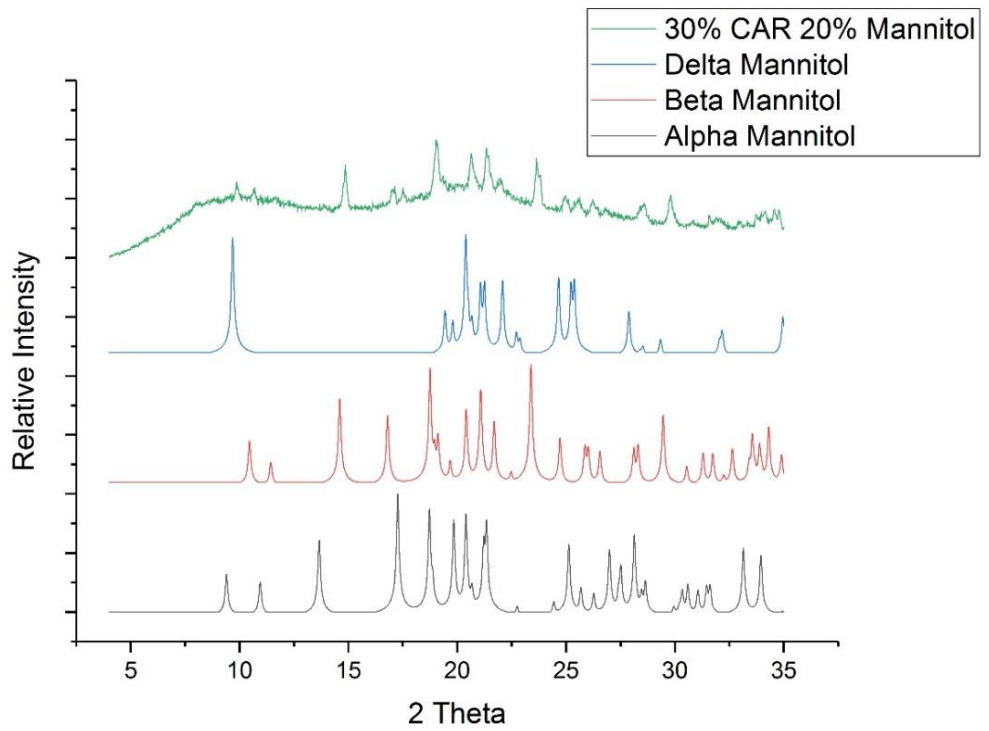
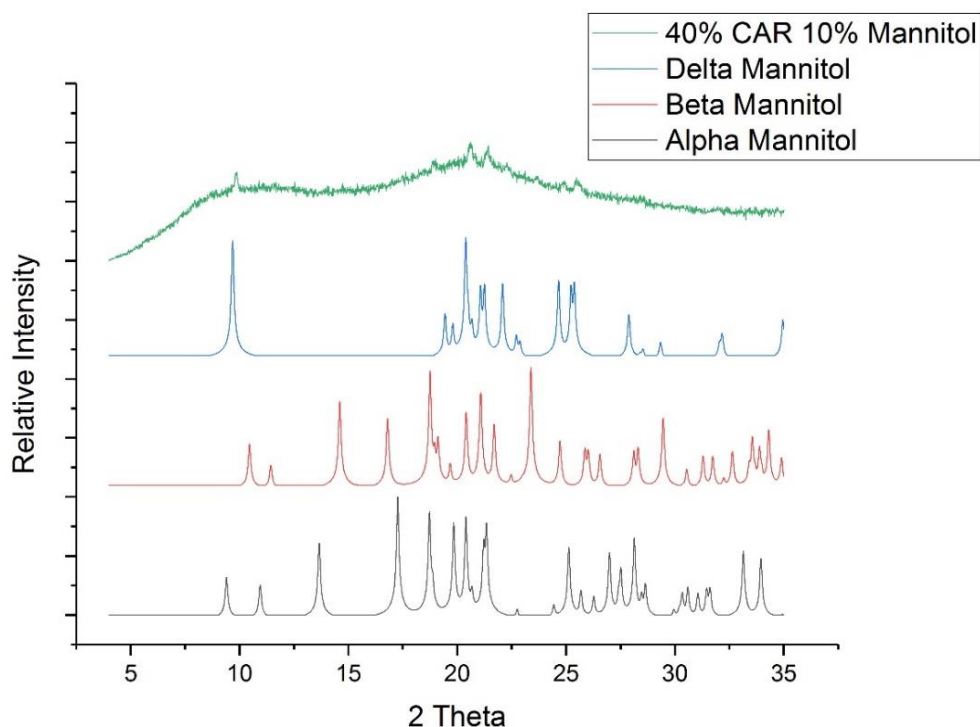


Figure 127 - 30% Carvedilol with Comparison of Mannitol Polymorphs



**Figure 128** - 40% Carvedilol with Comparison of Mannitol Polymorphs

It is difficult to determine from XRPD alone the precise nature of the crystallinity in each of these samples, due to the masking effect observed from the Affinisol™, but peaks corresponding to all three of the different polymorphs appear to be present. This is most easily seen in the formulations containing 10.5% and 30% carvedilol, where peaks are more defined and there is a strong indication that both the alpha and beta polymorphs of mannitol are contained within the formulations. As mentioned in Section 4.3.3.3.2, the presence of small amounts of crystallinity does not seem to hinder printing of formulations, but large amounts of crystallinity result in a non viable filament for printing, therefore it is likely that this has been the cause of print failure for both the 10.5% and 30% carvedilol shown in Figure 125 and Figure 127.

#### 5.3.1.3.2 Differential Scanning Calorimetry (DSC)

In order to obtain as much information as possible, the following heating profile was selected for analysing samples: an initial heat of 0°C - 190°C at 20°C/min, followed by cooling from 190°C - 0°C at 20°C/min, followed by an isothermal segment for 2 mins at 0°C and a final heating of 0°C - 190°C at 20°C/min.

It was reasoned that an initial heat cycle would potentially be affected by any moisture in the system, or any effects due to samples being left over time, so two heating cycles were run in order to clarify and sharpen any peaks. This second heat cycle also aids in removing any effects caused by irregular coverage of the bottom of the DSC pan by the pelletised filaments,<sup>148</sup> as the first heat cycle completely melts the material to create an even layer. It should be noted that this second heat cycle is not then examining the initial filament material under investigation, but is still able to give an indication of how the material behaves post printing, given that sampling of printed tablets for DSC is difficult to carry out. A cooling cycle was also included with the hope that this would lead to easier identification of the glass transition temperature, or any recrystallisation events which may occur.

Analysis of the starting materials (Figure 129) was also carried out which confirmed that carvedilol melts at 119°C<sup>119</sup> and remains amorphous after being cooled and heated a second time. As it was also known that the mannitol starting material was present in the beta form (from initial XRPD analysis), melting and recrystallisation behaviour could also be confirmed, with the beta form again being the polymorph observed from the 170.5°C melting point:

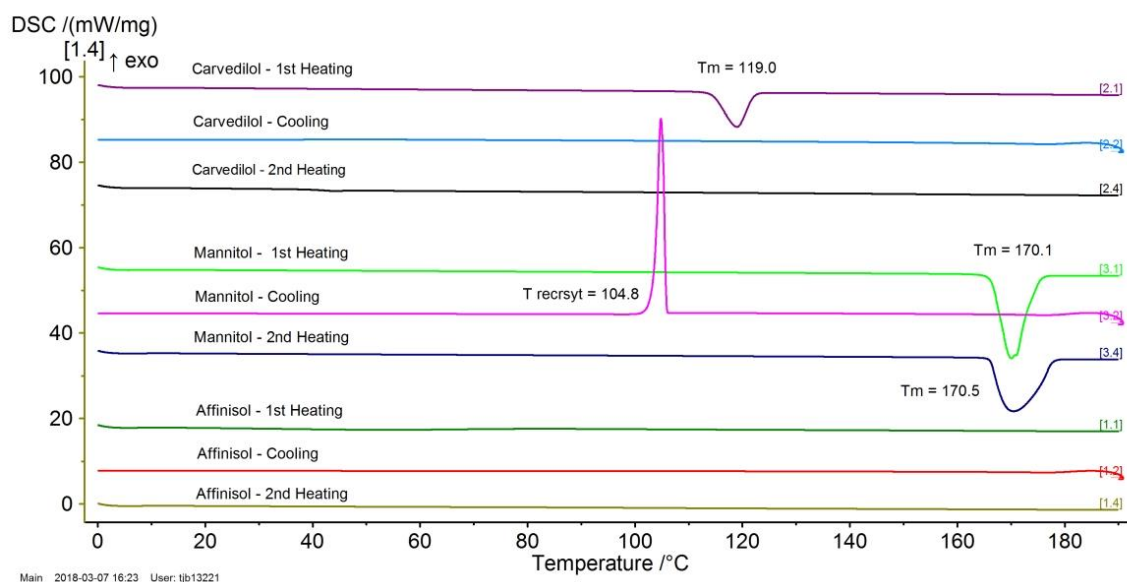


**Figure 129** - DSC Analysis of Starting Materials

*Population of a Ternary Phase Diagram to better understand Formulations for 3D Printing*

As changes observed in the DSC data are fairly constant, regardless of drug content, data from 20% carvedilol drug loading is used here to illustrate the changes observed when varying the mannitol content (Figure 130, Figure 131 and Figure 132), with all other DSC data of different drug loadings included in Appendix 7.6:

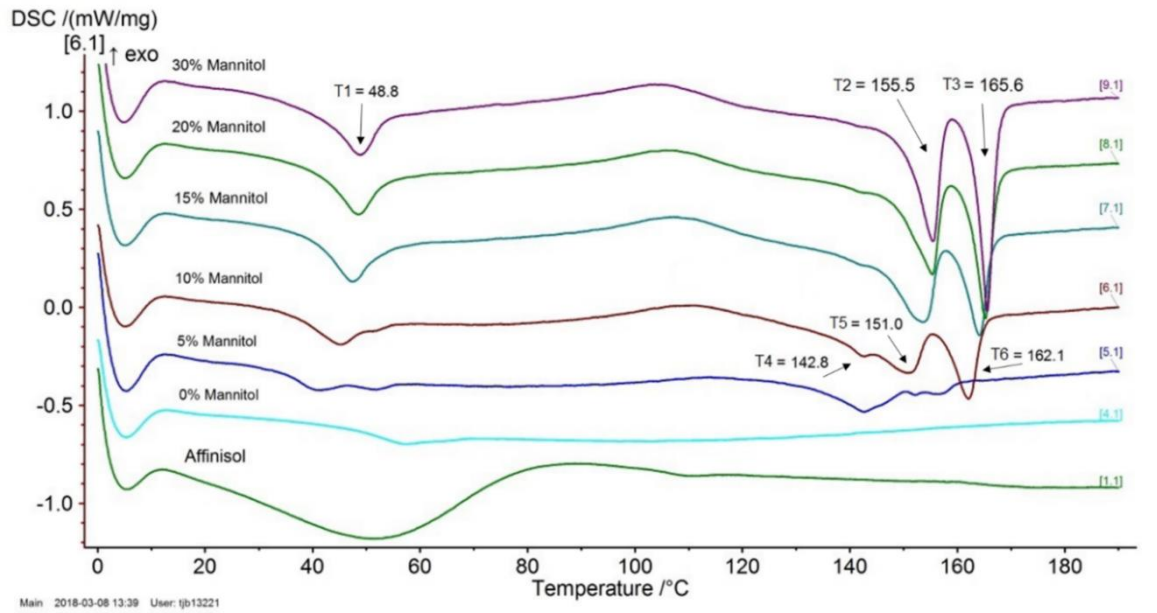


**Figure 130 - 20% Carvedilol Filaments (1st Heating)**

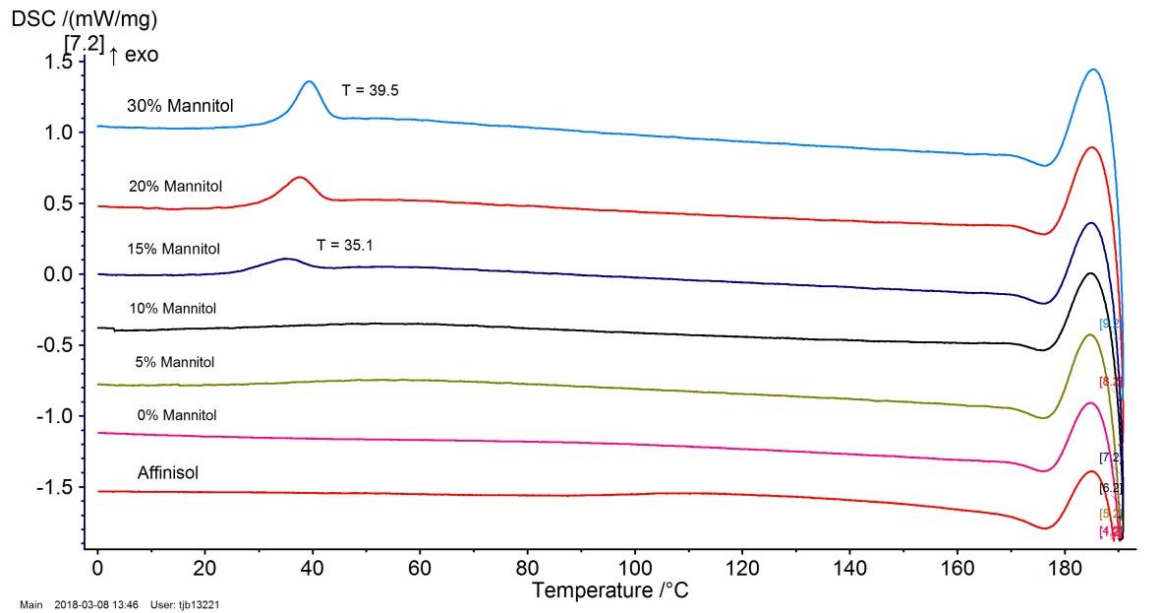


**Figure 131 - 20% Carvedilol Filaments (Cooling)**

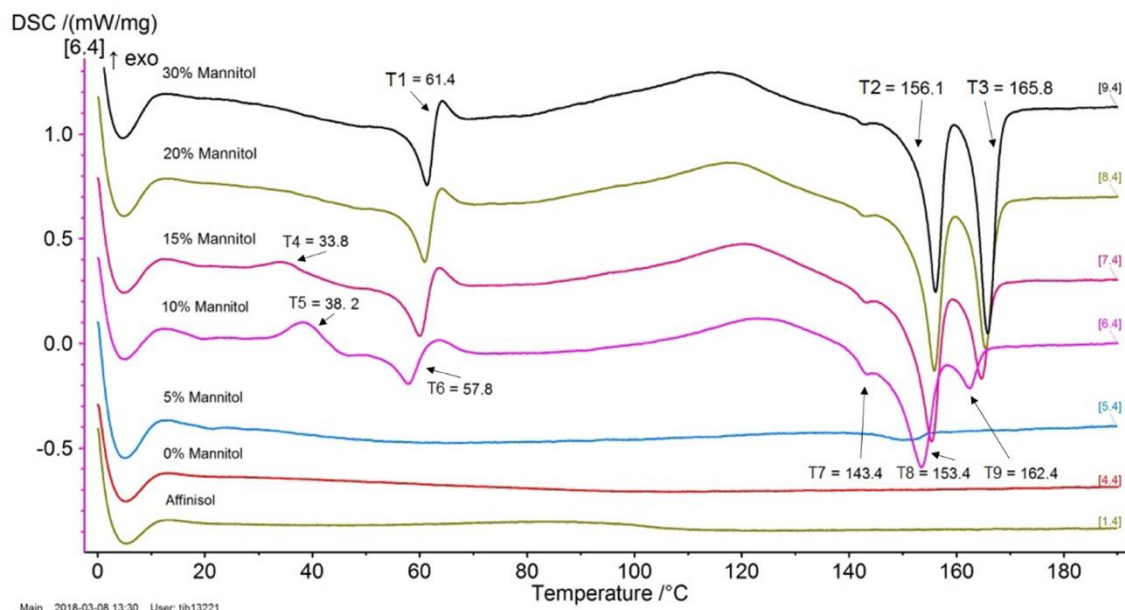


**Figure 132 - 20% Carvedilol Filaments (2nd Heating)**

When looking at the first heating for just the individual formulations and pure Affinisol™, the large broad peak observed in Affinisol™ is due to the presence of moisture, which should be removed in the second heat cycle. The  $T_g$  of Affinisol™ can also be seen, although very small, at approximately 110°C, which is close to that reported by Dow Chemicals (115°C).<sup>147</sup>

In the different mannitol formulations, there appears to be a small peak at approximately 50°C (T1) in all samples containing mannitol, followed by two sharp melting peaks, which gradually separate into a cluster of endothermic peaks between 140°C and 170°C (T2-T6), as the mannitol concentration decreases. Given the lack of evidence for crystalline carvedilol (mp 119°C) in the XRPD data, it is most likely that the observed peaks can be attributed to mannitol, which has three distinct polymorphs: alpha, beta and delta which melt at 165.3°C, 166.7°C and 156.2°C respectively.<sup>149</sup> Given the low intensity of these peaks in XRPD, it is difficult to identify if all these polymorphs are present, but the DSC seems to suggest that at least two are present in samples containing high mannitol concentrations, and potentially all three of these polymorphs could be present at low mannitol concentration, with the melting points depressed due to the presence of Affinisol™. The peak at 50°C is

likely attributed to a glass transition event, which is exhibiting enthalpic relaxation as characterised by the observed endotherm.<sup>150</sup>

On cooling, there is a peak at 39.5°C, which gradually decreases to 35.1°C as the mannitol concentrations decreases. This is likely due to recrystallisation of mannitol and may be depressed slightly due to increasing Affinisol™ concentration. It is also only visible at mannitol concentrations of 15% and higher, suggesting that the higher Affinisol™ concentration, present at lower mannitol concentrations, is stabilising the formulation in an amorphous form.

When looking at the events on the second heating, peaks seem to be clearer and more defined, allowing for easier identification. Peaks only start to appear once a mannitol concentration of 10% has been reached, again suggesting that samples below this concentration remain stabilised in an amorphous form. At samples of 20% mannitol and above, there appears to be a glass transition, followed by immediate recrystallisation at 61.4°C (T1), the literature suggests that this recrystallisation results in the alpha polymorph being produced.<sup>151</sup> The analysis then goes on to show a broad exothermic event, immediately followed by two distinct melting peaks at 156.1°C (T2) and 165.8°C (T3), likely corresponding to recrystallisation of another polymorph, followed by melting. When originally looking at this data, it was thought that these two melting peaks correspond to the alpha and delta polymorphs, due to the similarity of these melting peaks with reported literature values,<sup>149</sup> however this does not take into account the presence of a polymer, which could lower the observed melting peaks. When considering the presence of more peaks observed at lower mannitol concentrations, it is highly likely that these two melting peaks correspond to the alpha and beta polymorphs, which have depressed values due to the presence of Affinisol™. This is further supported by the continual depression of these peaks as the mannitol content decreases and the Affinisol™ content increases.

At a 10% and 15% mannitol concentration, there appears to be an exotherm at 38.2°C (T5) and 33.8°C (T4) respectively, followed by the same glass transition and immediate recrystallisation observed at higher mannitol concentrations, although appearing at the slightly lower temperature of 57.8°C (T6). Mannitol is known to

display 'polyamorphism',<sup>151,152</sup> so the exotherm most likely corresponds to a transition from one amorphous phase to another. Three different melting peaks are observed at higher temperatures, marked as 143.4°C (T7), 153.4°C (T8) and 162.4°C (T9) on Figure 132, which likely correspond to the three different melting peaks of the mannitol polymorphs, which have been depressed from that observed in the literature due to the high Affinisol™ content of the sample.

When considering the cooling profiles, which immediately precede this heating cycle, recrystallisation occurs in all mannitol samples of 15% and above, which may provide a reason as to why polyamorphism of mannitol appears to a lesser degree in the 15% formulation, and is not seen at all at increased mannitol concentrations. Given that there is already some recrystallisation of these formulations, along with a gradually increasing mannitol to Affinisol™ ratio, it is likely that there is already too much mannitol, or not enough Affinisol™ to stabilise any amorphous states, which explains the events seen in thermograms of 20% mannitol and above.

For 10% mannitol, which exhibits no recrystallisation on cooling, an amorphous state is initially stabilised, likely due to the higher Affinisol™ content, and displays the 'polyamorphism' discussed. Further heating shows three melting peaks, with one appearing to be the dominant peak over the other two. This would suggest that crystallisation of one polymorph is favoured over the other two in this system, but this may gradually convert to another over time, when comparing this to the first heat cycle. Due to the low intensity of the XRPD data, it is difficult to assign the true identity of these peaks, especially if they transform over time, further investigation, potentially with variable temperature XRPD, would be required to provide a definite explanation.

For the formulations containing 5% mannitol, there is no evidence of recrystallisation or polyamorphism, suggesting that this mannitol to Affinisol™ ratio is optimum if a stabilised amorphous formulation is required. Even through the presence of crystallinity does not impact the ability to print formulations below 30% mannitol in the system, structural integrity of the resulting tablets decreases as the mannitol content increases. This increased crystallinity could also impact the overall distribution of

carvedilol in the resulting dosage forms, therefore the amorphous formulations containing 5% mannitol would be preferred for future manufacture.

#### 5.3.1.4 Dissolution of Printed Tablets

As the original purpose of investigating the addition of mannitol to carvedilol/Affinisol™ formulations was with a view to improving the dissolution and release of the API from dosage forms, dissolution of all tablets which could be printed was investigated.

As with previous dissolution experiments, all tablets were subjected to dissolution analysis using a USP 1 dissolution test. Drug loading differed slightly between the different tablets (as noted by earlier HPLC analysis in Section 5.3.1.1), as did the weight of each tablet, but the approximate dose of the three different drug loadings were 20 mg for 10.5% CAR tablets, 40 mg for 20% CAR tablets and 60 mg for 30% CAR tablets. Samples were run for six hours and the following release profiles were obtained (Figure 133):

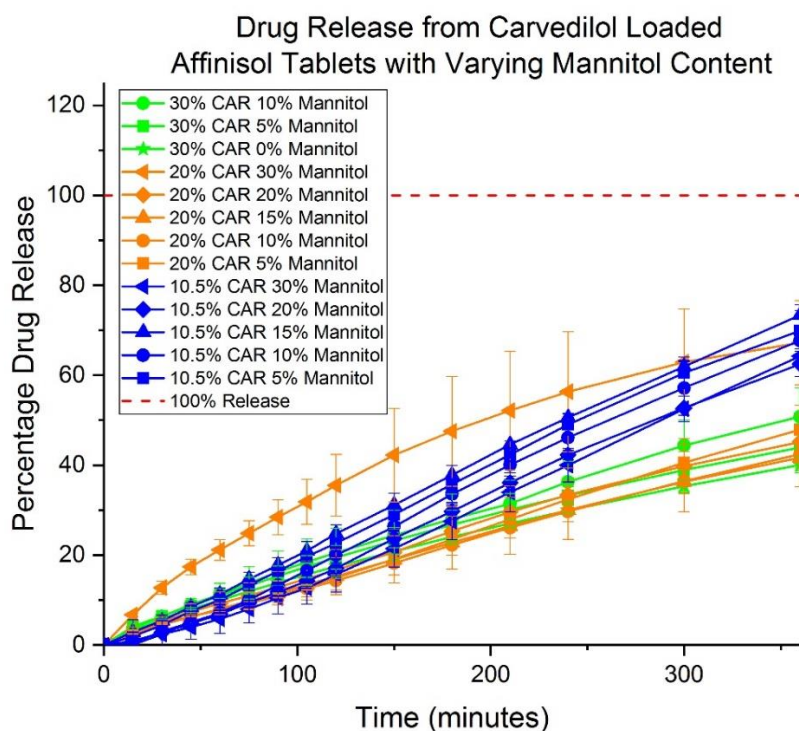


Figure 133 - Dissolution of Varying Mannitol and Carvedilol Content (n=3, ± standard deviation)



Considering differences between mannitol content and carvedilol content separately, these results suggest that the difference in release rate observed when varying mannitol is minimal, with no real improvement for any of the different drug loadings under investigation. Similarly to that observed in Section 4.3.3.6.1, it would appear that tablets with lower drug content (10.5% CAR) have a faster release rate than those with a higher drug content (20% and 30% CAR), but traditional release profiles which plot the data as 'percentage drug release' do not take account of the differing drug content in each of the tablets at the start of the dissolution experiment. As such, this data shows that tablets with 10.5% CAR are releasing more of their overall drug content within the timeframe of this experiment and are likely to achieve full release quicker than tablets with 20% or 30% CAR.

Given that these dissolution profiles seem to remain fairly linear, with the exception of 20% CAR 30% mannitol, release rate can be estimated by simple linear regression from plots of concentration vs time for the first 60 minutes. The tablets produced from the formulation containing 20% CAR 30% mannitol did not print very well and were excluded from the analysis due to discrepancies in the overall structure of the tablets, resulting in holes which penetrated into the internal structure. These holes allowed for the dissolution media to prematurely access the centre of these tablets, which would not occur in tablets which retained their structural integrity, and is likely the reason why the release of carvedilol from these tablets seemed improved relative to all other printed tablets.

Release rates (mg/min) were calculated based on 500 mL of dissolution media and normalised for weight (mg/min/g). These rates were then plotted in the following graph (Figure 134), to illustrate how the rates change with different mannitol and API concentrations:

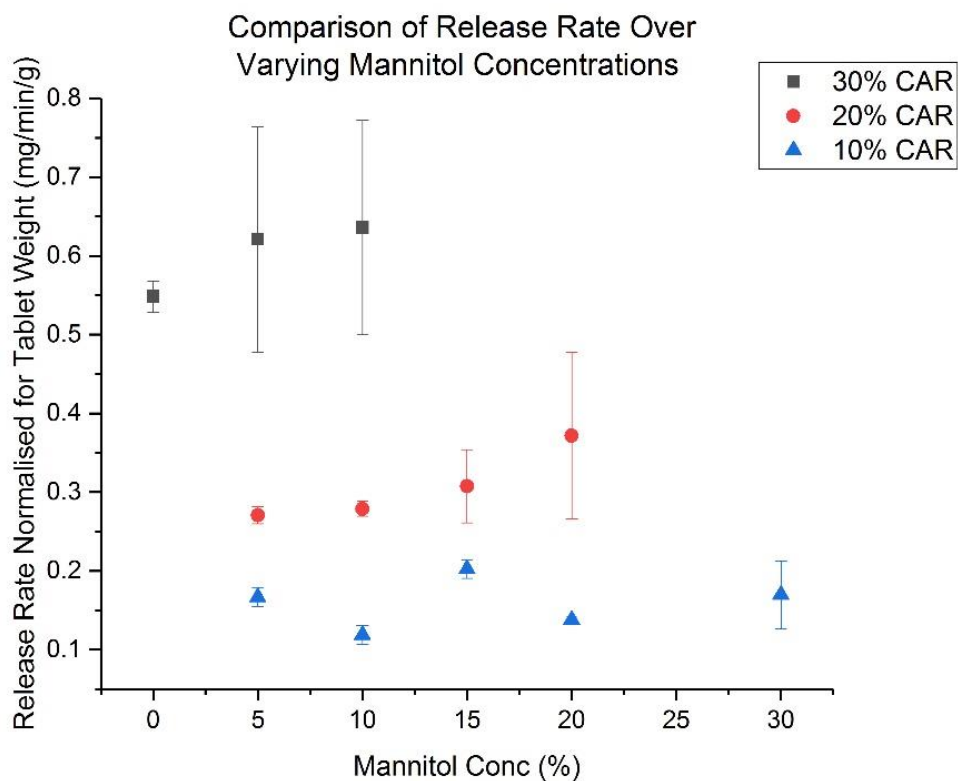


**Figure 134** - Release Rate over varying MAN and CAR loadings (n=3,  $\pm$  standard deviation)

When looking at release rate plotted against mannitol concentration, the most obvious trend seems to be the higher the drug loading, the faster the release rate. Changing the mannitol content doesn't seem to have any effect at all, although statistical analysis, using ANOVA calculations, should provide an idea as to whether the results are statistically different from one another. When comparing the results of Tukey analysis, these differences become clear (Figure 135 and Figure 136):

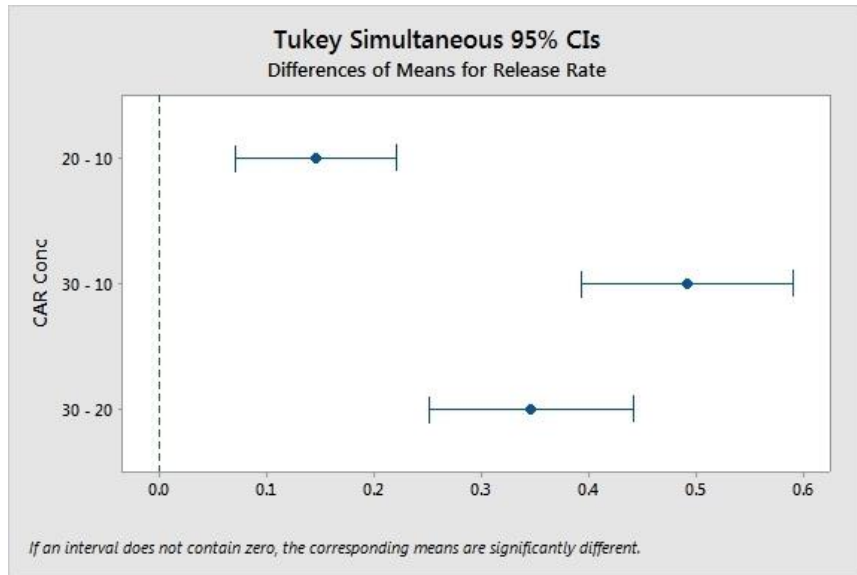


**Figure 135** - Tukey Analysis of Difference in Carvedilol Concentration

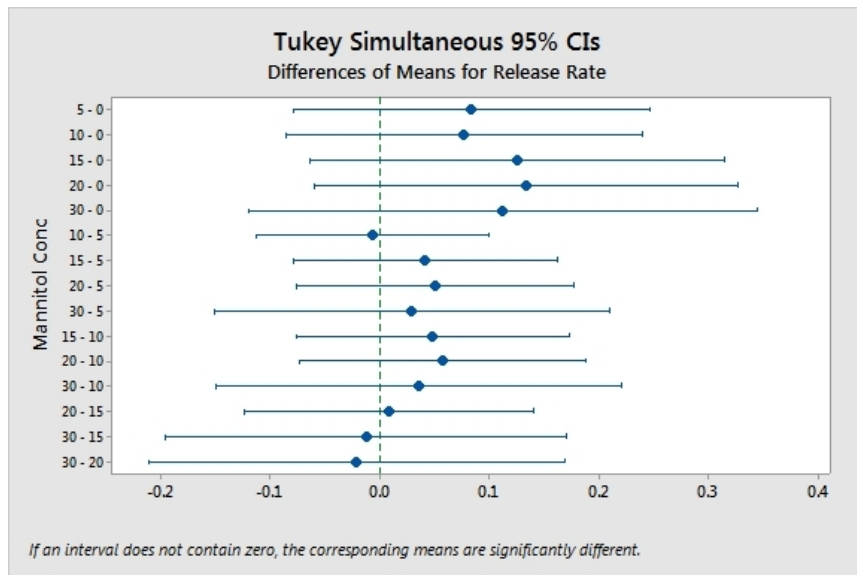


**Figure 136** - Tukey Analysis of Difference in Mannitol Concentration

When looking at the different drug loadings, it can clearly be seen that the differences observed between 10.5%, 20% and 30% drug loading are statistically relevant, and the conclusion that the rate increases with increasing drug loading is correct.

With regards to the differences observed between the mannitol concentrations, as all of these intervals contain zero, none of the mannitol concentrations produce results which are statistically different from one another. This means that the rate of release

does not improve or worsen regardless of the mannitol content of the formulation. As such, this allows for future manufacturing of these formulations to be based on conditions which gives the best processing results.

### **5.3.2 Highest and Lowest Achievable Dose**

As the investigation into various different mannitol and carvedilol concentrations was intended to cover the sustained release doses already available on the market (10-80 mg), attempts were made to investigate the highest and lowest possible drug loadings achievable in printed tablets, and how much drug is released during dissolution.

Two different sets of tablets were printed in order to determine the highest and lowest possible drug loadings which could be produced. A 10.5% carvedilol, 5% mannitol formulation was selected for the lowest dose, with an infill percentage of 10%, and a 30% carvedilol, 0% mannitol, with an infill percentage of 100% was selected for the highest dose. For the low drug loading, an infill of 0% was initially selected, but the top of the tablet had no structure to build upon, so an infill of 10% was determined to be the lowest infill which could be printed.

#### **5.3.2.1 Dissolution Analysis of Printed Tablets**

As with previous dissolution experiments, all tablets were subjected to dissolution analysis using a USP 1 dissolution test. Samples were run for six hours and the following release profiles were obtained (Figure 137):

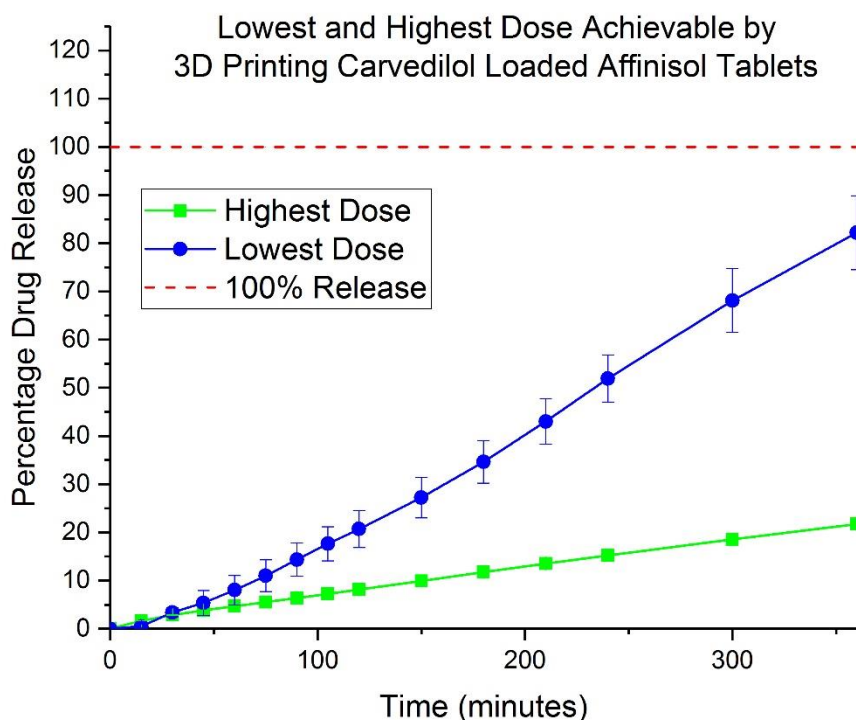


**Figure 137** - Dissolution of Highest and Lowest Achievable Dose (n=3 for highest dose and 2 for lowest dose,  $\pm$  standard deviation)

As expected, the release varies greatly between the two extremes of the doses chosen, but once again, traditional release profiles do not take account of the variation in drug content of the different tablets at the start of the experiment (approx. 16 mg vs 100 mg). Instead, this data highlights that the lowest dose tablets have released approximately 80% of their total content within the timeframe of the experiment, compared with the 20% released from the tablets produced with the highest dose. A closer look at the overall release rate for these two different designs, normalised for tablet weight, could provide further insight into the data.

Linear regression was, once again, used to calculate the release rates (mg/min) based on the volume of dissolution media remaining constant at 500 mL. These rates were again normalised for weight (mg/min/g) and plotted according to Figure 138, to illustrate how they change with different formulations:

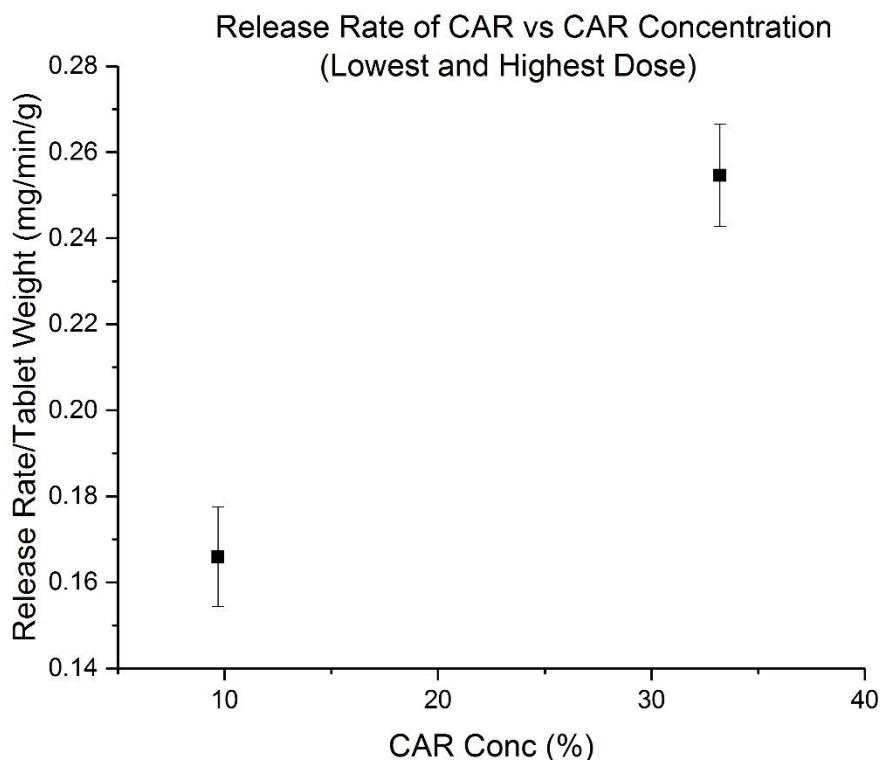


**Figure 138** - Release Rate of Carvedilol vs Carvedilol Content for Highest and Lowest Doses (n=3 for highest dose and 2 for lowest dose,  $\pm$  standard deviation)

When looking at release rate plotted against the carvedilol concentration, it appears that the higher the drug loading, the faster the release rate, which is difficult to determine when considering only data from traditional release profiles.

Given that there are only two data points, analysis was carried out using a Mann Whitney calculation in order to determine if there was any statistical difference in the release rate of these two doses. The results of this calculation indicate that there is no statistical difference between the release rates, which contradicts the findings obtained from previous dissolution experiments in Sections 4.3.3.6.1 and 5.3.1.4. It should be noted, however, that the number of tablets under investigation was only 3 for the highest dose, and 2 for the lowest dose, therefore it is likely that further investigation with more repeats would be needed to accurately determine if there is an overall difference in these release rates.

Based on the earlier HPLC data obtained in section 5.3.1.1, the drug loadings of the filaments used in the investigation were 9.7% w/w carvedilol for the lower drug loading, and 33.2% w/w carvedilol for the higher drug loading. Applying this to the tablets produced in this investigation, the lowest and highest possible doses achievable for a carvedilol/mannitol/Affinisol™ formulation produced by extrusion and printing are 16.8 mg and 101.5 mg respectively. While this does not cover the current range on the market of 3.125-25 mg for immediate release formulations, the controlled release range of 10-80 mg is closely aligned to these formulations. Further investigation into how these tablets are likely to behave within the body would be required to provide more insight into whether this is a suitable alternative to the current manufacturing procedure for carvedilol dosage forms.

### **5.3.3 Comparison to Direct Compression as a Manufacturing Method**

After carrying out experiments on the extrusion and 3D printing of various different compositions of carvedilol, mannitol and Affinisol™, along with the subsequent population of a ternary phase diagram of these components, it was reasoned that comparison with traditional tablet manufacture may offer insight into whether extrusion and subsequent printing provide any benefits over current manufacturing processes.

Using direct compression equipment, tablets were produced from three different formulations containing 10.5%, 20% and 30% carvedilol respectively and a constant mannitol concentration of 10%. Difficulty was encountered with poor flow of powder blends at 20% and 30% drug loading, and consistent tablet manufacture was not possible using the automated set up of the tablet press machinery. Instead, the die of the equipment was manually filled with each of the individual powder blends, and tablets produced in this fashion for comparison with 3D printing.

#### **5.3.3.1 Dissolution Analysis of Printed Tablets**

As with previous dissolution experiments, all tablets were subjected to dissolution analysis using a USP 1 dissolution test. Samples were run for six hours and the following release profiles were obtained (Figure 139):

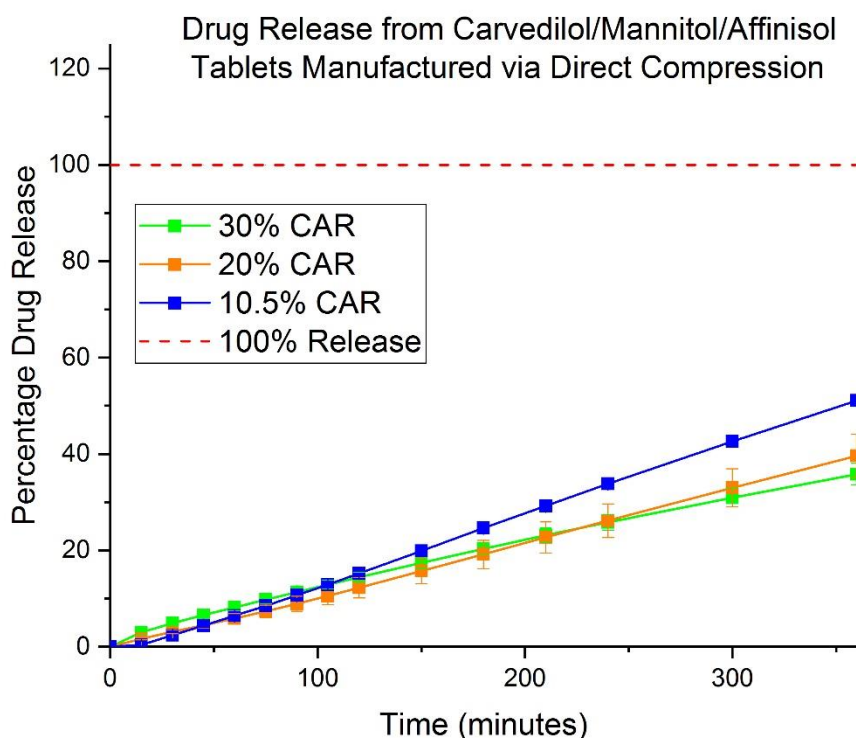


**Figure 139** - Dissolution of Formulations Manufactured via Direct Compression (n=3,  $\pm$  standard deviation)

On first examination of this data, the release profiles appear to be very linear with no evidence of any immediate release characteristics. This was also evident when examining the contents of the dissolution bath at the end of the experiment and finding partially dissolved tablets which appeared to have retained their original shape. This would suggest that the Affinisol™ is governing the release properties, rather than the specific manufacturing process, although the 30% CAR sample manufactured by direct compression does release more API in the 6 hour time period than its 3D printed, 100% infill counterpart in the previous section. Affinisol™ has been investigated for use in tablets manufactured by direct compression,<sup>153</sup> however it was concluded that it would be suitable for tablets manufactured for controlled release rather than any immediate release applications, which would support the findings observed here.

These results also suggest that there is not a huge difference in release rate across the different formulations, but again expressing the results as traditional release profiles



with 'percentage drug release' doesn't account for differences in drug loading or tablet weight for each of the different tablets under investigation. While these manually loaded samples were intended to be of similar weight, there were also still discrepancies due to poor flow and compressibility with higher drug loadings.

A more accurate way of comparing the release rate for these different tablets and formulations would be to look at the amount of drug released over time, and normalise for both tablet weight and surface area of each sample. Tablet weight is easily measured for each sample prior to dissolution, but the following surface area and volume were calculated for each of the formulations:

$$10.5\% \text{ CAR} - \text{Surface Area} = 268.6 \text{ mm}^2$$

$$- \text{Volume} = 318.1 \text{ mm}^3$$

$$- \text{Surface Area/Volume Ratio} = 0.84$$

$$20\% \text{ CAR} - \text{Surface Area} = 254.5 \text{ mm}^2$$

$$- \text{Volume} = 286.3 \text{ mm}^3$$

$$- \text{Surface Area/Volume Ratio} = 0.89$$

$$30\% \text{ CAR} - \text{Surface Area} = 240.3 \text{ mm}^2$$

$$- \text{Volume} = 254.5 \text{ mm}^3$$

$$- \text{Surface Area/Volume Ratio} = 0.94$$

Again, using linear regression, the following release rates (mg/min) were calculated according to the volume of the dissolution media, once again, 500 mL. This time, rates were normalised for both weight (mg/min/g) and surface area (mg/min/cm<sup>2</sup>) to account for any discrepancies observed between the individual tablets. These rates were then plotted in the following graphs (Figure 140 and Figure 141), and compared with 3D printed tablets, to illustrate how the rates change with different formulations across the two different manufacturing techniques:

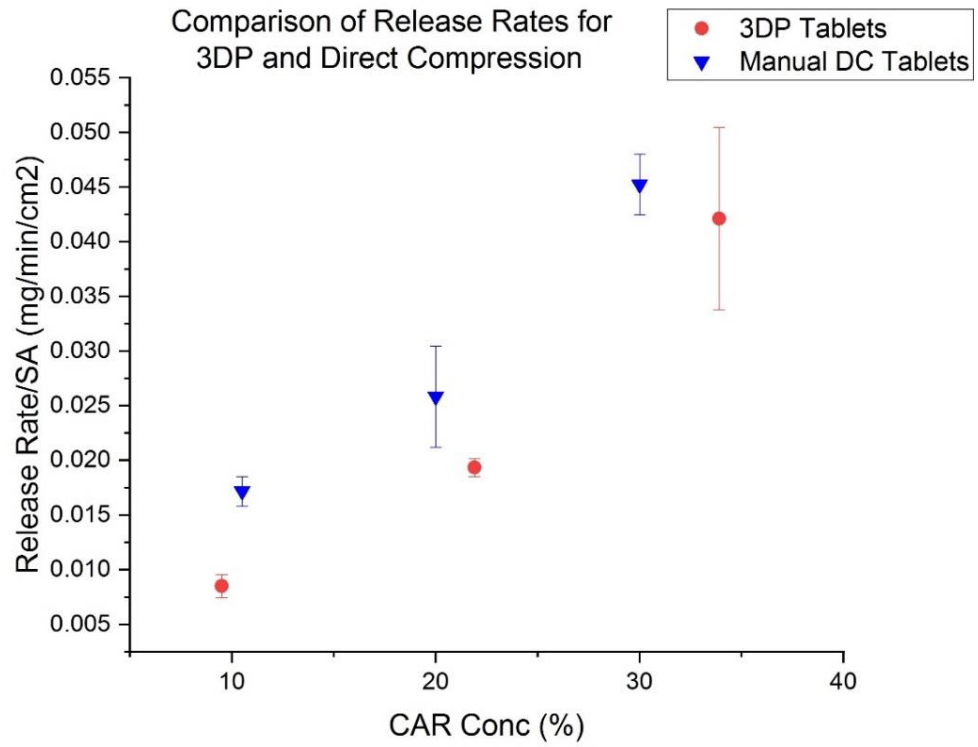


Figure 140 - Release Rates Normalised for Surface Area (n=3, ± standard deviation)

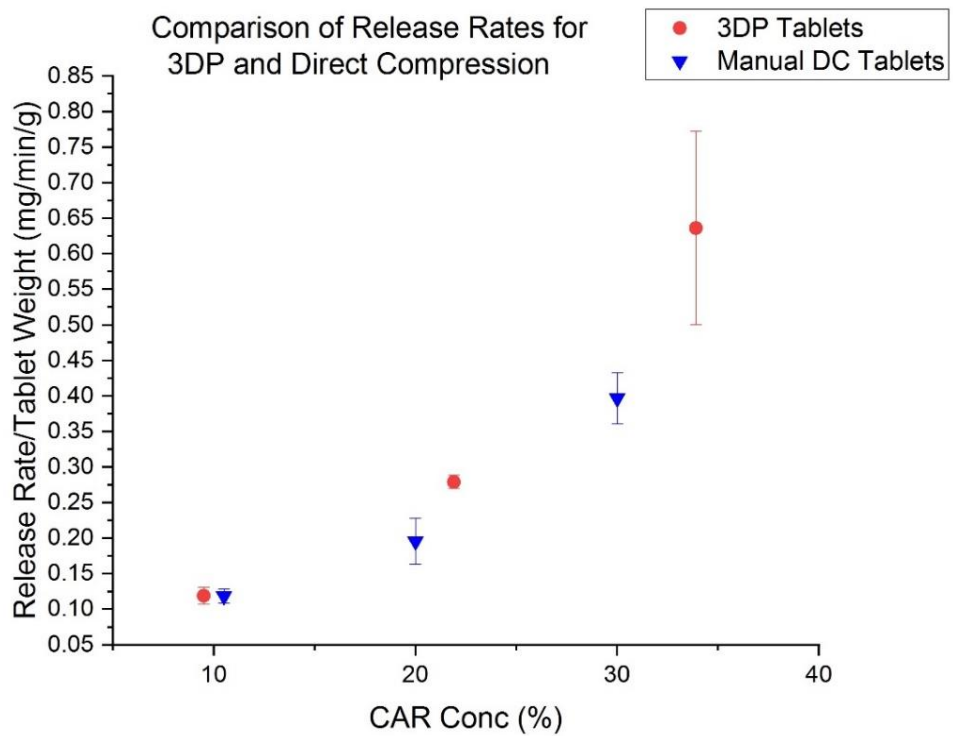
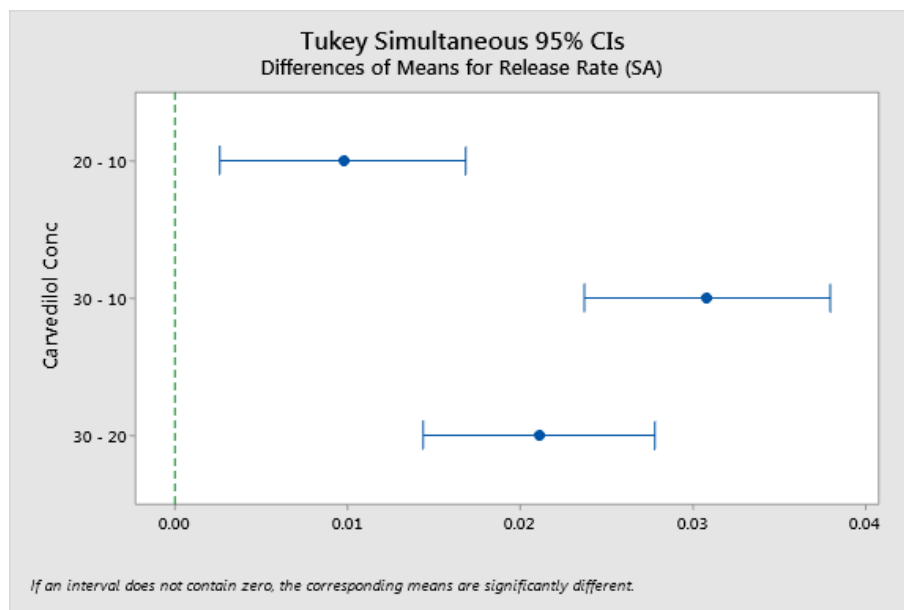


Figure 141 - Release Rates Normalised for Weight (n=3, ± standard deviation)

*Population of a Ternary Phase Diagram to better understand Formulations for 3D Printing*

When looking at these results, the major trend is the observed increase in dissolution rate as the drug loading increases. There is a very slight difference between the techniques when comparing the two graphs however - when normalised for tablet weight, 3D printing seems to offer that fastest release rate, but when normalised for surface area, direct compression seems fastest.

ANOVA calculations and Tukey analysis should provide an idea if the results are statistically different or not (Figure 142 and Figure 143):



**Figure 142** - Tukey Analysis of Carvedilol Content Normalised for Surface Area

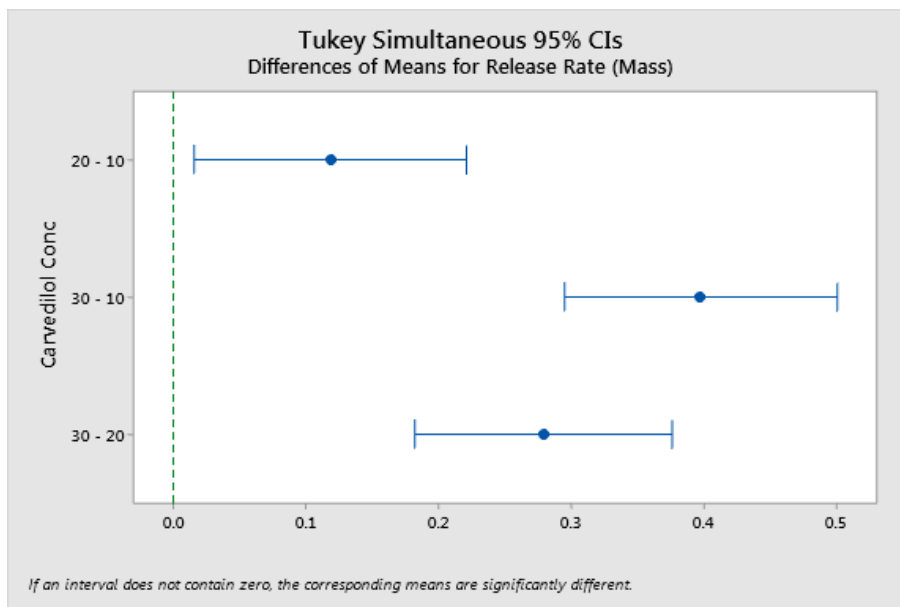


**Figure 143** - Tukey Analysis of Carvedilol Content Normalised for Tablet Weight

When looking at the carvedilol concentration in the different formulations (for both surface area normalised and tablet weight normalised samples), there is a statistical difference observed between all different drug loadings, and therefore, the observation that the rate increases as the drug loading increases is correct.

When carrying out Tukey analysis on the two different processes, neither of the confidence intervals included zero, therefore both 3DP and DC are statistically different from one another when looking at both samples normalised for surface area and for weight. Therefore, samples normalised for surface area show that direct compression offers the fastest release rate and samples normalised for tablet weight show that 3DP offers the fastest release rate.

Overall, it can be concluded that while there is a difference in release rate observed between direct compression and 3D printing, the major trend in increasing the rate is observed as an effect of carvedilol concentration, rather than an effect of any of the different processes.

When normalising the data for surface area, direct compression achieves the faster release rates, which could potentially highlight that the added manufacturing step of extrusion provides no added benefit to the production of carvedilol tablets when using

these materials. It should be noted, however, that calculation of the surface area is difficult for 3D printed tablets which, as a result of the manufacturing process, have many different grooves and ridges in the external structure. This could result in the release rates being normalised incorrectly, and the statistical analysis being incorrect.

When normalising the data for tablet weight, 3D printed tablets achieve the faster release rates, which could be a result of possible increased surface area (due to the aforementioned grooves and ridges) or the lower infill percentage of 30%, compared to the 100% infill of direct compression tablets. The manufacture of consistent tablets with 3D printing is also difficult to control, with the appearance of defects or holes in the surface, allowing the penetration of dissolution medium into the internal structure, further increasing the surface area.

While statistical analysis can provide further insight into these results, it should be noted that there was not a large sample size on which to carry out this analysis, so the conclusions may not give an accurate idea of the true effects.

#### **5.4 Conclusion and Next Steps**

Overall, when combining the results from all the different extrusion experiments looking at varying the concentrations of the three components: mannitol, carvedilol and Affinisol™, a suitable zone for manufacture of varying doses has been identified.

When looking at the different phase diagrams which have emerged from different analyses, along with complementary DSC and XRPD analyses, the area highlighted by the red box suggests the zone which is optimum for continued work in this area (Figure 144 and Figure 145):

*Population of a Ternary Phase Diagram to better understand Formulations for 3D Printing*

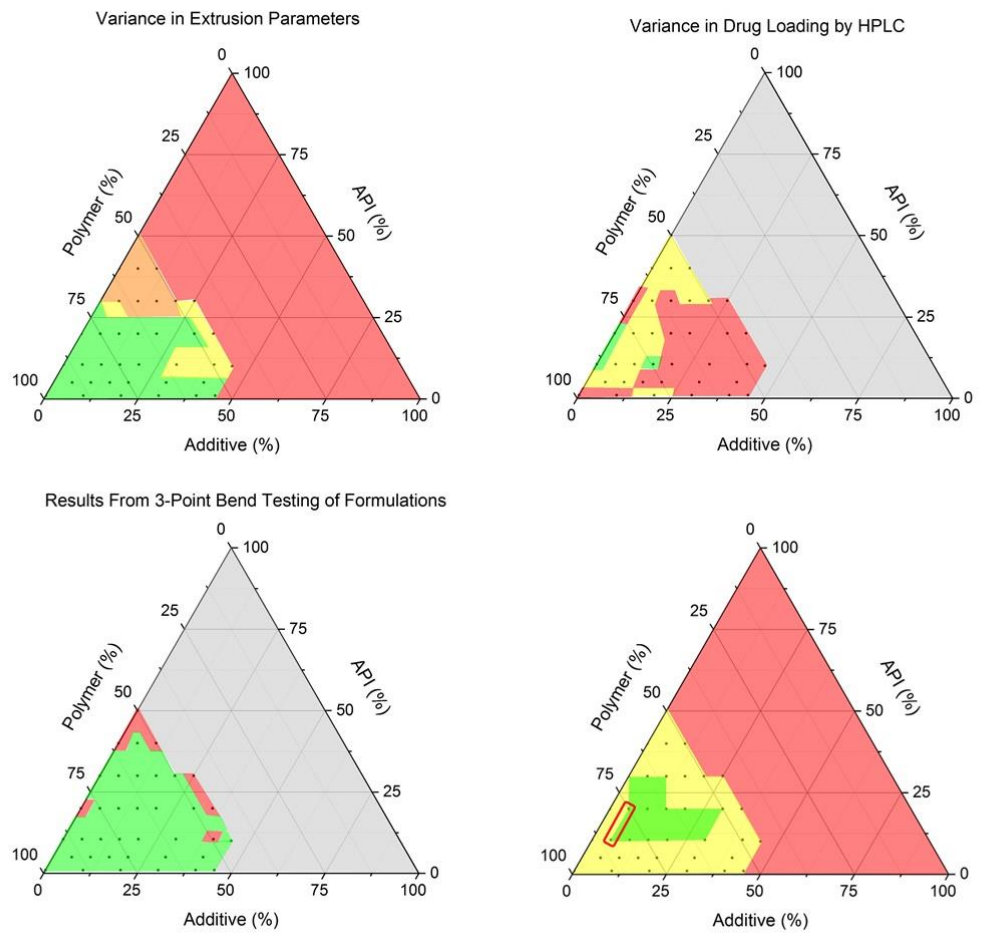


**Figure 144 - Ternary Phase Diagram Comparison**

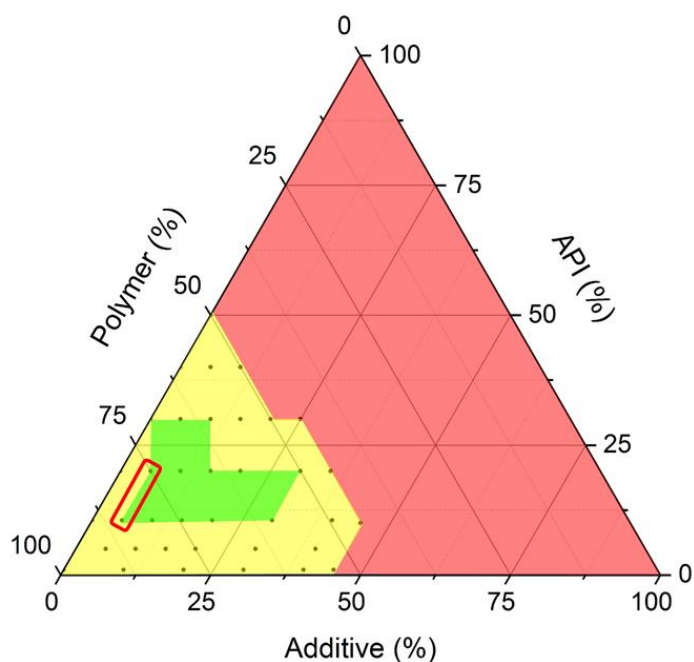


**Figure 145** - Optimum Operating Conditions as Identified from Experiments

This zone combines the reliability of extrusion parameters along with the printable zone identified from 3-point bend testing, and the ability to achieve the correct dose, as detected by HPLC. When comparing this to the known formulations which can be printed, the area contained within this red box is highlighted as having the ability to produce the most desirable results.

Dissolution experiments carried out on all the printable formulations, along with statistical analysis on the results, show that there is no benefit to increasing the mannitol concentration in terms of dissolution rate. The only observed improvement to the rate of dissolution is seen when increasing the drug loading. All formulations exhibit sustained release over the 6 hour time period investigated.

DSC and XRPD data suggest that carvedilol remains amorphous throughout the different formulations, but in order to preserve amorphousness in mannitol, at least over short time periods, mannitol concentration should not exceed 5%. While increased levels of crystallinity do not seem to have any effect on the printability or

dissolution of the tablets, the quality of prints decline somewhat as the mannitol content increases.

Despite not achieving immediate release through the use of mannitol in these formulations, it is clear that mannitol has the benefit of enabling printing when compared to 'blank' formulations, in drug loadings of 10.5% and 20%. Once a drug loading of 30% is reached, mannitol is no longer required for successful printing.

Further investigation with rheology and elongation experiments would be beneficial for understanding what parameters are necessary for successful printing, but time and equipment constraints meant that this was not possible for these experiments. Further investigation into different drug/polymer/additive combinations could also be beneficial in achieving immediate release 3D printed tablets.

The lowest and highest possible doses achievable for tablets produced via this method are 16.8 mg and 101.5 mg respectively. While this does not cover the current range on the market of 3.125 mg - 25 mg for immediate release formulations, it comes very close to matching the controlled release range of 10 mg – 80 mg, which fits well with the observed release mechanism.

When considering the overall process, and comparing to the current manufacturing method of direct compression, there doesn't seem to be a huge difference in observed release rates, leading to the question of whether the added processing step of extrusion is really beneficial to the overall process. When comparing dissolution data to that observed from the marketed controlled release formulation of carvedilol,<sup>154</sup> the data appears to be very similar with both the marketed capsules and the 3D printed tablets from this work showing a linear release profile over the first 6 hours of dissolution, with a similar percentage of drug being released for both formulations (approximately 60% for a 20 mg tablet). The data for the marketed formulations extends for a longer period of time and displays a first order release when observed for the full 24 hours, comparison of which wasn't possible with this work due to time constraints.

The only benefit of using the extrusion and printing manufacturing route, is the ability to potentially freely select a dose based on tablet size and infill percentage while



keeping the overall formulation the same. Given that the purpose of this research was to develop a method of doing just that, some level of success has clearly been achieved, but due to the early nature of this method development, further investigation is required.

## **6 Conclusions and Future Work**

### **6.1 Overall Conclusions**

Over the course of this research, the use of 3D printing has been investigated as a means to potentially provide access to personalised medicine. The first experimental chapter in this thesis looked at the use of PVA as a carrier polymer, with the addition of the chosen API, carvedilol, via a solution loading method. While the production of varying doses was possible by changing the infill percentage of the printed tablets, resulting in approximate doses in the range of 7-12 mg, these could not be increased any further due to limitations in the loading process. Various techniques were investigated in order to increase the API concentration in the filament, prior to printing, but a maximum drug loading of approximately 4% w/w was the highest concentration achievable within the filament. Various analytical techniques were applied in order to investigate the nature of the drug loading process and the drug distribution as a result of this process. Variation in drug loading was observed across the filament, which has not been discussed in the literature prior to this work, however this variation was shown to be ‘smoothed’ after printing. Nano-CT, although not investigated extensively, has also been shown to provide excellent visualisation of the internal structure of printed tablet and may offer added benefit to the future design of more complex dosage forms. While the dose achieved via this method is in the middle of the current market requirements for immediate release tablets, the mechanism of release from these final dosage forms was observed to be sustained release over six hours. Solution loading, using PVA as the carrier polymer, was therefore deemed unsuitable to match the current market requirements for production of carvedilol loaded 3D printed tablets, however it may be a suitable technique for manufacture of alternative APIs.

Expanding the research space further, the second experimental chapter of this thesis looked at increasing the drug loading in the filament by the use of hot-melt extrusion as a means of filament preparation. For continuity, PVA was again selected as the carrier polymer, but this resulted in difficulties with the production of suitable filaments for printing and highlighted the complex nature of this process and the need

for extensive research within the extrusion/printing area. After various different trials and the inability to resolve problems with PVA, Affinisol™ was instead selected as the carrier polymer, and work focused on the production of printable formulations, which also resulted in immediate release characteristics. Various different disintegrants (sodium chloride, glycine, cellulose, hydroxypropylcellulose, erythritol, mannitol and polyethylene glycols) and superdisintegrants (sodium starch glycolate and crosscarmellose sodium) were investigated, but none resulted in immediate release formulations, instead the conclusion that the notion of ‘disintegrant’ not necessarily being a sensible descriptor for additives to these dosage forms was determined. While investigating all these various additives, it was observed that Affinisol™ and carvedilol alone were not sufficient for the production of printable formulations, but required the addition of one of these ‘disintegrants’ for printing to be successful, despite the lack of improvement to the release mechanism. With the addition of one of these disintegrants (mannitol was deemed the most suitable) investigation into improving release through changes in surface area/volume ratio and infill percentage of tablets was carried out. This resulted in only very small improvements to the release rate, with 100% release still only occurring after six hours, even when applying the optimum experimental conditions. Given the materials available for manufacture and the type of 3D printing (fused filament fabrication) used in this research resulting in highly compacted dosage forms, it seems inevitable that sustained release should be the overall observed characteristic of any dosage forms produced in this way. Bearing all this in mind, further investigation into immediate release formulations with these components was deemed unsuitable, with a focus instead shifting to matching the controlled release formulations of carvedilol currently on the market.

The third and final experimental chapter of this thesis therefore looked at fully investigating the boundaries of the experimental space when including the three components – mannitol, carvedilol and Affinisol™ - in the production of the desired 3D printed dosage forms. By applying the construction of a unique phase diagram to this research, suitable ratios of each component were identified in order for the production of the final dosage forms to be successful, but this resulted in a very narrow window in terms of the operating parameters. This further highlights that the

manufacturing technique of fused filament fabrication, while displaying great potential in the field of pharmaceutical technology, is somewhat limited and care should be taken before fully abandoning any of the traditional routes of tablet manufacture. As an added piece of investigation, the hot-melt extrusion and 3D printing manufacturing technique was also compared with the traditional direct compression technique, still favoured in the majority of industrial settings, in order to determine if production is improved at all through the use of new technology. Results suggest that release rates are very similar across the different manufacturing techniques and further investigation would be required to determine which the ‘best’ technique is going forward. Despite these limitations and lack of overall improvement, a dose range comparable with the controlled release doses already on the market was successfully manufactured through 3D printing as a result of this research.

When considering the applicability of fused filament fabrication for the production of other formulations containing different APIs, it is hoped that the research within this thesis can provide a base from which to build upon. If using the same equipment as discussed within these experimental chapters, it should be noted that only thermally stable drugs should be investigated as temperatures up to 200°C are used throughout the manufacturing process. Very high dose drugs are also unlikely to benefit from this manufacturing technique given the requirement for at least 50% of the formulation to be reserved for the carrier polymer. Mechanical strength of any successfully extruded (or solution loaded) filaments must be assessed to determine if transfer to the printer is feasible and the use of additional excipients is more than likely also required in order for printing to be a success.

Overall, 3D printing offers a promising alternative to traditional manufacture, with the added benefit of being able to select different doses without complete re-formulation of the starting material – a positive consideration, even if there appears to be little improvements over other manufacturing techniques. Although this technique is still in its infancy, the speed with which the field of personalised medicine is advancing will no doubt have a favourable effect on any continued research within this area,

allowing more in-depth investigation into other multi-dose drugs currently on the market.

## **6.2 Further Work**

Despite the in-depth investigation carried out into various formulations suitable for 3D printing containing carvedilol, further work would still be beneficial in order to gain a greater understanding of the boundaries for successful manufacturing with these components.

As mentioned throughout this research, the inclusion of rheology as a means to investigate the polymer filaments may provide further insight into why some of the formulations fail to print. Further analyses into drug content of the formulations may also provide a greater understanding of the drug distribution within both filaments and tablets which would be beneficial for accurate dosing of patients.

Given the change observed in dissolution when adding holes to the tablet design, and the ability of CAD software to provide access to a whole range of alternative shapes when compared to conventional tablet design, further investigation into the role that dosage form structure has on dissolution properties is sure to provide interesting insights into how future formulations behave. The addition of increased complexity to designs could provide the ability to tweak the release kinetics between immediate and sustained release while still using the same feedstock filament prior to printing.

Furthermore, Affinisol™ is not the only polymer suitable for transfer from a hot-melt extruder to a 3D printer<sup>95,121,122</sup> and investigation into alternative carrier polymers may not only provide a greater range of components to choose from, but could also allow access to the elusive immediate release formulations which are also desired when using this 3D printing technique.



## 7.2 Feed Rate of Material Entering Extruder

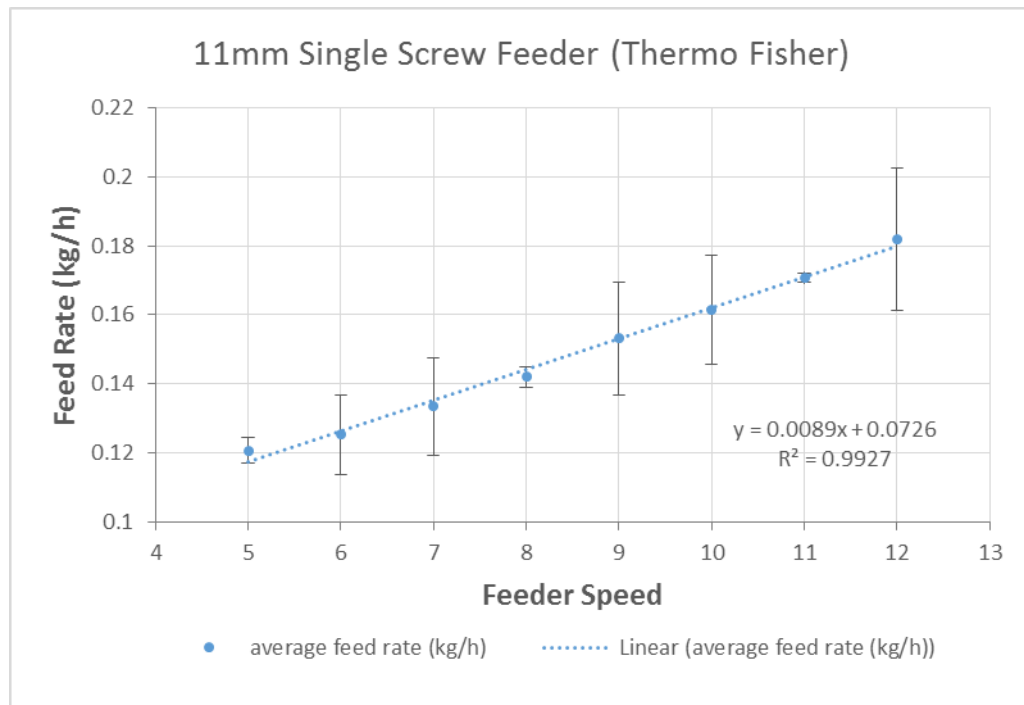


**Figure 147** - Feed Rate of Material Entering Extruder

**Table 45** - Feed Rate of Material Entering Extruder

Feeder Speed	Average Feed Rate (kg/h)	Stdev
5	0.121	0.004
6	0.125	0.012
7	0.134	0.014
8	0.142	0.003
9	0.153	0.016
10	0.161	0.016
11	0.171	0.001
12	0.182	0.021

## **7.3 Raman Mapping Images for Carvedilol Loaded Filaments and Tablets**

### **7.3.1 Carvedilol Loaded PVA Filaments**

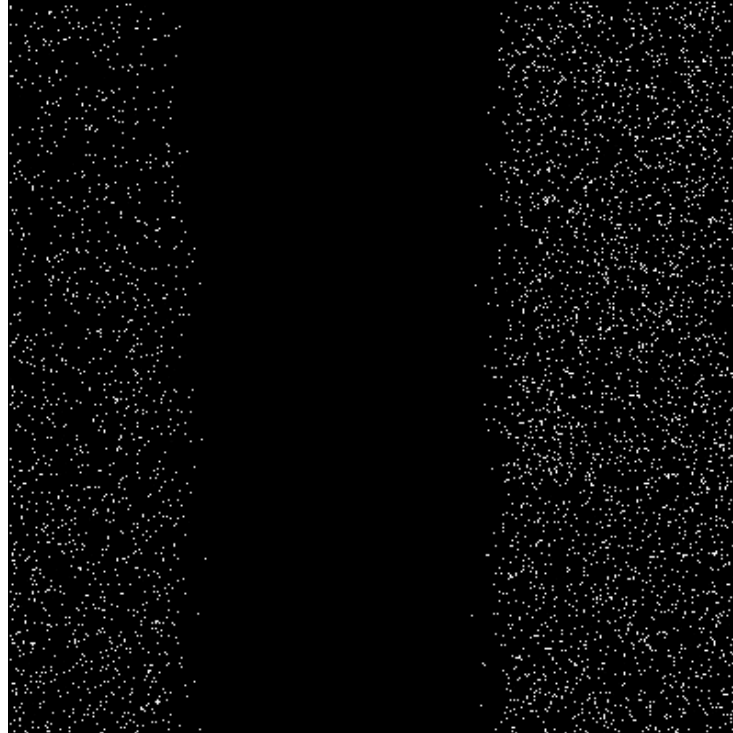


**Figure 148** - Black and White Map of Carvedilol



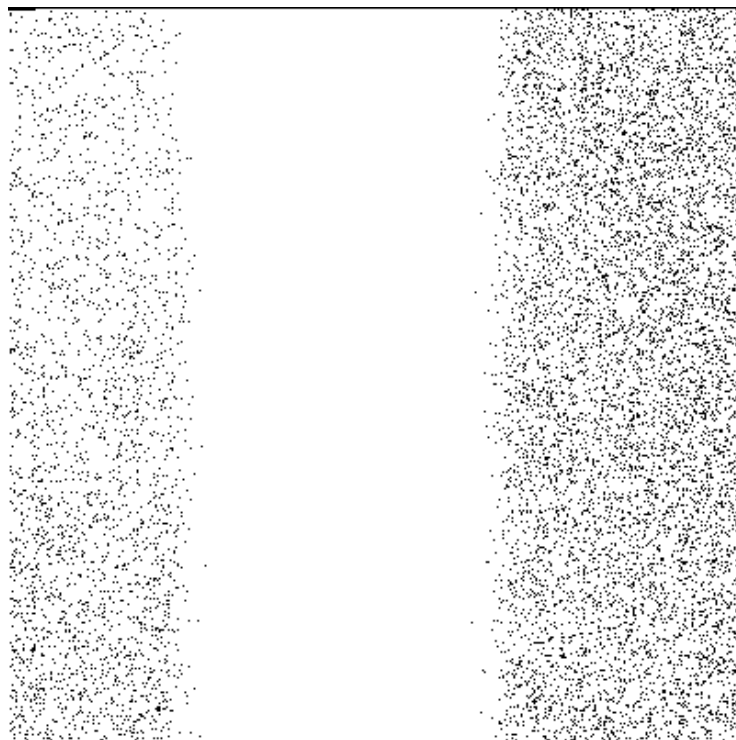


**Figure 149** - Black and White Map of PVA

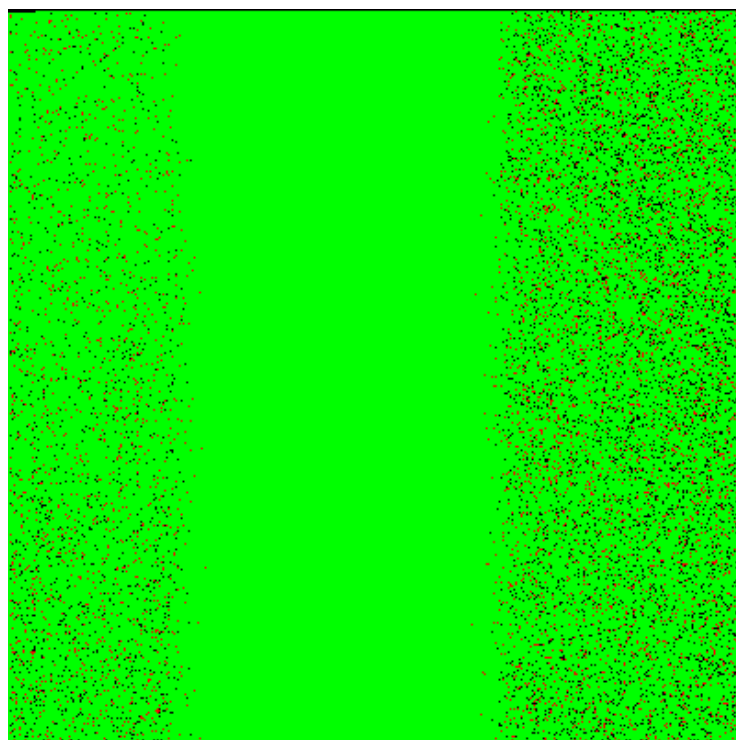


**Figure 150** - Colour Map Showing Green for PVA and Red for Carvedilol

### 7.3.2 Carvedilol Loaded PVA Printed Tablets

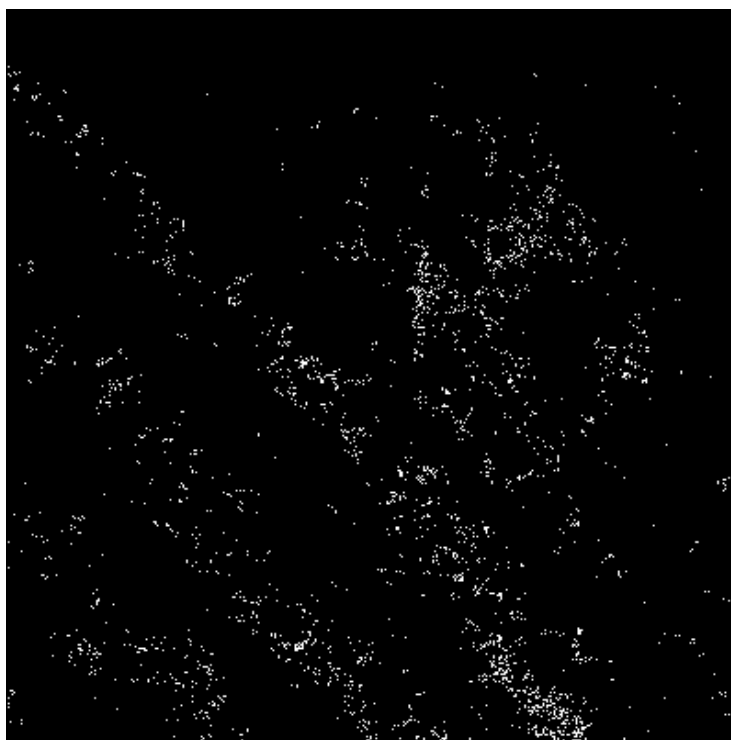


**Figure 151 - Black and White Map of Carvedilol**



**Figure 152 - Black and White Map of PVA**

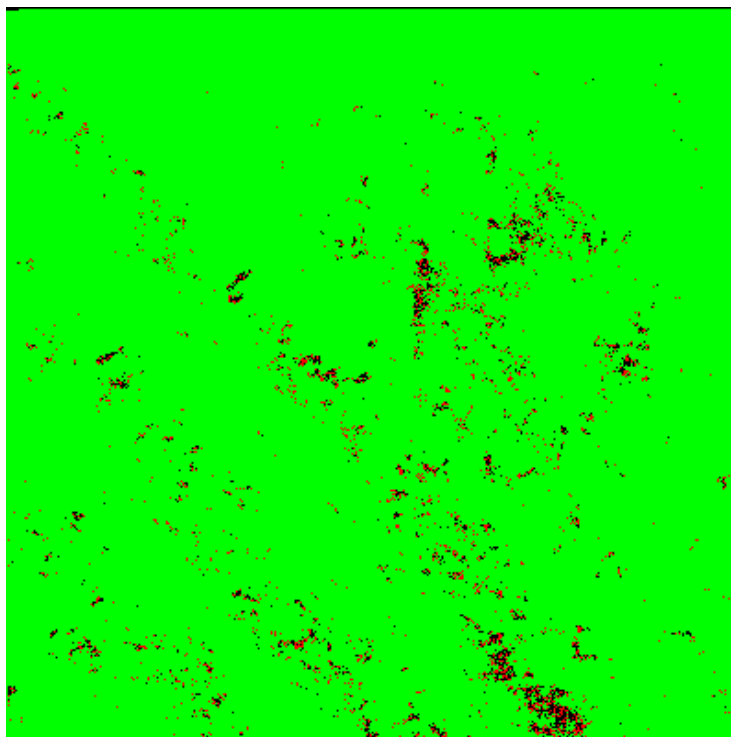


**Figure 153** - Colour Map Showing Green for PVA and Red for Carvedilol

#### 7.4 Stress versus Strain Graphs for Different CAR Drug Loadings

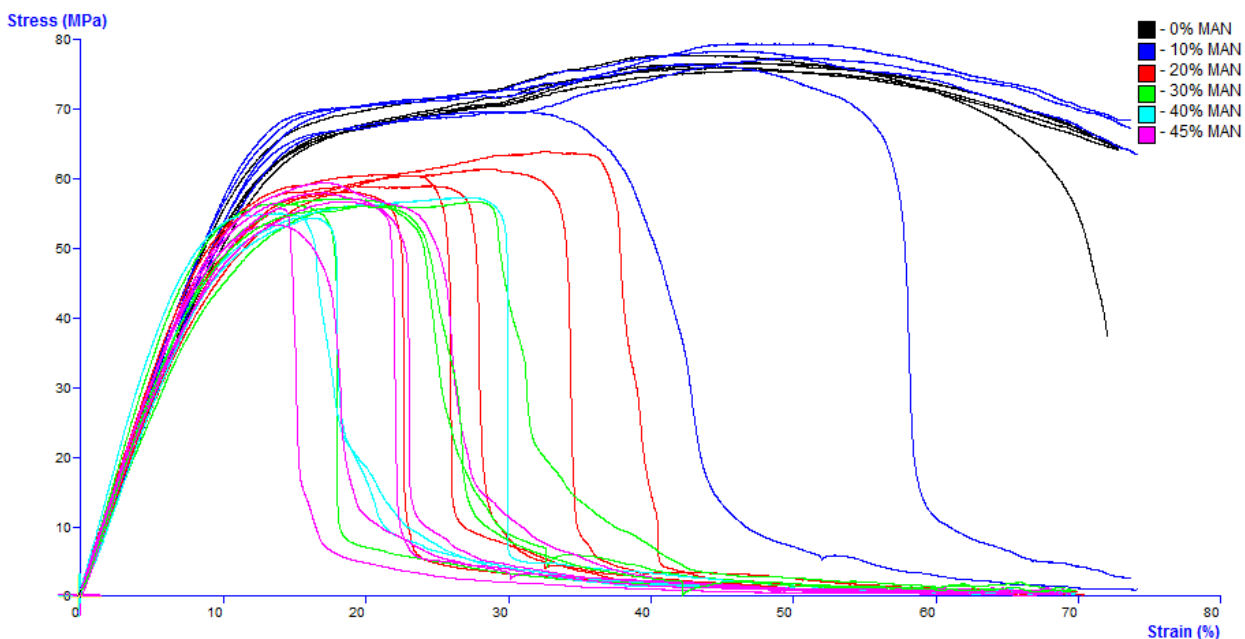


**Figure 154** - Stress versus Strain Graph for 1% CAR Drug Loadings

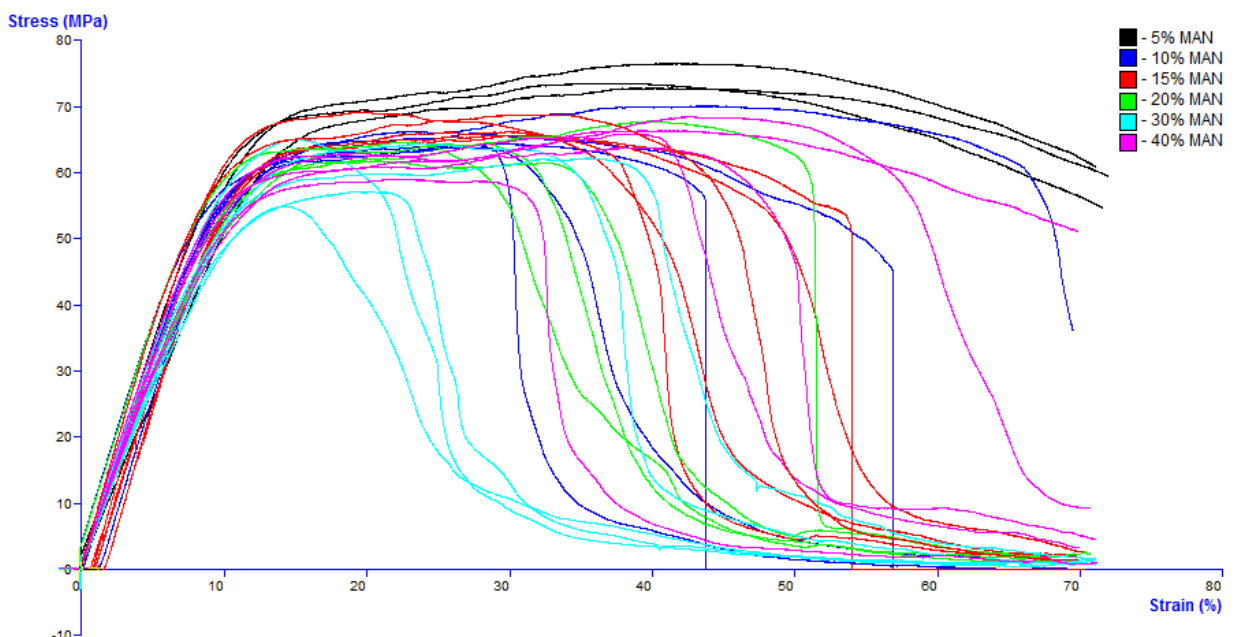


**Figure 155** - Stress versus Strain Graph for 5% CAR Drug Loadings

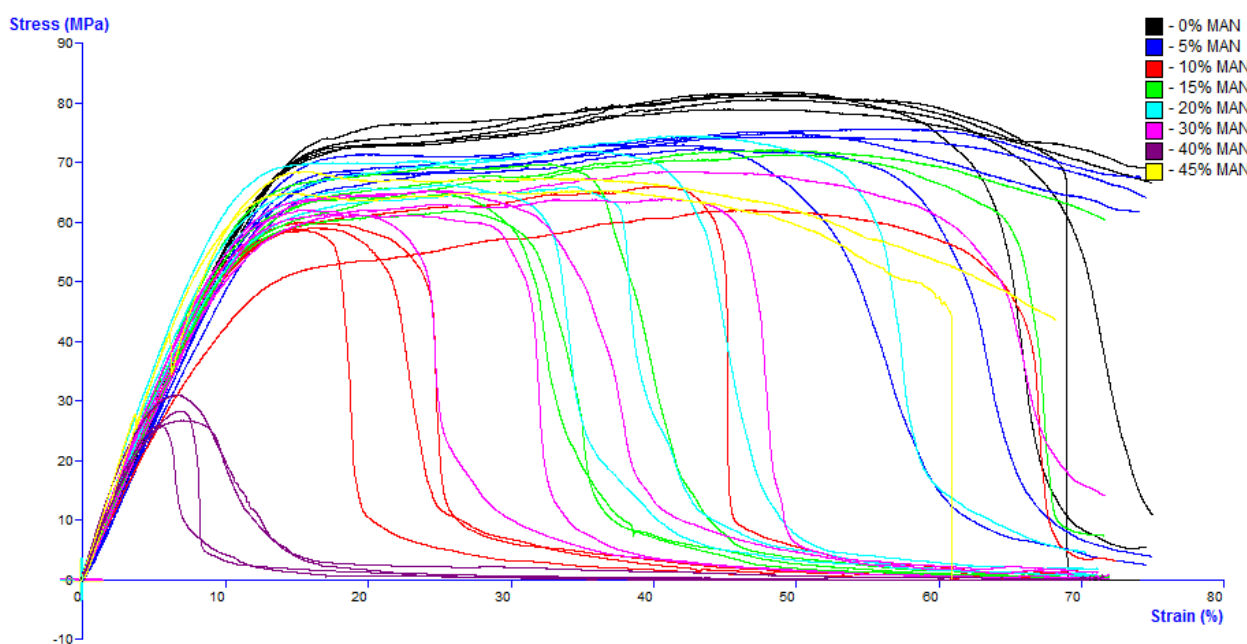


**Figure 156** - Stress versus Strain Graph for 10.5% CAR Drug Loadings

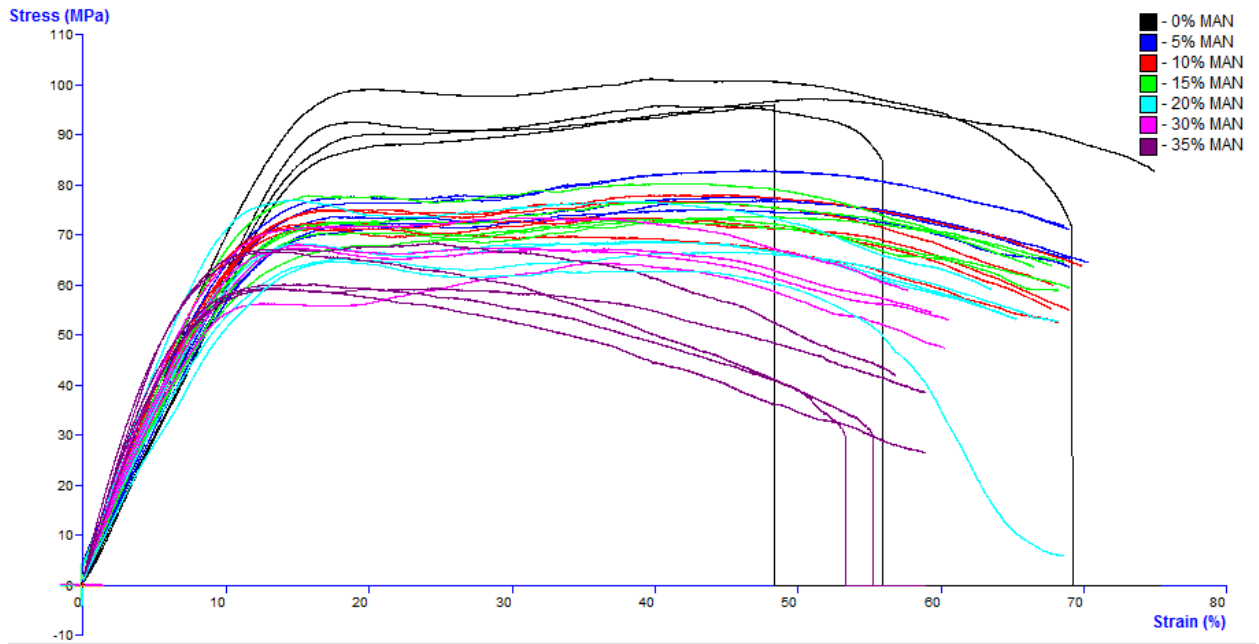


Figure 157 - Stress versus Strain Graph for 20% CAR Drug Loadings

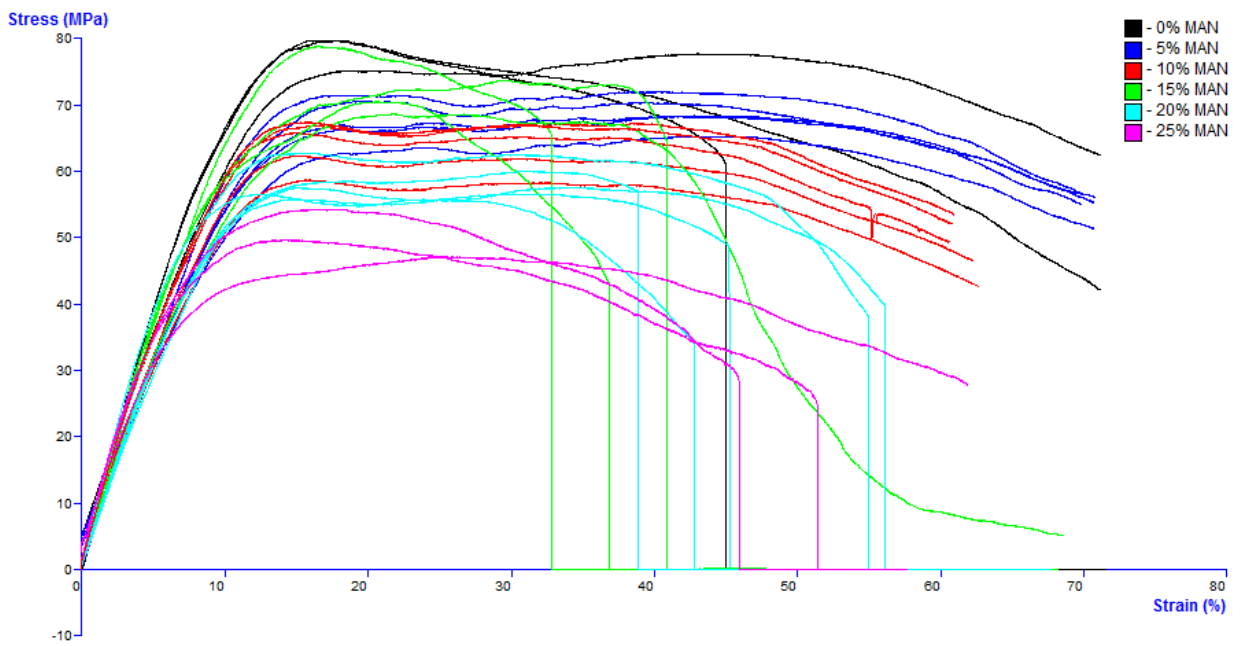


Figure 158 - Stress versus Strain Graph for 30% CAR Drug Loadings

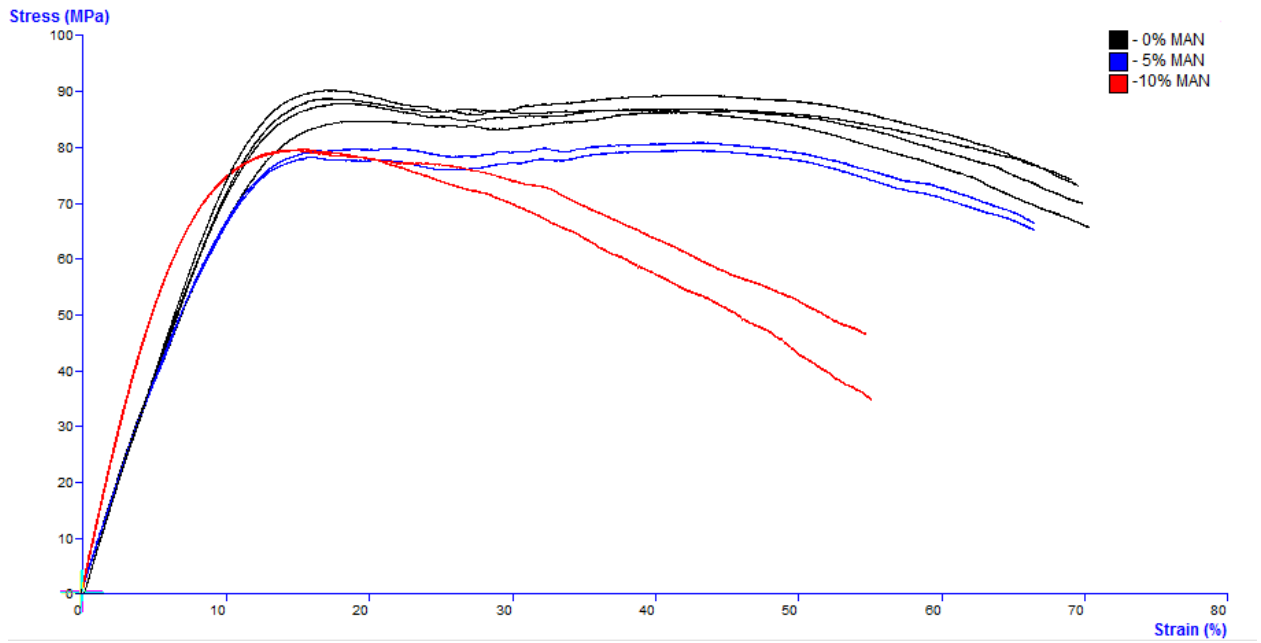


Figure 159 - Stress versus Strain Graph for 40% CAR Drug Loadings

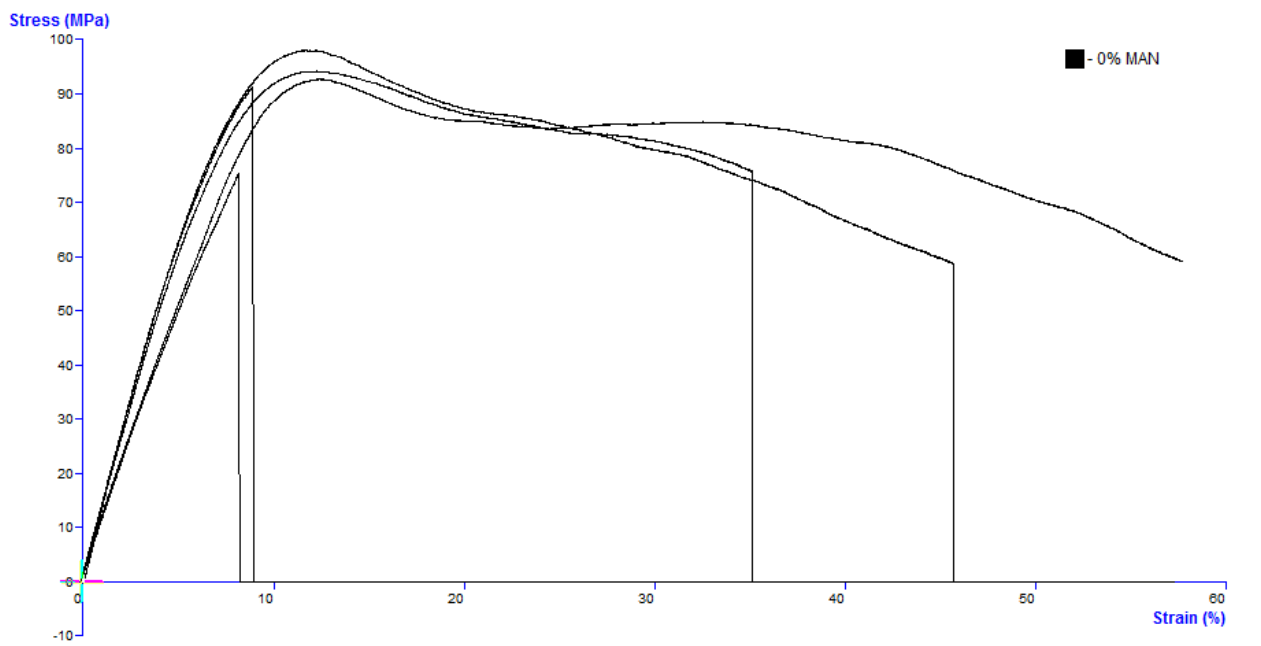


Figure 160 - Stress versus Strain Graph for 50% CAR Drug Loadings

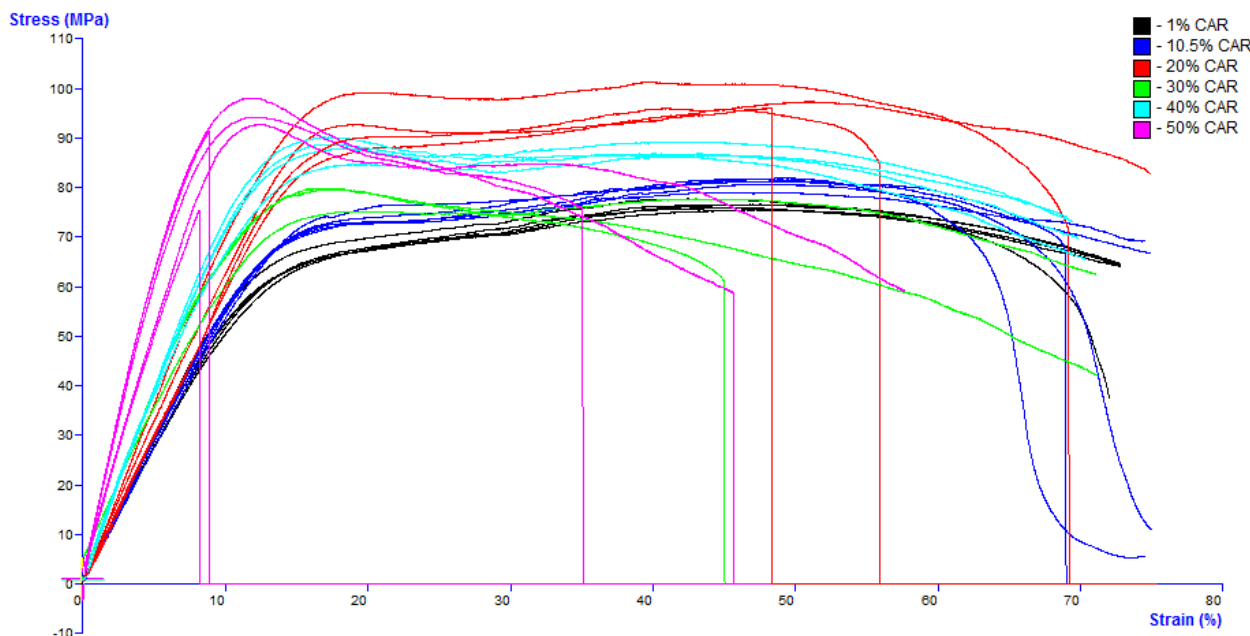


Figure 161 - Stress versus Strain Graph of Different Carvedilol Loadings at 0% Mannitol

### 7.5 Flexural Modulus and Maximum Stress Values for Ternary Phase Diagram Formulations

Formulation Composition	Flexural Modulus (MPa)	Maximum Stress (MPa)
PLA	8.1 ± 0.2	79.7 ± 3.2
1% CAR 0% MAN	5.7 ± 0.2	76.6 ± 0.8
1% CAR 10% MAN	5.9 ± 0.3	76.3 ± 3.9
1% CAR 20% MAN	5.8 ± 0.3	60.7 ± 2.2
1% CAR 30% MAN	6.1 ± 0.7	56.6 ± 0.5
1% CAR 40% MAN	6.4 ± 0.9	55.6 ± 1.6
1% CAR 45% MAN	6.3 ± 0.2	56.8 ± 2.3
5% CAR 5% MAN	6.0 ± 0.8	74.4 ± 2.0
5% CAR 10% MAN	6.5 ± 0.3	66.0 ± 3.6
5% CAR 15% MAN <sup>a</sup>	7.419 <sup>a</sup>	68.894 <sup>a</sup>
5% CAR 20% MAN	5.9 ± 0.2	64.8 ± 3.0
5% CAR 30% MAN	6.0 ± 0.6	60.8 ± 4.5
5% CAR 40% MAN	6.2 ± 0.4	64.8 ± 3.6
10.5% CAR 0% MAN	5.7 ± 0.2	81.0 ± 1.2
10.5% CAR 5% MAN	5.4 ± 0.3	74.2 ± 1.4

10.5% CAR 10% MAN	5.8 ± 0.5	61.3 ± 3.0
10.5% CAR 15% MAN	5.9 ± 0.3	68.1 ± 4.4
10.5% CAR 20% MAN	6.5 ± 0.6	69.9 ± 4.2
10.5% CAR 30% MAN	6.2 ± 0.4	64.4 ± 2.9
10.5% CAR 40% MAN	5.9 ± 0.4	28.2 ± 2.2
10.5% CAR 45% MAN	7.1 ± 0.3	66.0 ± 0.8
20% CAR 0% MAN	6.5 ± 0.6	97.7 ± 2.5
20% CAR 5% MAN	6.5 ± 0.3	78.3 ± 3.3
20% CAR 10% MAN	7.5 ± 0.5	84.8 ± 5.2
20% CAR 15% MAN	7.0 ± 0.6	75.6 ± 4.3
20% CAR 20% MAN	7.3 ± 1.4	70.0 ± 5.2
20% CAR 30% MAN	7.5 ± 0.6	68.5 ± 3.8
20% CAR 35% MAN	8.7 ± 0.6	63.0 ± 4.4
30% CAR 0% MAN	7.5 ± 1.0	79.2 ± 1.2
30% CAR 5% MAN	5.8 ± 0.6	69.0 ± 2.6
30% CAR 10% MAN	6.8 ± 0.5	64.4 ± 3.7
30% CAR 15% MAN	7.0 ± 1.1	69.8 ± 8.2
30% CAR 20% MAN	6.7 ± 0.9	58.8 ± 2.7
30% CAR 25% MAN	6.7 ± 0.6	49.3 ± 3.7
40% CAR 0% MAN	7.9 ± 0.2	88.5 ± 1.6
40% CAR 5% MAN	7.7 ± 0.2	80.2 ± 0.9
40% CAR 10% MAN	10.7 ± 0.02	79.6 ± 0.1
50% CAR 0% MAN	11.7 ± 1.6	90.5 ± 8.7

---

<sup>a</sup>An error with the equipment allowed only one sample to be analysed.



## 7.6 Supplementary DSC Data

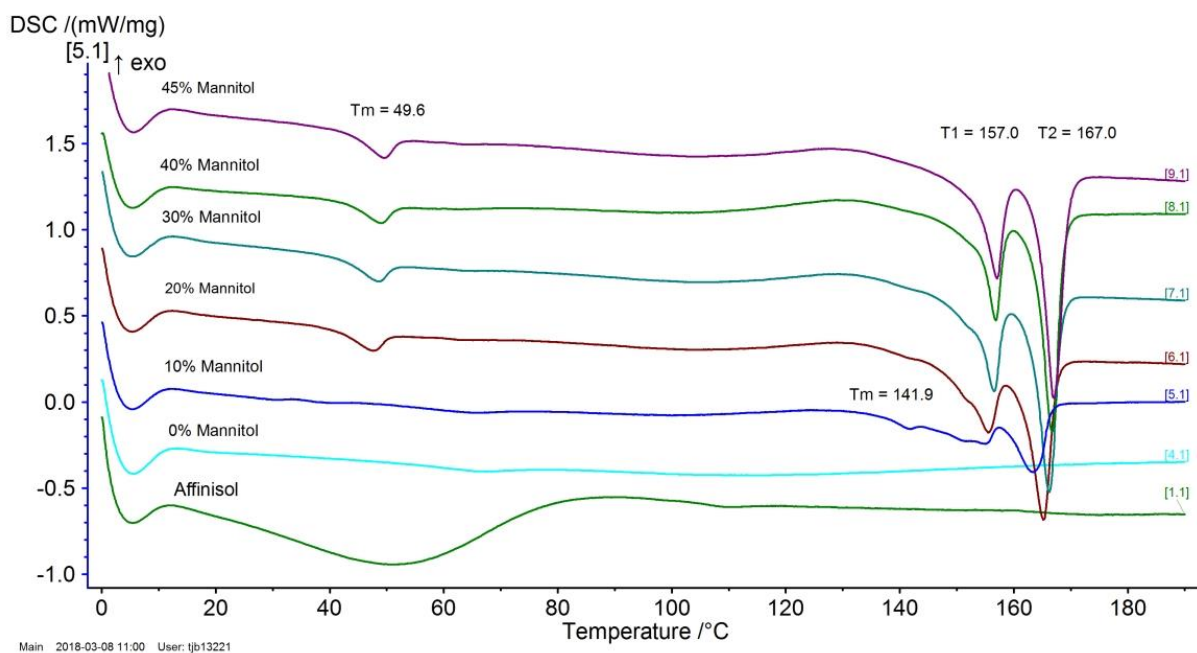


**Figure 162** - 1% Carvedilol Formulations 1st Heating

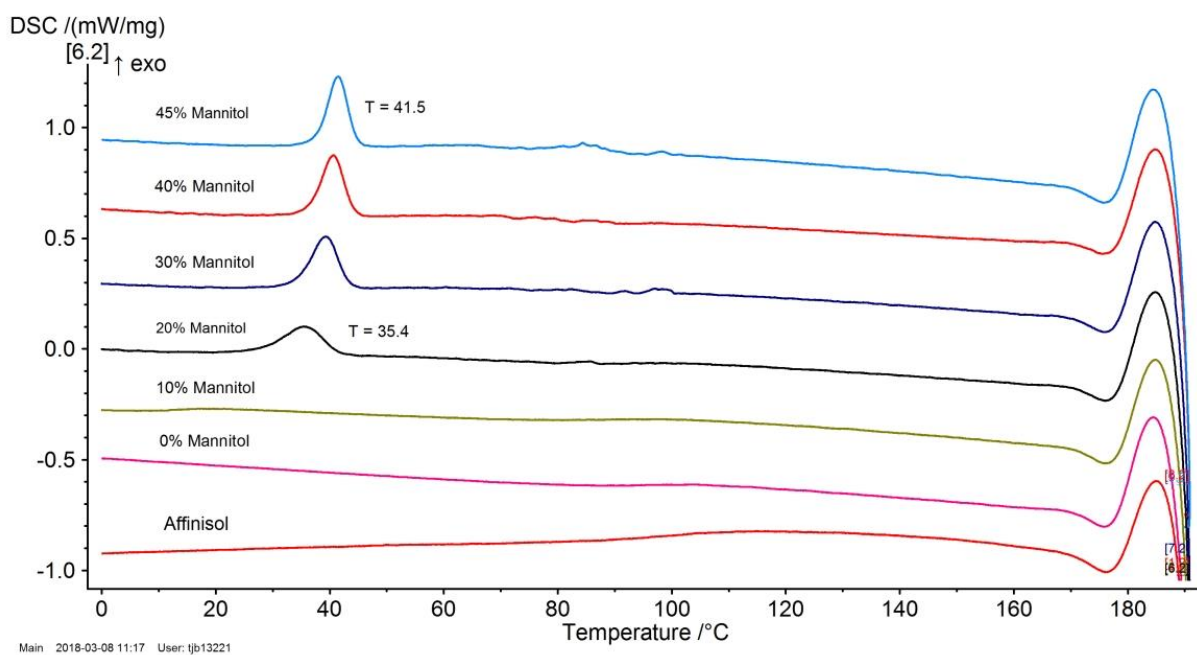


**Figure 163** - 1% Carvedilol Formulations Cooling

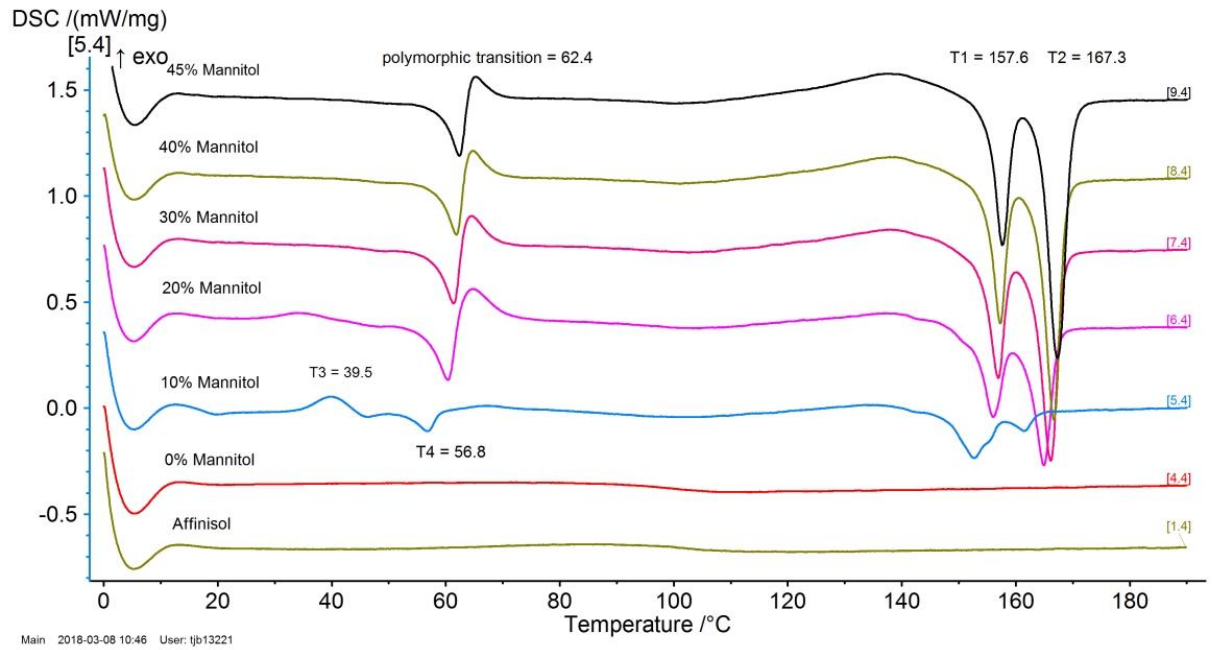


**Figure 164 - 1% Carvedilol Formulations 2nd Heating**

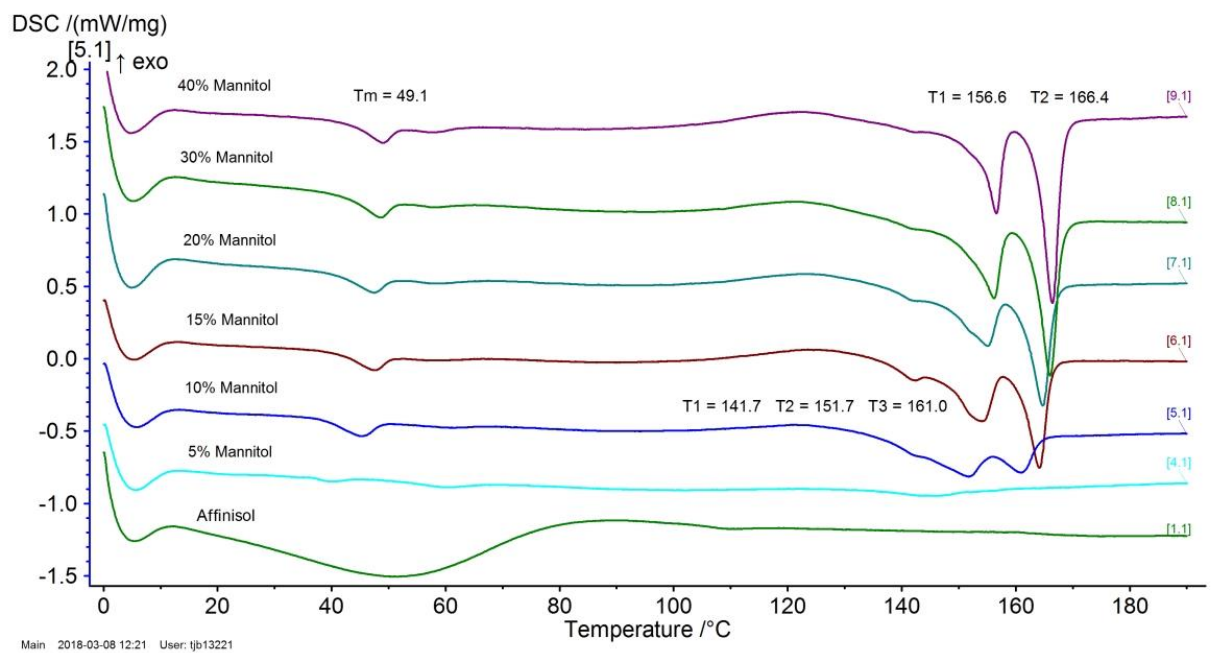


**Figure 165 - 5% Carvedilol Formulations 1st Heating**

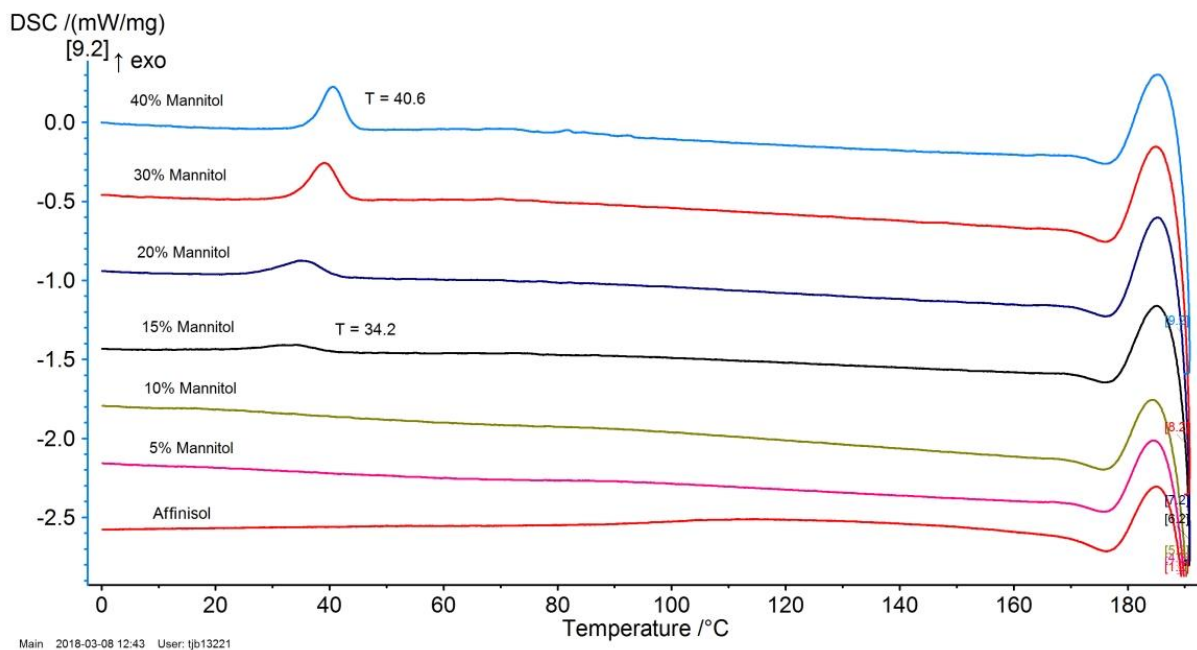


Figure 166 - 5% Carvedilol Formulations Cooling

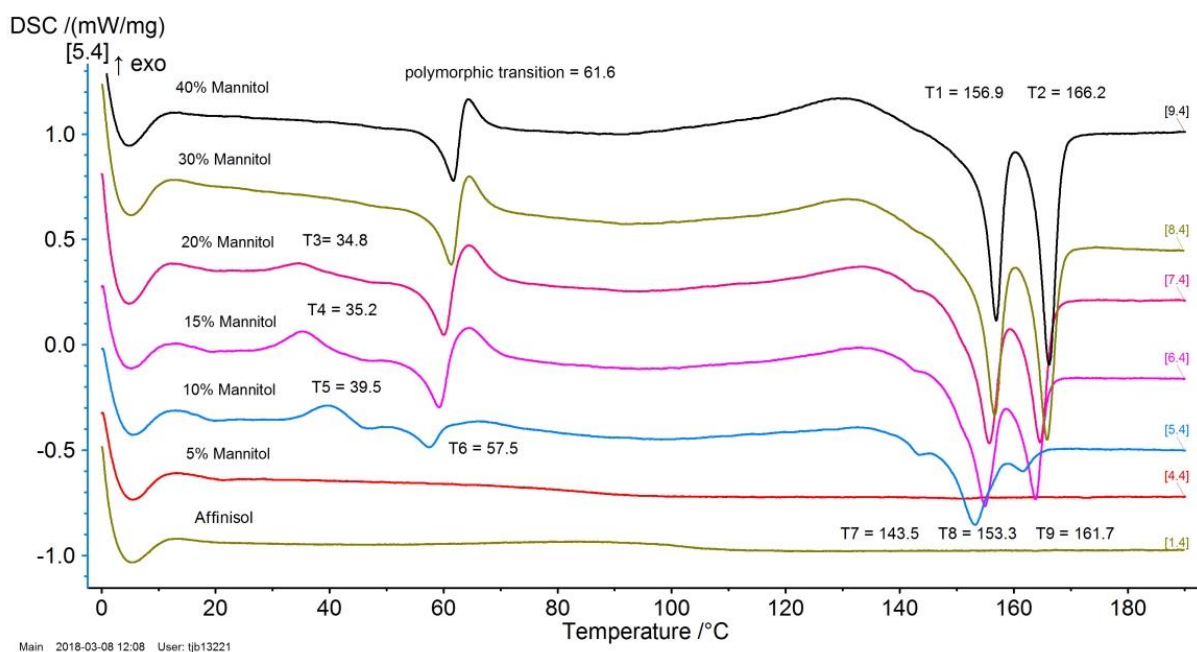
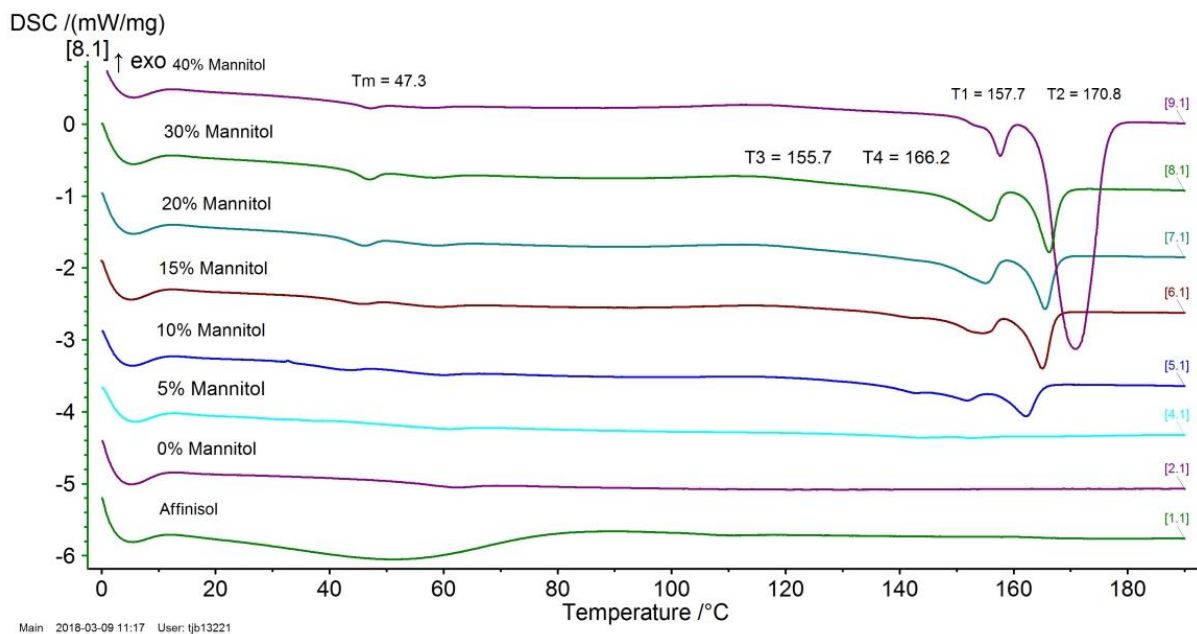
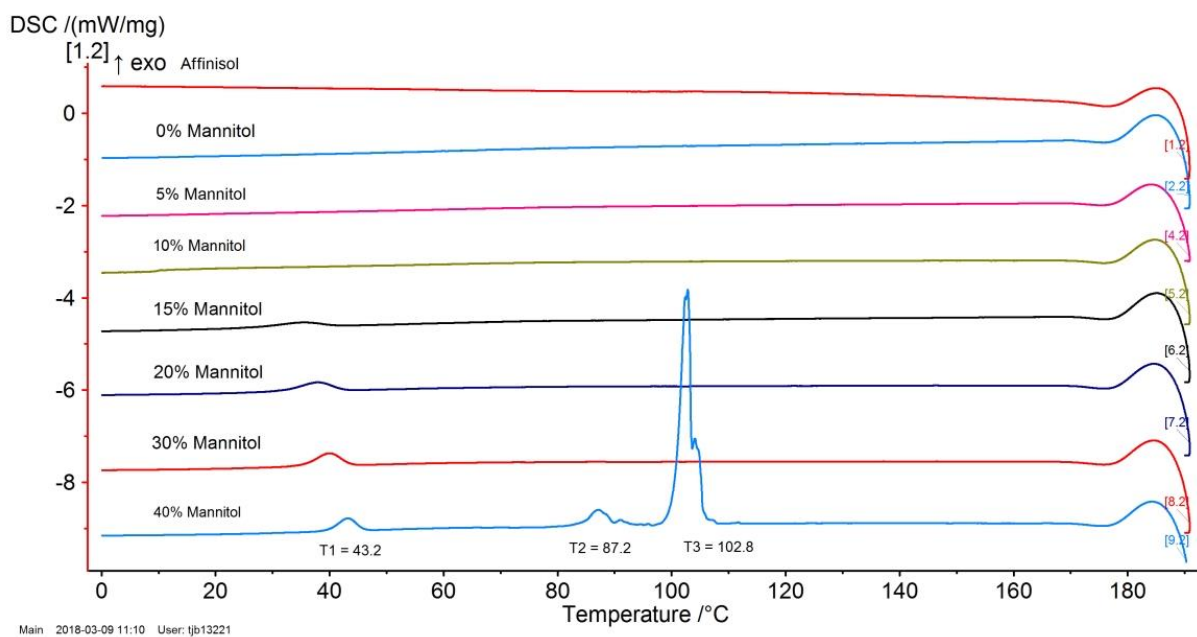


Figure 167 - 5% Carvedilol Formulations 2nd Heating



**Figure 168 - 10.5% Carvedilol Formulations 1st Heating**



**Figure 169 - 10.5% Carvedilol Formulations Cooling**

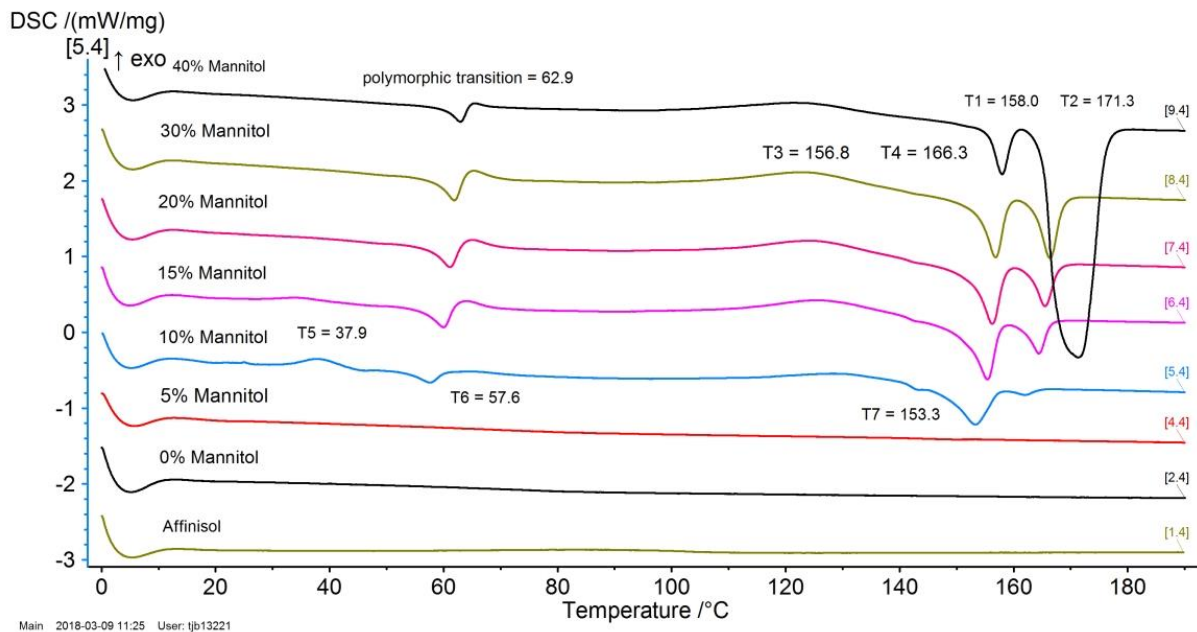


Figure 170 - 10.5% Carvedilol Formulations 2nd Heating

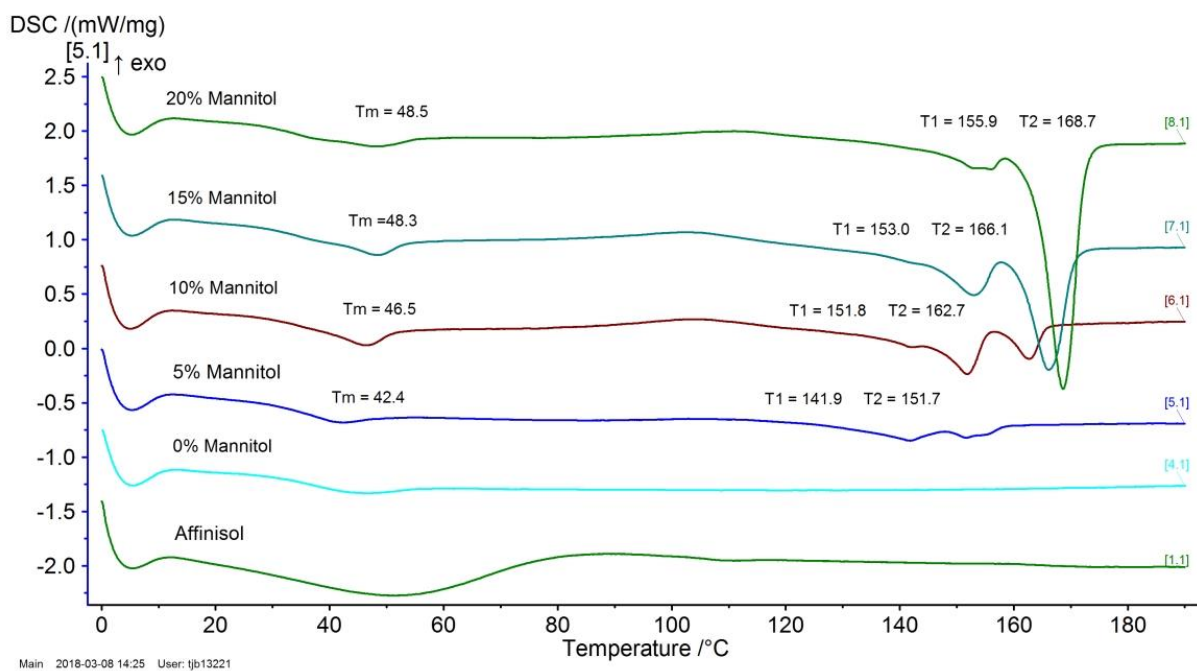


Figure 171 - 30% Carvedilol Formulations 1st Heating

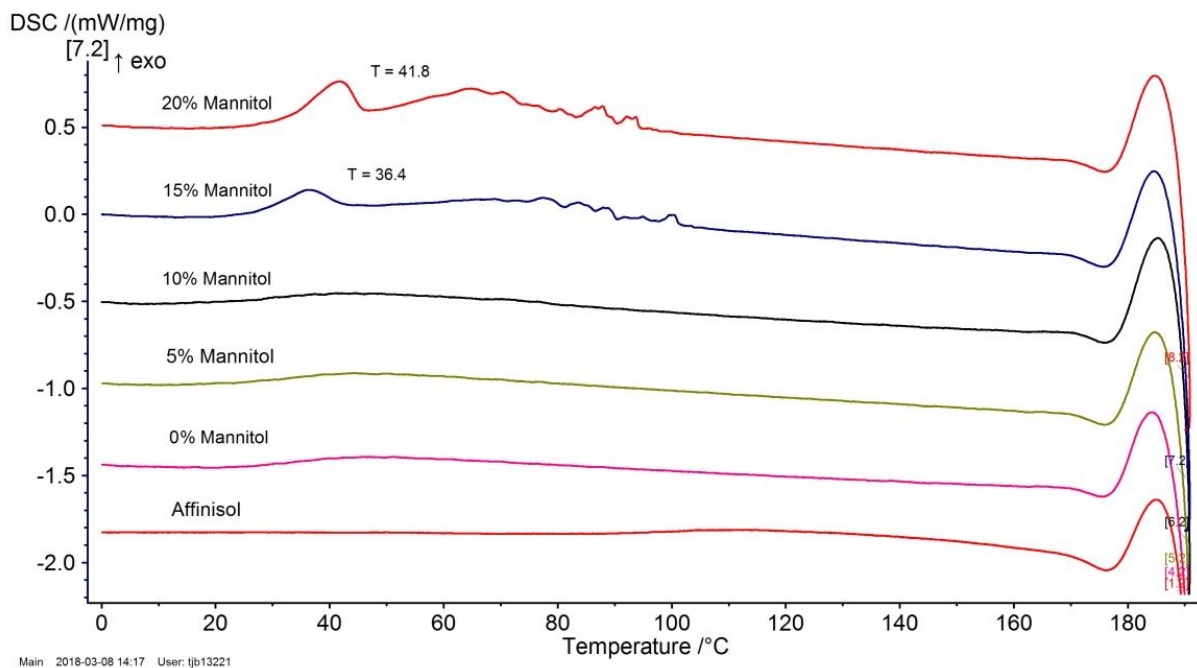


Figure 172 - 30% Carvedilol Formulations Cooling

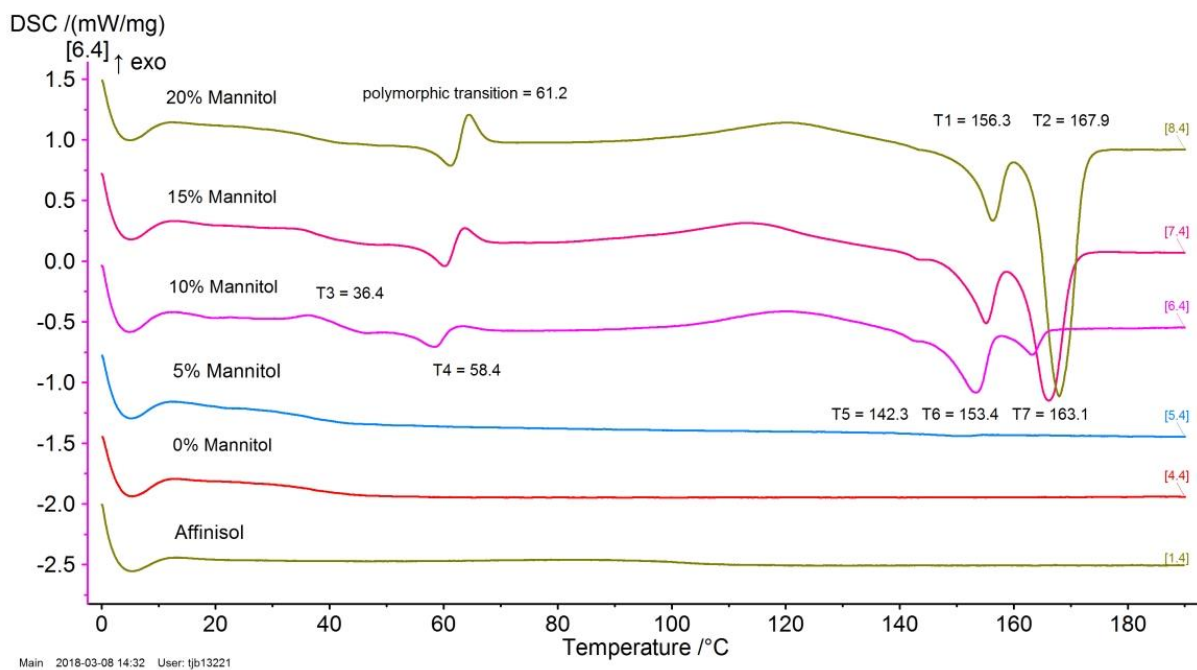


Figure 173 - 30% Carvedilol Formulations 2nd Heating

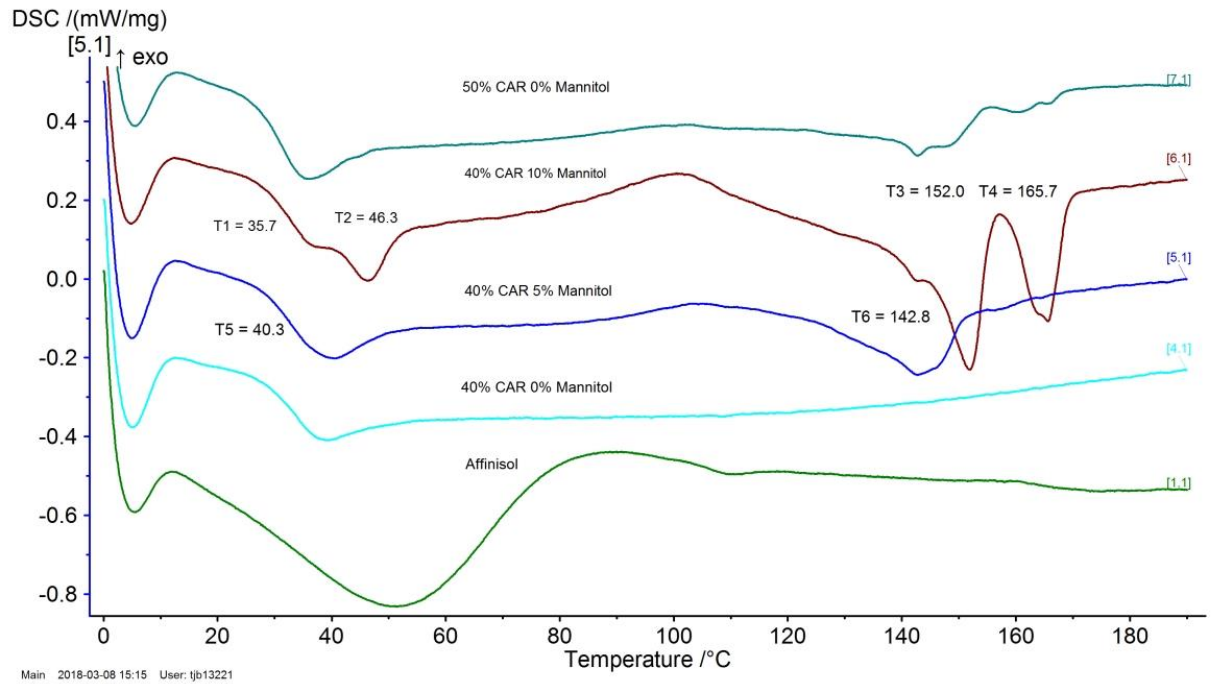


Figure 174 - 40% and 50% Carvedilol Formulations 1st Heating

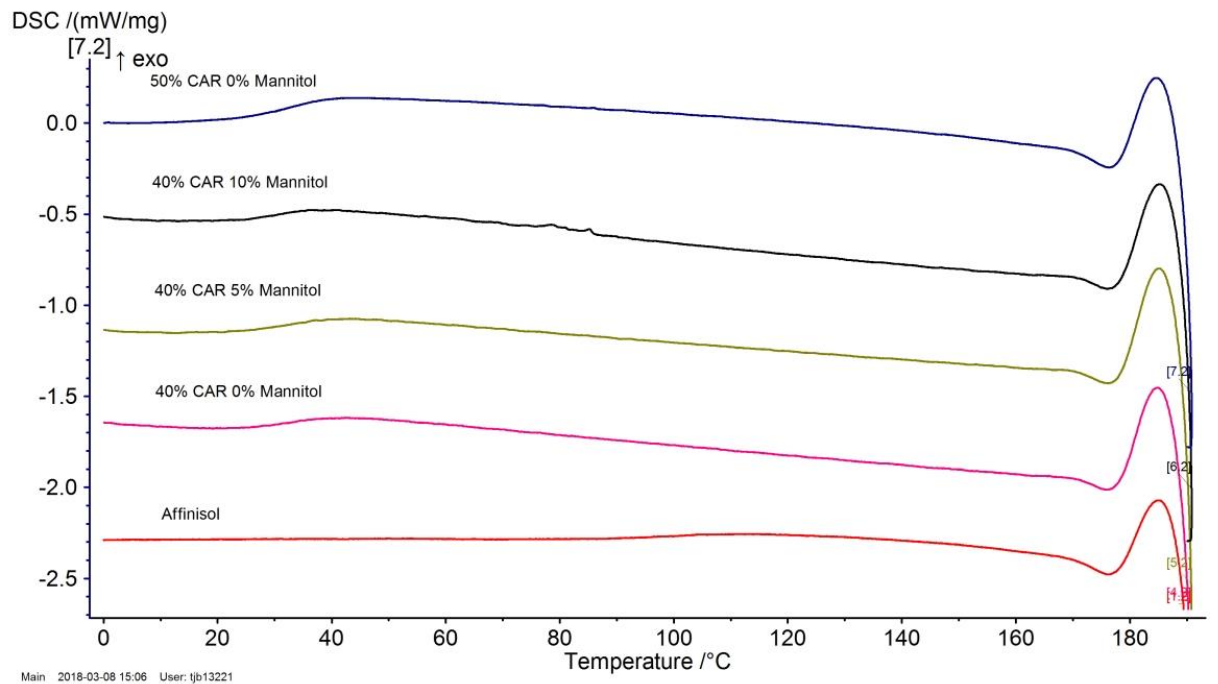
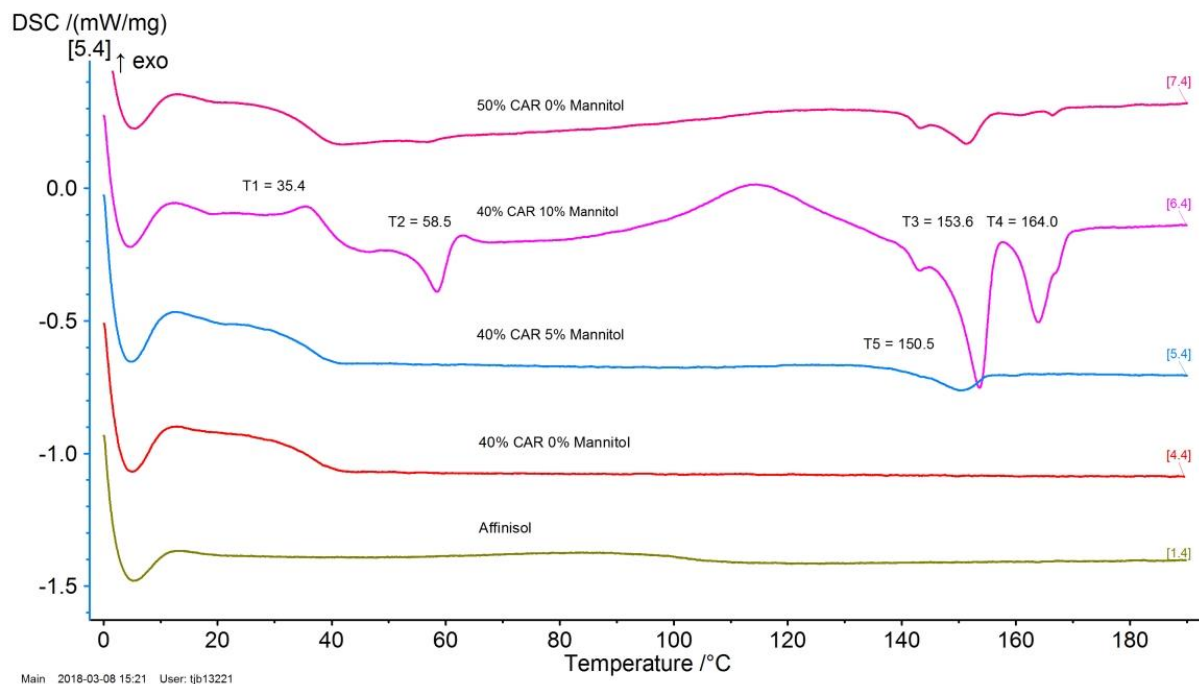


Figure 175 - 40% and 50% Carvedilol Formulations Cooling



**Figure 176 - 40% and 50% Carvedilol Formulations 2nd Heating**



## References

- <sup>1</sup> M. Saffran, G. S. Kumar, C. Savariar, J. C. Burnham, F. Williams, D. C. Neckers, *Science*, 1986, **233**, 1081-1084.
- <sup>2</sup> A. Fahr & X. Liu, *Expert Opinion on Drug Delivery*, 2007, **4**, 403-416.
- <sup>3</sup> H. van de Waterbeemd, E. Gifford, *Nat. Rev. Drug Discov.* 2003, **2**, 192-204.
- <sup>4</sup> A. Fasano, *J. Pharm. Sci.* 1998, **87**, 1351-1356.
- <sup>5</sup> S. V. Sastry, J. R. Nyshadham, J. A. Fix, *Pharm. Sci. & Technol. Today*, 2000, **3**, 138-145.
- <sup>6</sup> N. Pavurala, L. E. K. Achenie, *Computers and Chemical Engineering*, 2013, **57**, 196-206.
- <sup>7</sup> M. E. Aulton, *Pharmaceutics: the science of dosage form design*, Churchill Livingstone, New York, 2002.
- <sup>8</sup> P. M. Desai, C. V. Liew, P. W. S. Heng, *J. Pharm. Sci.* 2016, **105**, 2545-2555.
- <sup>9</sup> S. K. Joneja, W. W. Harcum, G. W. Skinner, P.E. Barnum, Jian-Hwa Guo, *Drug Dev. & Indust. Pharm.* 1999, **25**, 1129-1135.
- <sup>10</sup> H. Patel, V. Shah U. Upadhyay, *Int. J. of Pharm. & Life Sci. (IJPLS)*, 2011, **2**, 1006-1019.
- <sup>11</sup> J. Li, Y. Wu, *Lubricants*, 2014, **2**, 21-43.
- <sup>12</sup> British Pharmacopoeia Commission, *British Pharmacopoeia 2020: Appendix XII Recommendations on Dissolution Testing*, TSO, London, 2020.
- <sup>13</sup> M. P. Ratnaparkhi, P. Gupta Jyoti, *Int. J. of Pharm. Res. & Rev. (IJPRR)*, 2013, **2**, 11-21.
- <sup>14</sup> Y. Perrie, T. Rades, *Pharmaceutics – Drug Delivery and Targeting*, Pharmaceutical Press, London, 2012.
- <sup>15</sup> A. Kikuchi, T. Okano, *Advanced Drug Delivery Reviews*, 2002, **54**, 53-77.
- <sup>16</sup> <https://www.calpol.co.uk/our-products/get-the-dose-right> (Accessed 18/11/2019)
- <sup>17</sup> M. A. Azad, J. G. Osorio, A. Wang, D. M. Klee, M. E. Eccles, E. Grela, R. Sloan, G. Hammersmith, K. Rapp, D. Brancazio, A. S. Myerson, *Pharm. Res.* 2019, **36**, 167.
- <sup>18</sup> E. Fuenmayor, M. Forde, A. V. Healy, D. M. Devine, J. G. Lyons, C. McConville, I. Major, *Int. J. Pharm.* 2019, **558**, 328-340.
- <sup>19</sup> K. Wöstheinrich, P. C. Schmidt, *Drug Dev. & Indust. Pharm.* 2001, **27**, 481-489.
- <sup>20</sup> J. V. Santos, L. A. E. Batista de Carvalho, M. E. T. Pina, *AAPS PharmSciTech*, 2010, **11**, 1442–1448.
- <sup>21</sup> N. Shah, *Computers and Chemical Engineering*, 2004, **28**, 929–941.
- <sup>22</sup> A. A. Konta, M. García-Piña, D. R. Serrano, *Bioengineering*, 2017, **4**, 79.
- <sup>23</sup> M. Swan, *Int. J. Environ. Res. Public Health*, 2009, **6**, 492-525.
- <sup>24</sup> <http://mytorontocanadambastudentexperience.blogspot.co.uk/2012/10/personalized-medicine-or-p4-medicine.html> (Accessed 02/07/14)
- <sup>25</sup> M. J. Alomar, *Saudi Pharm. J.* 2014, **22**, 83-94.
- <sup>26</sup> K. Taylor, G. Harding, *Pharmacy Practice*, Taylor & Francis, London, 2001.
- <sup>27</sup> M. Kessel, *Nat. Biotechnol.* 2011, **29(1)**, 27-33.
- <sup>28</sup> B. Aksu, T. De Beer, S. Folestad, J. Ketolainen, H. Lindén, J. Almeida Lopes, M. de Matas, W. Oostra, J. Rantanen, M. Weimer, *Eur. J. Pharm. Sci.* 2012, **47**, 402-405.
- <sup>29</sup> C. Gao, L. Yu, S. Zeng, Y. Huang, Q. Zhou, *Ther. Clin. Risk Manag.* 2014, **10**, 217-227.
- <sup>30</sup> M. G. Kees, S. Weber, F. Kees, T. Horbach, *J. Antimicrob. Chemother.* 2011, **66**, 2330-2335.
- <sup>31</sup> S. Chien, T. G. Wells, J. L. Blumer, *J. Clin. Pharmacol.* 2005, **45**, 153-160.
- <sup>32</sup> E. Dolgin, *Nat. Med.* 2013, **19(2)**, 116-117.
- <sup>33</sup> P. B. Davis, U. Yasothan, P. Kirkpatrick, *Nat. Rev. Drug Discov.* 2012, **11**, 349-350.
- <sup>34</sup> I. Glurich, J. K. Burmester, M. D. Caldwell, *Heart Fail Rev.* 2010, **15**, 239-248.
- <sup>35</sup> Z. M. Zhao, S. Kansal, B. L. Bukaveckas, SmartWarf - A Portable Automated Warfarin Dosing Tool, *Proceedings of the 2009 International Symposium on Collaborative Technologies and Systems*, May 18-22, 2009, Baltimore, MD, USA, 348-355.
- <sup>36</sup> J. A. Hixson-Wallace, J. B. Dotson, S. A. Blakey, *Clin. Appl. Thrombosis/Hemostasis*, 2001, **7**, 33-37.
- <sup>37</sup> F. Denis, L. Viger, A. Charron, E. Voog, O. Dupuis, Y. Pointreau, C. Letellier, *Support Care Cancer*, 2014, **22**, 1467-1473.
- <sup>38</sup> G. S. Ryu, Y. J. Lee, *J. Manag. Care Pharm.* 2012, **18(6)**, 439-445.

- <sup>39</sup> P. Sobhani, J. Christopherson, P. J. Ambrose, R. L. Corelli, *The Annals of Pharmacotherapy*, 2008, **42**, 46-52.
- <sup>40</sup> K. Wening, J. Breitzkreutz, *Int. J. Pharm.* 2010, **395**, 174-181.
- <sup>41</sup> J. M. Rosenberg, J. P. Nathan, F. Plakogiannis, *J. Am. Pharm. Assoc.* 2002, **42(2)**, 200-205.
- <sup>42</sup> G. A. Green, C. Berg, N. Valdez, A. Kaplan, *Accuracy and ease of splitting scored Coumadin, Lanoxin and Toprol XL tablets*, 2009, Poster Presentation, AAPS, Los Angeles.
- <sup>43</sup> L. Solomon, A. S. Kaplan, *Method of administering a partial dose of a segmented pharmaceutical tablet*, 2010, US 0000007713547B2
- <sup>44</sup> K. Wening, J. Breitzkreutz, *Int. J. Pharm.* 2011, **404**, 1-9.
- <sup>45</sup> E. Kayitare, C. Vervaet, J.D. Ntawukulilyayo, B. Seminega, Van Bortel, J.P. Remon, *Int. J. Pharm.* 2009, **370**, 41-46.
- <sup>46</sup> <http://www.drugs.com/dosage/combivir.html> (Accessed 04/07/2014).
- <sup>47</sup> M. Alomari, F. H. Mohamed, A. W. Basit, S. Gaisford, *Int. J. Pharm.* 2015, **494**, 568-577.
- <sup>48</sup> E. Elele, Y. Shen, B. Khusid, *Appl. Phys. Lett.* 2010, **97**, 233501.
- <sup>49</sup> E. Elele, Y. Shen, R. Susarla, B. Khusid, G. Keyvan, B. Michniak-Kohn, *J. Pharm. Sci.* 2012, **101(7)**, 2523-2533.
- <sup>50</sup> N. Sandler, A. Määttänen, P. Ihalainen, L. Kronberg, A. Meierjohann, T. Viitala, J. Peltonen, *J. Pharm. Sci.* 2011, **100(8)**, 3386-3395.
- <sup>51</sup> P. A. Meléndez, K. M. Kane, C. S. Ashvar, M. Albrecht, P. A. Smith, *J. Pharm. Sci.* 2008, **97(7)**, 2619-2636.
- <sup>52</sup> S. Goodall, N. Chew, K. Chan, D. Auriac, M. J. Waters. *J. Aerosol Med.* 2002, **15(3)**, 351-357.
- <sup>53</sup> A. B. M. Buanz, M. H. Saunders, A. W. Basit, S. Gaisford, *Pharm. Res.* 2011, **28(10)**, 2386-2392.
- <sup>54</sup> R. Daly, T. S. Harrington, G. D. Martin, I. M. Hutchings, *Int. J. Pharm.* 2015, **494**, 554-567.
- <sup>55</sup> N. Genina, D. Fors, M. Palo, J. Peltonen, N. Sandler, *Int. J. Pharm.* 2013, **453**, 488-497.
- <sup>56</sup> F. Cilurzo, P. Minghetti, A. Casiraghi, L. Tosi, S. Pagani, L. Montanari, *Eur. J. Pharm. Biopharm.* 2005, **60**, 61-66.
- <sup>57</sup> A. J. Turner, PhD Thesis, University of Strathclyde, 2019.
- <sup>58</sup> N. Genina, D. Fors, H. Vakili, P. Ihalainen, L. Pohjala, H. Ehlers, I. Kassamakov, E. Haeggström, P. Vuorela, J. Peltonen, N. Sandler, *Eur. J. Pharm. Sci.* 2012, **47**, 615-623.
- <sup>59</sup> J. Gardan, *International Journal of Production Research*, 2016, **54**, 3118-3132.
- <sup>60</sup> K. Shahzad, J. Deckers, J. Kruth, J. Vleugels, *Journal of Materials Processing Technology*, 2013, **213**, 1484-1494.
- <sup>61</sup> H. Wu, W. Liu, R. He, Z. Wu, Q. Jiang, X. Song, Y. Chen, L. Cheng, S. Wu, *Ceramics International*, 2017, **43**, 968-972.
- <sup>62</sup> F. Ning, W. Cong, J. Qiu, J. Wei, S. Wang, *Composites Part B*, 2015, **80**, 369-378.
- <sup>63</sup> J. A. Inzana, D. Olvera, S. M. Fuller, J. P. Kelly, O. A. Graeve, E. M. Schwarz, S. L. Kates, H. A. Awad, *Biomaterials*, 2014, **35**, 4026-4034.
- <sup>64</sup> X. Wang, M. Jiang, Z. Zhou, J. Gou, D. Hui, *Composites Part B*, 2017, **110**, 442-458.
- <sup>65</sup> I. Gibson, D. Rosen, B. Stucker, *Additive Manufacturing Technologies - 3D Printing, Rapid Prototyping, and Direct Digital Manufacturing*, Springer, New York, 2015.
- <sup>66</sup> E. Sachs, M. Cima, J. Cornie, *Annals of CIRP*, 1990, **39(1)**, 201-204.
- <sup>67</sup> A. Gratton, *Comparison of Mechanical, Metallurgical Properties of 17-4PH Stainless Steel between Direct Metal Laser Sintering (DMLS) and Traditional Manufacturing Methods*, Proceedings of The National Conference On Undergraduate Research (NCUR) 2012, Weber State University, Ogden Utah March 29 – 31, 2012.
- <sup>68</sup> T. Duda, L. V. Raghavan, *IFAC-PapersOnLine*, 2016, **49-29**, .103-110.
- <sup>69</sup> Z. Liu, M. Zhang, B. Bhandari, Y. Wang, *Trends Food Sci. Tech.* 2017, **69**, 83-94.
- <sup>70</sup> J. I. Lipton, M. Cutler, F. Nigl, D. Cohen, H. Lipson, *Trends Food Sci. Tech.* 2015, **43**, 114-123.
- <sup>71</sup> M. S. Mannoor, Z. Jiang, T. James, Y. L. Kong, K. A. Malatesta, W. O. Soboyejo, N. Verma, D. H. Gracias, M. C. McAlpine, *Nano Lett.* 2013, **13**, 2634-2639.
- <sup>72</sup> N. Sandler, I. Salmela, A. Fallarero, A. Rosling, M. Khajeheian, R. Kolakovic, N. Genina, J. Nyman, P. Vuorela, *Int. J. Pharm.* 2014, **459**, 62-64.
- <sup>73</sup> W. E. Katstra, R. D. Palazzolo, C. W. Rowe, B. Giritlioglu, P. Teung, M. J. Cima, *J. Control. Release*, 2000, **66**, 1-9.
- <sup>74</sup> C. W. Rowe, W. E. Katstra, R. D. Palazzolo, B. Giritlioglu, P. Teung, M. J. Cima, *J. Control. Release*, 2000, **66**, 11-17.

- <sup>75</sup> [https://www.aprecia.com/pdf/ApreciaSPRITAMLaunchPressRelease\\_FINAL.PDF](https://www.aprecia.com/pdf/ApreciaSPRITAMLaunchPressRelease_FINAL.PDF) (Accessed 05/07/2018)
- <sup>76</sup> <https://aprecia.com/zipdose-platform/3d-printing.php> (Accessed 05/07/2018)
- <sup>77</sup> P. R. Martinez, A. Goyanes, A. W. Basit, S. Gaisford, *Int. J. Pharm.* 2017, **532**, 313-317.
- <sup>78</sup> L-T. Ng, S. Swami, C. Gordon-Thomson, *Radiat. Phys. Chem.* 2006, **75**, 604-612.
- <sup>79</sup> S. A. Khaled, J. C. Burley, M. R. Alexander, C. J. Roberts, *Int. J. Pharm.* 2014, **461**, 105-111.
- <sup>80</sup> A. Goyanes, A. B. M. Buanz, A. W. Basit, S. Gaisford, *Int. J. Pharm.* 2014, **476**, 88-92.
- <sup>81</sup> J. Skowrya, K. Pietrzak, M. A. Alhnan, *Eur. J. Pharm. Sci.* 2015, **68**, 11-17.
- <sup>82</sup> K. Pietrzak, A. Isreb, M. A. Alhnan, *Eur. J. Pharm. Biopharm.* 2015, **96**, 380-387.
- <sup>83</sup> A. Goyanes, H. Chang, D. Sedough, G. B. Hatton, J. Wang, A. Buanz, S. Gaisford, A. W. Basit, *Int. J. Pharm.* 2015, **496**, 414-420.
- <sup>84</sup> T. C. Okwuosa, D. Stefaniak, B. Arafat, A. Isreb, K. Wan, M. A. Alhnan, *Pharm. Res.* 2016, **33**, 2704-2712.
- <sup>85</sup> W. Jamróz, J. Szafraniec, M. Kurek, R. Jachowicz, *Pharm. Res.* 2018, **35**, 176.
- <sup>86</sup> A. Goyanes, C. M. Madla, A. Umerji, G. D. Piñeiro, J. M. G. Montero, M. J. L. Diaz, M. G. Barcia, F. Taherali, P. Sánchez-Pintos, M. Couce, S. Gaisford, A. W. Basit, *Int. J. Pharm.* 2019, **567**, 118497.
- <sup>87</sup> E. Prasad, M. T. Islam, D. J. Goodwin, A. J. Megarry, G. W. Halbert, A. J. Florence, J. Robertson, *Additive Manufacturing*, 2019, **29**, 100776.
- <sup>88</sup> Royal Pharmaceutical Society, *The British National Formulary*, 63rd Edition, Pharmaceutical Press, UK, March 2012.
- <sup>89</sup> J. S. LaFountaine, J. W. McGinity, R. O. Williams, *AAPS PharmSciTech*, 2016, **17**, 43-55.
- <sup>90</sup> M. Huang, X. Zhang, S. Chen, Y. Sun, Y. Xiao, J. Sun, M. Huang, S. Chen, F. Liu, *Pediatr. Cardiol.* 2013, **34**, 680-685.
- <sup>91</sup> M. Nishiyama, I. Park, T. Yoshikawa, Y. Hatai, M. Ando, Y. Takahashi, K. Mori, Y. Murakami, *Heart Vessels*, 2009, **24**, 187-192.
- <sup>92</sup> G. J. Fernandes, L. Kumar, K. Sharma, R. Tunge, M. Rathnanand, *J. Pharm. Innov.* 2018, **13**, 197-212.
- <sup>93</sup> S. M. Alshahrani, W. Lu, J. Park, J. T. Morott, B. B. Alsulays, S. Majumdar, N. Langley, K. Kolter, A. Gryczke, M. A. Repka, *AAPS PharmSciTech*, 2015, **16**, 824-834.
- <sup>94</sup> L. Martinez-Marcos, D. A. Lamprou, R. T. McBurney, G. W. Halbert, *Int. J. Pharm.* 2016, **499**, 175-185.
- <sup>95</sup> G. Verstraete, A. Samaro, W. Grymonpré, V. Vanhoorne, B. Van Snick, M. N. Boone, T. Hellemans, L. Van Hoorbeke, J. P. Remon, C. Vervae, *Int. J. Pharm.* 2018, **536**, 318-325.
- <sup>96</sup> <https://www.thermofisher.com/order/catalog/product/567-7600?SID=srch-srp-567-7600> (Accessed 13/01/20)
- <sup>97</sup> I. B. Hutchison, A. Delori, X. Wang, K. V. Kamenev, A. J. Urquhart, I. D. H. Oswald, *Cryst. Eng. Comm.* 2015, **17**, 1778-1782.
- <sup>98</sup> <https://www.simplify3d.com/support/materials-guide/pva/> (Accessed May 2018)
- <sup>99</sup> J. M. V. Alves, L. D. Prado, H. V. A. Rocha, *Pharm. Dev. Technol.* 2016, **21(7)**, 856-866.
- <sup>100</sup> S. E. Emshanova, *Pharm. Chem. J.* 2008, **42(2)**, 89-94.
- <sup>101</sup> Z. Zhou, C. Dunn, I. Khadra, C. G. Wilson, G. W. Halbert, *Eur. J. Pharm. Sci.* 2017, **99**, 95-104.
- <sup>102</sup> A. Goyanes, A. B. M. Buanz, G. B. Hatton, S. Gaisford, A. W. Basit, *Eur. J. Pharm. Biopharm.* 2015, **89**, 157-162.
- <sup>103</sup> V. G. Kadajji, G. V. Betageri, *Polymers*, 2011, **3**, 1979-2009.
- <sup>104</sup> E. Ha, J. Kim, S. Lee, W. Sim, J. Jeong, M. Kim, *J. Molecular Liquids*, 2019, **11**, 1622-1629.
- <sup>105</sup> J. G. Lyons, M. Hallinan, J. E. Kennedy, D. M. Devine, L. M. Geever, P. Blackie, C. L. Higginbotham, *Int. J. Pharm.* 2007, **329**, 62-71.
- <sup>106</sup> M. Ibrahim, M. Barnes, R. McMillin, D. W. Cook, S. Smith, M. Halquist, D. Wijesinghe, T. D. Roper, *AAPS PharmSciTech*, 2019, **20**, 195.
- <sup>107</sup> C. L. Hobday, C. H. Woodall, M. J. Lennox, M. Frost, K. Kamenev, T. Düren, C. A. Morrison, S. A. Moggach, *Nat. Commun.* 2018, **9**, 1429.
- <sup>108</sup> I. E. Collings, M. Hanfland, *Molecules*, 2019, **24(9)**, 1759.
- <sup>109</sup> <https://www.lpfrg.com/wp-content/uploads/2019/10/3D-Printer-Filament-Types-and-Uses.pdf> (Accessed 11/01/20)
- <sup>110</sup> <https://www.thingiverse.com/thing:724928> (Accessed May 2018)
- <sup>111</sup> <https://www.simplify3d.com/support/articles/multi-part-printing/> (Accessed March 2020)

- <sup>112</sup> N. Scoutaris, A. L. Hook, P. R. Gellert, C. J. Roberts, M. R. Alexander, D. J. Scurr, *J. Mater. Sci: Mater. Med.* 2012, **23**, 385-391.
- <sup>113</sup> M. Kyobula, A. Adedeji, M. R. Alexander, E. Saleh, R. Wildman, I. Ashcroft, P. R. Gellert, C. J. Roberts, *J. Controlled Release*, 2017, **261**, 207-215.
- <sup>114</sup> A. Goyanes, J. Wang, A. Buanz, R. Martínez-Pacheco, R. Telford, S. Gaisford, A. W. Basit, *Mol. Pharmaceutics*, 2015, **12**, 4077-4084.
- <sup>115</sup> W. Meng, J. Dvořák, R. Kumar, R. Hofmeister, F. Štěpánek, R. Ramachandran, F. J. Muzzio, *Advanced Powder Technology*, 2019, **30**, 1765-1781.
- <sup>116</sup> M. Alhijaj, P. Belton, S. Qi, *Eur. J. Pharm. Biopharm.* 2016, **108**, 111-125.
- <sup>117</sup> M. Alhijaj, S. Yassin, M. Reading, J. A. Zeitler, P. Belton, S. Qi, *Pharm. Res.* 2017, **34**, 971-989.
- <sup>118</sup> S. J. L. Billinge, T. Dykhne, P. Juhás, E. Božin, R. Taylor, A. J. Florence, K. Shankland, *Cryst. Eng. Comm.* 2010, **12**, 1366-1368.
- <sup>119</sup> L. D. Prado, H. V. A. Rocha, J. A. L. C. Resende, G. B. Ferreira A. M. Rangel de Figueiredo Teixeira, *Cryst. Eng. Comm.* 2014, **16**, 3168.
- <sup>120</sup> <https://www.fda.gov/media/133650/download> Accessed (29/12/2019)
- <sup>121</sup> J. Zhang, X. Feng, H. Patil, R. V. Tiwari, M. A. Repka, *Int. J. Pharm.* 2017, **519**, 186-197.
- <sup>122</sup> A. Melocchi, F. Parietti, A. Maroni, A. Foppoli, A. Gazzaniga, L. Zema, *Int. J. Pharm.* 2016, **509**, 255-263.
- <sup>123</sup> N. G. Solanki, M. Tahsin, A. V. Shah, A. T. M. Serajuddin, *J. Pharm. Sci.* 2018, **107**, 390-401.
- <sup>124</sup> M. Sadia, B. Arafat, W. Ahmed, R. T. Forbes, M. A. Alhnan, *J. Control. Release*, 2018, **269**, 355-363.
- <sup>125</sup> C. F. Lerk, G. K. Bolhuis, A. H. de Boer, *J. Pharm. Sci.* 1979, **68**, 205-211.
- <sup>126</sup> C. Chebli, L. Cartilier, *Int. J. Pharm.* 1998, **171**, 101-110.
- <sup>127</sup> J. Fukami, E. Yonemochi, Y. Yoshihashi, K. Terada, *Int. J. Pharm.* 2006, **310**, 101-109.
- <sup>128</sup> R. Hamed, A. Awadallah, S. Sunoqrot, O. Tarawneh, S. Nazzal, T. AlBaraghthi, J. Al Sayyad, A. Abbas, *AAPS Pharm. Sci. Tech.* 2016, **17** (2), 418-426.
- <sup>129</sup> K. Yuvaraja, J. Khanam, *J. Pharm. Biomed. Anal.* 2014, **96**, 10-20.
- <sup>130</sup> M. Lawson, *Sugar alcohols. Kirk-Othmer Encyclopedia of Chemical Technology*. John Wiley & Sons Inc, New York, 2000.
- <sup>131</sup> J. C. Price, in *Handbook of Pharmaceutical Excipients, Polyethylene glycol* ed. A. H. Kibbe, American Pharmaceutical Association and Pharmaceutical Association, Washington, 2000, pp. 392–398.
- <sup>132</sup> K. O'Donnell, M. W. Kearsley, *Sweeteners and Sugar Alternatives in Food Technology*, Wiley-Blackwell, Chichester, 2012.
- <sup>133</sup> [https://www.pharma.dupont.com/content/dam/dupont/amer/us/en/nutrition-health/general/pharmaceuticals/documents/Download\\_Affinisol%20HPMC%20HME%20Brochure.pdf](https://www.pharma.dupont.com/content/dam/dupont/amer/us/en/nutrition-health/general/pharmaceuticals/documents/Download_Affinisol%20HPMC%20HME%20Brochure.pdf) Accessed (10/02/2023)
- <sup>134</sup> E. Bordos, M. T. Islam, A. J. Florence, G. W. Halbert, J. Robertson, *Mol. Pharmaceutics*, 2019, **16**, 4361-4371.
- <sup>135</sup> S. A. Khaled, M. R. Alexander, R. D. Wildman, M. J. Wallace, S. Sharpe, J. Yoo, C. J. Roberts, *Int. J. Pharm.* 2018, **538**, 223-230.
- <sup>136</sup> J. Conceição, X. Farto-Vaamonde, A. Goyanes, O. Adeoye, A. Concheiro, H. Cabral-Marques, J. M. S. Lobo, C. Alvarez-Lorenzo, *Carbohydrate Polymers*, 2019, **221**, 55-62.
- <sup>137</sup> H.S.Kim, G.A.Jeffrey, R.D.Rosenstein, *Acta Crystallogr.* 1968, **B24**, 1449.
- <sup>138</sup> W.Kaminsky, A.M.Glazer, *Z.Kristallogr.* 1997, **212**, 283.
- <sup>139</sup> C.E.Botez, P.W.Stephens, C.Nunes, R.Suryanarayanan, *Powder Diffr.* 2003, **18**, 214.
- <sup>140</sup> H. Shihora, S. Panda, *JPSBR*, 2011, **1** (3), 148-153.
- <sup>141</sup> S. A. Khaled, J. C. Burley, M. R. Alexander, J. Yang, C. J. Roberts, *Int. J. Pharm.* 2015, **494**, 643-650.
- <sup>142</sup> A. Goyanes, P. R. Martinez, A. Buanz, A. W. Basit, S. Gaisford, *Int. J. Pharm.* 2015, **494**, 657-663.
- <sup>143</sup> H. E. Gültekin, S. Tort, F. Acartürk, *Pharm. Res.* 2019, **36**, 128.
- <sup>144</sup> B. Arafat, M. Wojsz, A. Isreb, R T. Forbes, M. Isreb, W. Ahmed, T. Arafat, M. A. Alhnan, *Eur. J. Pharm. Sci.* 2018, **118**, 191-199.
- <sup>145</sup> A. Gokhale, *Pharm. Tech.* 2014, **38**(5).
- <sup>146</sup> British Medical Association, Royal Pharmaceutical Society, (2018). *BNF 75*, London, BMJ Group and Pharmaceutical Press.

147

[http://msdssearch.dow.com/PublishedLiteratureDOWCOM/dh\\_0954/0901b803809543f4.pdf?filepath=dowwolff/pdfs/noreg/198-02327.pdf&fromPage=GetDoc](http://msdssearch.dow.com/PublishedLiteratureDOWCOM/dh_0954/0901b803809543f4.pdf?filepath=dowwolff/pdfs/noreg/198-02327.pdf&fromPage=GetDoc) Accessed (05/07/2018)

<sup>148</sup> W. Steinmann, S. Walter, M. Beckers, G. Seide, T. Gries, in *Applications of Calorimetry in a Wide Context - Differential Scanning Calorimetry, Isothermal Titration Calorimetry and Microcalorimetry*, ed A. A. Elkordy, IntechOpen, London, 2013, ch. 12, pp. 281-283.

<sup>149</sup> M. G. Cares-Pacheco, G. Vaca-Medina, R. Calvet, F. Espitalier, J.-J. Letourneau, A. Rouilly, E. Rodier, *Int. J. Pharm.* 2014, **475**, 69-81.

<sup>150</sup> J. A. Baird, L. S. Taylor, *Advanced Drug Delivery Reviews*, 2012, **64**, 396-421.

<sup>151</sup> M. Zhu, L. Yu, *J. Chem. Phys.* 2017, **146**, 244503.

<sup>152</sup> M. Zhu, J.-Q. Wang, J. H. Perepezko, L. Yu, *J. Chem. Phys.* 2015, **142**, 244504.

<sup>153</sup> P. Khatri, P. Katikaneni, D. Desai, T. Minko, *Journal of Drug Delivery Science and Technology*, 2018, **47**, 461-467.

<sup>154</sup> [https://www.accessdata.fda.gov/drugsatfda\\_docs/nda/2006/022012s000\\_ClinPharmR.pdf](https://www.accessdata.fda.gov/drugsatfda_docs/nda/2006/022012s000_ClinPharmR.pdf) Accessed (10/03/2023)